UNIVERSITY OF Southampton
School of Engineering Sciences

Bioengineering Sciences Research Group

Development of Computational Biomechanical Tools to Assess the Performance of the Resurfaced Hip Joint

Alexander Stephen Dickinson, December 2010

Thesis for the degree of Doctor of Philosophy

Supervisors: Dr M Browne and Dr A C Taylor

Knowledge Transfer Partnerships

FINSBURY ORTHOPAEDICS

Funded by a UK Government Technology Strategy Board
Knowledge Transfer Partnership with Finsbury Orthopaedics Ltd.

and

the Engineering and Physical Sciences Research Council

UNIVERSITY OF SOUTHAMPTON

ABSTRACT

SCHOOL OF ENGINEERING SCIENCES
BIOENGINEERING SCIENCE RESEARCH GROUP

Doctor of Philosophy

Development of Computational Biomechanical Tools to Assess the Performance of the Resurfaced Hip Joint

by Alexander Dickinson

Hip resurfacing shows good clinical results as a treatment for osteoarthritis in young male patients. However, there is room for improvement in survivorship and patient scope: occasional femoral neck fractures and femoral prosthesis loosenings occur, and concerns regarding the effects of metal ions released by wear particles contraindicate resurfacing in female patients. Both failure modes are multi-factorial but evidence suggests that biomechanical factors are involved. Finite element analysis is used to study the biomechanics of the resurfaced hip, but there have been contradictions between the findings of previous investigations, which could be linked to simplifications of the prosthesis positioning and implant-bone interface conditions compared to the *in-vivo* scenario. This thesis comprises three studies, investigating the biomechanics of the resurfaced hip. The effects of prosthesis sizing and positioning were investigated, and a new model for predicting progressive bone adaptation around the prosthesis was developed. Finally, these techniques were used to test the feasibility of a new design, informed by analysis of traditional designs.

In the first study, the effects of prosthesis sizing and varus-valgus positioning were investigated. Corroborated by clinical observations, the results indicated that under-sizing the prosthesis would reduce the strain in the femoral neck, potentially contributing to prosthesis loosening through stress shielding. The results also indicated the role played by the prosthesis stem and its bore in fracture of the femoral neck and proximal stress shielding.

In the second study, a combined bone defect healing and remodelling algorithm was developed to allow the progressive bone adaptation around the prosthesis to be predicted. The addition of defect healing to previous pure remodelling algorithms allowed the model to replicate the full set of radiographic changes observed clinically around the prosthesis.

In the final study, the findings of the biomechanical studies and their analysis methods were applied to a new design concept: a short stemmed resurfacing head, which could utilise ceramic materials. The model predicted a reduced risk of femoral neck fracture and prosthesis loosening for this design. The results gave a first indication that a ceramic resurfacing prosthesis would be feasible, providing an answer to concerns over metal ion release effects and potentially broadening the patient cohort.

CONTENTS

FIGURES

TABLES

ACKNOWLEDGEMENTS

The last four years have been both the most challenging and the most rewarding yet, and – difficult as it was at times – I'm so glad to have done it. But it would have been a lot harder and a lot less fun without the help some great colleagues and friends who all need to be thanked.

Dr Andy Taylor talked me into it in the first place, and his infectious enthusiasm convinces you that anything is possible. Thanks to Andy for giving me some huge responsibilities and for letting me jump in way out of my depth.

Dr Martin Browne helped me to turn all that enthusiasm into this thesis; in short I can't imagine a better Boss. Thanks to Martin for showing me how it's done, and for never allowing me to take things even remotely seriously.

This would have been very dry indeed without Team Finsbury. It was hugely motivational to work with you all, and to know that the research might make a difference in the outside world. I'm proud of what we achieved! It was a pleasure working with Anne, the Great Mike Tuke (who appreciates a real car), Katherine, Rod, Russell, Xiao and everyone else in Leatherhead. Most of all though I have to thank Dr Jeffers. When I grow up I'm going to be *just like you*.

Several consultant orthopaedic surgeons also helped me to link this to the real world, and were always keen to let me observe their work and to answer my questions. In particular, thanks to Mr Jeremy Latham from Southampton and Dr David Young from Melbourne, for providing example radiographs and photos to illustrate this work.

Team Southampton: the Bio Research Group is easily the Best Research Group, and it was huge fun to be part of. From the University and besides, for all the bike rides, laps of the sports hall, mountains climbed, skied down (and fallen off), boat races, road trips, New Forest and Isle of Wight adventures, Cake Fridays and voyages around the world, thanks to Adam, Aida, Anna, Becky, Catherine, Clint, Chris, Dave, Dunc, GavMan, Hatice, Hamid, Faye, Francis, Holly, JoJo, Lucy, Mamadou, Mari, Mav, Meadhbh, Mike, NJOS, Norm, Olly, Pete W_1, Pete W_2, Pramod, Rich, Rob, Stéphane and Tobes.

But the most important team is my family. I simply couldn't have done this without you chaps supporting me, or without being able to escape now and again.

This is for my Coach, my Nutritionist and my Big Brother.

ABBREVIATIONS

ALVAL	Condition, Aseptic lymphocyte-dominated vasculitis-associated lesions
ASR	Articular Surface Replacement (Prosthesis, DePuy)
AVN	Avascular Necrosis (condition)
BC	Boundary Conditions
BHR	Birmingham Hip Resurfacing (Prosthesis, Smith&Nephew)
BMD	Bone Mineral Density
CF-PEEK	Carbon Fibre Reinforced Polyetherether Ketone (bearing material)
CoCr	Cobalt Chromium (bearing alloy)
CS	Coordinate System
qCT	(Quantitative) Computer Tomography
DEXA	Dual Energy X-Ray Absorptiometry
DIC	Digital Image Correlation
DOF	Degree of Freedom
FDA	US Food and Drug Administration
FE or FEA	Finite Element (Analysis)
FOS	Factor of Safety
JCF	Joint Contact Force
MCFA	Medial Circumflex Femoral Artery
MoM	Metal-on-Metal (bearing combination)
MPE	Metal-on-Polyethylene (bearing combination)
NICE	National Institute for Clinical Excellence
OA	Condition, Osteoarthritis
PMMA	Polymethyl methacrylate (acrylic) (bone cement polymer)
RA	Condition, Rheumatoid Arthritis
RHR	Resurfacing Hip Replacement
SED	Strain Energy Density
THA or THR	Total Hip Arthroplasty or Replacement
XLPE	Cross Linked Polyethylene (bearing material)

1 INTRODUCTION

1.1 Motivation

Resurfacing hip replacement shows good clinical results, in particular for young, active male patients [1]. However, it has proven unsuitable for the treatment of older, female patients for several reasons, including the requirement of high quality bone in the femoral head and neck to support the prosthesis without fracture [2], adverse bone remodelling in the femoral neck [3, 4], and the risks of sensitivity reactions and the longer term effects of metal ions [5]. Femoral neck fracture and narrowing are believed to be multi-factorial phenomena and frequently linked to surgical error, poor patient selection and abnormal load events, although both may have links to biomechanics including prosthesis design and positioning [6].

Computational modelling is a predictive tool for the mechanical performance of structures, and is particularly relevant to biomechanical research owing to the complexity, expense and ethical issues associated with *in-vivo* models. Accordingly, finite element analysis (FEA) modelling techniques have been developed to replicate the behaviour of biological tissues supporting prosthetic devices. In an attempt to find a biomechanical explanation for fracture and adverse remodelling of the femoral neck in the resurfaced hip joint, the results of several computational stress analysis studies have been published which have made predictions of the stress and strain distribution in the bone supporting resurfacing prostheses. Early, simplified FE models demonstrated a reduction in stress within the resurfaced femoral head [7-9] and biomechanical analysis showed that varus orientation increases the risk of femoral neck fracture [10]. Later, more detailed, patient specific models with geometry and materials properties based on Computer Tomography (CT) scans were used to obtain more precise, absolute bone strain predictions [11-18].

These studies have focussed in particular on traditional prosthesis designs, considering the effects of different prosthesis-bone interface conditions, fixation methods including cementless and cemented fixation with different cement mantle thicknesses, and variations in prosthesis positioning including varus-valgus orientation and incomplete prosthesis seating. The results have confirmed the roles of several suspected, clinically observed risk factors in the failure of the resurfaced hip, and have developed guidelines for the optimal fixation of traditional prosthesis designs [12, 14, 17]. Concerning

prosthesis positioning, for example the effects of varus-valgus orientation, contradictory results have been obtained by several groups [15, 16, 18]. Furthermore, previous studies have made considerable simplifications of the true clinical conditions, with regard to implant positioning and sizing strategies, and in the representation of the implant stem-bone interface. Only some of the characteristic patterns of bone remodelling around the resurfacing head prosthesis have been replicated by simulations, indicating that there is scope for research into the interaction between different biomechanical processes at work following surgery, including adaptive bone remodelling, bone failure, and the healing and adaptation of the implant-bone interface.

The majority of studies in the literature discuss the use of existing hip resurfacing prostheses. However, there is limited discussion of the use of computational modelling in pre-clinical analysis, and application of the understanding of existing failure modes in the development of new designs. Some aspects of prosthesis design, for example the bearing surface geometry, may be restricted owing to functional constraints including the impingement-free range of motion. Other aspects are more open to development, for example the metaphyseal stem. Evidence to support this as a focus for research includes observations of radiographic changes around the stem [3, 4] which indicate that, contrary to its intended function as a non-load bearing alignment guide, it plays a role in load transfer into the medial cortex and away from the femoral head and proximal neck. Unlike the bearing surface, the stem is a design feature which could be changed easily and without affecting the primary function of the prosthesis and resurfaced joint.

Clinical evidence has suggested that there is scope for improvement of the biomechanics of traditional hip resurfacing prostheses, but the use of more biocompatible implant materials should also be considered. In order to circumvent the perceived adverse effects of metal ion release from the currently used Cobalt Chromium (CoCr) alloys, non-metallic structural biomaterials could be employed. However, to permit the use of non-metallic biomaterials, prosthesis design changes would be necessary; for example, when employing bioceramics, tensile stress should be minimised to prevent prosthesis fracture. A computational preclinical analysis tool that could evaluate the response of hip biomechanics and the implant structure to new prosthesis designs and materials would be very beneficial in the development of new prostheses.

1.2 Objectives

The objectives of this project were to develop finite element models of the proximal femur with a resurfaced femoral head, and to use them to investigate several patient, surgical, and implant design factors to understand in greater detail the biomechanical causes behind the failure modes of hip resurfacings.

Successful proof of concept of these methods has implications for prosthesis design development. In terms of biomechanical response, several goals can be immediately identified, including reduced risks of femoral neck fracture, adverse bone remodelling and prosthesis loosening, and greater tolerance to surgical and patient variation. To illustrate this, a case study was conducted with a proposed new resurfacing head design. While the detailed analysis of prostheses featuring non-metallic biomaterials was beyond the scope of this biomechanical research, the new design concept was influenced by the eventual goal of employing structural bioceramics, to improve biocompatibility and broaden the patient cohort to include the young female.

Figure 1 is a flowchart showing the approach taken towards the planned research, and will be repeated in skeleton form on the first page of each chapter in this thesis, highlighting how that chapter fits into the overall structure.

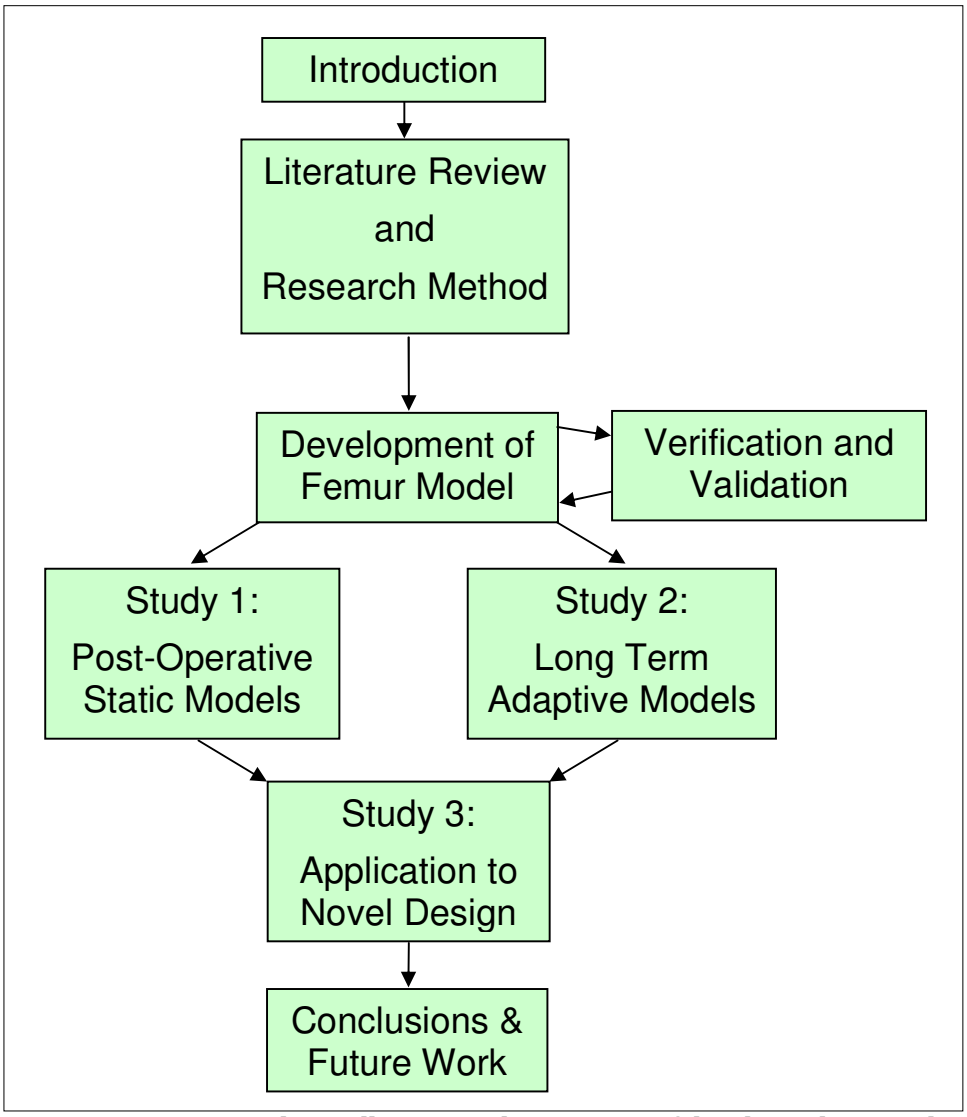

Figure 1: Project Roadmap, illustrating the Structure of the Planned Research

2 LITERATURE REVIEW AND RESEARCH METHOD

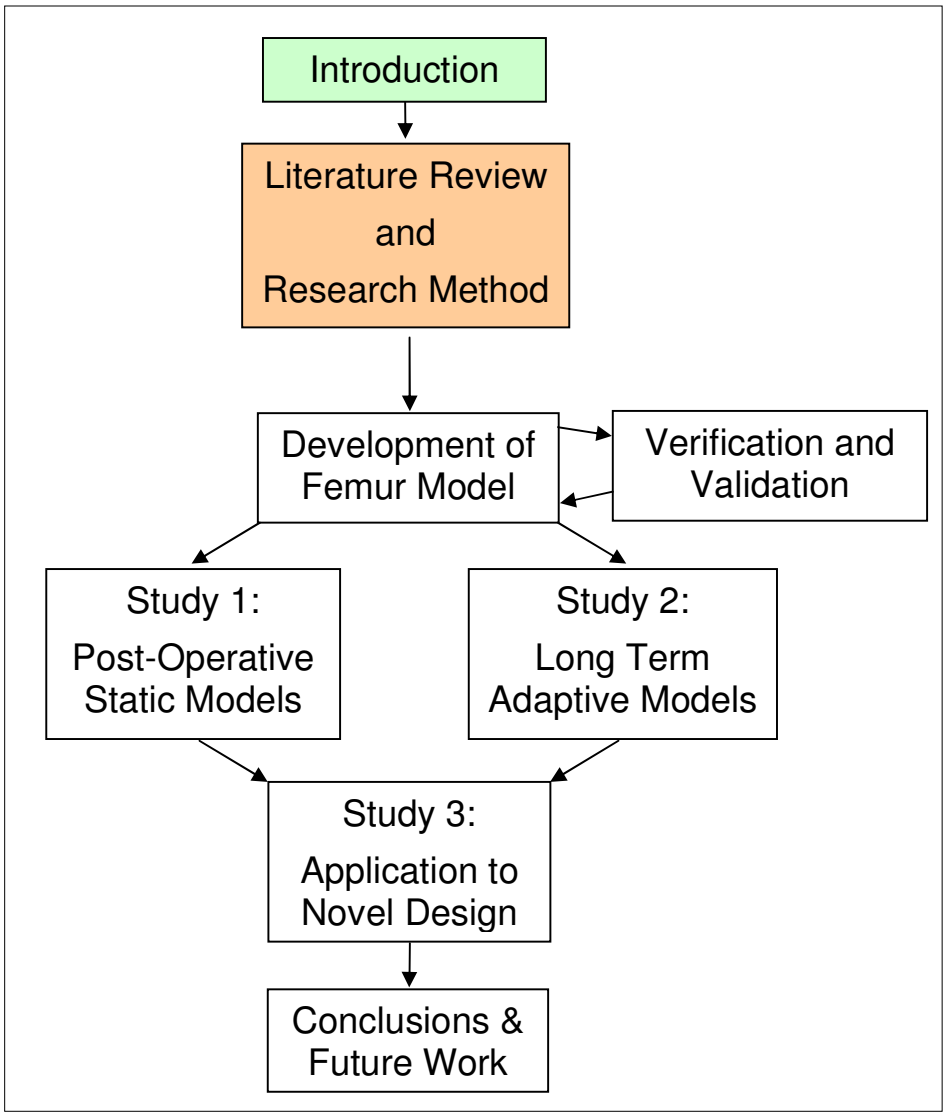

This study uses computational biomechanical models to predict the clinical performance of resurfacing hip prostheses. A thorough literature survey was conducted, with focus in two main areas. First, considering the clinical aspects, the causes of hip degeneration and the state of the art of surgical interventions were investigated, and the scope for improvement was summarised. Second, the biomechanics of the resurfaced hip were considered. The literature was reviewed for the biomechanics of the hip joint, details of the mechanical properties of bone, and its failure and adaptation processes. The state of the art of computational mechanical modelling of bone and prosthesis-bone interfaces, including failure, healing and adaptation was discussed, with particular application to hip resurfacing. Finally, this led to a justification of the research method.

2.1 Part 1: The Hip Joint, Degeneration, Treatments and Complications

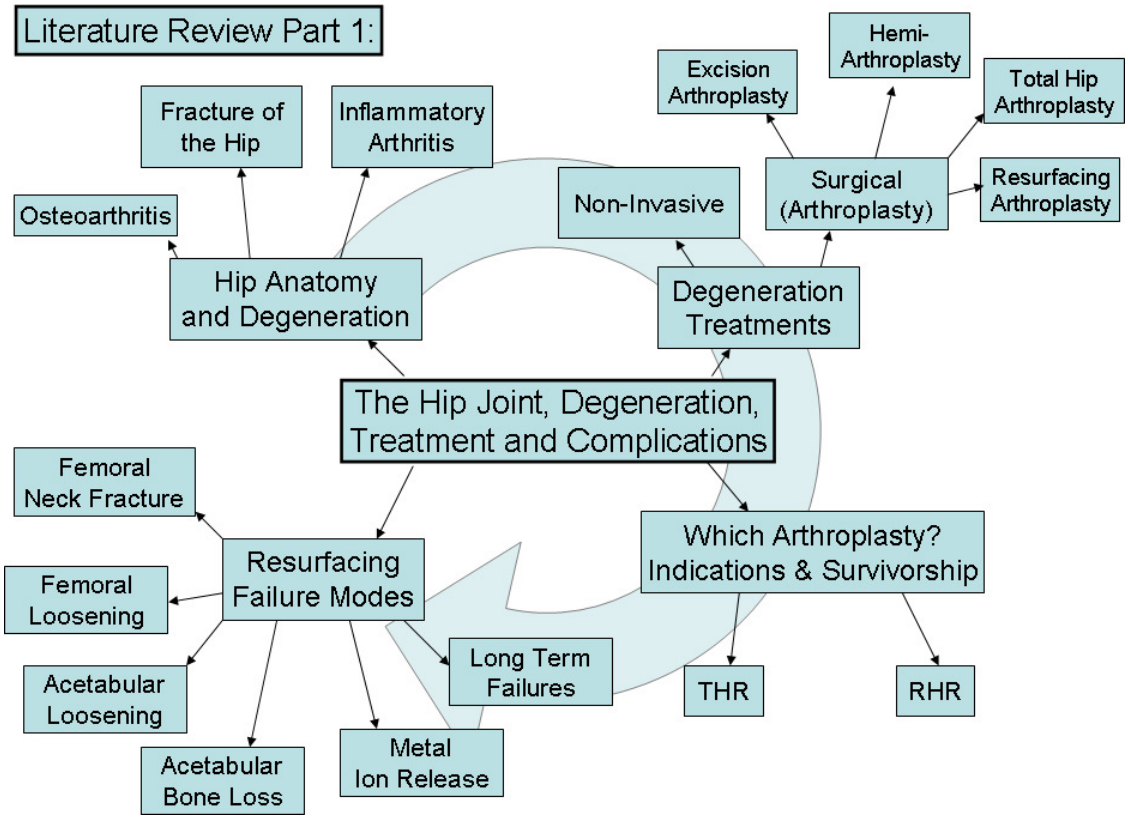

2.1.1 Joint Anatomy and Degeneration

The human hip consists of a ball and socket joint, as shown in Figure 2, capable of tri-axial articulation. The ball bearing is the femoral head, located at the proximal end of the femur, and the socket bearing is the acetabulum, located at the junction of the three pelvic bones [19].

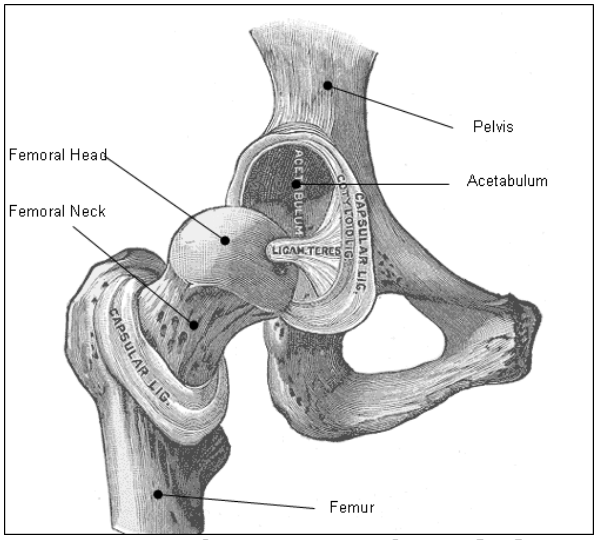

Figure 2: The Hip Joint Laid Open [19]

The hip is a synovial joint with a thin connective tissue called hyaline articular cartilage on each bearing surface, allowing low friction and wear articulation by deforming under load to give a large contact area and exuding lubricating synovial fluid, reducing the bearing surface stress. The joint is surrounded by a capsule consisting of two membranes. The outer fibrous membrane is a ligament structure which stabilises the joint, and the inner synovial membrane produces lubricating synovial fluid.

A main joint of the lower limb, the hips are involved in a very wide range of activities so their degradation can have a severe effect upon quality of life. The hip joint can be damaged by a number of diseases and injuries, the most common of which are described in the following sections.

Osteoarthritis (OA)

OA is the degradation of the articular cartilage and affects 5 million people in the UK, nearly 8% of the population [20], typically from 50-60 years. The cartilage structure is degraded by abrasion and adhesive wear, following damage in trauma or as a result of stiffening of the cartilage with ageing which reduces its effectiveness as a micro-elastohydrodynamic and lubricant exuding bearing surface [21]. This wear causes inflammation and can lead to disabling pain in the joint. The joint has very limited capacity to repair or regenerate damaged cartilage, so surgical intervention is often necessary to permit an OA sufferer to return to normal activity. All national joint replacement registers quote primary

osteoarthritis as the most common indication for hip replacement, accounting for approximately 75% of primary operations [22-25].

Fracture of the Hip

The second most common indication for hip replacement at approximately 12% of operations [22, 24] is fracture of the femur, specifically the femoral neck, in trauma or domestic injuries in the older patient who has lower bone quality as a result of conditions such as osteoporosis [26]. Avascular necrosis (AVN) of the femoral head can result from haematoma or displaced fracture healing because blood is supplied to the femoral head from arteries around the femoral neck. Once AVN occurs, the eventual consequence can be femoral head collapse, destroying the function of the joint.

Inflammatory Arthritis

A second major type of arthritic degeneration of joints is inflammatory arthritis, such as Rheumatoid Arthritis (RA), affecting approximately 1% of the global population [27]. It is an autoimmune attack against the synovium and articular tissue caused by aggressive tissue growth known as pannus, and causes swelling, pain and joint deformity. Inflammatory arthritis is responsible for approximately 4% of primary hip replacements [22-24].

Other Conditions

There are several other joint degeneration conditions listed as low incidence indications for hip replacement by the Swedish Register. These are femoral head necrosis (where the cause of the blood supply disruption is related to drugs, including steroids or alcohol, or is unknown), childhood disease causing deformity, imperfect joint alignment and loading, and loss of bone structure due to tumour excision.

2.1.2 Treatment of Joint Degeneration

Non-Invasive Treatments

A number of non-surgical treatments can be used to treat joint degeneration, particularly for arthritic disease, where the underlying bone structure is relatively healthy and disease is restricted to the joint's bearing surfaces. To reduce inflammation and pain, local hydrocortisone or anaesthetic injections, or systemic anti-inflammatory or analgesic drugs may be prescribed [28].

Surgical Treatments

In advanced cases of cartilage degeneration, or where the support bone structure has deteriorated (in the case of fracture, bone necrosis or deformity), surgical intervention may be necessary. In the case of RA a synovectomy may be performed to excise the inflamed joint lining. Where joint deformity limits function or causes abnormal cartilage wear, osteotomy is used, where a surgical fracture is created and re-set to the correct joint geometry. However, for all the listed indications, arthroplasty is a common treatment. Arthroplasty is defined as surgical repair of the joint articulation and has a number of forms, characterised by the amount of bone excised and the method of reconstruction of the articulation:

Excision Arthroplasty

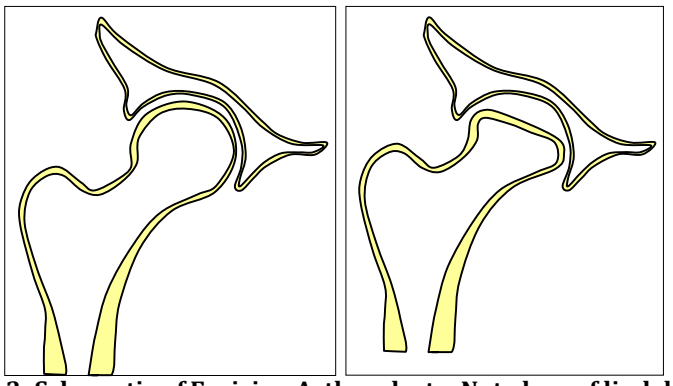

Figure 3: Schematic of Excision Arthroplasty. Note loss of limb length.

This involves simply the excision (cutting and removal) of the damaged tissue, following which articulation occurs between a fibrous pad which forms at the cut surfaces or with interposed tissue (Figure 3). This is commonly carried out in the thumb or toe, but clearly joint function will be limited, particularly in highly loaded joints such as the hip, so is used only in preference to arthrodesis (fusion).

Hemiarthroplasty

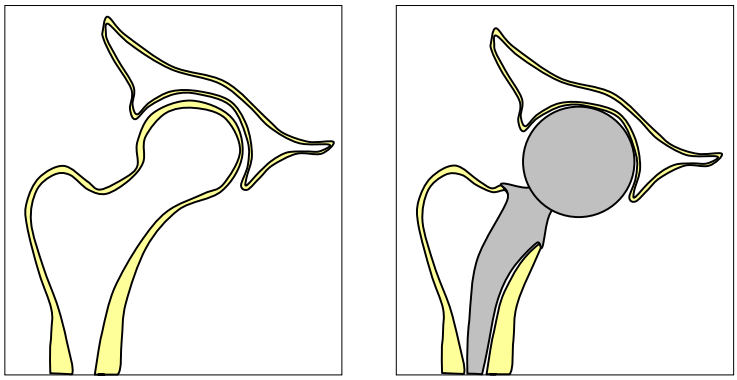

Figure 4: Schematic of Hemiarthroplasty

Hemiarthroplasty involves the replacement of one of the joint surfaces with an artificial bearing surface which articulates with the other, retained, natural joint surface. This is used in the hip when the surface of the femoral head is replaced with a large diameter metallic or ceramic ball mounted on a metal intermedullary stem and articulates with the acetabular cartilage. Hemiarthroplasty is indicated by advanced osteonecrosis [29], or femoral neck fracture when a healthy acetabular surface still exists.

Total Hip Arthroplasty

Total Hip Replacement (THR, Figure 5) involves reconstruction of both bearing surfaces of the joint. Traditional THR implants feature a ball and socket bearing couple, typically of smaller articulating diameter than the healthy joint, with the ball mounted on a metallic stem which fits in a reamed channel in the femur. The first successful examples were produced by Charnley [30], and by McKee and Watson-Farrar [31], shown in Figure 6.

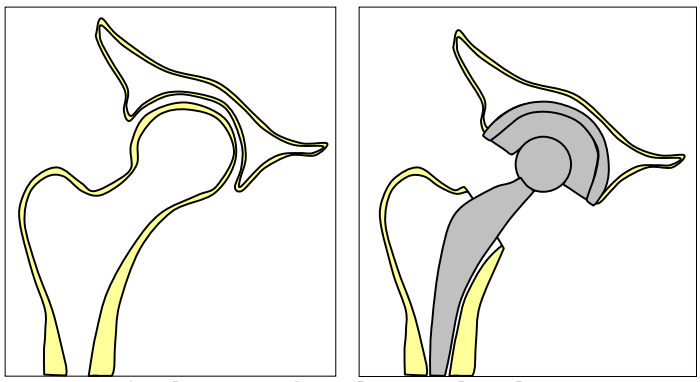

Figure 5: Schematic of Total Hip Arthroplasty

Figure 6: Charnley (Johnson & Johnson) and McKee-Farrar Total Hip Replacement Implants (Reproduced and adapted with permission and copyright © of the British Editorial Society of Bone and Joint Surgery) [31]

Resurfacing Hip Arthroplasty

Resurfacing Hip Replacement (RHR, Figure 7) replaces both bearing surfaces but is designed to conserve as much bone as possible. As explained earlier, OA is the most common single indicator for hip joint replacement, and as it affects only the contact surfaces, it is unnecessary to replace the whole joint so the bearing surfaces alone can be excised and replaced. Several clinical attempts at hip resurfacing were made between the 1960s and 1980s [30, 32-38], but the first widely successful RHR implant was the Birmingham Hip Resurfacing (BHR, Smith & Nephew), developed in the early 1990s and introduced in 1997 and accounting for up to 10% of hip arthroplasty procedures in certain markets [25, 39]

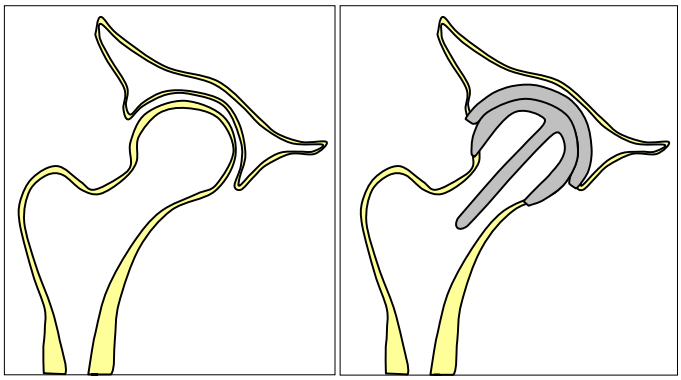

Figure 7: Schematic of Resurfacing Hip Arthroplasty

Figure 8: The Birmingham Hip Resurfacing (BHR) Implant [2]

2.1.3 Which Arthroplasty?

The choice of surgical treatment depends on the patient's indicating condition and their wider aetiology, with each type of arthroplasty suiting particular patient groups. Excision arthroplasty can be considered as a last resort when revision THR is impossible, and hemiarthroplasty has been shown clinically to be suitable only for young patients with high quality articular cartilage [40], who only represent a very small percentage of patients in comparison to those with osteoarthritic joint degeneration. Therefore, THR and RHR patient demographics are considered in detail.

Total Hip Replacement

Developed originally during the 1960s, modified, modular versions of Charnley's prosthesis continue to be the state of the art in THR surgery today. THR prostheses have particular benefits for patients with femoral neck fractures and AVN of the femoral head, as these regions of bone are replaced completely. THR benefits older patients with lower quality bone, because the implant features its own support structure for the bearing surfaces, in the form of the femoral stem. Furthermore, THR surgery is an established procedure which represents low risk to both patients and surgeons. National joint arthroplasty registers have produced excellent long term survivorship data for THR, stating survivorship of 73% at 25 years (Sweden [22]), 63% at 24 years (Finland [23]) 80% at 17 years (Norway [24]). More recently implanted prostheses show improved survivorship short-term, of approximately 95% at 10 years [22-24], illustrating improved implant technology and surgical technique.

Resurfacing Hip Replacement

If OA occurs in younger patients, it is likely that the patient would easily outlive current THR implants due to the patient's longer life expectancy, and the higher loading which they exert on their joints. Revision surgery would then be required, involving further bone removal, and since any remaining bone may be of lower quality due to age related osteoporosis or bone adaptation related resorption, the procedure would be more difficult, with less long term strength. As noted earlier, osteoarthritis affects only the bearing surfaces of the joint so further bone resection is unnecessary if the patient has sufficiently good quality bone to support a resurfacing implant. If the femoral head and neck are retained, femoral revision surgery is equivalent to a primary THR procedure, and the associated higher survivorship would be expected; this was the original concept of RHR surgery. Accordingly, NICE (the National Institute for Clinical Excellence) [41] recommends RHR surgery for patients below 65, and the main benefits include:

- lower wear compared to small bearing THR implants, particularly relevant to younger patients,
- bone conservation, facilitating revision surgery,
- retention of more natural geometry and operation of the joint [34], giving more natural load transfer and stress distribution, which reduces loosening associated with adverse bone adaptation and may reduce patient perception,
- reduced risk of dislocation of the joint, owing to the larger head diameter [42], and
- shorter postoperative recovery time.

The 2008 Australian National Joint Replacement Registry report [39] contained the most comprehensive RHR data at the time of writing, and reported that the cumulative revision percentage of all resurfacing and primary total hip replacement operations were 4.6% and 3.4% respectively at 7 years. Their data is plotted on Figure 9, which shows that the increased revision level for RHR implants arises largely from failures in the first post-operative year. Critically, their data indicates that survivorship is considerably higher in young patients than the elderly (3.6% at 7 years for patients under 55 years old, compared to 9.9% at only 5 years for patients over 75 years) in direct contrast to their THR data. Revision rates were even lower in male patients than females (2.9% revised at 7 years for males, compared to 6.5% for females at only 5 years).

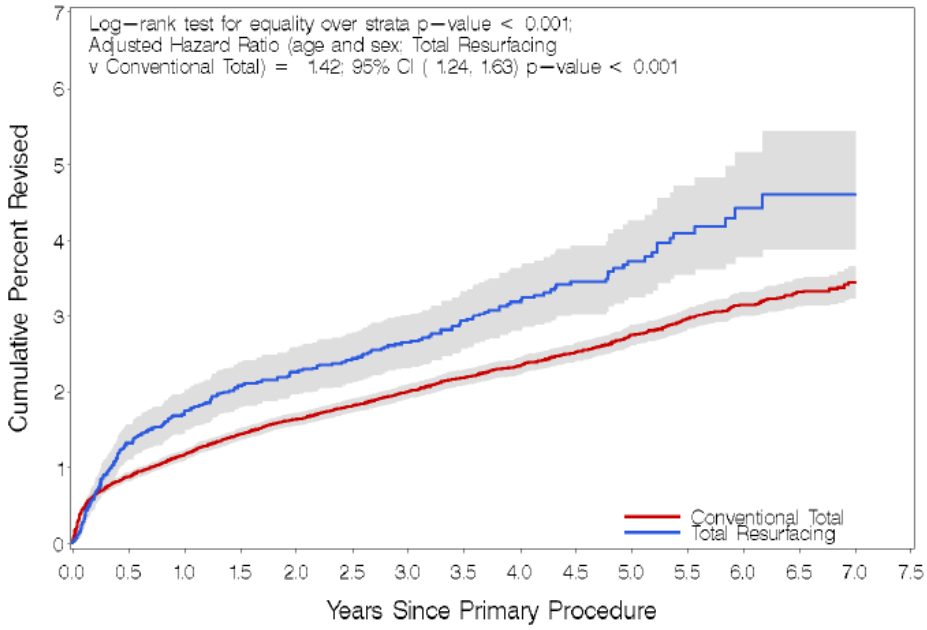

Figure 9: Cumulative Revision of Resurfacing and Total Hip Replacement Implants [39]

This generalised clinical data shows that excellent results can be achieved in the young, male patient group but some improvement is necessary for resurfacing surgery to become as successful as total hip replacement for as broad a group of candidate patients. The possible reasons for these trends in survivorship are discussed later with consideration of the causes for failure of RHR implants.

2.1.4 Failures in Resurfacing Hip Replacement

Thanks to modern design techniques, improved materials technology and stringent standard certification processes, it is unusual for failures of joint replacement implants to be caused by implant failure or gross wear. Instead, failures tend to occur in the supporting bone or at the interface between the implant and the bone. The main mechanical failure mechanisms seen in all hip replacements and those specific to resurfacing are shown in Figure 10, and described below.

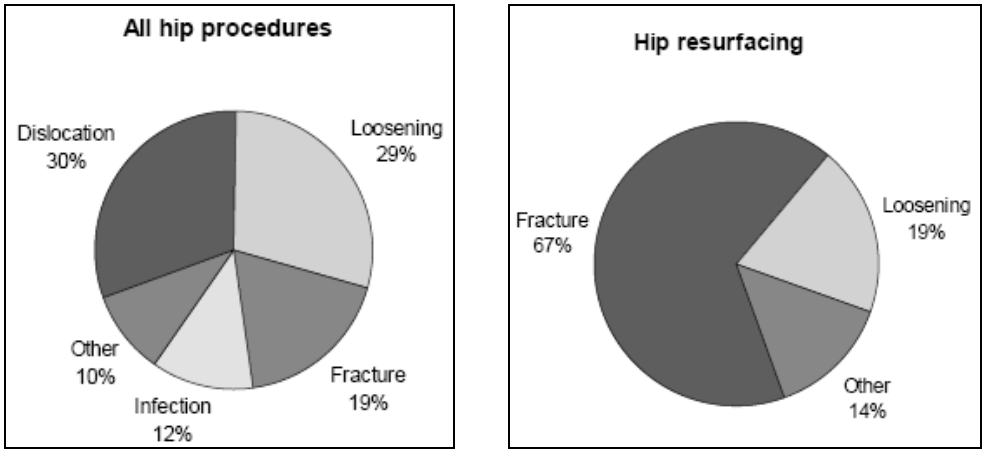

Figure 10: Reasons for Revision in All Hip Replacements and Specific to Resurfacing. Goldman Sachs and the Australian National Joint Replacement Registry (2004) [43, 44].

Femoral Neck Fracture

Early hip resurfacing implants featured cobalt chromium (CoCr) metal on high density polyethylene (HDPE) bearings, and studies by a number of groups [2, 6, 45-50] showed that since polyethylene cups were replaced with metal, the main early failure mechanism became femoral neck fracture, particularly within the first six months postoperatively. Surgical technique is responsible for a considerable proportion of these fractures, having weakened the femoral neck due either to:

- improper seating of the femoral head, leaving a ring of exposed reamed cancellous bone at the head-neck junction which is incapable of adequate load transfer [6],
- neck notching, where the lateral cortex of the femoral neck is grazed by the cylinder cutter during preparation of the femoral head [47, 50, 51],
- aggressive removal of osteophytes on the anterior cortex, again causing a stress concentrating notch [51], or
- excess varus positioning of the implant [10, 47, 52-54].

To avoid femoral neck fracture, 5-10° valgus implant alignment is recommended for safe implant-bone load transfer, thanks to theoretical, experimental and modelling studies [10, 15, 54]. Morlock et al [49] observed different modes of periprosthetic fracture, identifiable by morphology and the time post-operatively to occurrence. In 267 retrieval cases, they identified that 46% involved fracture originating at the rim of the femoral implant after an average of 99 days - probably linked to neck notching (Figure 11), incorrect implant alignment or incomplete seating (Figure 12). Later, with an average postoperative age of 262 days, another 20% of failures occurred inside the femoral head, which were

linked to necrosis due to microfractures from surgery or potentially thermal necrosis from bone cement polymerisation. The same group [48] found excessive cement penetration (greater than 5mm) into the cancellous bone inside the resurfacing head in 63% of the 55 early failure patients in their study. Thermal osteonecrosis could be a high possibility in such patients as a higher volume of bone cement in a thicker mantle has a higher peak polymerisation temperature [55]. The incidence of these failure modes could be reduced by improving surgical technique and instrumentation, and more careful application of bone cement, allowing more accurate femoral head preparation and full implant seating before cement polymerisation is too advanced.

Impaction in the surgical procedure may weaken the femoral neck by creating microfractures. This damage may also be initiated during femoral head preparation which exposes the neck to torsion loads, which it does not experience in normal activity. Moreover, two groups [56, 57] observed high incidence of neck fractures in patients with bilateral hip resurfacing. In addition to normally occurring bone microfractures, in the second operation the femoral neck in the contralateral hip may be damaged by impaction loads transmitted through the pelvis to the operating table. Improved surgical technique may solve this problem, either through reduction or removal of impaction loads, a patient position which stresses the contralateral hip less, or longer interoperative time.

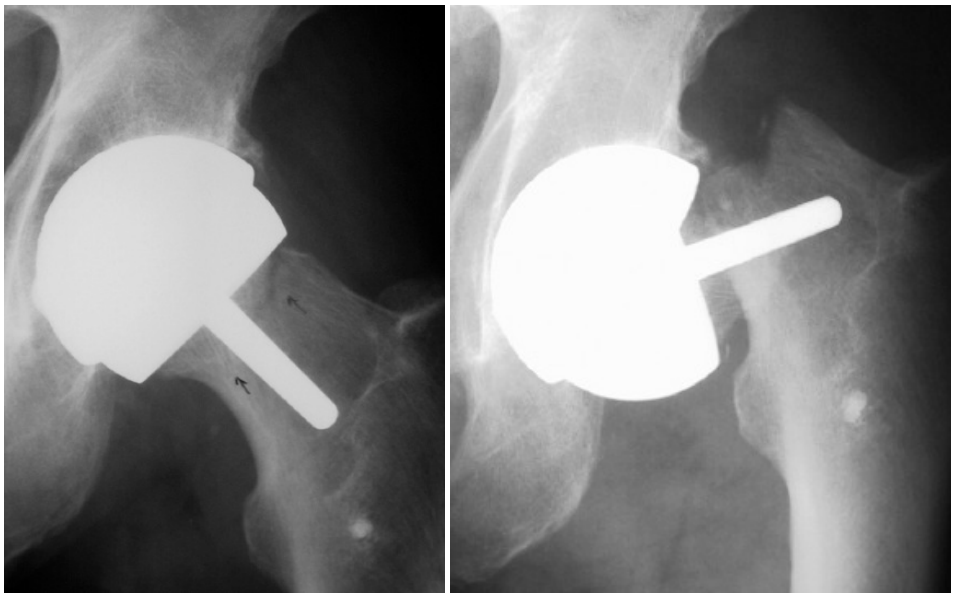

Figure 11: X-rays of a Resurfaced Hip with Notched Superior Femoral Neck and Initiated Fatigue Cracks (left) and after Fracture (right) [50]

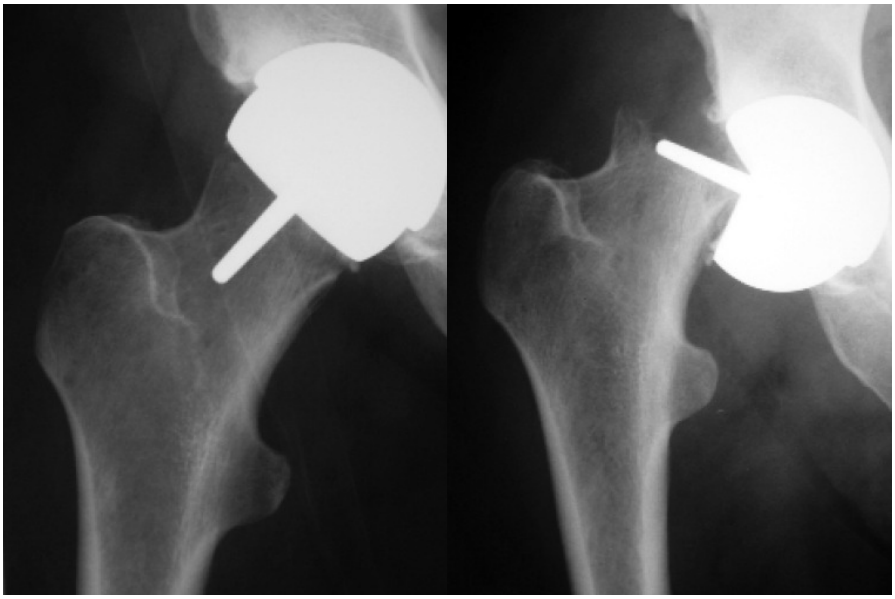

Figure 12: X-rays of a Resurfaced Hip with an Incompletely Seated Implant Postoperatively (left) and after Fracture (right) [58].

Another suggested significant cause for femoral neck fractures was secondary osteonecrosis. Two groups [46, 59] have presented histological samples from failed resurfacings with evidence of established osteonecrosis in all cases where the failure mode was femoral neck fracture, and where the femoral head blood supply had been undisturbed prior to surgery. It was suggested that the extent of 'vascular insult' in surgery due to mechanical and thermal injury determined whether or not a patient would develop osteonecrosis. Beaulé et al [60] note that bone resection, particularly around the postero-lateral femoral neck area, should be minimised to avoid avascular necrosis, as this region contains the Medial Femoral Circumflex Artery (MFCA), which is the main blood supply to the femoral head (Figure 13).

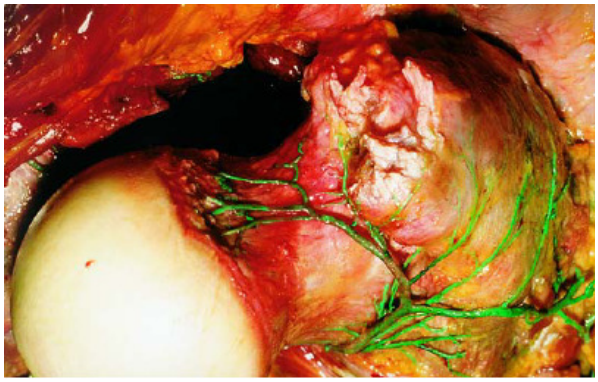

Figure 13: Photograph of the left Proximal Femur, showing the MFCA (Medial Femoral Circumflex Artery) and its perforation Reproduced and adapted with permission and copyright © of the British Editorial Society of Bone and Joint Surgery [61]

Steffen et al [62] showed that tissue oxygenation concentration in the femoral head fell by 62% on average during surgical approach and by 80% at the end of surgery, and was completely disrupted in 3 patients of 10. In other studies, Amarasekara et al [63] recorded four times the mean reduction in femoral head blood flow when the posterior approach was used, in comparison to the trochanteric flip approaches, and Steffen et al [64] showed that the antero-lateral approach only temporarily disrupted the blood supply whereas it had not recovered by the end of surgery using the posterior approach. It was accepted that the time required for the blood supply to recover following surgery was not recorded, so the clinical implication of these measurements was unknown, however in those patients where blood supply is more greatly disrupted, lasting bone damage is more likely.

In addition to the mainly surgery-related factors, patient factors are believed to contribute to femoral neck fracture. A possible cause for femoral neck fracture is inadequate support from the host bone arising from insufficient bone quality preoperatively due, for example, to osteoporosis or femoral head cysts. More than one group [47, 65] have identified a significantly higher risk for the older, overweight female patient, and Amstutz et al [6] identified cystic degeneration as a contributory factor in early neck fractures. Shimmin et al also reviewed the influence of prosthesis size on failure [66], and identified increased risks of femoral neck notching and cement over-penetration in smaller patients. As such, it is clear that patient selection is one of the most critical aspects of resurfacing surgery.

Femoral Osteolysis

Medium term failures by femoral implant loosening or femoral neck fracture have been identified [2, 46, 47, 67], caused by gradual support bone degeneration. Radiographically visible signs of degeneration, such as femoral neck narrowing, have been studied widely [3, 42, 45, 68-72]. A typical case is shown in Figure 14 with a radiographic measurement technique, although more pronounced narrowing tends to precede failure. It is of most concern in the tensile-loaded superior femoral neck, and the favoured explanations are stress shielding and blood supply disruption, although the precise mechanism is unclear. These studies suggest alternative or additional causes including impingement on the rim of a poorly aligned acetabular cup, and the action of macrophages in an inflammatory osteolytic reaction to wear particles.

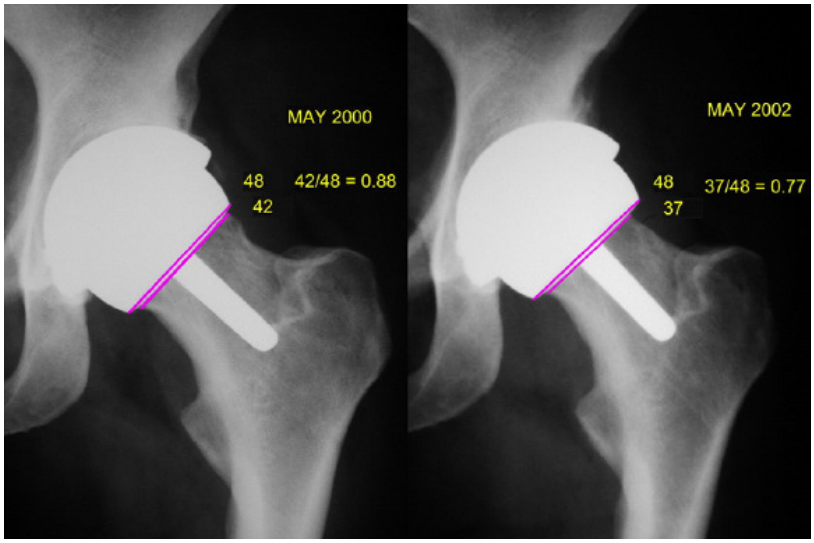

Figure 14: X-ray evidence of Femoral Neck Narrowing after 2 years [72]

The cited studies have identified varying degrees of femoral neck narrowing and an incidence of radiographically measurable narrowing in up to 90% of patients [3, 42, 45, 68, 70, 72], with particularly high incidence in joints which failed due to femoral loosening [68]. Hing et al's study [3] was the most comprehensive, considering various risk factors and monitoring progression over 5 years. Female gender and valgus neck-shaft angle were identified as statistically significant risk factors, and valgus implant alignment and smaller implant sizes were potential risk factors without statistical significance. Again, no link to clinical failure was identified in this shorter term study, and narrowing was seen to stabilise with no significant change seen between radiographs taken at three and five years. This was corroborated by Spencer et al [72] who saw stabilisation after 2 years, with up to 7 years follow-up. Finally, Katrana et al [70] identified a significantly higher incidence of neck narrowing in patients with cementless implants compared to cemented femoral heads, although this could be design- as well as fixation-related.

As femoral neck fracture tends to occur early, there is insufficient time for this remodelling to occur and no link between early fracture and neck narrowing has been drawn. However, femoral aseptic loosening must be of concern for these patients, and late femoral neck fracture, particularly in the event of trauma or later bone quality reduction due to osteoporosis, could also become a risk. Recently, longer term, progressive failures by femoral aseptic loosening and head collapse have become apparent [69, 71, 73], shown in Figure 15.

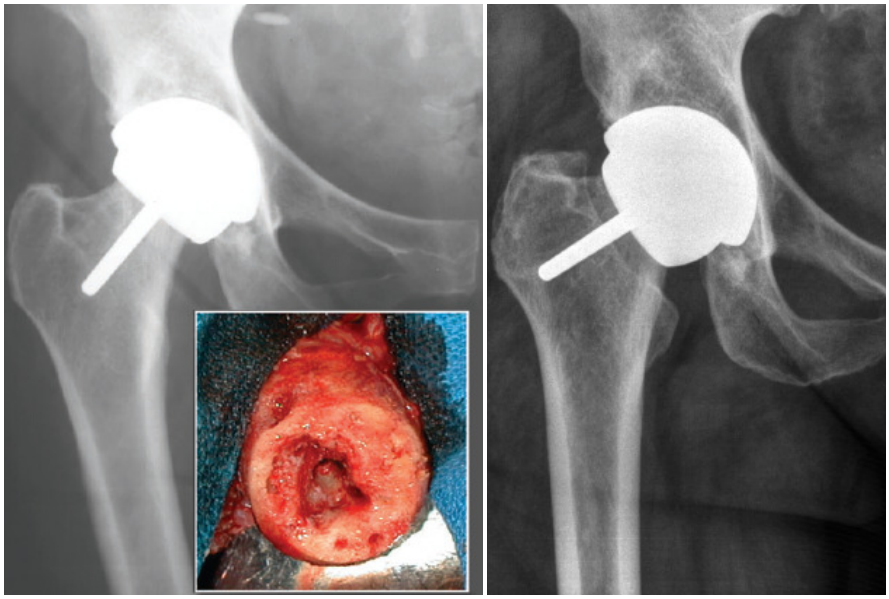

Figure 15: X-Ray Evidence of Femoral Head Subsidence, Varus Shift and Loosening from 1 (left) to 5 (right) years, and the Femoral Head showing Cystic Degeneration (Inset) [73]

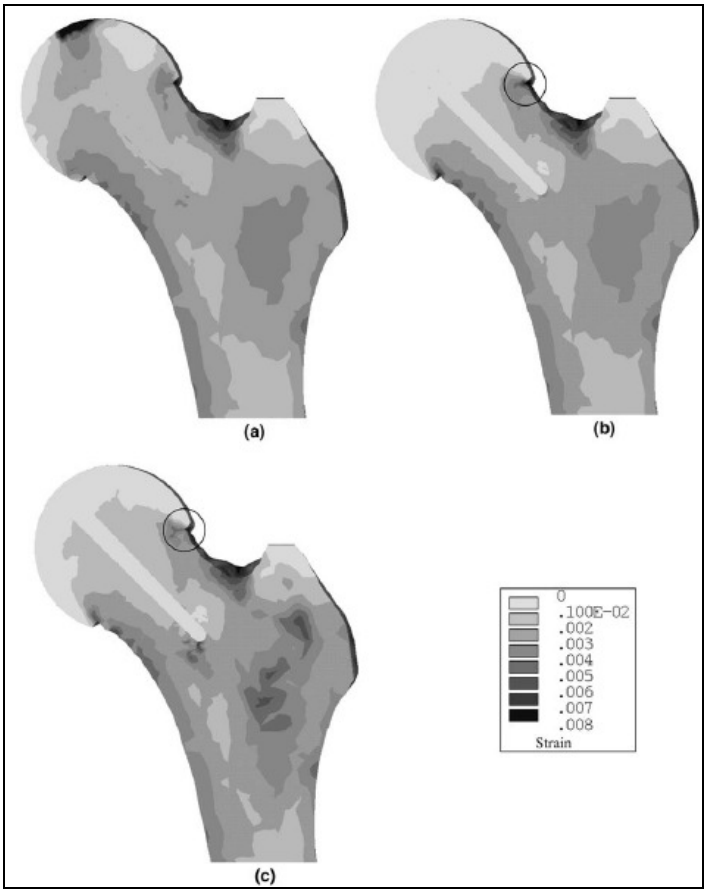

Figure 16: Proximal Femur Strain Distribution (a) Preoperatively, (b) Immediately Postoperatively and (c) after Remodelling. Ringed is a Strain Concentration in the Superio-lateral Neck Cortex, relieved by Remodelling [13].

Dual Energy X-ray Absorptiometry (DEXA) studies [74-77] have showed increased Bone Mineral Density (BMD) in the medial femoral neck, and on the lateral side immediately below the implant-bone junction following an initial BMD drop. This is consistent with finite element (FE) computational simulations by Watanabe et al [9], Taylor [12], Ong et al [14] and Gupta et al [13], which predict increased strain here, and initially appears inconsistent with neck narrowing. Indeed, Gupta's results (Figure 16) show that this strain concentration could be relieved by a remodelled increase in bone density, the opposite of stress shielding. However, the DEXA data considers the whole femoral neck bone region rather than just the surface, where the resorption occurs. In order for the implant to remain stable, a net increase in BMD across the whole neck would be required to counteract a reduction in bone volume on its surface. Conversely, implant loosening would be consistent with bone density loss inside the femoral head, as predicted by these FE analyses but which cannot be visualised *in-vivo* by X-ray, CT or DEXA studies as the radiopaque implant material obscures the interior bone. However, this effect has been identified in retrieved resurfaced femoral heads [78, 79], as shown in Figure 17.

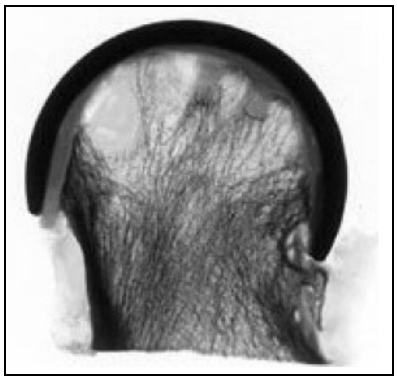

Figure 17: X-ray of a Femoral Head Section showing Resorption [78]

Alternatively, if the neck cortex stress concentration leads to microfractures under stumbling loads or impingement with the cup rim, damage at the head-neck junction may also contribute to neck narrowing. Simple tests have shown that the range of motion (ROM) of resurfaced hips is actually lower than that of THR hips [80, 81], although the ROM is still sufficient for normal activities. However, in cases of poor implant position impingement is more likely to occur in normal use, potentially leading to bone damage at the head-neck junction. Microfractures at this stress concentration would reduce the local stiffness, potentially redirecting the load path to the implant's metaphyseal stem and the medial neck cortex, which would bypass the lateral femoral neck cortex and could cause bone resorption. This would be particularly marked in patients who have experienced trauma, have poor bone quality or an

excessively low cup inclination or anteversion and therefore superior neck impingement, but trabecular densification around the stem and in the medial neck are in fact common radiographic observations [4, 74, 75, 82].

Pollard et al [4] reported 'pedestal' signs of densification around the stem tip in 60% of RHR patients, of which 50-55% showed further densification of the medial cortex. This is illustrated in Figure 18 [14] which shows the formation of a neo-cortex around the tip of a BHR stem, indicating positive bone remodelling. However, failure still occurred as stem break-out, probably due to some traumatic event or strain overload despite the remodelling. Beaulé at al [68] noticed radiolucency in this region in 3 of the 10 patients who displayed neck narrowing in their study, also suggesting migration or stem break-out. This is open to argument however: radiolucency could indicate either an interfacial gap due to prosthesis migration after overload and failure, or bone resorption due to stress shielding. Contrary to Beaulé's observations, McMinn [42] saw no correlation between neck narrowing and femoral radiolucencies.

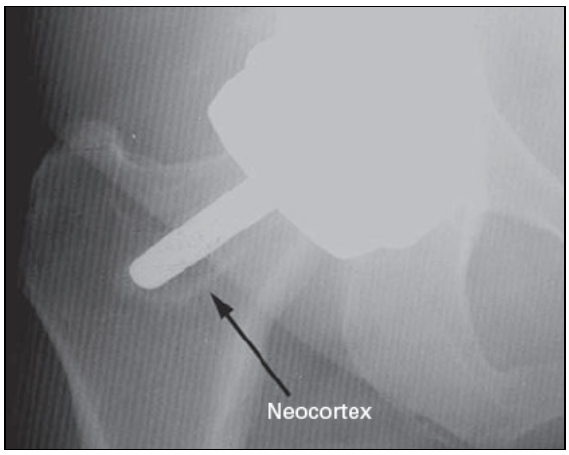

Figure 18: Evidence of Neo-cortex in Femoral Stem Bore (Radiopacity) and Stem Break-Out (Radiolucency) around a BHR Implant Reproduced and adapted with permission and copyright © of the British Editorial Society of Bone and Joint Surgery [14]

Acetabular Osteolysis

The most common failure mode of all THR implants and early RHR implants is aseptic loosening. This was responsible for 60% of THR revisions on the Swedish Hip Register since 1979 [22] and approximately 70% of revisions in a number of studies of early Metal-Polyethylene (MPE) resurfacing implants summarised by Thompson [83]. Charnley [84] observed in a clinical study and later Schmalzreid et al [85] showed through histological analysis of autopsy specimens that the major cause

of aseptic loosening was osteolysis- a biological immune response, not a mechanical effect- which can occur when particles are generated by wear at the joint bearing surfaces. The particles diffuse into the bone-implant interface region and activate macrophages which attempt to destroy them. The enzymes they release also damage surrounding tissue, weakening the implant-bone fixation and leading to loosening (observed as a change of the cup angle) and potentially migration of the cup (observed as it subsides superiorly into the pelvis), where the bone ceases to support it properly. This causes inflammation and pain, and ultimately affects the joint geometry and motion range.

Since the removal of polyethylene from resurfacing hip replacements, the incidence of osteolysis has been reduced dramatically [2], because the wear volumes from MoM bearings are up to two orders of magnitude smaller than for M-PE implants [86, 87], and the particles have lower osteolytic potential due to their smaller size [88-92]. However, wear particle osteolytic potential is cumulative, so osteolysis may still occur in very high wear MoM bearings [93]. Known as metallosis, in these cases sufficient metal debris is present that the periprosthetic tissues are stained black. Metal wear particles are smaller, so the specific surface area of wear particles is still considerable despite the lower overall volumetric wear of MoM bearings [88], and this is reported to be the controlling factor in wear-induced osteolysis [94, 95]. Excessive metal bearing wear may occur due to excessive cup inclination [49, 71, 95], where the bearing wear patch reaches the cup rim on bedding-in wear and the generation of lubricating fluid-film is disrupted, so a steady state of low wear is never reached.

Wear particles may not be the sole cause of osteolysis. It has also been identified in the presence of inflammatory markers in the joint fluid, particularly where the fluid has direct access to a cut bone surface [96], as may occur in cases of incomplete implant seating or incorrect alignment. However, these cases are rare and may be linked to preoperative inflammation or poor surgical technique, and the bulk of the evidence shows that osteolysis is only responsible for a minority of failures in hip resurfacing in the absence of implant malpositioning [45, 50]. The implication is that wear particle induced osteolysis may have been solved by the removal of polyethylene bearings, provided that the alignment of the MoM bearing is sufficiently accurate that excessive wear does not occur.

Metal Ion Release

Although wear-induced osteolysis has been largely mitigated through the use of metal-on-metal bearings, the main wear-related concern now relates to the effects of ion release due to corrosion of wear particles in an aggressive bio-environment [97]. Research continues into the effects of metal ions, particularly shortly post surgery when ion release levels are high due to the reduced pH associated with inflammation increasing corrosion and a 'running-in' effect increasing wear [98].

Increased cobalt and chromium ion levels have been detected in patients with MoM bearings compared to those with MPE or CoC implants, and the general population [99-105], and significantly higher levels are measured in patients with larger diameter RHR patients compared to small diameter THRs [106]. Possible effects are both local and systemic, because wear particles are present in the periprosthetic tissue but their ionic corrosion products attach to erythrocytes (red blood cells) which transport them around the entire body [107]. Metal ions have been located in local bone marrow, distant lymph nodes, the liver and spleen, and necrosis and fibrosis in the lymph nodes have been observed using optical and electron microscopy. Effects are pronounced in loose, fretting implants or those with high bearing wear [108]. Suggested effects of metal particles and ions are:

- *Cytotoxicity and Metallosis:* where macrophagic response to wear particles causes pain and inflammation, causing cell death and tissue necrosis [92, 109]. This is observed in patients with poorly oriented implants which demonstrate high wear, which is responsible for the large wear particle volume.
- *Hypersensitivity (ALVAL):* without excessive wear particle levels, an inflammatory response can occur which is activated by lymphocytes, and only subsides on revision to a Cobalt and Chromium-free prosthesis [110]. This is termed ALVAL (aseptic lymphocyte-dominated vasculitis-associated lesions) and symptoms are pain, effusion and occasionally osteolysis. It is hard to diagnose and dermal screening tests are unreliable [111] but is estimated to have normal incidence of up to 1% [112, 113], and around 60% in patients with a failing implant [111].
- *Pseudotumour:* presenting similarly to ALVAL but containing aseptic, benign, cystic or solid soft tissue masses, so called 'pseudotumours' have been found after approximately 5 years follow-up [5, 71]. Again, the incidence is estimated at 1% [5] and may be more common in cases of poor implant alignment.
- *Carcinogenicity and Mutagenicity:* there is concern that in the long term, cobalt and chromium ions may cause an increased risk of some cancers, specifically haematopoietic cancers and leukaemia. Visuri et al [114] examined all the epidemiological data available to quantify the relative cancer risk

to MoM hip arthroplasty patients and concluded that despite a relative leukaemia risk of 3.77 for MoM compared to M-PE patients, with reductions in the risk of stomach, colon and rectum cancer, the overall risk of all cancers compared to the general population was 0.95 (95% CI 0.8-1.1), or essentially unchanged. Indeed, hip replacement gives increased life expectancy over the general population (standardised mortality ratio 0.94). Longer term study is necessary to identify whether cancer incidence shows latency. The effects of tobacco and asbestos can be latent for several decades [115].

- *Teratogenicity:* some concerns exist regarding the risk of congenital malformations in children of resurfacing patients. This cannot be tested ethically, but is studied in case reports [116, 117]. There have never been any reported cases of birth defects, although contradictory evidence has been collected of the transmission of metal ions across the placenta. Healthcare guidance suggests that patients of childbearing age should be educated regarding teratogenic risks, be offered alternative (e.g. ceramic) bearing implants, or aim not to conceive before the end of the bedding-in wear phase.

Long Term Failure – Friction and Wear?

Although there is limited evidence for hip resurfacings beyond approximately 10 or 11 years, early metal on metal hip replacements have survived for more than twenty years [2, 118, 119]. When this review was conducted, only one study by Tuke et al [120] was found in the literature which attempted to predict long term failures of MoM hip resurfacings, through modelling validated by a retrieval analysis. They proposed a third stage in the wear life, at 'end point' where the bearing friction rises as the contact patch grows to reach approximately 75% of the bearing surface. High friction was identified as the cause of late aseptic loosening, at up to twenty years in their study. However, by avoiding all these failure modes, outstanding performance can be achieved: the final retrieved implant studied survived to thirty four years, and was revised for stem fracture.

2.1.5 Failure Modes- Summary and Scope for Improvement

- The two main mechanical failure modes of current femoral resurfacing prostheses are femoral neck fracture, and aseptic loosening through remodelling of the support bone. It is accepted that these failures may be linked to a number of additional, surgery and patient related causes, but the role of implant design is considerable.
- There are a range of concerns and actual risks associated with the metal ions released by MoM bearing wear particles. The incidence of some risks may be reduced by ensuring low implant wear through correct alignment, but to answer all of the concerns, an alternative, metal free implant material could be employed.
- Should all shorter term risks be avoided, long term failures are probably wear-related so again, use of a lower wear bearing material would prolong implant life.
- Acetabular failures are likely to be related to surgical technique, in terms of poor alignment leading to excessive wear and metallosis or osteolysis, or excessive bone resection. There appears to be limited necessity for improvement of structural design of the metal acetabular cup, but there may be scope for development of cups using alternative bearing materials including structural bioceramics or advanced polymers, to reduce wear related effects or cup thickness and bone resection.
- Patient selection is also critical to ensure that bone quality is sufficient to support the implant, and that bone geometry allows optimal implant alignment (low cup inclination and valgus femoral head alignment). A large head-neck diameter ratio may also be ideal, so that a small femoral head and therefore small acetabular cup can be used, conserving acetabular bone which aids revision.

Having identified the scope for improvement of resurfacing hip replacement prostheses, with particular focus on prosthesis mechanical design and the use of alternative structural biomaterials, it is necessary to understand the biomechanics of the hip joint and the materials involved, particularly the bone structure of the hip and its mechanical behaviour. This is discussed in the second half of the literature review.

2.2 Part 2: Biomechanics of the Hip Joint, and Computational Modelling

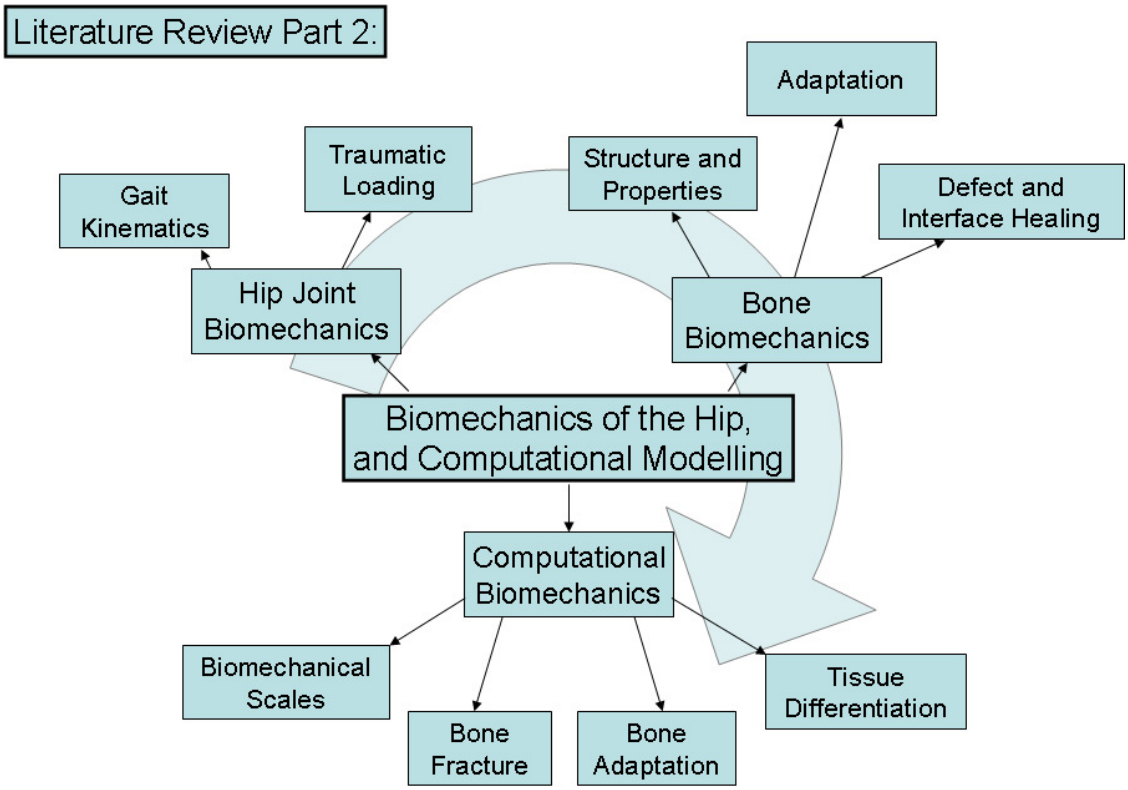

2.2.1 Macro-Scale Biomechanics of the Hip Joint

In order to design prostheses for replacement of the hip joint, the forces exerted upon it must be understood, and these are related to activity and the joint's range of motion. The hip may also be loaded abnormally, as a result of trauma. This section will review the loads which a hip prosthesis and the supporting bone must sustain.

2.2.1.1 Normal Gait Kinematics

The hip is capable of articulation in flexion-extension, abduction-adduction, and internal-external rotation (Figure 19). Figure 20 shows the range of these motions which are required for normal gait, from electro-goniometric measurements [121].

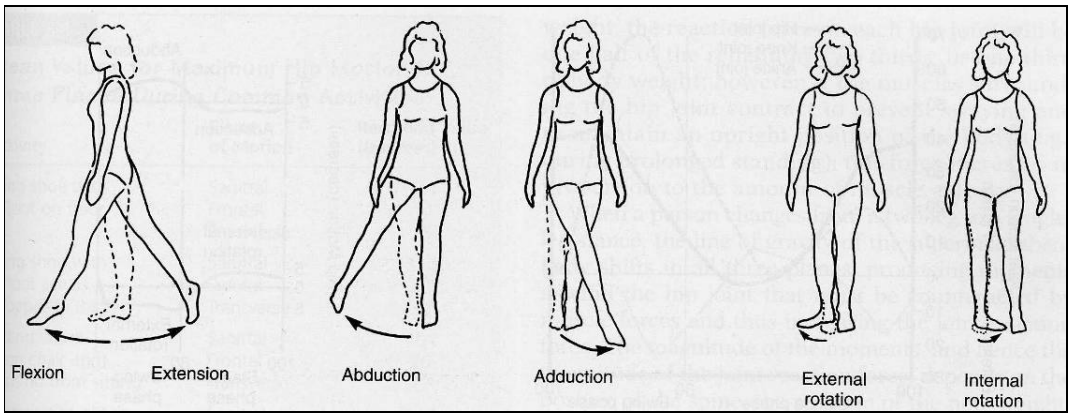

Figure 19: Degrees of Freedom of the Hip Joint [121]

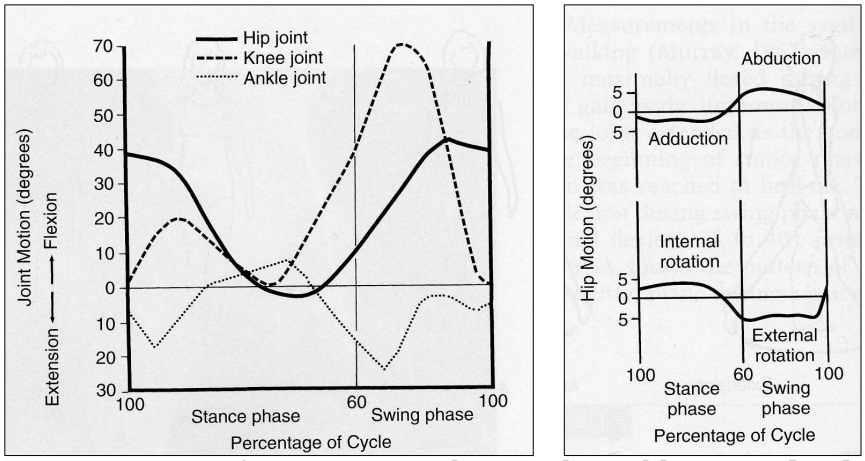

Figure 20: Range of Motion in Normal Gait, and a Healthy Patient [121]

Table 1: Extreme Ranges of Motion Required for Normal Activities [122]

Motion	Range /°	Activity
Flexion – Extension	124	Tying Shoe with Foot on Floor
Abduction – Adduction	28	Squatting
Internal - External Rotation	33	Tying Shoe with Foot across Opposite Thigh

Although this shows that normal gait requires approximately 45° of Flexion-Extension and 10° of Abduction-Adduction and Rotation, additional motion is required for other day-to-day activities. Data for activities requiring more extreme ranges of motion is included in Table 1.

The bearing contact force across the hip joint - the Joint Contact Force (JCF) - arises from the dynamic load of the body weight and additional muscle forces which stabilise the joint. These may be predicted by inverse dynamics as explained in a summary of work by Paul in 1976 [123], whereby estimates of reaction forces and moments at the lower limb joints are calculated using filmed kinematic data and ground reaction force measurements from a load cell, obtained in a gait lab. The most cited work in this area was conducted by Bergmann et al [124, 125] who also inferred joint contact forces from total hip replacement prostheses instrumented with strain gauges. Although inter-patient variation is high, and absolute values are limited in accuracy as a result of experimental uncertainty and small patient cohorts, there are clear trends in joint contact force data. Bergman et al's data in Figure 21 [125] shows that joint contact forces are cyclic, with the resultant force showing two peaks- one at the heel strike, and another immediately before toe lift-off.

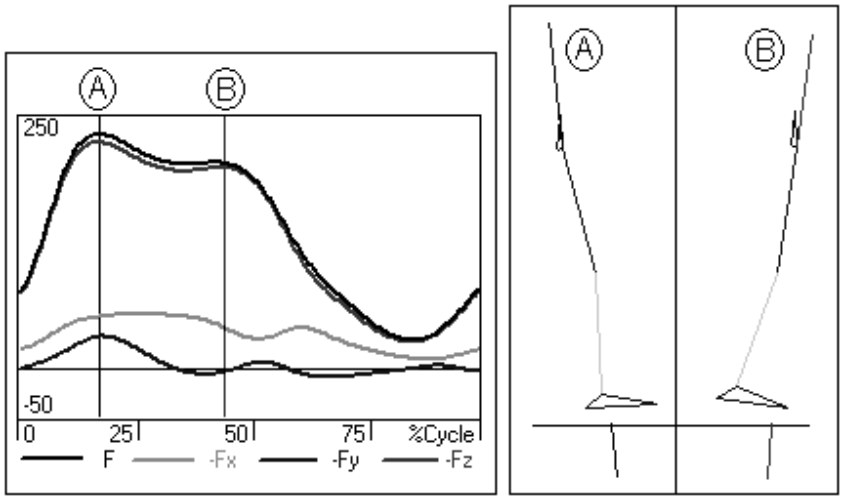

Figure 21: Joint Contact Force Data from Bergmann et al [125], with Peaks at Heel Strike (A) and Toe-Off (B) marked.

Table 2: Typical Peak Joint Contact Forces and Directions for Normal Activities and Experimentally Determined Fracture Load Ranges in Traumatic Events [124-130]

Activity	Peak Joint Contact Force	Angle in Frontal Plane	Angle in Sagittal Plane
Normal Walking	238 %BW	13.4°	8.2°
Stair Ascent	251 %BW	13.8°	14.5°
Stair Descent	260 %BW	13.1°	7.7°
Standing Up	190 %BW	15.9°	4.9°
Stumbling	3-16kN	8°	0°
Falling	0.6-4.6kN	120° (See Figure 25.)	60° to Neck (See Figure 25)

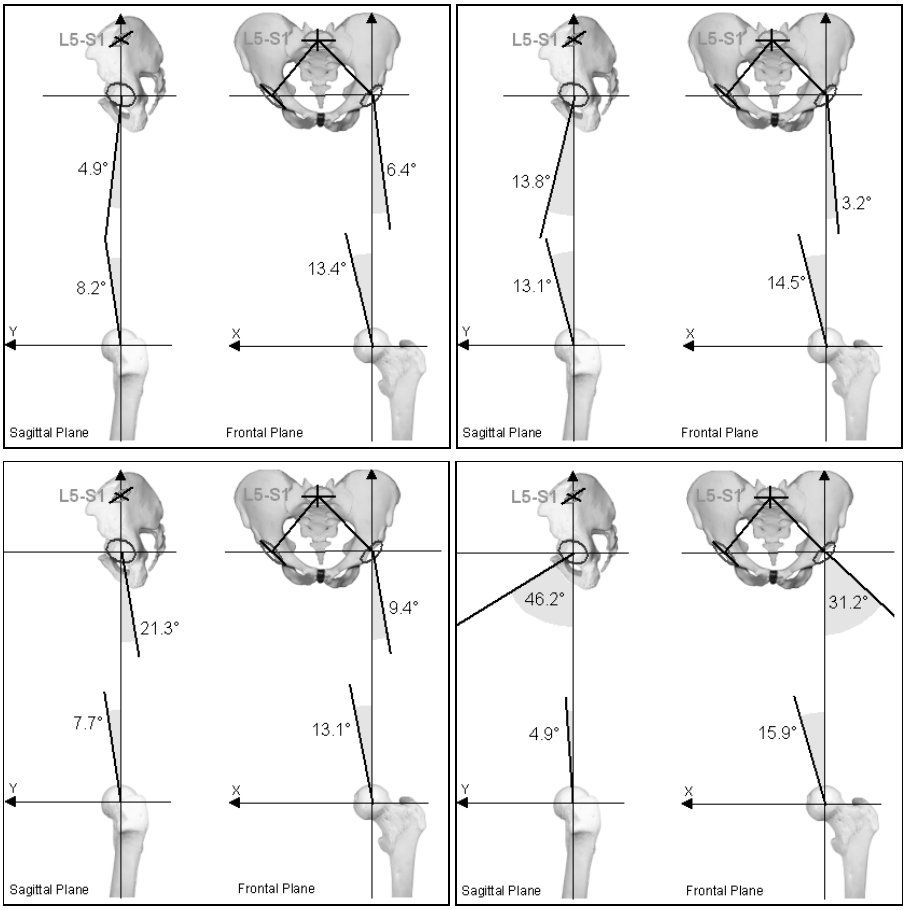

Figure 22: Peak JCF Directions in the Femur and Pelvis CS for (clockwise from top left) Gait, Stair Ascent, Stair Descent and Standing Up Load Cases. Modified from Bergmann et al [125]

Typical peak joint contact forces were reported in Bergman et al's 2001 study [125]. They recommended that implant testing should consider walking and stair climbing, the highest magnitude normal activities, although there are other activities which exert lower magnitude forces on the joint at more extreme angles, such as rising from seated and squatting. Average forces and their directions measured across the cohort of patients are given in Table 2 and illustrated in Figure 22. These were calculated for the femur and pelvis coordinate systems (CS), by finding the direction of the joint contact force using its x, y and z components in the lab coordinate system, and subtracting the femoral flexion, extension and rotation angles and the pelvic anterior/posterior and left/right tilt respectively.

2.2.1.2 Traumatic Joint Loading

Table 2 includes traumatic loading data from an earlier study by Bergmann et al [124], which reported loads in a similar direction but of much higher magnitude, resulting from an accidental stumble. Cristofolini et al [126] investigated spontaneous fractures using a combination of mechanical testing of cadaveric bones and FE analysis. They found that the worst-case stance loading scenario leading to spontaneous fracture occurred with loading on the femoral head at 8° to the femoral shaft. The mechanical test set-up for this scenario is shown in Figure 23.

In addition to stumbling, falling is a common, more severe traumatic event in the elderly. To identify high risk patients for femoral neck fracture, several groups [129, 131-133] have investigated the loads arising from a fall on the hip. They used loading occurring from an 'oblique fall backwards and to the side' in their early cadaveric femoral neck fracture studies [129, 131], and a mechanical test set-up representing this scenario is shown in Figure 25. Both groups replicated their tests with finite element models [134]. Most recently, instead of modelling an isolated femur under quasi-static loading conditions, Majumder et al [127, 135] produced a dynamic FE analysis model of the full torso under impact loading, including soft tissue structures and plastically deformable bone materials properties, to understand better the contact loads sustained under sideways falling. Whilst it may be a considerable task to reproduce their explicit FE model, their results may be used as more representative boundary conditions for the standard, isolated femur models. In this case, they found that a peak load of 8.3kN (or approximately 1100% Bodyweight) resulted at the joint contact zone, with the impact lasting

approximately 50ms (Figure 24) for an average speed fall, and extrapolated their data for a range of fall velocity and soft tissue thickness values.

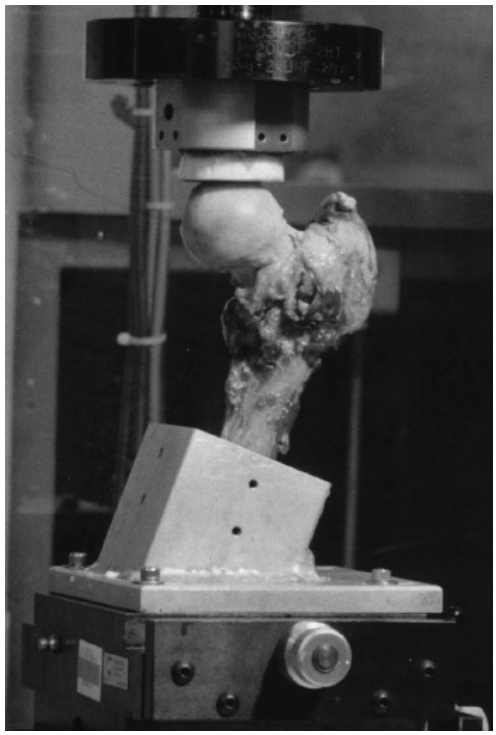

Figure 23: Mechanical Test Conditions Representing Normal Service Loading [129]

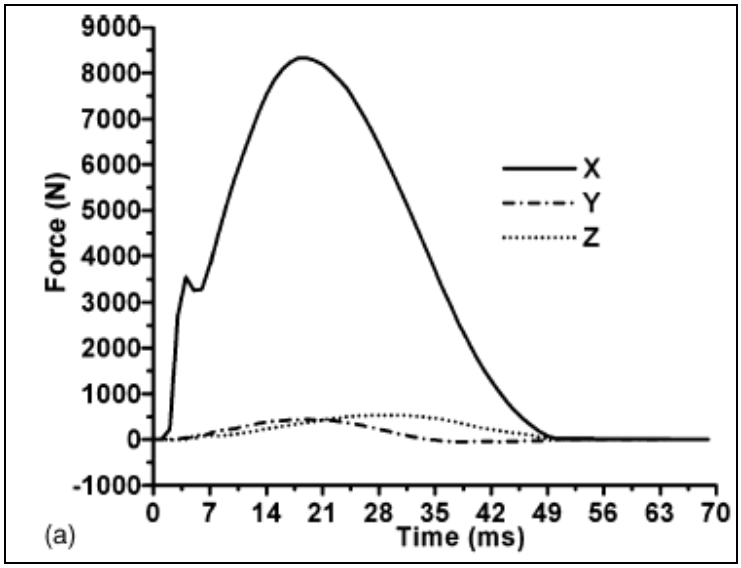

Figure 24:Simulated Impact Force-Time History in an Oblique Fall on the Hip [127]

Considering ramp loading as opposed to impact, typical experimental values for femoral neck fracture strength range from 0.6–4.6 kN (under loading from oblique falling [129]) to 3–16 kN (under

stance loading [128-130]). It is likely that the strength of an implant will exceed this range of loads, particularly if it is designed to pass US FDA (Food and Drug Administration) acceptance criteria [136]. Failure of an implant is most likely to occur if it is poorly aligned, resulting in rim loading following impingement or partial subluxation [137]. Also, an implanted bone may be further weakened by a misaligned implant than it would be with ideal surgical technique (Section 2.1.4). Therefore, to account for the envelope of possible *in-vivo* conditions, the following studies should be undertaken:

- prediction of bone failure and remodelling stimulus under gait and stance loading conditions,
- prediction of bone failure under traumatic loading conditions, and
- prediction of implant failure under extreme loading from trauma or incorrect alignment.

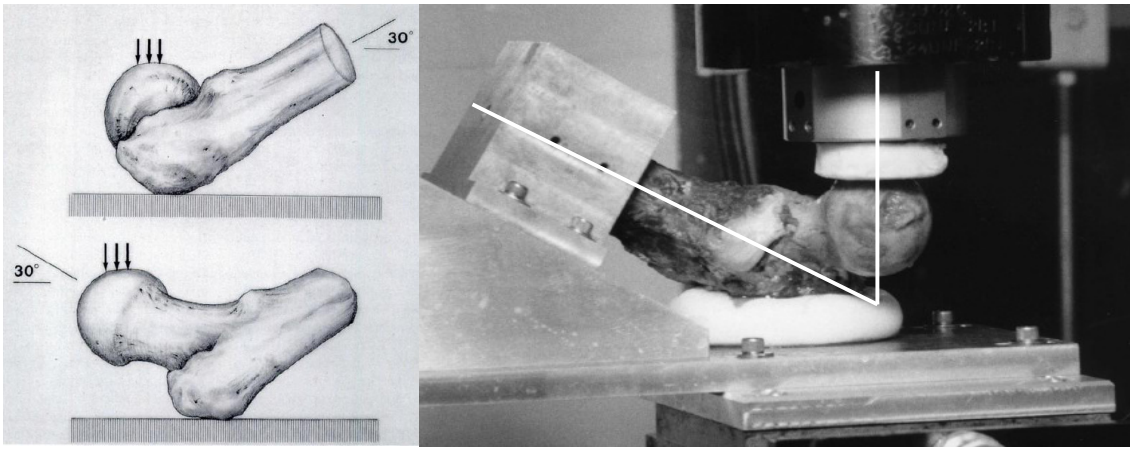

Figure 25: Mechanical Test Conditions representing Trauma- an Oblique Fall – Schematic (left) and Photo of Experimental Set-Up (right) [129, 131]

2.2.2 Micro-Scale Biomechanics of Bone and Implant-Bone Interfaces

When a prosthetic joint is being designed and analysed, the behaviour of the supporting bone must be understood. This section considers the structure and mechanical properties of bone, its modes of failure, adaptation to changes in loading and damage repair mechanisms. Prosthesis-bone interface biomechanics is also discussed briefly. This will allow the processes of bone fracture, remodelling, gap filling and prosthesis loosening to be understood.

Structure of Bone

Bone contains two different macroscopic structures, which evolve in response to the loads it experiences. Figure 26 shows the typical structure of a long bone, such as the femur, tibia or fibular. This consists of a hard outer shell of 'compact' or 'cortical' bone of lamellar structure, and inner regions of cellular 'spongy' or 'cancellous' bone with an open porous cellular structure of rod like trabeculae. The dense cortical structure constitutes the majority of the bone structure in the body, supporting tensile and compressive stresses and allowing attachment of ligaments and tendons for muscle loading. Highly vascular cancellous bone structures are located at the epiphyses of long bones and inside vertebrae, and support compressive loads.

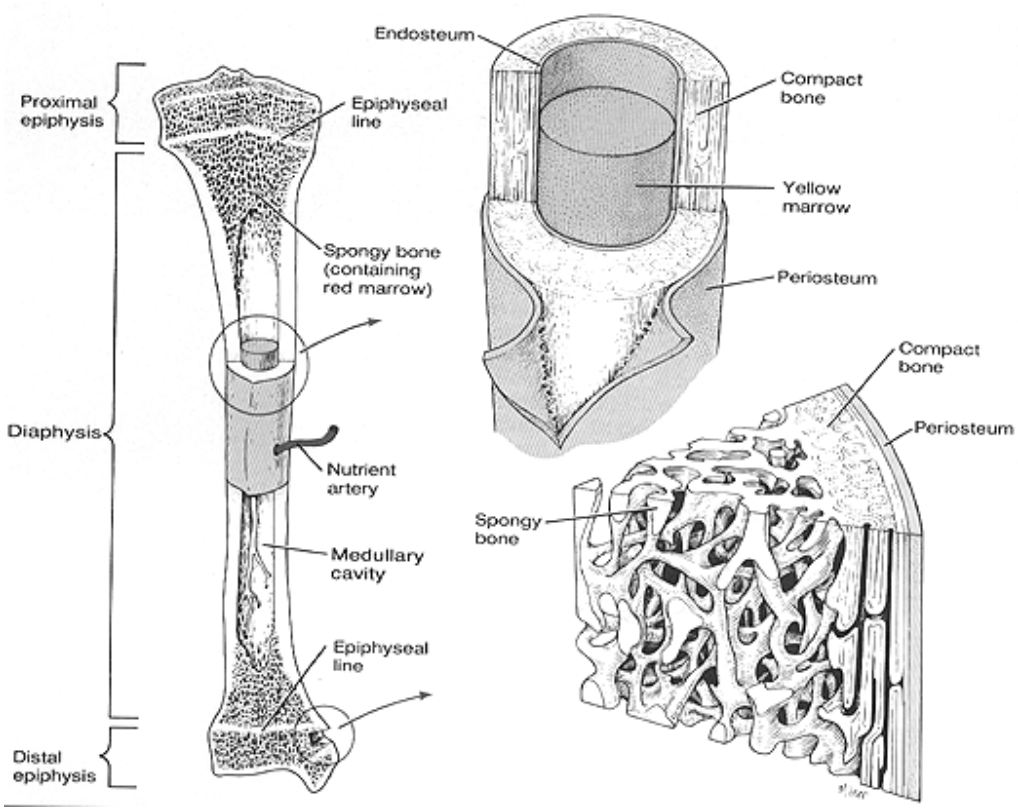

Figure 26: Bone Structures [138]

Bone consists of cellular organic and mineral, inorganic phases. The mineral phase, approximately 60-70% by mass, contains mainly a calcium phosphate which contributes stiffness and strength to the bone. 5-8% is made up by water, and the organic cellular matrix forms the balance. The organic component contains cells which perform maintenance of the bone: osteoclasts destroy damaged bone, osteoblasts back-fill with new bone mineral material and osteocytes (mature bone cells) are believed to act as sensors to regulate the process. These cells are known collectively as the Basic Multicellular Unit

(BMU), whose activity is illustrated in Figure 27. As osteocytes sense bone damage, osteoclasts travel along the trabecular surface resorbing material and forming a resorption cavity, which is refilled with new tissue by osteoblasts.

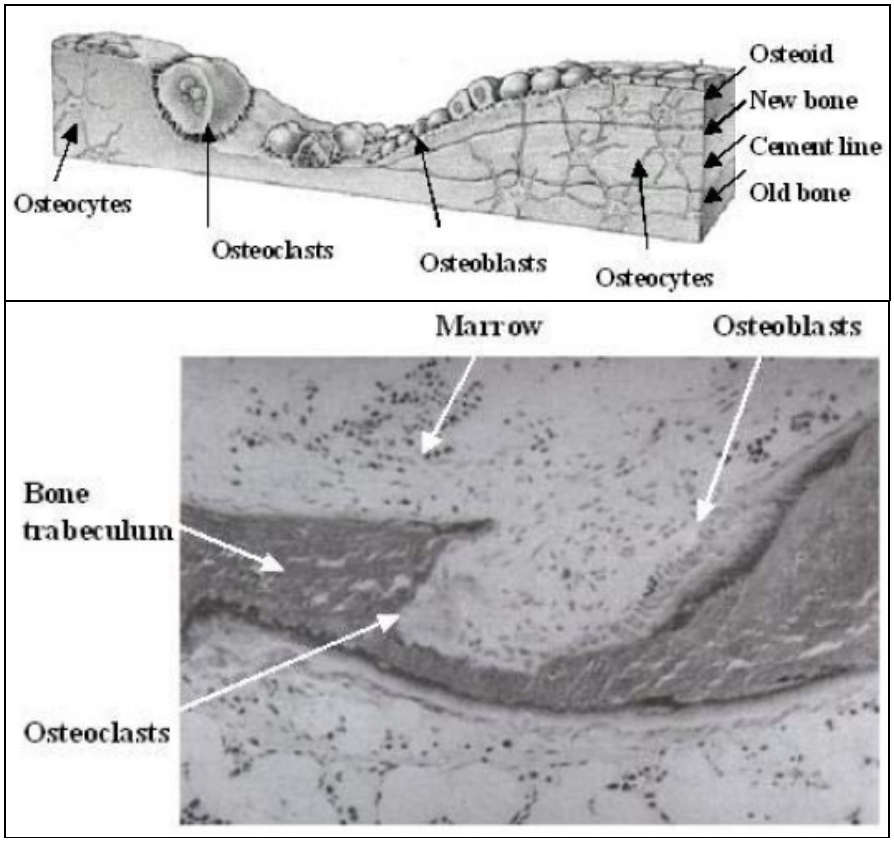

Figure 27: Schematic (top) and Histology (bottom) Images of BMU Activity on a Trabeculum [139].

Cortical Bone Materials Properties

Review articles present results of considerable mechanical testing on the macroscopic mechanical properties of cortical bone, giving values for properties including the Young's Modulus, Poisson's ratio, tensile and compressive strengths. Many factors affect these properties, particularly viscoelasticity, dynamic strain rates and the age of the subject. Cadaveric tissue measurements are also subject to inaccuracy from loss of sample moisture, and inhomogeneity with loading direction and anatomic location. However, under physiological strain rates (up to $0.1s^{-1}$) and for appropriate moisture material, longitudinal Young's Modulus is reported to be approximately 17GPa, with ranges from 14.1GPa (compression) to 24.5GPa (tension). Similarly there is a wide range of Poisson's ratio values, from 0.08 to 0.45 in human bone. Longitudinal strength values are reported to be on average 133MPa and

193MPa in longitudinal tension and compression respectively, and 51MPa and 133MPa in transverse tension and compression respectively [140, 141].

Cancellous Bone Materials Properties

As a cellular structure, cancellous bone can be considered on a continuum level, with mechanical properties which are dependent on its density (ρ). For the Young's Modulus 'E', many groups have attempted to fit empirically an exponential relationship of the form:

$$E = A\rho^{B} \qquad \textbf{Equation 1}$$

Morgan and Keaveny [142] and Morgan et al [143] reported empirical fits for this relationship for several anatomical sites and found considerable variation along with relatively low regression coefficients. A survey of modulus-density relationships using mechanical testing and FE analysis [144] identified the closest correlation, from Morgan et al [143]:

$$E = 6850\rho^{1.49} \qquad \textbf{Equation 2}$$

Figure 28 shows the relative strength for cancellous (ρ≈0.3g/cm^3) and cortical bone (ρ=1.73g/cm^3), for one strain rate, indicating a linear strength-density relationship. However, the yield *strain* of bone may instead be considered independent of density within an anatomic location according to mechanical tests by Morgan and Keaveny [142], at approximately 0.7-0.85% in compression and 0.61% in tension. This is thought to arise because cancellous bone adapts on the micro-scale through densification or resorption so that its continuum scale yield strain is approximately constant.

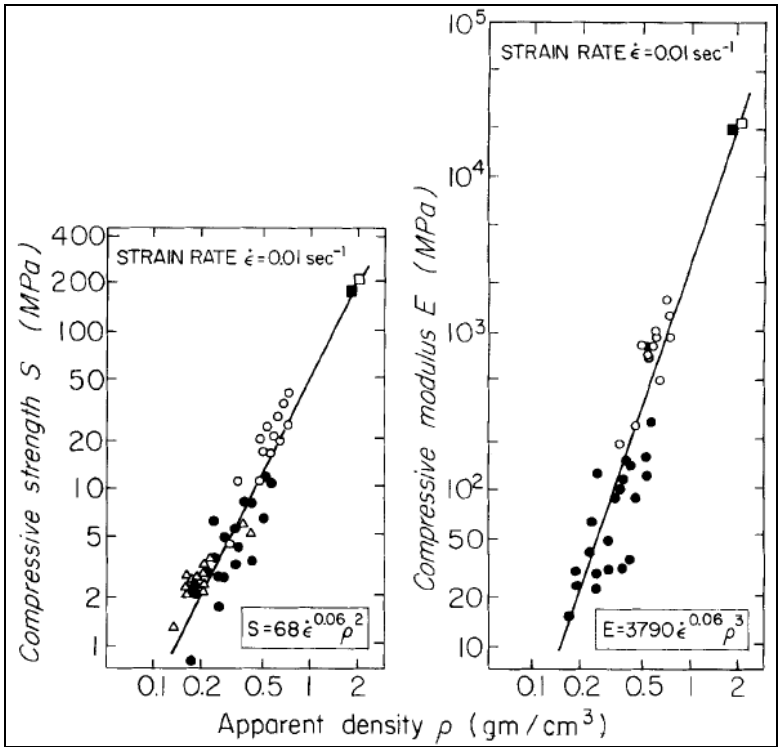

Figure 28: Mechanical Properties of Bone for Varying Density [140]

Adaptation of Bone

Bone is a self optimising structure, responding to the loads it experiences by a process called remodelling. Bone is in a state of continuous renewal, and remodelling is the process by which the structure can adapt to support an increase in loads, or to remove bone from regions in which it is unloaded. Remodelling occurs in two ways:

- internal remodelling- changing the porosity of the cancellous bone, and
- external remodelling- changing the outer dimensions of the cortical bone.

When bone loading increases relative to its normal state, material is deposited by internal or external remodelling, and vice versa. This effect is beneficial to sportsmen, allowing their skeletons to support high loads. However, for hospital patients confined to bed for extended periods, inactivity leads to increased fracture risk caused by a loss of bone density. Mathematical rules have been fitted to the process according to Wolff's law of 1870 [145] (discussed in detail later).

In localised areas, adverse bone remodelling is observed around joint prostheses, caused by stress shielding. The presence of a stiff metallic stem alters the load path through the bone, as stress follows

the stiffest path. In a hip implanted with a THR, this path is through the implant and into the diaphyseal cortical bone, so the stress bypasses the proximal bone structure which is then resorbed [146]. This can be seen on the x-rays in Figure 29, where bone density and cortex thickness has increased around the distal stem but considerable resorption has occurred more proximally. An advanced loss of bone density will provide inadequate implant support leading to loosening and increased fracture risk, and may leave the bone with insufficient strength even to support a revision implant.

Figure 29: Postoperative (left) and 7-Year (right) THR X-Rays showing Proximal Bone Resorption and Distal Periprosthetic Bone Densification [146]

Biomechanics of Defect and Implant-Bone Interface Healing

The repair of orthopaedic injuries is thought to be controlled by a process of sequential tissue differentiation. In bone fracture healing [147], osteochondral defect repair [148] and implant-bone interfacial adaptation, precursor mesenchymal stem cells (MCSs) are involved in the healing of the defect. MSCs are unspecialised cells which maintain an 'undifferentiated phenotype until they are exposed to the appropriate signals' [149], at which point they can differentiate into connective tissue cells. MSCs may be introduced on a scaffold to support the repair of large defects [150], but without intervention, smaller, stable defects will be populated by granulation tissue containing MSCs. They derive from the bone marrow, and it is thought that they migrate towards an injury site in the body to perform tissue repair. MSC differentiation can produce fibrous tissue, cartilage, muscle, marrow and bone through transformation into fibroblasts, chondrocytes, myoblasts, stromal cells and osteoblasts. Connective tissue differentiation is influenced by several stimuli including growth factors, changes in oxygen tension (hypoxia) and mechanical loading. For example, Matsuda et al [151] found that growth factors and hypoxia activate protein kinases which promote osteoblast proliferation, whereas mechanical strains activated different kinases, which promote cell growth arrest and apoptosis. Therefore it was suggested that a balance between the two environmental pathways determines connective tissue differentiation and growth.

Consideration of the mechanical stimulus is of particular interest in orthopaedic scenarios. Angele at al [152] found that mechanical stimuli could enhance tissue generation in a chondrogenic medium, and Altman et al [153] showed that tissue differentiation could be controlled in the absence of cell growth factors, by mechanical stimuli alone. In a well vascularised orthopaedic surgery site, it may be assumed that there is always a sufficient supply of growth factors to stimulate osteoblast proliferation, and since the high rate of proliferation leads to local hypoxia at the cellular level [154], it can be suggested that the pathway of MSC differentiation is influenced particularly by mechanical stimulation. Suggestions of the transduction mechanism (by which mechanical stimuli are converted into chemical activity in the cell, leading to differentiation) include strain reception, changes to nutrient and metabolite transfer rates through hydrostatic pressure, and cell binding [153]; in engineering terms, deviatoric or dilatational bulk strains [155], and relative interfacial 'micromotion' [156]. These stimuli will be discussed in the remainder of this chapter.

Strain Stimulated Tissue Differentiation – In Bulk Bone

Perren [157] suggested in simple terms that the tissue in a fracture site responds to the 'Interfragmentary Strain' (IFS), promoting the formation of a tissue type of sufficient stiffness to support the applied load without failing. In order for osteogenesis to occur, the fracture must first be stabilised by the formation of soft tissue. Artificial fracture stabilisation or fixation can be used to assist this. Pauwels [158] considered the action of two mechanical stimuli: shear and hydrostatic stresses, representing shape and volumetric changes – deviatoric and dilatory. This approach has a stronger biomechanical foundation, as it may link the specific orientation of cells in each tissue type to the mechanical stimulus they experience, promoting chondrogenesis under compression, or highly directional ligamentous and tendonous tissue formation under shear strain. Further tissue differentiation to permit ossification through both endochondral and intramembranous routes would then be possible, as illustrated by Figure 30.

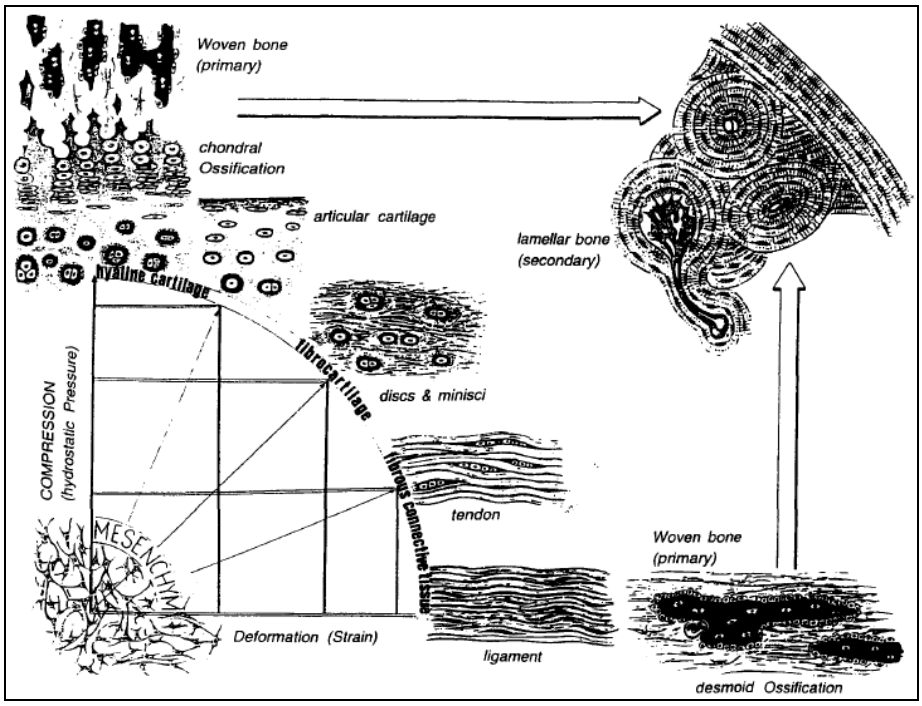

Figure 30: Proposed Tissue Differentiation Routes under Mechanical Stimuli according to Pauwels (adapted by Weinans and Prendergast [159])

The advantage of the shear and hydrostatic stress approach is that the two stimuli isolate two forms of mechanical deformation: hydrostatic or 'dilatational' stresses represent volumetric changes, and shear or 'deviatoric' stresses represent geometric distortion without a volumetric deformation. Carter et al [155] attempted to quantify the effect of the two mechanical stimuli combined with

vascularisation, considering intermittent, peak cyclic stresses resulting from typical biomechanical loading. They suggested that high magnitude shear or tensile hydrostatic stress would result in fibrous tissue formation, even if normal loading is minor and only a very small number of such loading cycles are experienced. Conversely, with good vascularity and in more stable conditions giving lower magnitude stress, they suggested that osteogenesis would be possible. Their model promoted chondrogenesis under compressive hydrostatic stress, and even under low magnitude tensile hydrostatic stress in cases of avascularity. The model is illustrated in Figure 31.

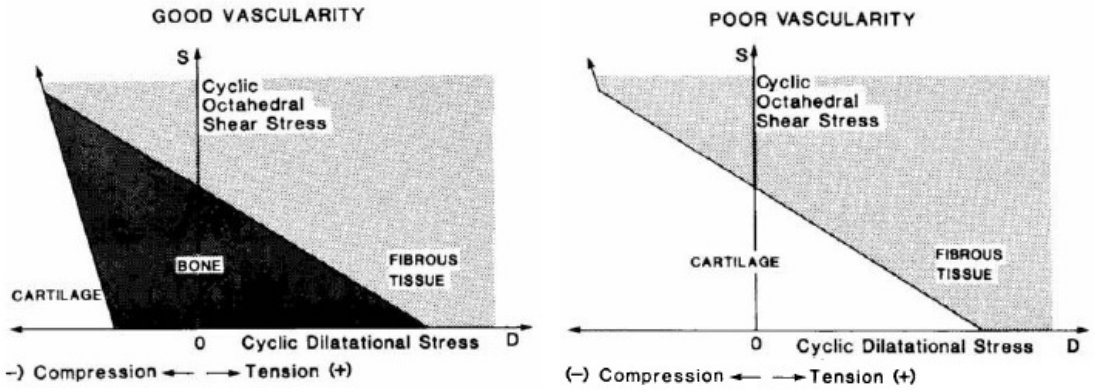

Figure 31: The Carter Model of the Influence of Mechanical Stimuli on Tissue Differentiation [155]

Micromotion Stimulated Tissue Differentiation – at Bone-Implant Interfaces

Long term aseptic loosening of cementless prostheses may occur as a result of wear particle induced osteolysis, but initial implant fixation may never be achieved if there is excessive relative movement between the implant and the supporting bone. In the case of large 'micromotion' or 'dynamic motion' as defined by Speirs et al [156], 'nonmineralized connective tissue' can form at the interface [160] which has insufficient strength to support the implant. Canine studies have shown that movements above 150μm lead to a fibrous interface, whereas with small micromotions (in the range of 20μm-56μm), osseointegration can be achieved [160-162]. Prediction of the implant-bone micromotion is therefore beneficial in the analysis of prospective designs, and influences the transfer of load from the implant to the bone, which will affect its remodelling behaviour.

Summary

Femoral neck fracture and femoral prosthesis loosening are two main failure modes of traditional hip resurfacing prostheses. An understanding of bone failure, and bone adaptation both in bulk and at implant-bone interfaces could aid in informing the more reliable use of contemporary designs and in the development of new prosthesis concepts. The next section of the review will describe biomechanical modelling techniques which have been produced in an attempt to simulate these phenomena.

2.2.3 Finite Element Analysis and use in Pre-Clinical Research

Theory of Finite Element Analysis

Finite Element Analysis is a computational tool which allows deformation, strain and stress analysis of structures with geometry and materials properties too complicated for deterministic analysis. The method is based on the one dimensional Hooke's Law:

$$F = kx \qquad \textbf{Equation 3}$$

where F is the applied force on the spring, k is its stiffness – a function of the spring's cross section and the properties of its material – and x the resulting extension. The FEA method expands this into a matrix system, whereby a complicated structure is discretised into small, regular 'Finite Elements' and continuity is defined at the junctions between the elements or 'Nodes'. Thus the Hooke's Law equation is expressed in vector and matrix form as:

$$\{F\} = [k]\{x\} \qquad \textbf{Equation 4}$$

where [k] is the stiffness matrix, which contains the geometric and materials properties of the structure. Forces are applied to nodes in the loaded regions of the structure, and certain nodes are constrained against motion, and with inversion of the stiffness matrix the system is solved as:

$$\{x\} = [k]^{-1}\{F\} \qquad \textbf{Equation 5}$$

Using the displacement field throughout the structure, the strain can be calculated, followed by the stress with knowledge of the stiffness of each element.

FE analysis can be faster and less expensive than mechanical testing, and can provide full-field stress data throughout a structure, compared to data at single surface points as would be obtained with strain gauges, or on the external surface of the structure as in photoelasticity. FE is particularly beneficial in pre-clinical analysis of biomechanical structures, where there is limited scope for experimentation by *in-vivo* or cadaveric *in-vitro* mechanical testing owing to high levels of subject variability, ethical constraints and cost. FE permits the comparative performance of a number of prosthesis designs to be investigated, and the full effects of surgical and patient variability to be predicted.

FE Analysis of Biomechanical Structures

In micro-scale bone modelling, individual trabeculae of the bone structure are studied (Figure 32 left). However, when a whole bone or implant is to be modelled, the scale of individual trabeculae is very small compared to the whole structure, so it is not feasible to represent both in the same model. Therefore, in macro-scale modelling, continuum mechanics are used for the elements constituting the bone, where changes to the trabecular microstructure within each element are represented by changes to its material properties (Figure 32 right). As this study considers the effects of resurfacing implants on bone, macro-scale, continuum methods are considered.

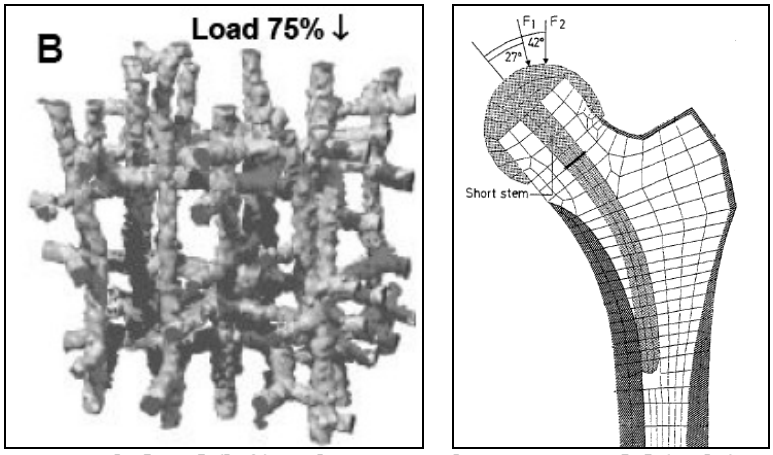

Figure 32: Micro-Scale [163] (left) and Macro-Scale Continuum [8] (right) Bone Models.

FE Analysis of Bone Fracture

Owing to its complex, inhomogeneous structure, it is not possible to define a single failure criterion for bone, such as peak von Mises stress as would be used in a plastically yielding metal structure. Numerous approaches have been made to study bone fracture loads and locations, both in the analysis of implanted bones and, more fundamentally, in the analysis of the risk of fracture of the femur in the elderly. The discussion in the literature is of the choice of failure criterion in the FE model: the ratio of a peak or equivalent stress or strain to a strength value, and definition of failure when the first element in the model fails, or when a set volume of elements has failed. Previously used approaches are discussed below.

Lotz et al [164] conducted mechanical tests and FE modelling studies in parallel and investigated von Mises stress, Hoffman yield and von Mises strain criteria to their FE stress data to form a predictive tool for fracture in the femur. The Hoffman yield criterion is essentially a von Mises stress criterion

where different tensile and compressive strengths are used. They identified that the von Mises strain was the most reliable criterion, predicting fracture loads for gait and falling load cases to within 8%, but they failed to reproduce the failure mode and location in their simulations. Locations were predicted more reliably by subsequent work using a model incorporating material nonlinearity [165].

Keyak et al [129] employed a 'Factor Of Safety' (FOS) principle to a von Mises Stress yield criterion in their first study, obtaining a strong linear correlation between experimental and FE predicted fractures when a contiguous volume of 400mm^3 of bone exceeded their individually calculated, density dependent yield strengths. This technique does not require peak values, which are subject to errors in FEA, and they very reliably reproduced fracture modes and locations. However their method underestimated strength quite considerably. Further work by Keyak and Rossi [132] compared the performance of several criteria: Hoffman stress, a Hoffman strain analogue, maximum normal stress, maximum normal strain, maximum shear strain, Coulomb-Mohr and modified Mohr theories (which combine tensile and compressive factors). Unlike Lotz et al [164], Keyak and Rossi [132] found that the strain based theories gave worse predictions than the von Mises stress and shear based methods. This was corroborated recently by Duchemin et al [128] who obtained excellent correlation between their tests and FE models with a von Mises stress criterion requiring failure of 50 elements (of unreported volume) to cause bulk failure.

As identified in the results from Morgan and Keaveny [142] and Bayraktar et al [166], strain must be a simpler, more reliable metric than stress, owing to its independence from density which removes an empirically fitted estimation step from the calculation. Schileo et al [144] argued that the difference in findings between these results is probably down to errors in strain prediction, and as mentioned earlier, identified the most reliable stiffness-density relationship from the candidates in the literature to improve strain prediction. In their most recent work they successfully fitted an asymmetric peak principal strain criterion in FE models to experimental tests of femurs under stumbling loading, and showed it to give a far more reliable prediction of failure load and precise location than von Mises stress or asymmetric peak principal stress. Their study used cortex strains only, and stumbling loading, which is a possible limitation. Failures under stumbling or gait loads tend to originate from the surface, but this is not necessarily the case in a sideways fall (where failures may be intertrochanteric [129]) or in an implanted bone where the internal trabecular structure is placed under additional strain.

In summary, it is suggested that the most effective failure criterion will be a combination of those listed above: an asymmetric, maximum principal strain based criterion. The strain approach minimises the number of assumptions required, since a separate yield strength value need not be calculated for each element. Instead, the density independent yield strain of bone can be exploited.

FE Analysis of Bone Adaptation

The stimulus for remodelling is not known for certain. It is thought to be linked to strain or damage: mechanical loading results which could be sensed by osteocytes. A number of groups have produced continuum-scale finite element models employing remodelling algorithms using these stimuli, which are corroborated with *in-vivo* evidence, most notably the groups in Nijmegen [167-169], Trinity College Dublin [170], and Zaragoza [171, 172]. Other groups have demonstrated that structural optimization theories permit similar predictions of anisotropic bone adaptation [173, 174], albeit at high computational expense.

Specific Strain Energy Stimulated Remodelling

The first comprehensive remodelling algorithm, using strain related stimulus to simulate site specific remodelling both internally and externally, was described by Weinans et al [169], summarised as follows. The remodelling stimulus at each location in the bone, the specific strain energy (strain energy per unit bone mass), is calculated by:

$$S = \frac{U}{\rho} \qquad \textbf{Equation 6}$$

where 'S' is the specific strain energy, 'U' is the strain energy density (SED) over a daily loading cycle and 'ρ' is the bone density. Carter et al [175] proposed that the effects of 'n' different load cases could be included in the stimulus, using a weighted average of the strain energy density values 'U_i'. This was simplified by Huiskes et al [168] for equally weighted load cases to:

$$U = \frac{1}{n}\sum_{i=1}^{n} U_i \qquad \textbf{Equation 7}$$

Carter showed that this approach could reproduce physiological cancellous bone macrostructure in a 2D iterative remodelling study using three load cases: the point of peak load during walking and the two extremes of flexion-extension motion.

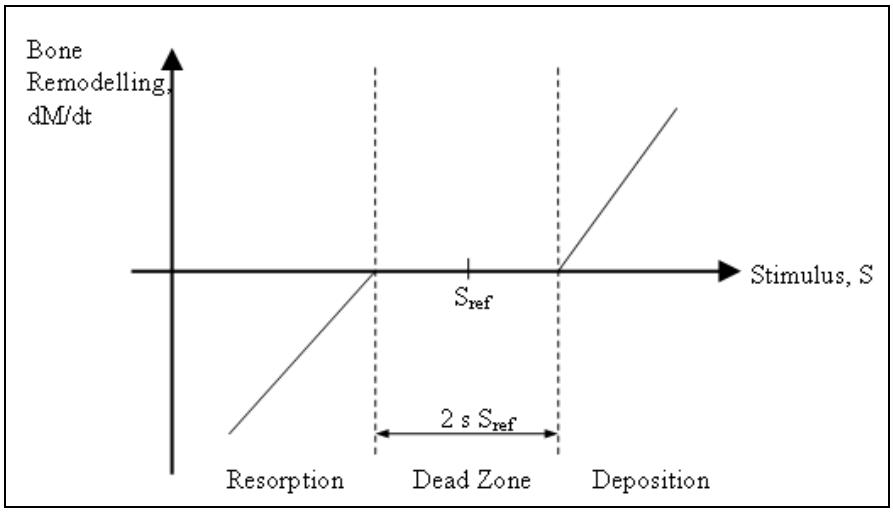

Figure 33: Bone Remodelling behaviour according to the Stimulus, Specific Strain Energy

Continuum remodelling simulation theories aim to equalise the specific strain energy 'S' at each location with its value in healthy, un-implanted bone, 'S_{ref}', by changing the bone mass 'M' through internal or external remodelling. The actual stimulus is the percentage change in specific strain energy, '$(S-S_{ref})/S$'. Bone deposition (positive rate of change of bone mass, dM/dt) occurs when 'S' is greater than the reference value, and resorption when 'S' is lower. However, as Frost [176] identified, there is a threshold stimulus-change from the natural level ($|S-S_{ref}|$) below which the bone is unresponsive and remodelling does not occur. This is known as the 'dead zone', shown in Figure 33. The remodelling process can be expressed as:

Remodelling- Bone Resorption, dM/dt < 0	No Remodelling- Lazy-Zone dM/dt = 0	Remodelling- Bone Deposition dM/dt > 0
when		
$S \le (1-s)S_{ref}$ **Equation 8**	$(1-s)S_{ref} < S < (1+s)S_{ref}$ **Equation 9**	$S \ge (1+s)S_{ref}$ **Equation 10**

Theory suggests that bone can only be resorbed or deposited at a free surface, implying that the cortical thickness 'x' can change and that cancellous pores may change size altering the density 'ρ', but that no new pores form. This was quantified by Martin [177] who developed an area density function to define the free surface area for bone cellular activity as a function of bulk bone density, and current studies factor this into their remodelling rate constants. This gives the maximum potential remodelling

rate for a bone density of 1.125g/cm^3, and effectively zero remodelling rate for bone densities of 0 and 1.73g/cm^3, where there is complete resorption or zero porosity.

With this approach, the Nijmegen model [169] showed that realistic internal remodelling was achieved by direct variation of the bone density with an upper limit equal to the cortical bone density, 1.73gcm^{-3}, where porosity reaches zero. Lower limits of cortex thickness of 0.005mm and bone density of 0.01gcm^{-3} were used to aid model convergence. Thus, internal and external remodelling rates were expressed by the following ordinary differential equations:

Internal Remodelling	External Remodelling
$\frac{dM}{dt} = \rho A \frac{dx}{dt}$	$\frac{dM}{dt} = V \frac{d\rho}{dt}$
x > 0.005mm	0.01 < ρ < 1.73 gcm^{-3}
Equation 11	**Equation 12**

For a chosen time step size Δt, the change in cortex thickness Δx or cancellous density Δρ can be calculated for each element and each time step using forward Euler integration, allowing site specific remodelling:

$$\rho^{i+1} = \rho^i + C\left(S - [1 \pm s]S_{ref}\right)\Delta t \qquad \textbf{Equation 13}$$

and

$$X^{i+1} = X^i + D\left(S - [1 \pm s]S_{ref}\right)\Delta t \qquad \textbf{Equation 14}$$

where C and D are constants determining the rates of each kind of remodelling [169], a function of the free surface area of the bone for cellular activity [177].

Damage Stimulated Remodelling

Still working isotropically, Prendergast and Taylor [170] used an alternative remodelling stimulus: damage accumulation. They proposed that under normal conditions, at remodelling equilibrium, bone contains damage in the form of 'inter-constituent microcracks'. Damage is a theoretical quantity with a value between 0 (intact) and 1 (failed), and the normal damage level is denoted 'ω_{RE}', equal to the

damage repair capacity. Under increased homeostatic stress relative to the natural equilibrium level, the damage level must rise to a level 'ω', so the change in accumulated damage 'Δω' is given by:

$$\Delta\omega = \omega - \omega_{RE} \qquad \textbf{Equation 15}$$

This change in accumulated damage 'Δω' was used as the remodelling stimulus. The level of bone deposition 'X' is proportional to the stimulus using 'C' as a rate constant, so that the deposition rate is:

$$\frac{dX}{dt} = C\Delta\omega \qquad \textbf{Equation 16}$$

$$\frac{dX}{dt} = C\int_{t_0}^{t}\left(\dot{\omega} - \dot{\omega}_{RE}\right)dt \qquad \textbf{Equation 17}$$

As such, knowledge of the absolute levels of damage is not required: the rate of bone deposition can be calculated using only the rates of damage accumulation and repair. These can be quantified under fatigue loading using the 'remaining life' approach to quantify damage under fatigue loading. This states that for n_i cyclic loads resulting in cyclic stress of $\Delta\sigma_i$, the damage is equal to:

$$\omega = \frac{n_i}{N_{fi}} \qquad \textbf{Equation 18}$$

where N_{fi} is the number of cycles to failure at that load and clearly when N_f cycles are reached, damage $\omega=1$ and the element fails. As with the specific strain energy stimulated remodelling, the theory of Carter et al [175] is used and the remodelling stimulus is averaged over 1 day, experiencing n_i cycles of m different loading levels:

$$\omega = \sum_{i=1}^{m}\frac{n_i}{N_{fi}} \qquad \textbf{Equation 19}$$

As damage increases linearly from 0 to 1 under one load level, the rate of damage over time at one load level is equal to:

$$\dot{\omega} = \frac{1}{N_{fi}} \qquad \textbf{Equation 20}$$

The fatigue life is obtained using an empirical relationship from Carter et al [178]:

$$\log\left(N_f\right) = H\log\left(\Delta\sigma\right) + JT + k\rho + M \qquad \textbf{Equation 21}$$

where $\Delta\sigma$ is the cyclic stress, T is the temperature in °C, ρ is the density in gcm^{-3}, and H, J, K and M are constants. Finally, Euler integration is used to calculate the change in damage accumulation over a time step Δt:

$$\Delta\omega^{i+1} = \Delta\omega^{i} + \left(\dot{\omega} - \dot{\omega}_{RE} \right)\Delta t \qquad \textbf{Equation 22}$$

and the algorithm can be applied to each element in an FE model, solving iteratively.

Optimisation Based Remodelling Methods

There is an argument that biomechanical models should consider a measure of the anisotropy of bone mechanical properties. The Zaragoza group developed a damage-repair approach to bone remodelling considering a 'fabric tensor' [171] which considers both mechanical properties and bone damage to be directional, and expressed in tensor form. Their modelling process combined damage stimulated anisotropic internal remodelling with external remodelling through biomimetic Computer Aided Optimization (CAO) [179] which allows growth aligned with the stimulus gradient, rather than normal to the existing surface. Their application of the damage concept was also slightly different, interpreting damage as a measure of porosity. This process has been employed in simulation of *in-vivo* animal tests and remodelling around the proximal femur containing a THR implant [171, 172] and expanded most recently to consider metabolic activity and bone mineralisation [180], and Paris Law fatigue damage accumulation principles [181]. Although this method is designed to model anisotropic effects, it requires an initial assumption of the material anisotropy. As the process was developed and applied to 3D bone models [171, 172], the approach was to model first a homogeneous, isotropic material bone subjected to walking loads for up to 300 days worth of remodelling, to allow a representative density and anisotropy situation to develop before implantation and the full simulation. Although this creates perhaps a more generalised, less patient-specific model, this initial case is highly dependent on human interpretation.

Finally, research into the micro-scale remodelling behaviour of the trabecular structure was reported by Jang et al [182] using Surface Topology Optimisation, whereby a set bone material volume is redistributed in order to minimise a weighted sum function of the bone mass and total strain energy [183]. This process has also been coupled with external remodelling of cortical bone [184] and used to predict the effects of implantation [174], but the complexity was such that at the time of writing, computational expense has constrained its use to 2D models.

Combined Stimulus Methods

McNamara and Prendergast [185] summarised the argument that both strain and damage may affect remodelling, using a micro scale model of single trabeculum with a combined strain and microdamage stimulus. Their model predicted that damaged bone could be resorbed and repaired by the combined stimuli when a mechano-regulatory system was used. That is, strain and damage stimuli were both able to act, with the strain stimulus prioritised below a critical damage level, and damage stimulus prioritised above it. As well as giving good results on the micro-scale 2D model, this approach has been expanded onto a continuum level, as in the study by Scannell and Prendergast [186].

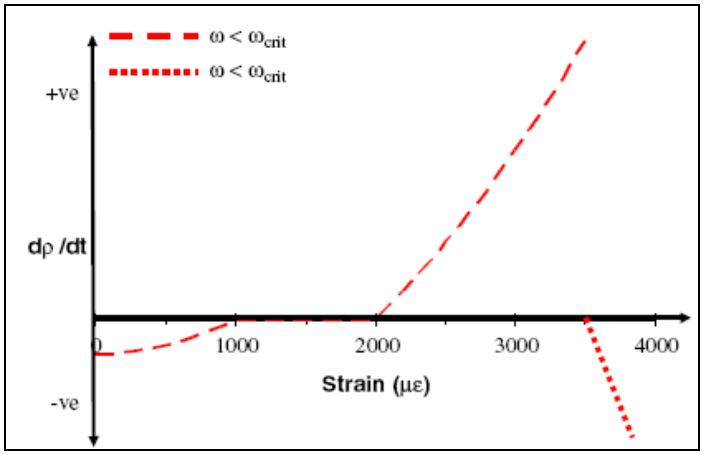

Figure 34: Strain and Damage Stimulated Bone Adaptation by Mechano-Regulation [185]

FE Analysis of Tissue Differentiation

Despite only recent confirmation of the role of mechanical stimuli in tissue differentiation, attempts to simulate fracture healing by this method were reported as early as 1979 [157, 158]. Carter et al's more detailed, two stimulus approach was reported in 1988 [155], where the octahedral shear stress 'S' and dilatational hydrostatic pressure 'D' were defined as functions of the principal stresses σ_1, σ_2 and σ_3:

$$S = \tfrac{1}{3}\left[(\sigma_1 - \sigma_2)^2 + (\sigma_2 - \sigma_3)^2 + (\sigma_3 - \sigma_1)^2\right]^{\frac{1}{2}} \quad \textbf{Equation 23}$$

$$D = \tfrac{1}{3}(\sigma_1 + \sigma_2 + \sigma_3) \quad \textbf{Equation 24}$$

They investigated the relative importance of the two mechanical stimuli, combining them in a single parameter 'OI', the Osteogenic Index:

$$OI = \sum_{i=1}^{c} n_i \left(S_i + kD_i \right)$$ **Equation 25**

for 'c' separate load cases over the course of a day, 'n' representing the number of load cycles experienced of the 'ith' load case, and where 'k' was an empirically fitted constant to weight the relative effects of the stimuli. They applied this analysis to a two dimensional FE model of fracture healing under compressive and bending loads. They found that hydrostatic stress had a more pronounced effect than shear, with predicted tissue phenotype distributions most representative of *in-vivo* observations when $k \geq 2$. Although their models were considerable simplifications, they agreed with early global and histological trends in as diverse cases as initial fracture fixation [155], foetal metaphyseal (chondro-osseous) development [187] and implant-bone interfaces [188, 189], and formed the quantitative basis for more detailed studies. However, further modelling research has since shown that the predictions obtained from the Osteogenic Index approach becomes less valid with progressive tissue differentiation [190].

Claes and Heigele [191] developed this theory and identified quantified stimulus limits for differentiation into different tissue types (Figure 35), obtaining the values empirically from comparison to histological results from an ovine model of fracture healing and showed them to be valid also for drill hole defects [192]. In the low stiffness tissue initially present in an injury site, with a Young's Modulus in the order of 1MPa, their predictions of the relative importance of hydrostatic and shear stresses were consistent with Carter et al's [155].

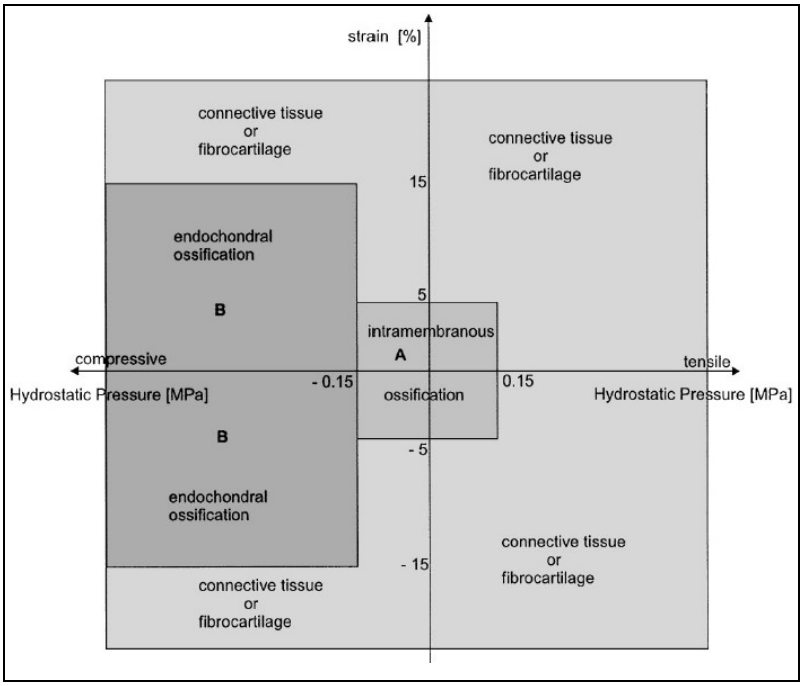

Figure 35: The Claes and Heigele Model of the Influence of Mechanical Stimuli on Tissue Differentiation [191]

The Osteogenic Index approach was developed in a different manner by Prendergast et al [188, 193] who considered combined effects of strain and a more explicit quantification of interstitial fluid velocity, by modelling bone as a biphasic poroelastic material with solid and fluid contributions to its mechanical properties. Huiskes et al [194] then quantified limits of these stimuli to promote proliferation of different phenotypes, again through empirical fit to an animal model, but this time using a porous implant-bone interface.

This approach was employed by Lacroix et al [195-197] in the simulation of fracture healing, and they introduced an adaptive feature to their model, simulating cell diffusion into the granulation tissue at the fracture site:

$$D\nabla^2 n = \frac{dn}{dt} \qquad \textbf{Equation 26}$$

where D is a diffusion constant and n is the concentration of cells in an element. This was followed by simulation of gradual tissue adaptation based on the strain-fluid velocity stimulated differentiation model, and the stiffness of the healing tissue was allowed to evolve using the rule of mixtures:

$$E = \frac{n^{\max} - n}{n} E_{granulation} + \frac{n^{\max}}{n} E_{tissue} \qquad \textbf{Equation 27}$$

where E is the resulting tissue stiffness, $E_{granulation}$ and E_{tissue} the stiffnesses of granulation tissue and the tissue phenotype which is evolving, and n/n^{max} the fractional cell concentration. This was smoothed over ten successive days of simulation, to prevent artificially fast adaptation and numerical instability [195].

This approach has since been applied to osteochondral defect filling [198], and implant-bone interfacial tissue adaptation [199]. The effects of different cell dispersal mechanisms were studied by Pérez and Prendergast [200] in an implant-bone interfacial gap model, considering diffusion and preferred-direction random-walk mitosis models. The methods they studied gave similar evolutions of tissue stiffness but different tissue type patterns, and they lacked histological evidence to indicate which method was preferable. A more recent study by Isaksson et al [201] sought to compare the previously mentioned biomechanical stimuli, to identify the approach which corroborated clinical evidence most closely. They found that all the methods gave similarly representative simulations of fracture healing, but demonstrated the importance of including resorption feedback capabilities and showed that in isolation, the deviatoric strain stimulus produced results closer to clinical observations than the dilatational volumetric (hydrostatic pressure) stimulus. As such, similarly to bone remodelling, a pure mechanical simulation method may produce valid results for tissue differentiation simulations, because the strain stimulus dominates and the interstitial fluid pressure may be captured indirectly by consideration of mechanical hydrostatic pressure.

2.2.4 Research Method: Critical Review and Scope for Further Research

This final section of the literature review chapter contains a critical review of the existing biomechanical studies reported in the literature which have considered the resurfaced femoral head and neck. It identifies areas in which further research is required, and justifies the objectives and approach adopted for this research project.

Previous Modelling Techniques

The first study which employed 3D geometry representative of the full proximal femur was reported by Watanabe et al [9], who studied the differences in von Mises stress and minimum principal (compressive) strain between natural and resurfaced femurs. Their model contained fewer than 5000 elements owing to computational constraints at the time. Several studies have been published since, [11-18, 202-206], with geometry and materials properties from CT scans and over 100,000 degrees of freedom.

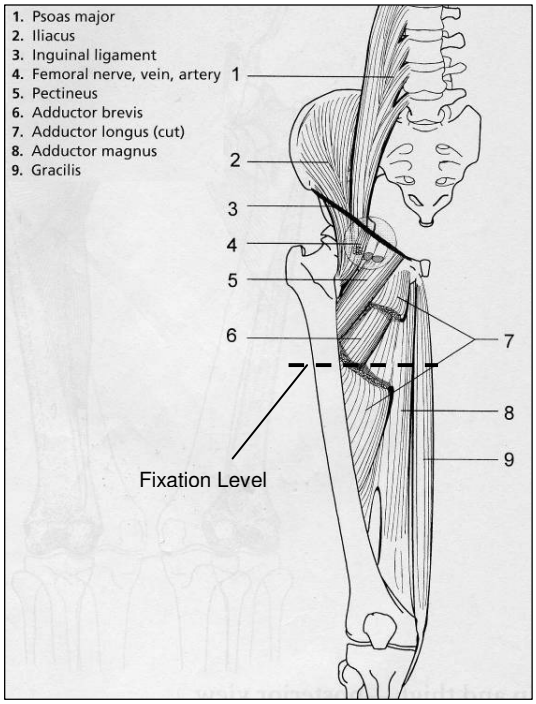

Figure 36: Anterior View of the Pelvic and Femoral Muscles with their Attachment and Origin Locations [207].

Studies have indicated that the inclusion of particular muscle groups and the location of the fixed boundary conditions have considerable effects on the bone strains in the proximal femur. Speirs et al [208] investigated the effects of constraining the femur at the diaphysis or the knee condyles, and the inclusion of various muscle forces. The two rules they used to describe the adequacy of the boundary condition sets were a physiological displacement of the femoral head under load, and small reaction forces at the fixed nodes indicating force and moment equilibrium in the structure. Their conclusion was that a full set of muscle forces and fixation at a single node at the knee joint centre produced the most accurate results across the entire femur. This approach is crucial where the full strain field in the femur is of interest. However, its complexity may be an unnecessary expense for analysis of implants in

the proximal femur alone, particularly resurfacing implants whose influence extends to the femoral head and neck only. Speirs et al [208] ruled out the mid-shaft constraint approach owing to excessive reaction forces and large joint centre displacements under load. However, they did not remark for this model that the inclusion of muscle forces considerably reduced the reaction forces at the fixed nodes; that is, the reaction forces at the fixed nodes indirectly represent the muscle forces. Their other concern was that a large displacement of the joint centre generates artificially high bending moments, but their 'mid-shaft' constraint was approximately two-thirds along the femur. Femoral head displacement would be reduced by applying the mid-shaft constraint higher, and this may be justified physiologically if constraint is applied at the centroid of the attachment areas of the muscles which provide the vertical force equilibrium in the system (the hip adductors and flexors, Figure 36), approximately one third of the length of the bone from the proximal end.

Polgár et al [209] also investigated distal and mid-shaft constraints and the application of various muscle groups. Their concern with constraint was excessive strain 'up to about 25-30mm above the level of fixation', however this is far from the region of interest in resurfacing implant analyses, and the joint centre displacement for this arrangement was close to physiological levels. As Taylor [12] noted, strain artefacts at constrained nodes must be expected in the finite element method, so the distribution of strains is of most importance, rather than peak values. This mid-shaft fixation approach must be used with care in THR prosthesis models, where the stem approaches the constraint location and the strains in that area *are* of interest.

The simplified muscle force approach was found to be valid in earlier work by Stolk et al [210] who identified that the most significant muscle group for FEA of an implanted hip was the abductors. It was found that the abductor muscle force could reduce peak cement stresses by up to 50%, whereas the iliotibial tract muscles and adductors had a much lesser effect. This would only be valid for the mid-shaft constrained model, as the attachment areas for many of the muscles apart from the abductors would be close to the constraint and, again, have little effect on strains and serve only to reduce the reaction forces at the constrained nodes.

In summary, provided that the strain near the constrained nodes is not of interest, it can be argued that it is representative to use mid-shaft constraint and the abductor muscles alone, so long as the location of the constraint is chosen carefully.

Previous Variables Investigated

The main focus of the existing resurfacing studies has been periprosthetic fracture of the femoral neck, and remodelling around the prosthesis, with the study variables of:

- comparison of the implanted and natural femora, statically [9, 11, 12, 16, 17] and adaptively [13, 203],
- the effect of reduced support bone quality [11, 202]
- implant stem diameter [12, 202] and the extent of stem-bone contact [12, 18, 203, 205],
- implant stem length [8, 202]
- implant fixation, including cemented vs. cementless fixation [14] and cement mantle thickness [12, 17, 202],
- the extent of implant-bone bonding [12, 14, 15, 202, 203],
- implant orientation, including varus-valgus orientation [14-16, 202] and exposure of cancellous bone [15], and
- implant material, comparing Cobalt Chromium to Alumina Ceramic [202, 205].

In addition to these 'normal' positioning studies,

- the effects of femoral neck notches of varying sizes was researched by a combined mechanical testing and simple FE analysis investigation [204].

A summary of previous resurfaced femur computational studies is given in Table 3.

Table 3: Approach Taken in Previous Resurfaced Femur FE Studies (Cont'd Over)

Study, Year	Focus	Geometry	Mesh	Boundary Condition	Loads	Algorithm / Output Measure
Watanabe et al 2000 [9]	Understanding Biomechanics of Implanted Femur. Fracture Stress and Stress Shielding	Simplified 3D	Linear Tets (4k) Homogeneous	JCF and Abductors, Fixed Distally	3 Points in Gait	Fracture: von Mises Stress Remodelling: Min Principal Strain
Taylor 2006 [12]	Change in Load Transfer and Peak Strains vs Stem Bonding, Contact Length, Diameter, and Cement Thickness	CT, Human	Linear Tets (1.5-6.5mm) Heterogeneous	JCF and Abductors, Fixed Distally	Gait	Load Transfer: Comparative Pre- to Postoperative Strains Fracture: Equivalent Strain
Gupta et al 2006 [13]	Adaptive Remodelling	CT, Human	Nonlinear Tets (69k) Heterogeneous	JCF, Abductors, Vastus, Ilio-tibial Tract, Fixed Distally	Gait, Stair Climbing	Remodelling: Strain Energy Density
Long and Bartel 2006 [15]	Peak Cement Stress, Max and Min Strains, Load Distribution vs Varus/Valgus, Exposed Cancellous, Bonded/Sliding	CT, Human	Linear Hexahedra (38k) Heterogeneous	JCF and Abductors, Fixed Distally	Gait	Split between Cylinder, Chamfer, Prox. and Dist. Stem Load Transfer
Little et al 2007 [11]	Neck Fracture Risk vs Resurfacing, Reduced Strength with Age and Osteoporosis	CT, Human	Nonlinear Tets (76k) Heterogeneous	JCF and Muscles, Fixed Distally	Gait	Fracture Risk from Ratio of Peak Principal Stresses to Strengths

Table 3 cont'd: Approach Taken in Previous Resurfaced Femur FE Studies

Study, Year	Focus	Geometry	Mesh	Boundary Condition	Loads	Algorithm / Output Measure
Radcliffe and Taylor 2007 [16, 17, 202]	Change in Load Transfer and Peak Strains vs [202] Stem Diameter and Length (normal or extra long), Stem Bonding, Patient Weight, Bone Quality, Cement Thickness [17] and Varus-Valgus orientation [16] Ceramic Implant Material [202]	CT, Human, Multi-Femur	Linear Tets 1.5-2mm (ROI) 4-5mm (Distant) Heterogeneous	JCF and Abductors, Fixed Distally	Gait	Load Transfer: Comparative Pre- to Postoperative Strains Fracture: Equivalent Strain
Ong et al 2006 [14], 2008 [18]	Remodelling Stimulus vs Cemented/Cementless and Bonded/Sliding [14] Remodelling Stimulus and Cement-Implant Stress vs Varus-Valgus and Stem Over-Reaming [18]	CT, Human	Linear Hexahedra (153k), Shells (7k) Heterogeneous	JCF and Abductors. 'Mid-diaphyseal' Fixation	Gait	Remodelling: Strain Energy Minimum Principal Stress
Pal et al, 2009 [203, 205]	Adaptive Remodelling [203]. Remodelling Stimulus vs Stem-Bone Contact, and Implant-Cement / Cement-Bone Debonding. Ceramic Implant Material[205].	CT, Human	Nonlinear Tets (98k) Heterogeneous	JCF, Abductors, Vastus, Ilio-tibial Tract, Fixed Distally	Gait, Stair Climbing	Remodelling: Strain Energy Density

Previous Findings

The general findings of the previously published hip resurfacing biomechanical studies of hip resurfacing are as follows:

- reduced superior femoral head strain consistent with stress shielding and increased strain around the prosthesis stem, potentially leading to pedestal line formation [8, 9, 12-14, 79]
- increased strain shielding for stems with larger diameters [12], longer lengths [8] and greater extents of stem-bone contact [8, 12, 18, 202, 203, 205],
- increased femoral neck strain concentrations for larger diameter, longer stems [202], and very thin cement mantles [202],
- increased strain shielding with a bonded shell [14, 15, 203], with a bonded stem [8, 12, 14, 15, 17, 79, 203], and (to a lesser extent) with a thicker cement mantle [17, 202], and
- reduced peak femoral neck strains (indicating a reduced femoral neck fracture risk) with valgus implantation [15, 16, 202], fully covered cancellous bone [15], if the prosthesis torque is lower [202], and if femoral neck notching is avoided [204].

Some contradictory findings have been reported, particularly considering the influence upon strain shielding of:

- varus-valgus prosthesis angle ([16, 202] vs [18, 79]) and
- stiffer ceramic implant materials ([202] vs [205]).

Most recently, the benefit of multi-femur analyses in capturing the range of inter-patient variability has been demonstrated [16, 17, 202, 211].

2.2.5 Scope for Further Research

While investigating the biomechanics of the resurfaced hip, and in the pre-clinical analysis of new prosthesis designs, there are clear benefits to static models, showing the instantaneous post-operative remodelling stimulus, and to long term adaptive models, predicting the dynamic remodelling behaviour.

In the listed previous studies, there has been substantial research into the biomechanics of the resurfaced hip considering a range of variables, but some results have been contradictory, for example the effects of implant orientation on bone remodelling (Ong et al [79] vs Radcliffe et al [16]), and the influence of prosthesis material (Radcliffe [202] vs Pal et al [205]). In these studies, a quantified comparison of long term bone adaptation predictions with clinical evidence has been lacking. Furthermore, all the reported studies have simplified the stem-bone interface, although it has been shown that conditions at this interface are influential upon the remodelling behaviour. In traditional resurfacing head designs, the stem tapers along at least a portion of its length, but the bore drilled for it is parallel sided, so a void exists around the tapering portion of the stem postoperatively. In order for clinically observed bone densification around the stem tip to occur, this void must re-fill gradually, but this has also not been considered in previous studies, which have assumed one of two extremes: either a sustained gap, or perfect implant-bone contact.

Advances in computational resources now allow increasingly complex scenarios to be modelled. Therefore there is scope to revisit some of the previously researched variables, taking care to simulate clinically representative implant positioning and implant-bone interfaces. In addition, the application of advanced bone healing simulation methods in conjunction with bone remodelling algorithms may allow more clinically representative long term behaviour of the biomechanical adaptation of the femoral head and neck to resurfacing to be captured in a pre-clinical analysis model.

2.3 Summary, and Plan for the Research Project

The goal of the research is to develop computational biomechanical tools which replicate the clinical behaviour of replacement joint prostheses more closely than current models, and use them to identify areas in which the survivorship of current prosthesis designs may be improved. Despite good medium term clinical performance of resurfacing hip replacement, there is clear scope for improvement in mechanical and biological terms.

- revision of a hip resurfacing may be necessary due to mechanical failures such as periprosthetic bone fracture or resorption and loosening. These failure modes may be influenced as much by surgical, clinical and patient selection issues as by the prosthesis design, but improved design with the goal of higher tolerance to variation and error is worth researching.
- the local and systemic biological effects of the current Cobalt Chromium prosthesis alloys are not fully understood, but to build on technology from total hip replacement, the use of ceramic biomaterials would circumvent these concerns.

Furthermore, despite considerable research into the biomechanics of the resurfaced hip, there is justification for the development of a new resurfaced femur computational model:

- of the studies conducted to date, detailed instantaneous postoperative performance predictions have been made, but there has been some contradiction in results.
- no adaptive model has been produced which has corroborated clinical behaviour quantitatively. Therefore, the new model would aim to generate for the first time clinically representative, long term predictions of the adaptive biomechanical response of the hip to resurfacing.

The research will be conducted and presented around the following structure:

- Development and validation of finite element models of the resurfaced femoral head, with a focus on clinically representative implantation and simulation of bone adaption,

and for the case study:

- use of the FE models to understand the biomechanical causes of femoral neck fracture and implant loosening, and
- use of the FE models and their predictions to inform on the development of a new RHR prosthesis design, with the aims of incorporating geometry to improve biomechanical performance and eventually, ceramic materials.

3 METHODOLOGY

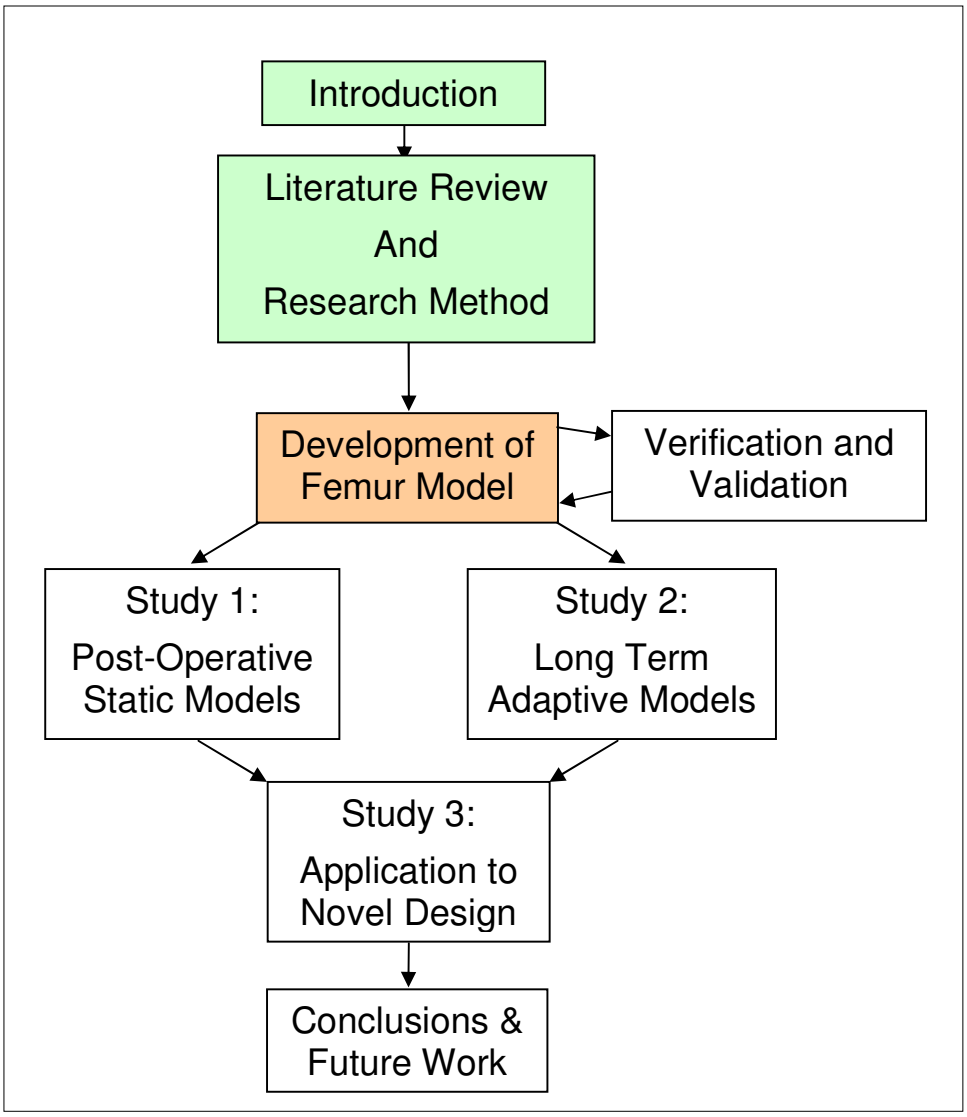

3.1 Purpose

A three-dimensional mechanical finite element model of the implanted femur is useful for analysis both of the strain in the bone, and of the stresses in the resurfacing head prosthesis. For the purposes of this study, a femur FE model was developed to allow prediction of the femoral neck fracture risk and remodelling stimulus in the proximal femur following resurfacing. With a prediction of the remodelling stimulus, the adaptive remodelling behaviour of the bone can be projected at low computational expense, and given more processing time, progressive bone adaptation around the prosthesis can be predicted.

3.2 Development of the Resurfaced Femur Model

3.2.1 FE Model Geometry and Mesh

A model of the proximal femur was developed in this study, based upon past techniques described in the literature review. Geometry and materials properties were derived from a CT scan of a 63 year-old male patient (height 1.77m, weight 85kg) with no known orthopaedic disease. A stereolithography (.stl) surface mesh of the femur was obtained from a library held in the research group, which had been produced using AMIRA software (Visage Imaging, Carlsbad, USA). NURBS geometrical surfaces were fitted to the geometry using SolidWorks 2007 CAD software (Dassault Systemes SolidWorks Corp., Concord, USA) and surgical cuts were performed using CAD models of surgical cutters, preparing the bone in a manner representative of that achieved in surgery. Several different implant design, positioning and sizing strategies were studied, so the precise details of the surgical cuts will be given when each model is presented.

The geometry was imported into ANSYS 12 structural FE software (ANSYS Inc, Canonsburg, USA), where it was meshed with second order tetrahedral elements. The mesh density was varied from a fine 2.5mm edge length in the femoral head, neck and intertrochanteric regions (the region of interest), to a coarse 6.0mm edge length in the femoral shaft.

The resurfacing head prosthesis was map-meshed by sweeping the geometry in segments, using second order hexahedral elements (Figure 37). A mesh with 1.0-2.0mm side length was used, with

quadratic elements at a high density (1.0mm element side length) on the surface of the bone where it was in contact with the stem or cylindrical faces of the implant, to obtain high accuracy contact stresses. The completed intact femur model contained approximately 110,000 elements and 170,000 nodes. The implanted model contained approximately 100,000 elements and 160,000 nodes.

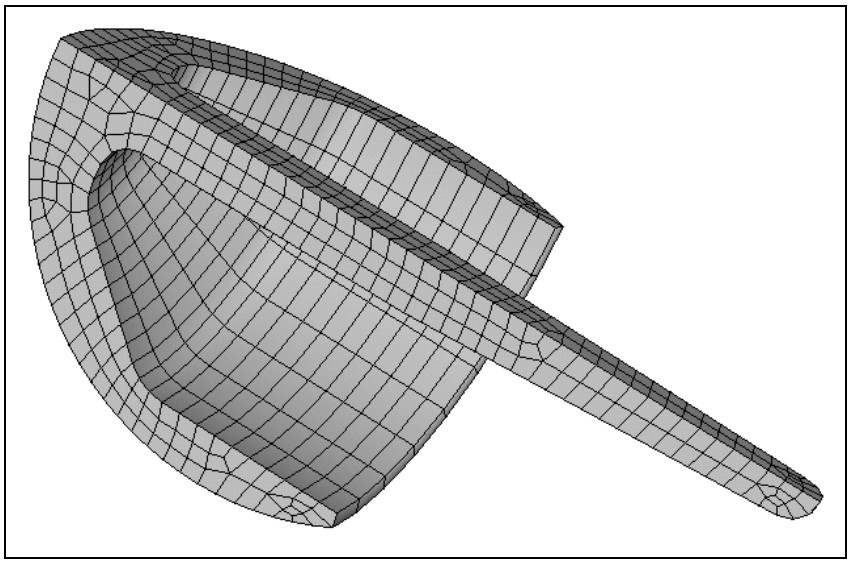

Figure 37: Mapped Mesh of one Quarter Segment of the Resurfacing Head Prosthesis

Preliminary study showed that although mesh convergence by model stresses and strains was achievable within feasible limits of solution time, the direct comparison of bone strains in the remodelling stimulus calculation was more sensitive to element size. The intact bone model was produced pre-partitioned at the surgical cut for the prosthesis (Figure 38), so that the elements in the intact and resurfaced models were identical and remodelling stimulus results would not be subject to averaging errors.

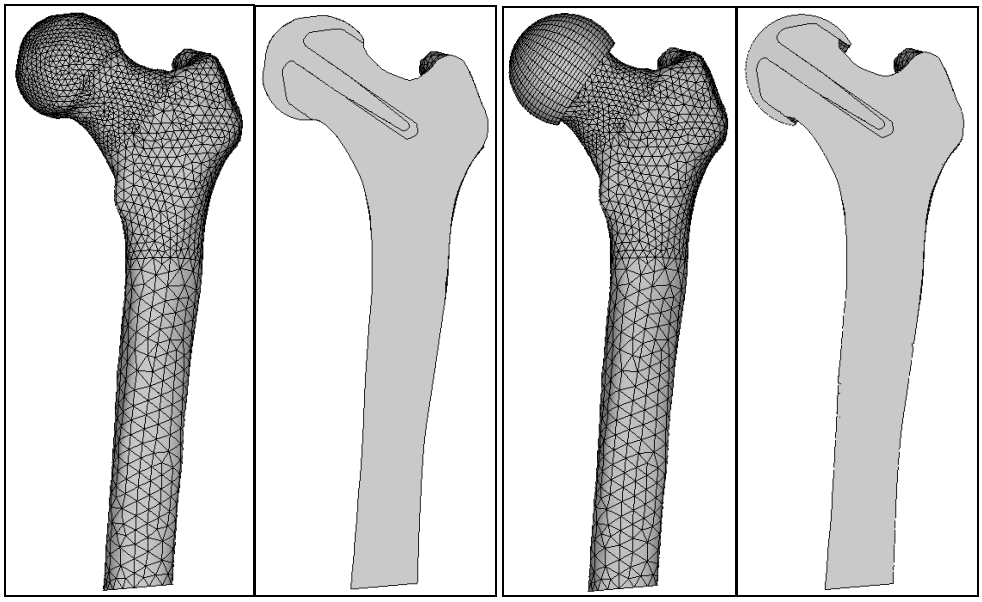

Figure 38: Full and Cross-Section Meshes of the Intact (left) and Resurfaced (right) Proximal Femur showing Partitions for the Resected Bone, Prosthesis and Stem Bore.

3.2.2 Materials Properties

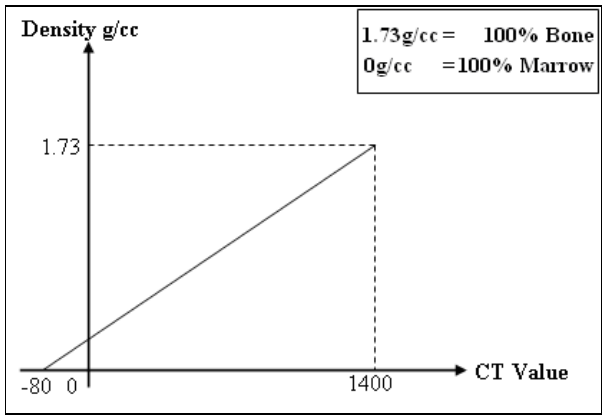

Figure 39: CT Greyscale to Bone Density Calibration Curve. Example CT Values are given, as they are specific to each scan.

Materials properties were applied to the solid elements using BoneMat freeware (Istituto Ortopedico Rizzoli di Bologna, Italy) [212], which calculates a weighted average of the greyscale values of the voxels in the CT scan corresponding with each finite element in the model. Then, the CT greyscale units were scaled into density values using a linear relationship whereby bony regions were considered to contain a mixture of mineral and marrow materials. In the absence of calibration bars of known materials in the scans, the average greyscale values of regions containing 100% marrow (the femoral canal) and 100% mineralised bone (the femoral mid-shaft cortex) were read and scaled using

corresponding relative densities of 0 and 1.73gcm^{-3} respectively to obtain the linear greyscale-density conversion function (Figure 39).

Using the density values in each element, the bone material was given linear isotropic mechanical properties. The isotropic material simplification is common in the implanted and intact femur bone modelling studies in the literature, because the determination of anisotropic materials properties is not possible using standard CT data [132]. In order to capture material orthotropy, either several directional stiffness and failure constants must be assumed, or a heterogeneous pseudo-physiological materials properties map is established through iterative remodelling from a homogeneous, isotropic initial condition [171, 172]. Both options are dependent upon human interpretation, and good correlations have been obtained between computational and experimental models without introducing these additional assumptions [128, 130, 132]. The case is similar with the assumption of linear elastic behaviour of the bone material [213]. The Young's Modulus was determined using the empirical relationship from Morgan et al [143] found by Schileo et al [144] to provide the closest correlation between FE modelling and cadaveric tests (Equation 28), and a plot of the resulting mechanical properties of the proximal femur is given in Figure 40.

$$E = 6850\rho^{1.49} \qquad \textbf{Equation 28}$$

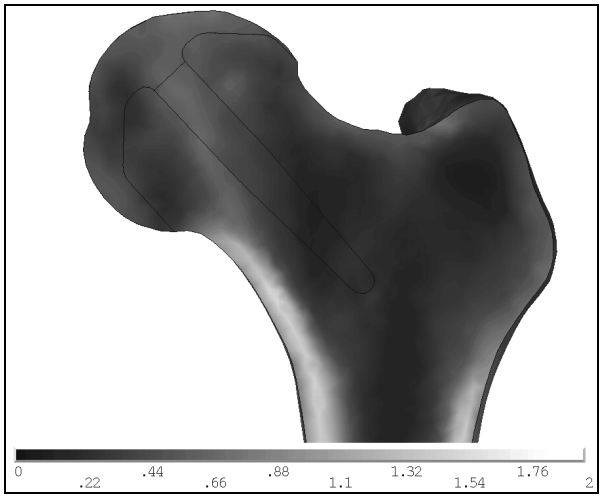

Figure 40: Contour Plot of Bone Density in the Proximal Femur Model. Units g/cm^3.

Unlike models from previous studies, no separate volume of elements was defined for the cement mantle in the implant-bone construct. Instead, a group of elements within a specified distance from the cut cancellous implant-bone interface was selected using a search algorithm, and their collective Young's moduli modified to that of PMMA bone cement (E=2.8GPa, Poisson's Ratio =0.3 [12]). This permitted a variety of cement mantle thicknesses and geometries to be simulated with the same meshed model, improving model flexibility considerably. For the variables investigated in this thesis, a single cement mantle nominal thickness of 3mm was used. This resulted in a cement mantle a minimum of 2-3 elements thick with the minimum 1.0mm thick elements in this region. By ensuring the mesh size was below the cement mantle thickness, large stiffness discontinuities were avoided which could otherwise result if excessively large, potentially cortical bone surface elements remained unselected by the search algorithm.

3.2.3 FE Model Loading and Boundary Conditions

The model of the proximal femur was loaded under stance (normal gait and stumbling) conditions as shown in Figure 41, and sideways falling conditions as shown in Figure 42, and the magnitudes and directions of joint contact forces (JCF) and muscle forces (ABD) are included in Table 4 and Table 5 respectively. Gait loading was used for the analysis of bone remodelling, and stumbling and sideways falling loads were used for the analysis of femoral neck damage initiation.

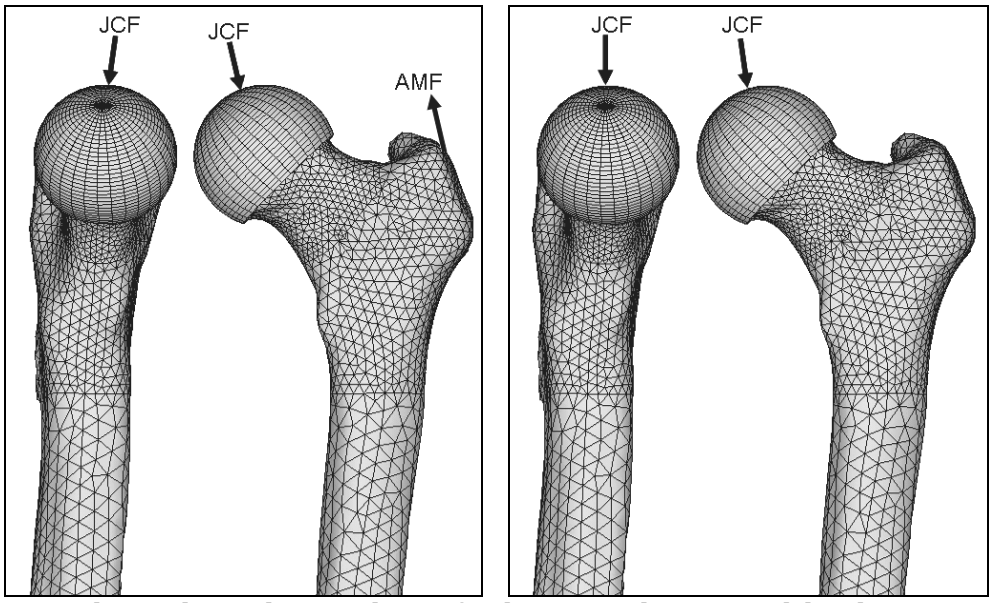

Figure 41: Loading and Boundary Conditions for the Proximal Femur Model under Stance Loading Conditions: Normal Gait (left) and Stumbling (right)

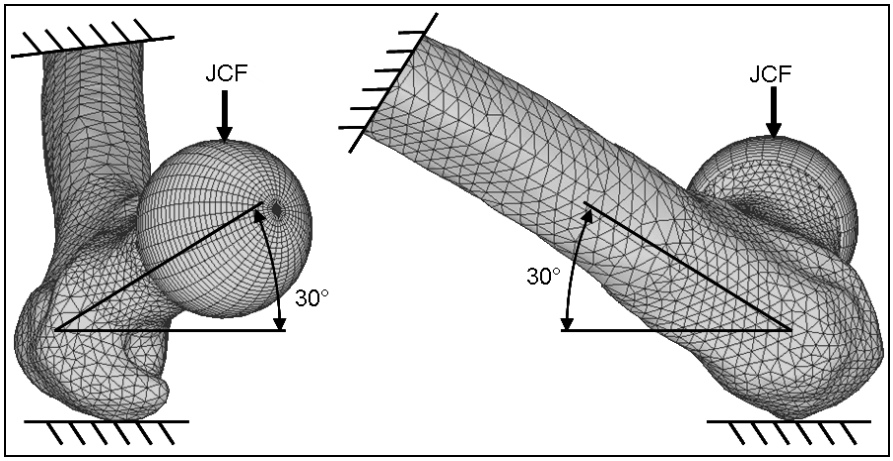

Figure 42: Loading and Boundary Conditions for the Proximal Femur Model under Traumatic Falling Loading Conditions

Table 4: Joint Contact Force Magnitudes and Directions for the Normal Gait, Stumbling and Oblique Falling Loading Scenarios Modelled

Scenario	Joint Contact Force / N	Angle in Frontal Plane	Angle in Sagittal Plane
Normal Gait	2,500	13.4°	8.2°
Stumbling	7,500	8°	0°
Falling	2,500	120° (See Literature Review)	60° to Neck (See Literature Review)

Table 5: Muscle Force Magnitudes and Directions for the Normal Gait, Stumbling and Oblique Falling Loading Scenarios Modelled

Scenario	Muscle Force / N	Angle in Frontal Plane	Angle in Sagittal Plane
Normal Gait	833	12°	0°
Stumbling	0	-	-
Falling	0	-	-

Several modelling studies have focussed purely on the boundary conditions and muscle force application on FE models of the proximal femur, discussed in the Literature Review. It was proposed that the fixation of the model should be located one-third of the length of the femur from the proximal end, relating approximately to the centroid of the adductor muscle location. Therefore the reaction forces generated at this constraint would refer implicitly to the forces applied by these muscles, and yet any strain artefacts associated with the constraints would be sufficiently far from the region of interest that they would not invalidate the bone strain and remodelling stimulus values in the region of interest.

Forces representing the joint contact and abductor muscle loads were applied to areas of nodes on the surface of the model representing the bearing contact patch and muscle attachment regions. Muscle forces were applied uniformly over the muscle attachment areas, but in the definition of the joint contact force, a non-uniformly distributed pressure was applied to the joint contact patch [12]. Using a spherical search algorithm, a circular group of nodes was selected on the surface, and a second algorithm was written to apply force to each node using a circular pressure distribution as exists in Hertzian contact mechanics [214]. The contact patch was calculated to be approximately 10mm in diameter, according to spherical Hertzian contact. The mean pressure 'P_m' was calculated using the contact force 'W' and the patch area, of radius 'a':

$$P_m = \frac{W}{\pi a^2} \qquad \textbf{Equation 29}$$

Then the maximum pressure P_0 is given as:

$$P_0 = \frac{3P_m}{2} \qquad \textbf{Equation 30}$$

Finally, the circular distribution of pressure as a function of the distance 'r' from the centre of the patch is given by:

$$P(r) = P_0\sqrt{1-\frac{r^2}{a^2}} \qquad \textbf{Equation 31}$$

The proportion of the patch surface area associated with each node in the selection was calculated, and used with its distance from the patch centre to weight its contribution to the overall contact patch force. This resulted in a discretised version of the pressure distribution shown in Figure 43.

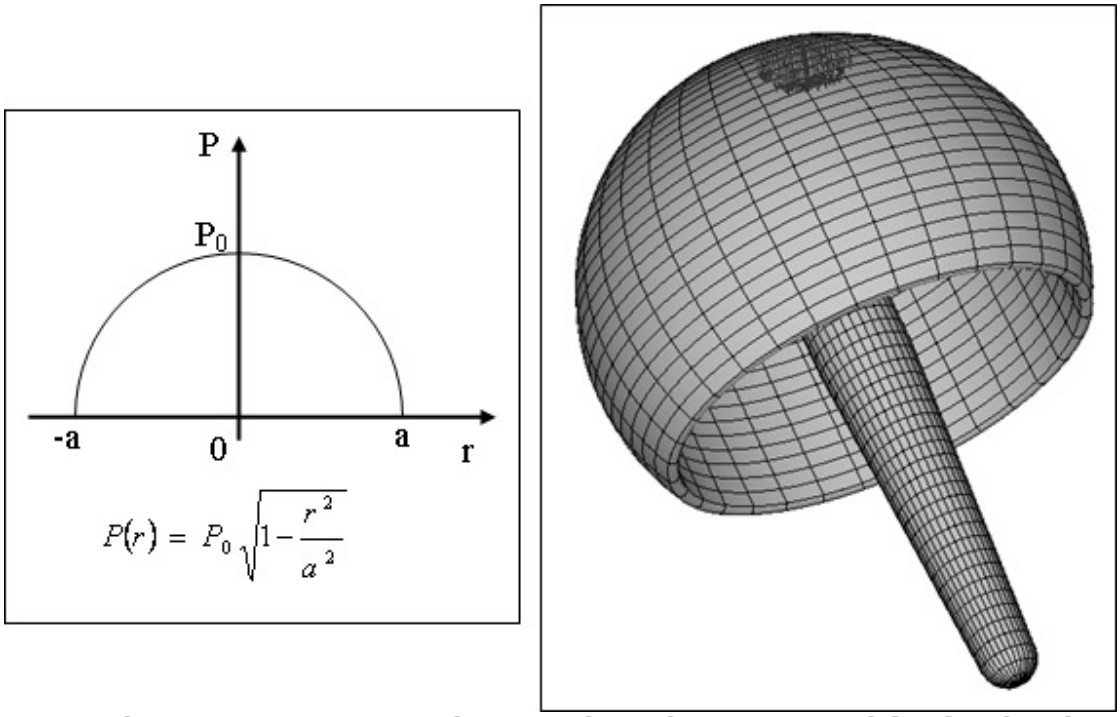

Figure 43: Circular Hertzian Pressure Distribution on the Implant Contact Patch [214], and Application to FE Model

The joint contact force alone was used in the simulation of the traumatic events, on the basis of Cristofolini et al's [126] cadaver tests and models. Their conclusion was that it is not necessary to include muscle forces explicitly when simulating fractures, as the joint contact force alone (which is generated in part by the muscle forces) is sufficient for agreement between simulated predictions and physical test results. They observed minimal local strain differences in the femoral head and proximal neck when the muscle forces were neglected, so to avoid introducing further assumptions, muscle forces were neglected from the traumatic load cases in the present study.

3.3 Model Outputs

3.3.1 Bone Fracture Analysis Method

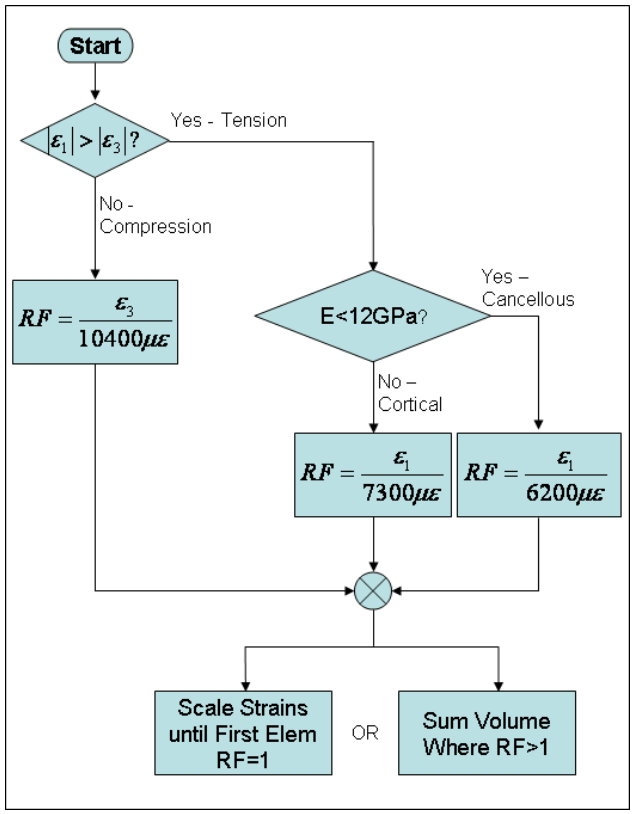

Figure 44: Flow Chart for Calculation of the Damage Initiation Load and Damaged Bone Volume at a Set Load, in an Implanted Proximal Femur

A bone fracture load analysis based on the most recent method validated by Schileo et al [130] was employed. It was judged that the most effective failure criterion was a combination of those employed in previous studies discussed in the Literature Review [128, 129, 132, 164, 165]: an asymmetric, maximum principal strain based criterion. Unlike stress, the strain approach minimises the number of assumptions required, since a separate yield strength value need not be calculated for each element. Instead, the approximately density independent yield strain of bone was exploited. Unlike Schileo et al's criterion [130] though, failure in the cortical and cancellous bone was considered, to include the possibility that following resurfacing or in a sideways fall, fracture could initiate internally rather than at the cortex. As in Schileo et al's [130] study, the risk of fracture 'RF' was calculated for each element (Figure 44). Two logical tests were used, to identify whether the bone element is primarily in tension or compression, and whether it can be treated as cancellous or cortical bone. Then its individual risk of failure was calculated as the ratio of the appropriate tensile or compressive principal strain to the

tensile or compressive yield strain (Bayraktar et al [166]). Finally, the two outputs used to analyse the femoral neck fracture risk were:

- the load at which bone yield initiated in the bone, through linear scaling of peak strains in the highest RF element in the model, and
- the volume and distribution of yielding bone for a given load, from the sum of volumes and locations of elements with RF greater than unity.

3.3.2 Pure Remodelling Bone Adaptation

The remodelling stimulus in the bone was analysed considering the pre- and post-operative cases. Strain Energy Density (SED) was used as the stimulus, being the most commonly used in the literature to date and for which all the empirically fitted remodelling parameters have been determined. Initial study was conducted statically, by considering the immediately postoperative remodelling stimulus. The remodelling stimulus distribution was observed qualitatively with FE contour plots, and the volume of bone with a stimulus exceeding the threshold value 's' (±75%, [215]) was calculated for quantitative analysis. The volume of remodelling bone predicted for a second threshold stimulus 's=±50%' was also analysed, to represent a younger patient with a higher metabolism as would be expected to receive a hip resurfacing. The ±75% value was used as the most commonly employed value in the literature for similar studies [13, 186, 203], but more recent sensitivity analysis has shown that ±60% produced the best agreement between for total hip replacement patients [216]. The ±50% value was selected as an extreme limit for young hip resurfacing patients, so that a full range was considered.

Later, dynamic adaptive models were run which predicted the progressive remodelling behaviour. Using Euler forwards integration to simulate adaptive remodelling in each element, the governing equations of the remodelling process were:

$$\begin{aligned} \rho_{n+1} &= \rho_n + a(\rho)\tau\left[S-(1-s)S_{ref}\right]\Delta t \quad && if \;\; S < (1-s)S_{ref} \\ \rho_{n+1} &= \rho_n && if \;\; (1-s)S_{ref} \le S \le (1+s)S_{ref} \\ \rho_{n+1} &= \rho_n + a(\rho)\tau\left[S-(1+s)S_{ref}\right]\Delta t \quad && if \;\; S > (1+s)S_{ref} \end{aligned}$$

Equation 32

The rate constant for remodelling 'τ_s' was 130g^{2}mm^{-2}J^{-1} per month [169]. The time step size 'Δt' was limited, to prevent inaccuracies in the progression of the solution and aid numerical convergence. The

most highly stimulated element in the model was allowed to experience a density change of 10% of the cortical bone density, or 0.173g/cm^3 [186] (Equation 33). Then a new structural analysis was run to obtain updated remodelling stimulus levels, which change as a result of the bone density adaptation:

$$\Delta t = \frac{0.173}{\left\{\tau_s a(\rho)\left[S-(1\pm s)S_{ref}\right]\right\}_{\max}}$$

Equation 33

The density of each element was limited to 1.73g/cc or 0.05g/cc, representing 100% theoretical density cortical bone and complete resorption respectively. SED stimulated remodelling was not combined with damage stimulation using the approach employed by Scannell and Prendergast [186], because preliminary study showed that with the ideal implant positioning and cement mantles modelled, strains would be below the levels reported to generate critical damage under normal gait loading (4000-10,000με [176]) within the simulation periods used. Instead, a maximum limit of the bone remodelling rate was applied for each element, calculated using a maximum lamellar bone deposition rate of 5.5μm/day [217], the element's density and Martin's surface area density function [177]. The remodelling simulation process is illustrated in flow chart form in Figure 45. The solutions were run until 24 months, according to available quantitative clinical data for corroboration of results.

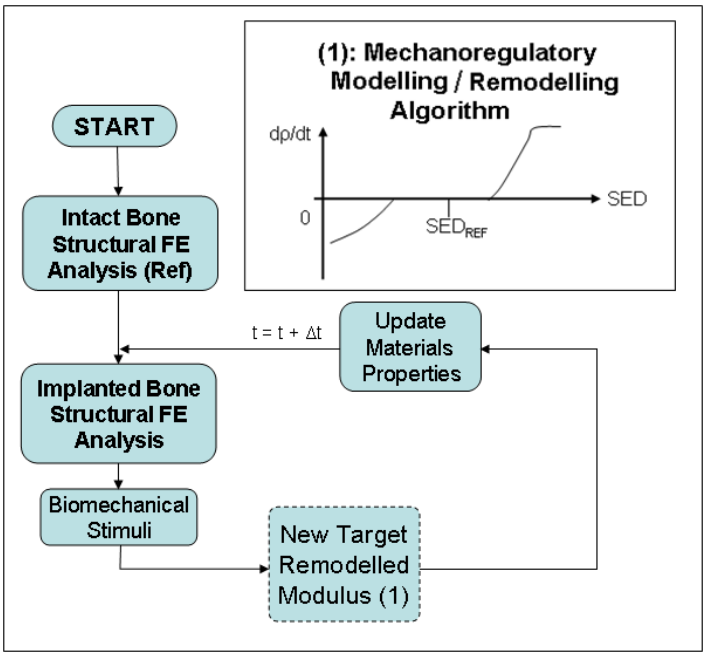

Figure 45: A Flow Chart of the Adaptive Remodelling Process

3.3.3 Combined Healing and Remodelling Bone Adaptation

Bone Healing Method

In order to assess the importance of the gradual healing of voids around the prosthesis arising from surgical cuts a healing module was added to the bone adaptation algorithm. This was based on the tissue differentiation fracture healing models produced by the Trinity College Dublin group [196, 197]. The basic quasi-static FE model of the resurfaced femur was used as the start point for the healing model, with tissue differentiation applied initially to the void around the tapering portion of the prosthesis stem. This region was map meshed like the prosthesis, with second order hexahedral elements in order to obtain high through-thickness results accuracy and allow progressive gap filling. Meshing was controlled in order to fit nominally seven elements through the thickness of the healing gap, as shown in Figure 46. Owing to the tapering shape of the void, this was necessarily reduced to a single element thickness at its proximal edge, but the most elements possible were fitted into the void thickness whilst observing element aspect ratio shape quality limits as recommended for the software used.

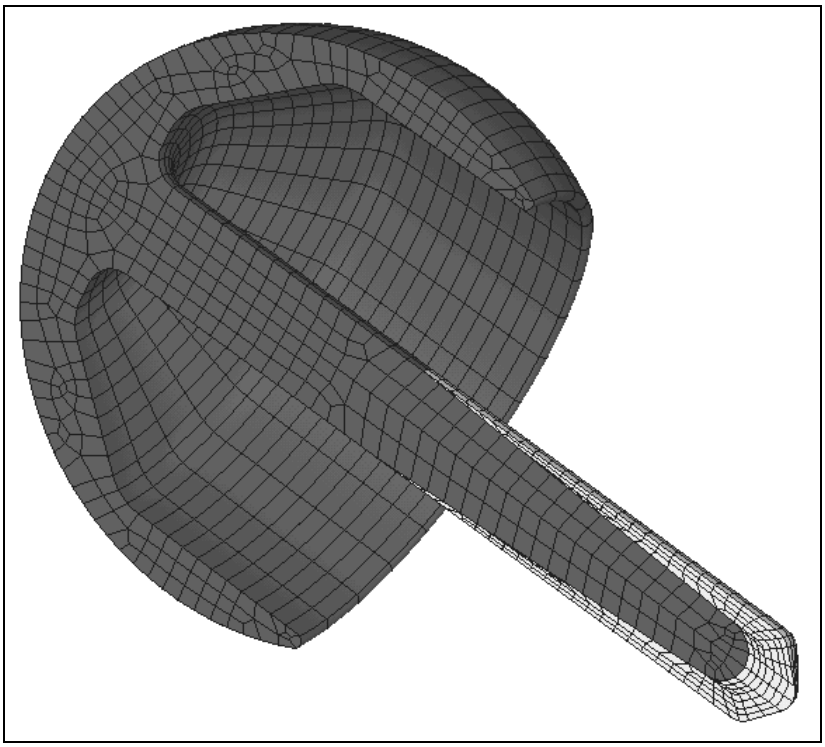

Figure 46: The Map Meshed Prosthesis and Stem-Bore Defect

First, an intact analysis was run to obtain initial reference remodelling stimulus levels. Then, iterative implanted structural analyses were run. The defect around the implant stem was filled initially

with granulation tissue which is infiltrated by mesenchymal stem cells by diffusion [197], representing the combined effects of cell migration and proliferation. The diffusion of stem cells was modelled using Equation 34, where '[c]' is the cell concentration, initially zero throughout the defect. Diffusion was driven by the percentage cell concentration in the mature bone at the cut surface, and a zero diffusion boundary condition was imposed on the surface of the implant. 'D' represents the diffusion coefficient of 2.37mm^2 per day [196, 218]. With this approach, the equilibrium cell concentration in the defect would be such that the resulting pattern of density of any bone re-filling the defect would be projected from the cut surface of the bone, which is more logical than a single, uniform density. This diffusion analysis was run iteratively with 1 day time steps.

$$\frac{d[c]}{dt} = D\nabla^2[c] \qquad \textbf{Equation 34}$$

The differentiation and maturation of these cells was then modelled using a smoothed mechanical stimulation process [197]. The differentiation of the stem cells into a target phenotype (fibroblasts, chondroblasts or osteoblasts) according to mechanical conditions was controlled using dilatational hydrostatic pressure and deviatoric equivalent strain stimuli (Table 6) from Claes and Heigele, assuming good vascularity [191]. These cells were then allowed to mature to form fibrous tissue, cartilage or bone. At each iteration, the stimulated phenotype was identified for each element and its new target modulus 'E_{n+1}' was calculated with Equation 35, by a rule of mixtures using the fractional cell concentration ($[c]/[c]^{max}$), the target tissue modulus 'E_{tissue}' and the granulation tissue modulus '$E_{granulation}$':

$$E_{n+1} = \left(\frac{[c]}{[c]^{\max}}\right)E_{tissue} + \left(\frac{[c]^{\max} - [c]}{[c]^{\max}}\right)E_{granulation} \qquad \textbf{Equation 35}$$

The E_{tissue} values are given in Table 6 [201]. The temporal smoothing of the formed tissue's modulus to give its final value '$E_{n+1,smoothed}$', was achieved by averaging the target value with the modulus values from the 9 preceding days [195], as in Equation 36:

$$E_{n+1,smoothed} = \frac{1}{10}\sum_{i=n-9}^{n+1} E_i \qquad \textbf{Equation 36}$$

and this value was used to update the structural model's mechanical properties.

Table 6: Healing Defect Tissue Phenotype Properties and Stimulus Levels [184, 188, 189, 194]

Tissue Phenotype	Young's Modulus /MPa	Strain Stimulus / %		Hydrostatic Pressure Stimulus / MPa
Granulation Tissue	1	-		-
Fibrous Tissue	2	- >5 <-5	 and and	>0.15 >-0.15 >-0.15
Cartilage	10	>15 <-15	and	<-0.15
Bone (Endochondral Ossification)	1000 (Immature) 6000 (Mature)	-15 to 15	and	<-0.15
Bone (Intramembranous Ossification)		-5 to 5	and	-0.15 to 0.15

Combined Bone Healing, Modelling and Remodelling Algorithm

The tissue differentiation defect healing module was combined with the remodelling simulation process as illustrated in flow chart form in Figure 47, in a similar method to that used by Liu and Niebur [218]. This allowed the following processes to be captured by the model:

- remodelling of mature bone,
- differentiation of stem cells in granulation tissue in the defect into mature tissue, and
- modelling of immature bone in the defect.

The remodelling process shown in Figure 45 was augmented, so that once an implanted structural analysis had been completed, the cell phenotype of each tissue element was interrogated, and either the bone remodelling adaptation process or the tissue differentiation defect healing process was applied:

- in mature bone, a remodelling step was completed to obtain the element's remodelled modulus,
- in soft tissue, a healing step was completed, to obtain the element's target tissue phenotype and modulus, and
- in immature bone, target moduli from both modelling and healing processes were obtained, and the larger value selected. The immature bone modelling process was identical to the mature bone remodelling process, except that a single reference strain value of 2000με was used, with a threshold stimulus value of s=±33% [217, 219, 220].

In soft tissue and immature bone elements, the modulus was smoothed (Equation 36). Finally, as explained earlier for numerical convergence, each element's new modulus value was compared to its value at the last structural solution. Repeated adaptation calculations were performed until the largest element modulus change in the model reached 0.173g/cc, at which point a new FE iterative loop was begun, with a new structural solution.

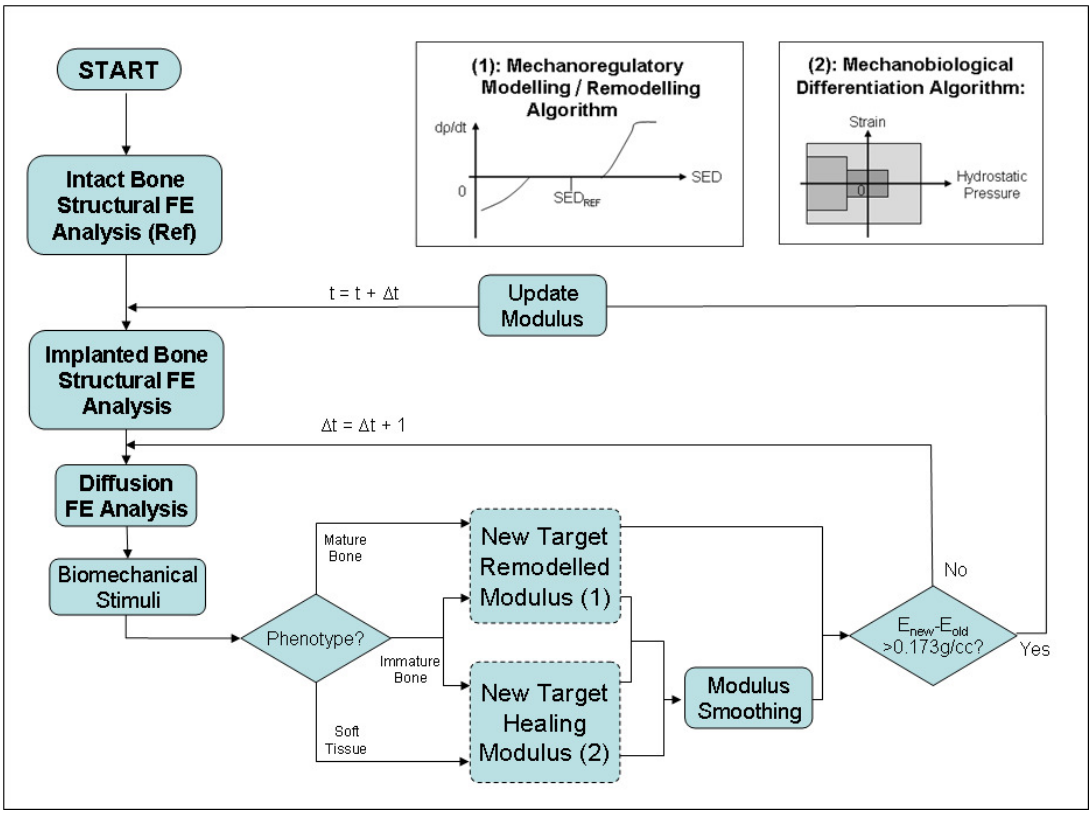

Figure 47: A Flow Chart of the Combined Adaptive Remodelling and Tissue Differentiation Process

4 VERIFICATION AND VALIDATION

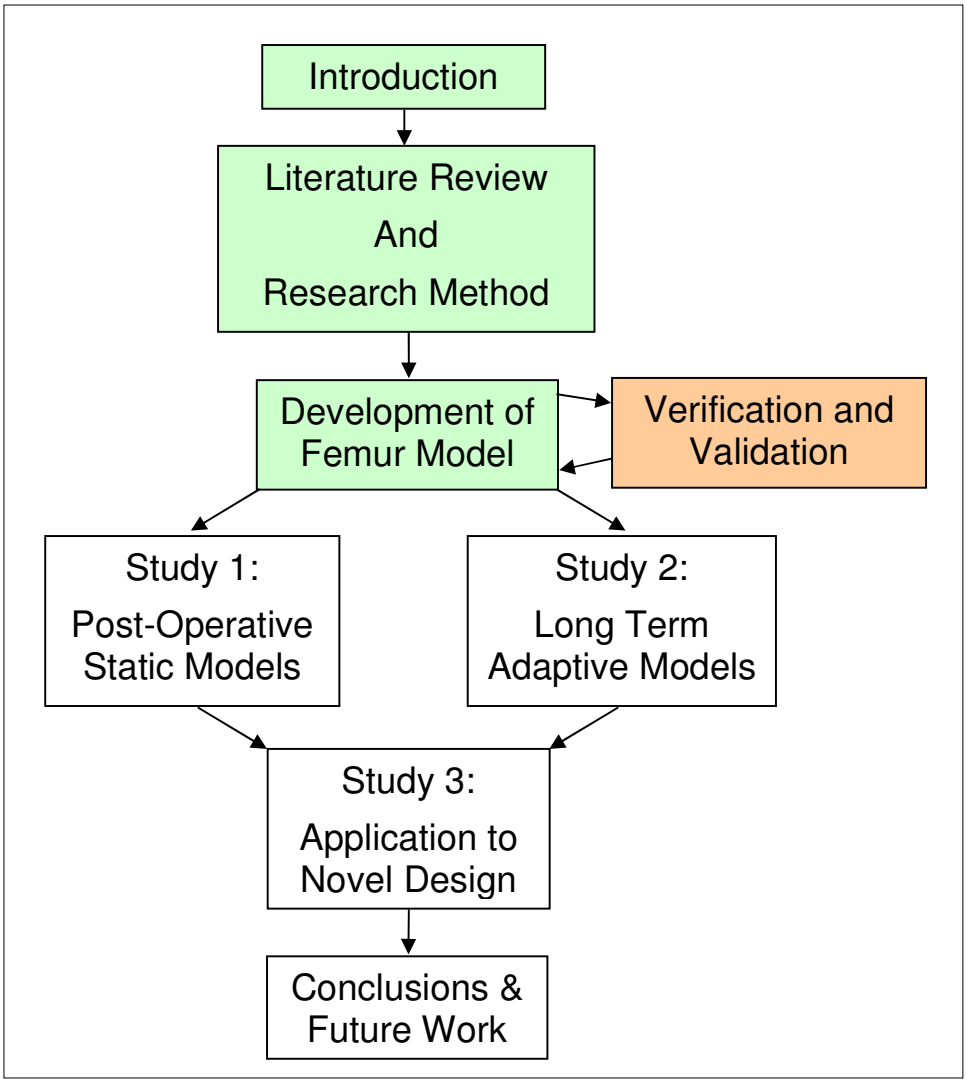

A part of the results reported in this chapter (the Digital Image Correlation model validation study) was presented at the 6th World Congress on Biomechanics, Singapore, August 2010.

This has also been accepted for publication as a journal article:

Dickinson, AS, Taylor, AC, Ozturk, H, Browne, M: *Experimental Validation of a Finite Element Analysis Model of the Proximal Femur Using Digital Image Correlation and a Composite Bone Model*. Journal of Biomechanical Engineering (Trans. ASME), 2011, IN PRESS.

4.1 Purpose

Particularly in biomechanical research, computational models are a representation of a physical theory of high complexity owing to the three dimensional geometry and loading scenarios, and inhomogeneous materials properties. It is of great importance to check that a model is 'verified and validated, and that its output is correctly interpreted before its predictions can be considered to have any clinical value' [221]. The following definitions must be considered:

- *verification:* assessment of the numerical accuracy of the model,
- *validation:* assessment of the ability of the model to replicate the intended physical scenario, and
- *output interpretation:* use of an appropriate mechanical performance or failure criterion for analysis.

Also important is:

- *corroboration:* the comparison of the results predicted by the model with other models reported in the literature, and with trends observed in clinical data.

This chapter contains details of verification checks carried out on the model before use, mechanical tests conducted for validation, and corroboration of the model's predictions.

4.2 Model Verification and Output Interpretation

There are a set of checks which can be made to verify an FE simulation, including mesh convergence analysis, assessment of convergence tolerances of non-linear simulations, and consideration of the individual sources of model nonlinearity, for instance, contact penetration. With regard to output interpretation, considerable experience with the selection of appropriate simulation outputs has been reported in the literature, specifically relating to biomechanical phenomena such as failure criteria for bone fracture, and stimuli for tissue adaptation and differentiation. The discussion of output interpretation was covered in the Methods and Materials section, and two verification tests are discussed in detail here:

4.2.1.1 Mesh Convergence Analysis

A mesh convergence analysis was conducted to verify the model, by meshing the femur using four different mesh density maps (Figure 48) with first and second order elements. The results are shown in Figure 49, using the internal bone fracture metric of the percentage volume of bone exceeding the yield strain: a second order criterion (strain related) was used as a more strict convergence indication than a first order criterion, such as deflection. Furthermore, given the number of interfaces in the model, peak stresses in the bone are treated with caution so a convergence criterion linked to the *distribution* of strain was used.

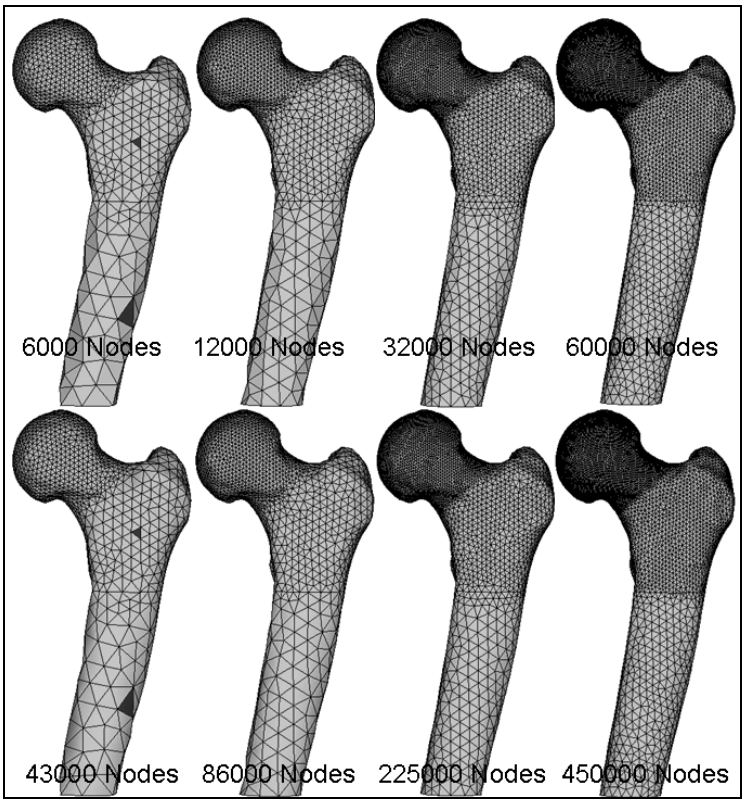

Figure 48: Four Mesh Density Verification Models featuring Approx. 6000 to 450,000 Nodes.

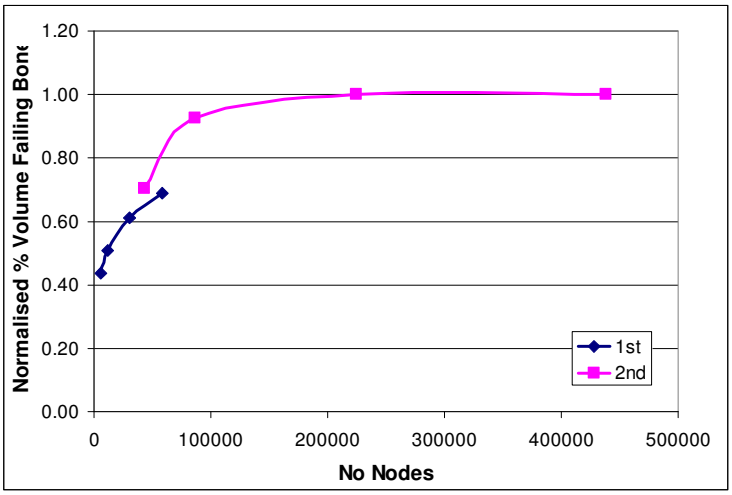

Figure 49: Mesh Refinement Verification Study. The effect of the Number of Nodes Defined, and the Mesh Type (1st or 2nd Order) on the Normalised Percentage Volume of Bone Exceeding Yield Strain.

A second order mesh with approximately 170,000 nodes was chosen. These models required approximately 2.5 - 5 hours solution time on a Viglen VIG397M workstation using an Intel Pentium III processor and 8GB RAM, running Windows x64.

4.2.2 Materials Properties Convergence Analysis

Further model verification was conducted by analysing the sensitivity of the materials properties definition. BoneMat software permits control of the number of materials properties which are used to represent the model, by definition of the minimum Young's Modulus increment between successive materials. Six models of the intact femur were solved, based on the mesh of verified density, and containing between 6 and 1715 materials properties (Figure 50). This was controlled by setting the minimum Young's Modulus increment between 5GPa and 10MPa. The results are given in Figure 51, and it was identified that the model outputs of the maximum defined Young's Modulus, peak von Mises stress and peak deflection all changed by less than 1% once 200 materials properties were used, which resulted from a minimum Young's Modulus increment of 100MPa.

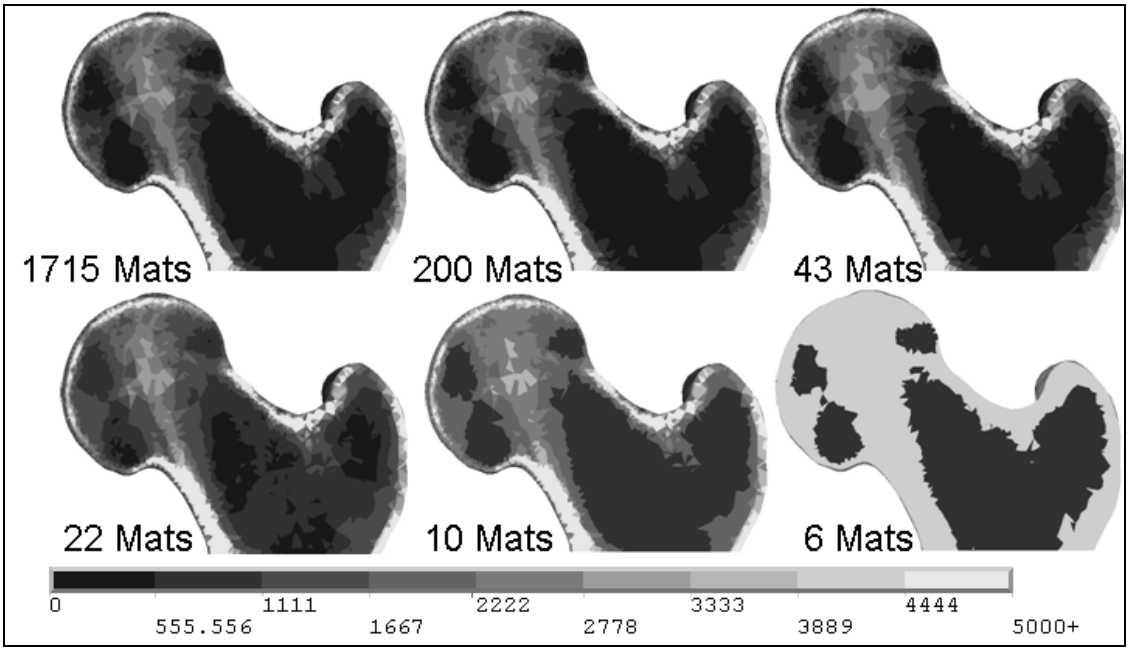

Figure 50: Six Materials Properties Verification Study Models featuring 6 to 1715 Materials. Plot shows Young's Modulus, units MPa.

In this case the peak values of the convergence criteria were used, as a stricter test. This was possible because the intact femur model was used, which features fewer interfaces than the implanted model, and therefore is less likely to feature interface stress or strain artefacts. The peak von Mises strain was used as the second order result criterion in addition to the Deflection, and the directly defined Young's Modulus.

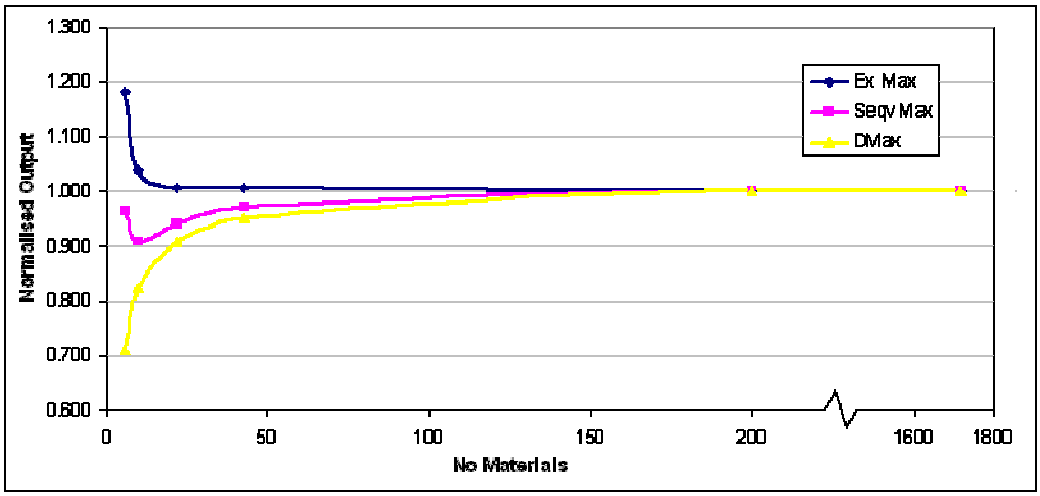

Figure 51: Materials Properties Verification Study. The effect of the Number of Materials Defined on the normalised outputs of Maximum Young's Modulus (Ex Max), Peak von Mises Stress (Seqv Max) and the Peak Deflection (DMax).

4.3 Model Validation

Complete proof or validation of any physical or mathematical theory is rarely achieved. Owing to inter-patient variability, the huge complexity of the *in-vivo* situation, and the ethical constraints of *in-vivo* experimentation, this is particularly difficult in biomechanical simulations. The validity of a model must still be assessed, and corroboration with clinical data is the default check to perform upon the predictions obtained from biomechanical FE models. This is a top–down approach, considering the final outputs of the model, so it is difficult to identify the source of any invalidity. To this end, a bottom–up approach may be preferable, which identifies the suitability of each stage of the modelling process. The main steps in the FE modelling process described previously which require comprehensive experimental validation are the processes of generating the model from the CT scan of a bone through image segmentation, CAD reconstruction and FE meshing. Furthermore, provided that an adequate set of boundary and loading conditions have been selected, the application of these loads to the model can be verified with a physical experiment. The purpose of the study reported here was to validate aspects of the FE model generation and solution process using a composite replica femur model, to give additional confidence in the model's predictions.

4.3.1 Experimental Validation Methods

For the validation of an FE model with mechanical testing, several strain measurement techniques are available. The most common is strain gauging, which has been used in several biomechanical model FE validation studies [144, 222, 223] and has the advantage of high accuracy when correctly attached to the specimen's surface, but the disadvantage of giving only discreet point strain measurements. This is a clear limitation in biomechanical modelling, where amorphous geometry and material inhomogeneity often lead to considerable strain variation across a structure.

To obtain strain data over a whole surface, photoelasticity [224] was the first established technique, which takes advantage of 'birefringence', whereby the refractive index of a transparent material changes under the application of strain, in proportion to the strain magnitude. A scale model of the structure of interest is produced from a photoelastic material, and plane polarised light is shone through it. The light is resolved into two waves by the strained material, parallel to the first and second principal strain directions, whose differing magnitudes cause the material to refract the two waves by

different amounts. This results in a phase shift, so that when the waves are combined they interfere, producing a fringe pattern which indicates the strain state, and the fringe packing indicates the strain magnitude. This has the advantage of producing field data on the surface of a structure, but the disadvantages that it requires a replica structure to be produced using a photoelastic material, and is best applied to planar structures experiencing plane stress conditions. For the application in question, bone is neither photoelastic nor a planar structure, so simplifying the structure to a planar model representation made from a homogeneous photoelastic material would make it very difficult to relate to the clinical situation. Reflection photoelasticity is an alternative method where a photoelastic coating is applied to a reflective specimen, permitting real components to be tested, but this technique is best suited to stiff, metallic structures and is intolerant to specimen curvature.

More recently, Digital Image Correlation (DIC) has been developed as an alternative approach which yields field strain data on the surface of a specimen [225, 226], providing high resolution strain magnitude and direction data, with greater tolerance to specimen curvature. DIC is an optical process, whereby the region of interest of a specimen is coated with a high contrast, random speckle pattern which is observed throughout a loading cycle using one or more digital cameras. Software is then used to calculate the absolute and relative displacements of 'facets', or square groups of pixels containing characteristic points in the speckle pattern, which are then used to calculate the loaded structure's deformation and, with comparison to an unloaded reference reading, its strain. Use of multiple cameras permits calculation of deformation and strain in three dimensions. The principle is shown in Figure 52.

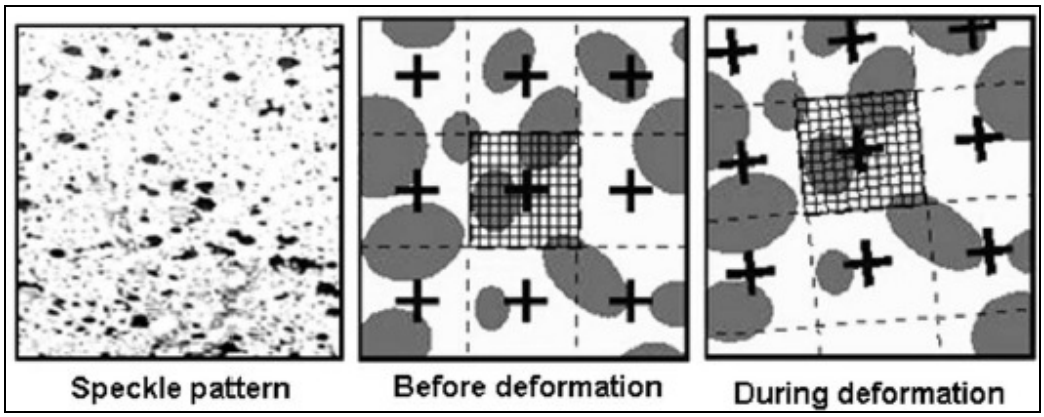

Figure 52: The Digital Image Correlation Process showing a Macroscopic Speckle Pattern and Tracking a Facet of Pixels through a range of Deformation [227]

To obtain truly full field strain measurements- within the three dimensional body of a structure- Digital Volume Correlation (DVC) can be used. This involves similar calculations to DIC, but uses voxels on a CT scan of a specimen and tracks reference features in its microstructure, such as that in trabecular bone. This method may afford the highest resolution data, and permits strain measurement for material internal to 3D structures, but the process is expensive and requires the specimen to be mechanically tested within a micro-CT scanner. This was possible for small scale trabecular bone specimens [228, 229] but infeasible for whole bone structures using the equipment available at the time of writing.

Two methods were selected for experimental validation testing of the model generation process: the gross deflection of the structure was measured with a dial gauge, and the surface strains were measured using digital image correlation.

4.3.2 Validation Methodology

For the purposes of cost, availability and reproducibility, the modelling process validation tests employed a 'Sawbone' composite replica femur (Sawbone AB, Malmö, Sweden). The replica femur was loaded and measurements of displacements and strains were obtained, for comparison to predictions from an FE simulation of the test, conducted prior to the test to avoid experimental bias:

Finite Element Analysis Methodology

A CT scan of the Sawbone was obtained and used to produce a structural FE model using the same process of segmentation, solid model generation and finite element meshing as applied in the main study models using clinical CT scans. The only departure from that technique was that the materials properties were applied explicitly, as the stiffness of the cortical and cancellous materials used in the Sawbone are essentially homogeneous and reported by the manufacturer.

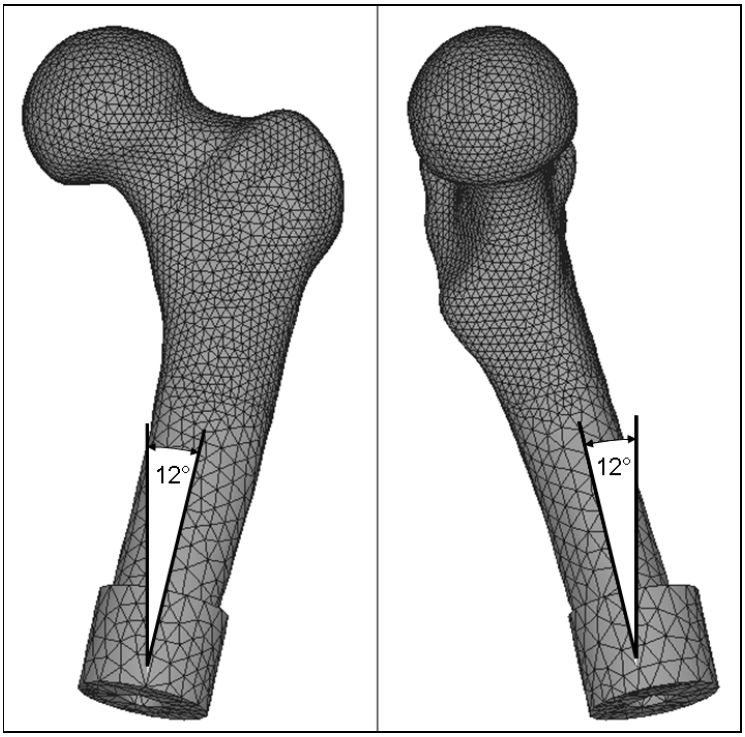

Figure 53: The Proximal Sawbone FE Model Geometry and Mesh

Figure 53 shows the geometry and mesh of the Sawbone FE model. The Sawbone was modelled as sectioned and fixed at a level 1/3 of the diaphyseal length below the greater trochanter in a block of PMMA resin, aligned so that the bone's mechanical axis was oriented with 12° of flexion and 12° of adduction. This represents an approximation of the combined angles of orientation of the femur and joint contact force (JCF) vector in gait [125], rotated in 3D space so that the JCF vector was aligned with the vertical, as in mechanical testing described later. A 1200N joint contact force was applied to a 20mm radius circular patch of nodes on the femoral head, and a 400N abductor muscle force to a triangular patch of nodes on the greater trochanter, both aligned with the local vertical direction. Material properties were obtained from the manufacturers of the Sawbone and the Technovit 3040 PMMA cement (Heraeus Kulzer GmbH, Germany) and applied to the model explicitly: Young's Modulus values of 16.35GPa and 0.145GPa were used for the cortical and cancellous bone materials respectively [230], along with 2.15GPa for the PMMA [231].

Mechanical Test Methodology

The FE model scenario was reproduced in a physical test. The level of 1/3 of the diaphyseal length of the Sawbone femur was measured below the greater trochanter for the constrained height, and a cut was made 30mm lower, using a custom made jig to ensure reproducible cut position and orientation (Figure 54).

Figure 54: Sawbone Cutting Guide

The bone was then mounted in PMMA to a depth of 30mm, in an aluminium cylinder with a key-way to prevent rotation of the bone under load. The mounted Sawbone is shown in Figure 55, with a lever system attached to the femoral head and greater trochanter, so that a single axis actuator could be used to apply joint contact and abductor muscle forces. Femoral head and greater trochanter interface components were manufactured using rapid prototyping from the CAD model of the Sawbone so that the face in contact with the Sawbone matched its amorphous geometry. The joint contact pad rested on the femoral head, but the greater trochanter pad was attached to the Sawbone with 2-part epoxy adhesive and three screws. The lever arm was designed such that it applied a 3:-1 ratio of joint contact to abductor muscle force; for example, applying 800N to the lever arm would exert 1200N on the femoral head, and 400N upwards on the greater trochanter.

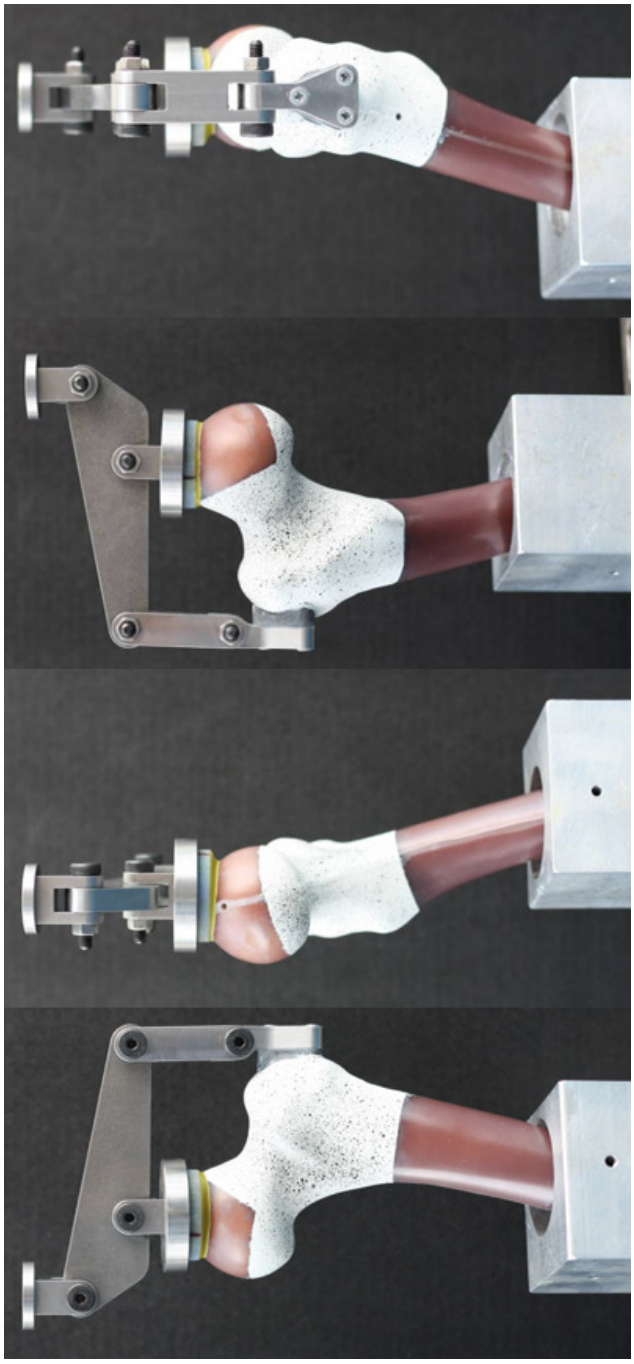

Figure 55: The Cut, Potted, Aligned Sawbone with Joint Contact / Abductor Muscle Loading Lever Arm Attached. Lateral, Posterior, Medial and Anterior Views (top – bottom).

For the DIC strain measurements, a pattern was applied with matt spray paint to a measurement zone on the proximal femur as shown in Figure 55, above the lesser trochanter. The pattern consisted of speckles up to a maximum of 1mm in diameter in a random distribution of size and location. A magnified image of the speckle pattern is given in Figure 56.

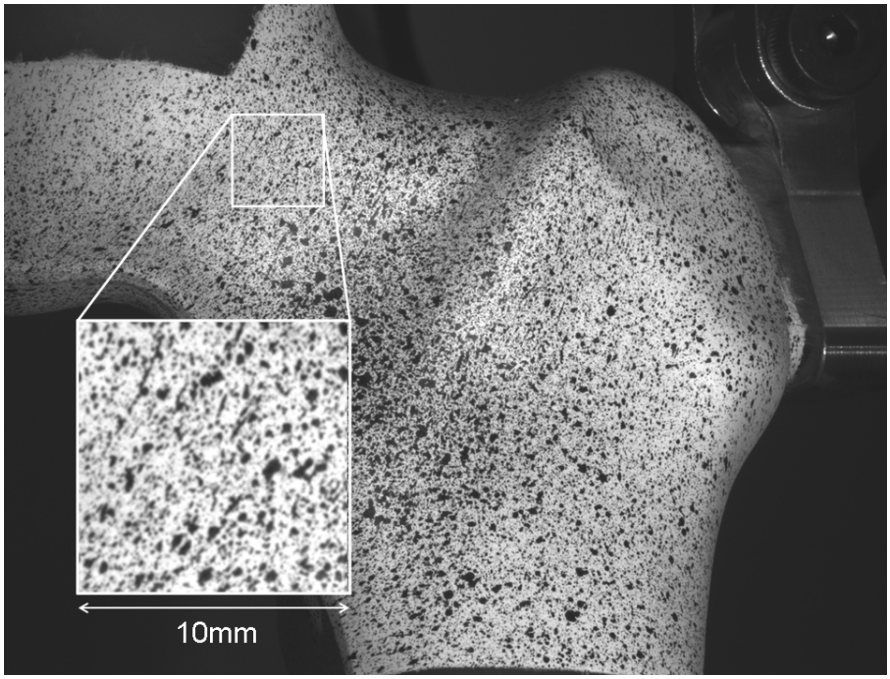

Figure 56: Digital Image Correlation Speckle Pattern

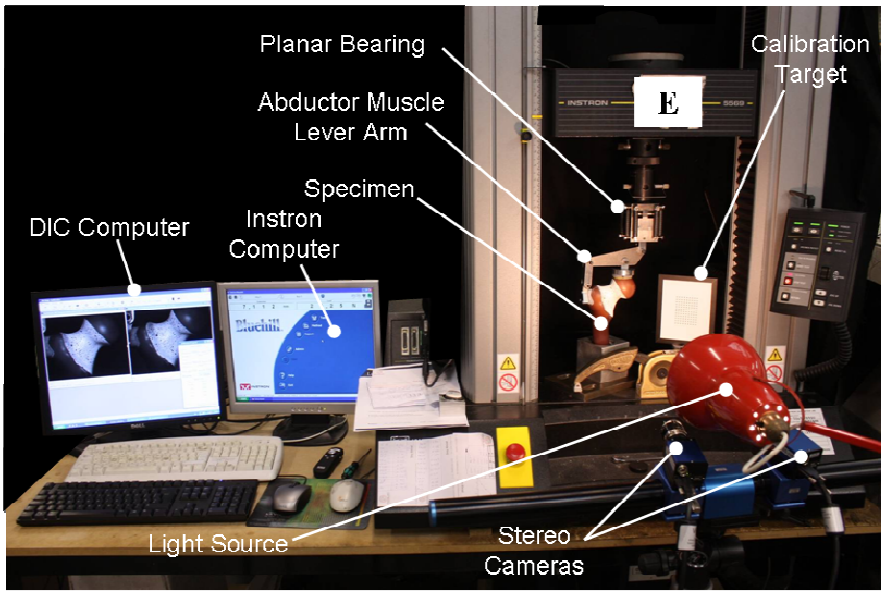

Figure 57: The DIC/Mechanical Test Experimental Setup

The Sawbone and loading jig were attached to an Instron 5569 Electromechanical axial test machine (Instron, Norwood MA, USA) with a ±2kN load cell and driven by Bluehill Software. The DIC test setup comprised dual 2MP digital cameras (Limess GmbH, Germany) fitted with Xenoplan f2.0/28 lenses (Schneider Optik, Kreuznach, Germany), and a desktop PC running VIC3D Software (Correlated Solutions Inc., USA). Figure 57 shows the experimental setup for the mechanical test specimen on the

test machine and the DIC equipment. The cameras were positioned at a distance of 330mm from the specimen, giving a pixel size of 0.059mm, and therefore the approximate minimum reliably visible speckle size of 0.1mm (2x2 pixels). In order to maximise the measurement sensitivity with minimal experimental error, the system was set up to minimise measurement noise. The specimen was lit so as to allow a 12.5ms exposure at f5.6 aperture opening, to give an optimal balance of exposure quality, contrast and depth of focussed field, determined in preliminary testing.

The strain was measured over three views of the model: anterior, posterior and medial. Two tests were conducted for each view:

- first, five repeated unloaded datasets were collected, for which the theoretically calculated strain would be zero. Therefore, any non-zero calculated strain would provide a measure of the sensitivity of the testing method (experimental error).
- second, five repeated datasets were collected for each view with the model unloaded, and then loaded with 500N, 750N, 1000N and 1200N joint contact forces. The repeat measurements would provide a measure of the variability of the testing method (experimental uncertainty). The FE strain data was down-scaled linearly to these applied loads for direct comparison. The strain was recorded in twenty-five 5mm^2 virtual strain gauges (Figure 58). In total, 625 data points were used to assess correlation (five repeats x twenty five strain readings x five loads).

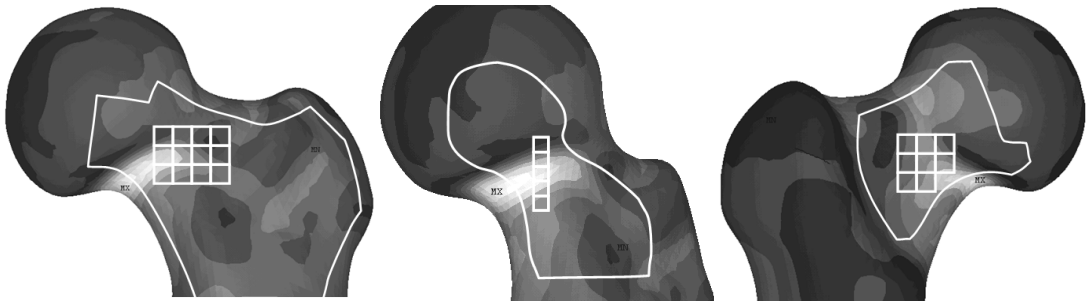

Figure 58: Measurement Gauge Areas

Finally, as a definitive test of model deformation, the deflection of the femoral head was measured under load using a dial gauge (Mitutoyo 2050-08, Mitutoyo Measurements, Japan). As shown in Figure 59, the dial gauge was mounted to the base plate of the specimen holder so that additional deformations of the surrounding test equipment were removed from the measurement, allowing direct comparison with the predicted deflection from the FE model.

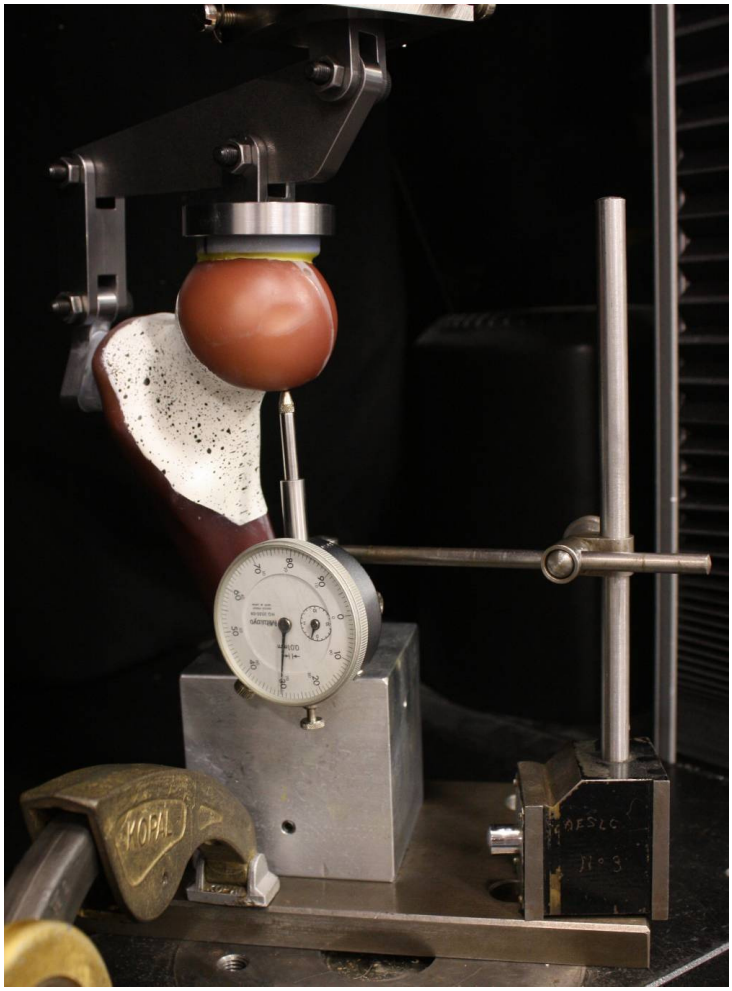

Figure 59: Measurement of Femoral Head Deflection under Load with a Dial Gauge

4.3.3 Validation Results and Discussion

First, to quantify the DIC strain measurement sensitivity, five unloaded measurements were taken and used to calculate the strain (theoretically zero), for each of the three views, and the resulting strain contour plots are included in Figure 60. The peak computed strain values are included in Table 7, both for the whole measurement area (overall peak value) and in the centre of the measurement area (based on five virtual strain gauge areas, mean plus three standard deviations), as it was observed that the highest magnitude error measurements occurred at the edges of the area of interest. This was attributed to the measurement discontinuity at the edge of the area of interest, in addition to the curvature of the specimen surface, as the errors were seen to be highest in the more curved medial and posterior faces.

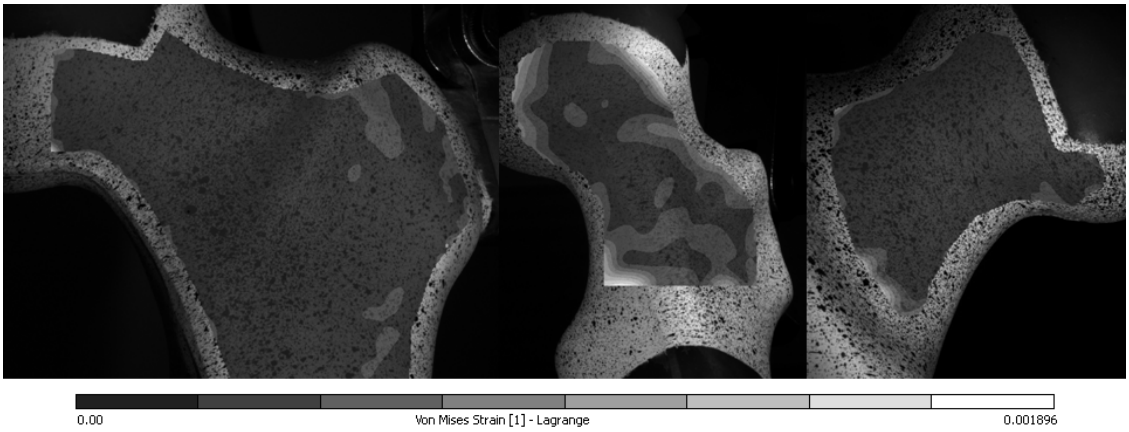

Figure 60: Strain Measurements in the Unloaded Sawbone in Anterior (left), Medial (centre) and Posterior (right) Views. Worst Measurements from Five are shown.

	View		
Strain Measurement Sensitivity	**Anterior**	**Medial**	**Posterior**
Peak Strain Error, Edge of Measurement Area	<±1250με	<±2250με	<±1100με
Maximum Six Sigma (Mean + Three S.D.) Error Values, Centre of Measurement Area	±110με	±360με	±140με

Table 7: DIC Strain Measurement Sensitivity Values

These worst case sensitivity and measurements on the medial surface are in line with values reported in the nearest comparable study in the literature [10] which quoted an error standard deviation of 300με, and considerably smaller than values reported for microstructure-scale studies [13,14]. The values for the less curved anterior and posterior surfaces are in line with the sensitivity quoted by the manufacturer, of 200με. Under 1200N the FE model predicted that the peak von Mises strain on the cortical surface was ~1900με at the inferior femoral head-neck junction, indicating that the measurement sensitivity and reproducibility were sufficient for this experimental setup, with the most reliable data on the anterior surface.

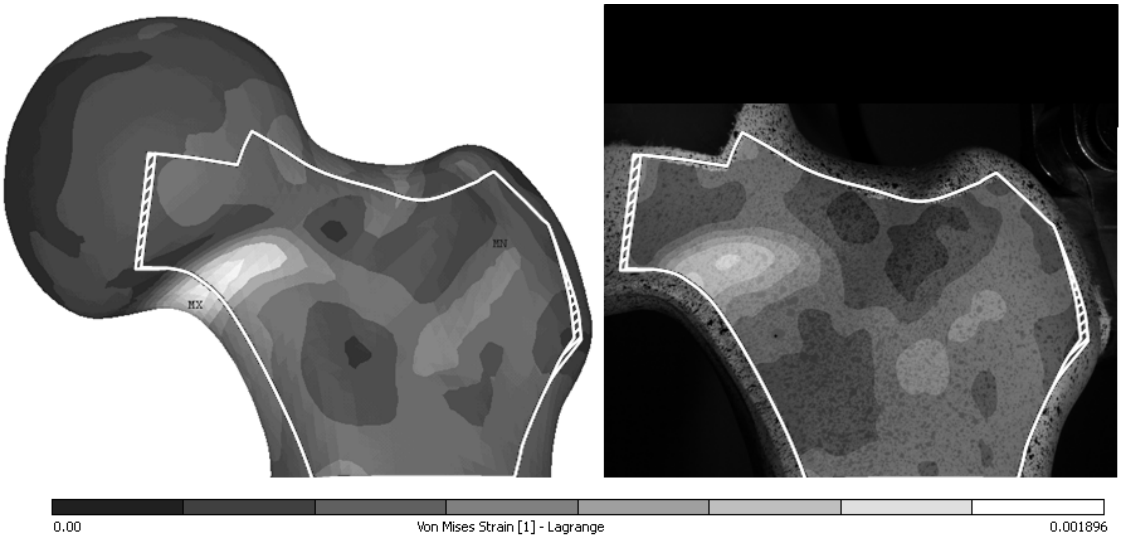

Figure 61: Finite Element Predicted (left) and DIC Measured (right) von Mises Strain on the Anterior Femoral Neck Surface. 1200N Joint Contact Force, 400N Abductor Muscle Force. High Error Regions Cross-Hatched.

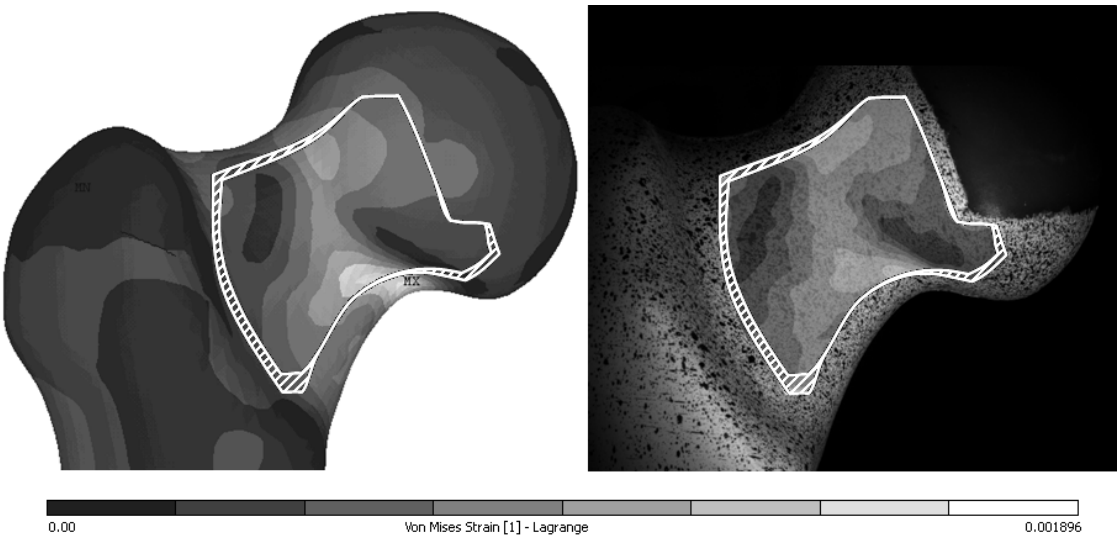

Figure 62: Finite Element Predicted (left) and DIC Measured (right) von Mises Strain on the Posterior Femoral Neck Surface. 1200N Joint Contact Force, 400N Abductor Muscle Force. High Error Regions Cross-Hatched.

Qualitatively, the measured strain patterns on the femoral neck were very similar to computational predictions. Figure 61, Figure 62 and Figure 63 show the FE predicted and DIC measured von Mises strains on the anterior, posterior and medial femoral neck surfaces respectively, allowing qualitative comparison. The contour magnitude scaling is the same for the two techniques, and the contour colours from the FE and DIC softwares are matched as closely as possible.

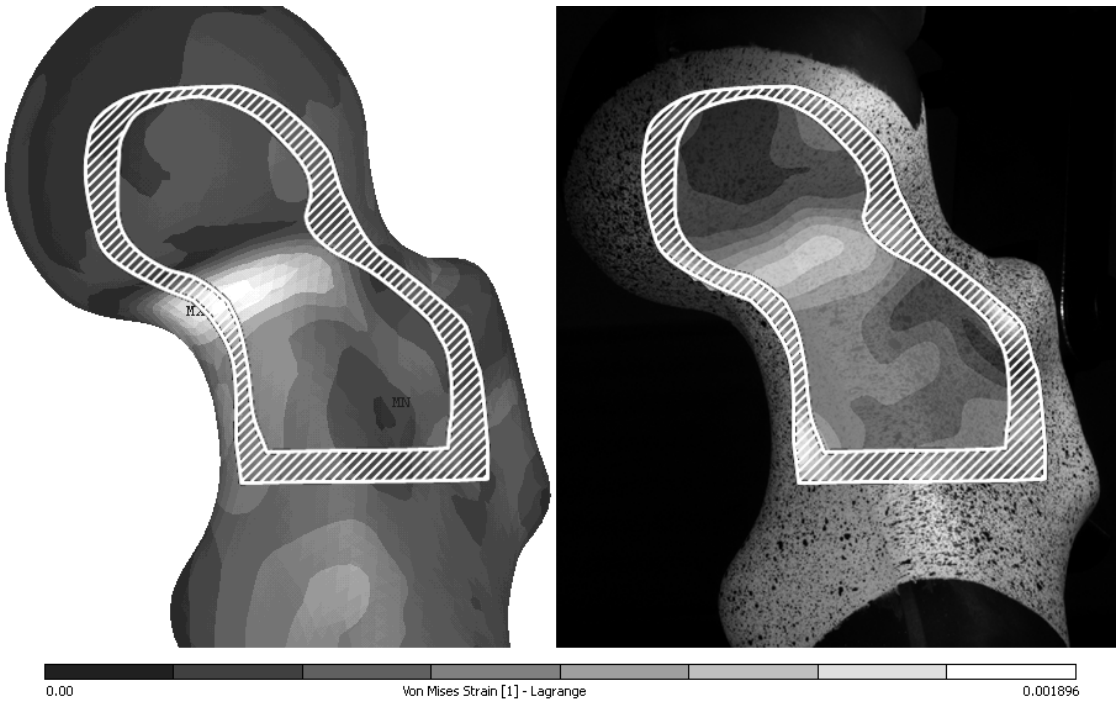

Figure 63: Finite Element Predicted (left) and DIC Measured (right) von Mises Strain on the Medial Femoral Neck Surface. 1200N Joint Contact Force, 400N Abductor Muscle Force. High Error Regions Cross-Hatched.

Cross-hatched zones on the plots indicate the region around the edge of the gauge area where the experimental error was highest, owing to specimen surface curvature. On the medial plot, it was harder to obtain clear DIC strain readings, particularly around the highly curved femoral head-neck junction and the edges of the gauge area where the viewing direction of the cameras was the most acute, but the overall pattern still corroborated the FE prediction.

In terms of quantitative analysis, first the gross deflections predicted by the FE model were compared to those measured in the test using the dial gauge, which resulted in the excellent agreement of a linear regression slope of 0.97 (D_{Test}:D_{FE}) and an R-Squared correlation value of 0.998. The reproducibility of the strain measurements was assessed by finding the standard deviation of the measurements averaged across the virtual strain gauge regions (Table 8). Quantified comparison between the two techniques was assessed by plotting the data on a scatter graph and fitting a linear trend by least squares regression.

The two techniques were in good agreement. Considering all the data, there was a linear regression slope of 0.90 (ε_{DIC}:ε_{FE}) and an R^2 correlation value of 0.86 between the simulation and the tests. For the anterior surface data alone, the agreement improved to give a regression slope of 0.93 and an R^2 correlation value of 0.92. The correlation was still clear despite the worst case of experimental errors, on the high curvature medial surface, for which the data displayed an R^2 correlation value of 0.83. The regression plot for the full dataset is shown in Figure 64. As the data in Table 7 and Table 8 suggest, the measurement error was up to three times as high for the medial face and intra-measurement variability was up to 4 times higher on the medial surface than the anterior and posterior surfaces, owing to its much higher curvature and strain gradient. In addition, the strain measurements obtained from the posterior surface were of lower magnitude and therefore had a lower signal:noise ratio, which explains the higher degree of scatter for the lower magnitude strain points on the regression plots. Therefore there was most confidence in the anterior data, so a regression plot was produced using the data from the anterior surface alone (Figure 65).

	View		
Measurement Repeatability Values for Three Faces. Averaged across All Gauge Areas	**Anterior**	**Medial**	**Posterior**
Standard Deviation	**±**15.9με	**±**68.7με	**±**22.3με
Six Sigma (3 S.D.)	**±**47.7με	**±**206με	**±**66.9με

Table 8: DIC Strain Measurement Reproducibility Values

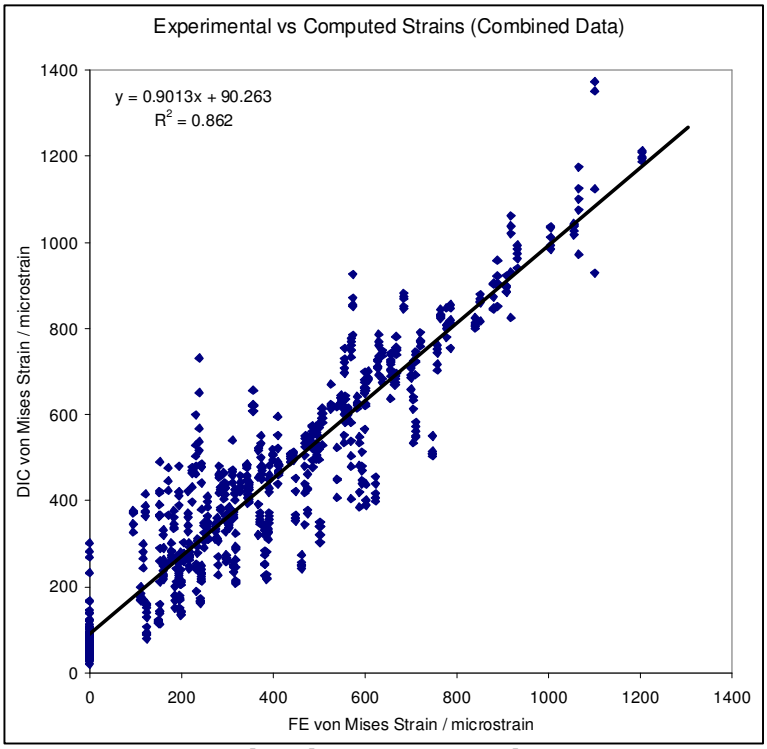

Figure 64: FE Predicted vs DIC Measured von Mises Strain. 625 Data Points (25 Gauge Areas x 5 Loads x 5 Repeats)

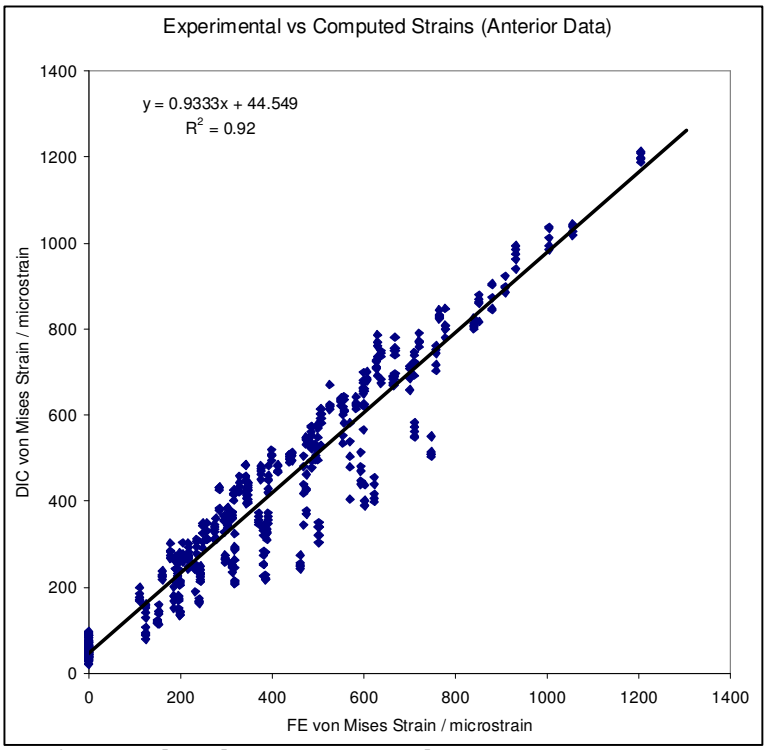

Figure 65: FE Predicted vs DIC Measured von Mises Strain. Anterior Data. 300 Data Points (12 Anterior Gauge Areas x 5 Loads x 5 Repeats)

The regression slopes showed good agreement, but indicate that the DIC technique may underestimate peak strains, particularly in high strain gradient regions owing to its spatial resolution. This is supported by the closer one-to-one agreement on the anterior surface than on the high curvature, high strain gradient medial surface. Possible solutions are discussed below.

The correlations achieved using DIC were in a similar range to reported values from the cited strain gauging studies from the literature [144, 222, 223], where R^2 correlation values of 0.89-0.91 were quoted. However, the DIC technique provided full field strain data compared to the discreet point data obtainable from strain gauging, and is potentially easier to use. Limitations of the DIC technique employed in this study included lower results accuracy on the high curvature medial femoral neck surface, and the necessity to use von Mises equivalent strains in the analysis, whereas the cited strain gauge studies [144, 222, 223] analysed principal strains. The experimental technique used in this study generated principal strains in two dimensions which could not be directly compared with the three dimensional principal strain data produced by the finite element model, other than for peak values. However, patterns of tensile and compressive strains from the two techniques were observed to be in qualitative agreement, and a clear quantitative correlation was confirmed using equivalent strain. Furthermore, the use of equivalent strain gives a non-zero axis intersection on the experimental vs. computational data correlation plots (Figure 64 and Figure 65) which graphically indicates the experimental error more clearly than principal strain plots would.

Where high gradient peak strains are missed due to measurement resolution, accuracy would be improved using a finer speckle pattern and a shorter camera-specimen distance. Additional non-planar cameras would resolve accuracy problems in regions of high curvature. Where apparatus is limited to two cameras, the main regions of strain concentration could be identified with measurements on a global view of the region of interest, followed up with more precise measurements taken close-up and using a finer speckle pattern, in this example at the medial femoral head-neck junction.

A possible general limitation of the DIC technique in the testing of tissue specimens is that it may be difficult to apply the speckle coating, upon which the results resolution and accuracy is highly dependent. However, this was achieved successfully in a much smaller, murine scenario by Sztefek et al

[227] and through careful preparation of the samples, they achieved similar sensitivity and repeatability measurements to those obtained with the ideal, clean, smooth, non porous composite bone in this study.

The main limitation of this section of the study is that assumptions still remain in the model generation process of materials properties assignment and model loading and boundary conditions. A particular source of inaccuracy in the model is the definition of the materials properties, which this experimental study neglects. These results act to validate the overall study model's geometry and meshing processes, and the application of the finite element solution method. Since the adaptive bone remodelling predictions obtained from the model in question were produced on a pre-operative to post-operative comparative basis, the effects of loading and materials properties assumptions may be reduced. With validation of the model generation process comes some confidence in the simulation's results. However, validation of the materials properties assignment by repeating the experiment using a cadaveric femur is an important extension of this work.

4.3.4 Validation Conclusion

Digital image correlation has proven value for strain measurement in biomechanical scenarios and as reported in this chapter, although full model validation will never be achieved with practical limits of physical testing, the technique produced evidence to support the validity of part of the FE model generation process from CT scans. Furthermore the results demonstrated the value of DIC for providing detailed, full field data for biomechanical model validation, with relative ease. For more complete validation evidence, the experimental – modelling comparison should be repeated with a cadaveric femur.

4.4 Model Corroboration with the Literature

Finally, to consider the overall outputs of the model, it was corroborated against results from the literature, considering specifically Taylor et al [232]'s *in-vivo* radiographic measurement of femoral deflections, Aamodt et al [233]'s *in-vivo* strain gauge measurements, and FE predictions from several groups [11, 12, 196, 201, 202, 222] for overall displacements of the model and strains in the cortex. Corroboration of the implanted models is included in each study's discussion section.

4.4.1 Model Displacements

Figure 66 shows the overall deformations of the loaded, intact femur under single leg stance. The magnitudes of these displacements can be compared to *in-vivo* measurements and finite element simulation data for corroboration, as in Table 9. Such data is limited, currently to Taylor et al's [232] which refers to measurements from two subjects only, with the X-Ray technique giving a quoted approximate accuracy of ±1mm. However, their hypothesis is that owing to muscle forces and overall compressive loading (rather than bending) the global displacements of the femoral head should be very small, with slight deflection medially and inferiorly.

Table 9: Corroborating the FE Model with X-Ray Measurements of Femoral Head Displacement

Direction	X-Ray Data [232]	FE Model
Medial	1.25mm (-1.5 to +4.0)	1.8mm
Posterior	-	0.63mm
Vertical	-1.5mm (0 to -3.0)	-0.89mm

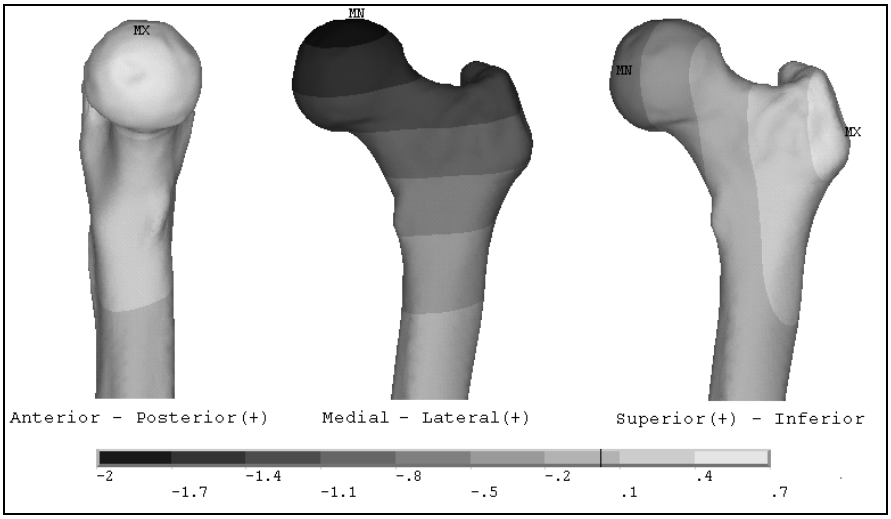

Figure 66: Deformations of the Loaded, Intact Femur

The model is in good agreement with the directions of deformation and the magnitudes are within the measured range, and it can be corroborated well with other FE studies which have focussed purely on application of boundary conditions [208, 209]. However, because model deformations could be tuned by adjustment of the boundary condition location, further corroboration using the model strains is essential.

4.4.2 Cortex Strains

Figure 67 shows a contour plot of the equivalent strain in the intact proximal femur under gait loading. For quantitative corroboration with other studies, plots of the strain were created along paths on the medial and lateral, and anterior and posterior aspects of the cortex, beginning at the femoral head equator and running distally to beyond the lesser trochanter. These are included as Figure 68 and Figure 69.

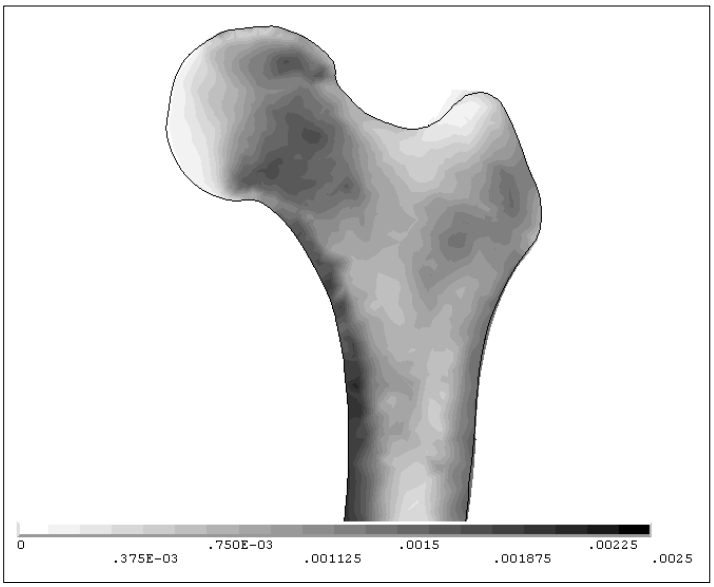

Figure 67: Contour Plot of Equivalent Strain on a Cross Section of the Proximal Intact Femur under Gait Loading.

To attempt quantitative corroboration, Figure 68 and Figure 69 include similar data from several other computational modelling studies [11, 12, 196, 201, 202, 222], in the form of the shaded boxes on the charts. These boxes indicate the range of strains predicted in the equivalent regions in the cited studies, scaled to represent the same applied joint contact force, and with artefacts associated with nodal force application removed where appropriate. This model's results lie almost entirely within the range of strains predicted by the other studies, with particularly close correlation of the medial and anterior strains. The lateral and posterior strains are also largely within the ranges predicted previously, but are towards the bottom of the range predicted in the femoral neck. Only two of the cited studies [11, 196]- which were associated- predicted such high femoral neck strains in these regions, so these may be peculiarities of the bones from which they created their FE models, for example a larger femoral head-neck diameter ratio. Clearly interpatient variability will have a considerable effect on the predictions generated by CT-derived FE models such as these, so reasonable corroboration is demonstrated because these results lie within the range of previous studies' results obtained using several different patient data sets.

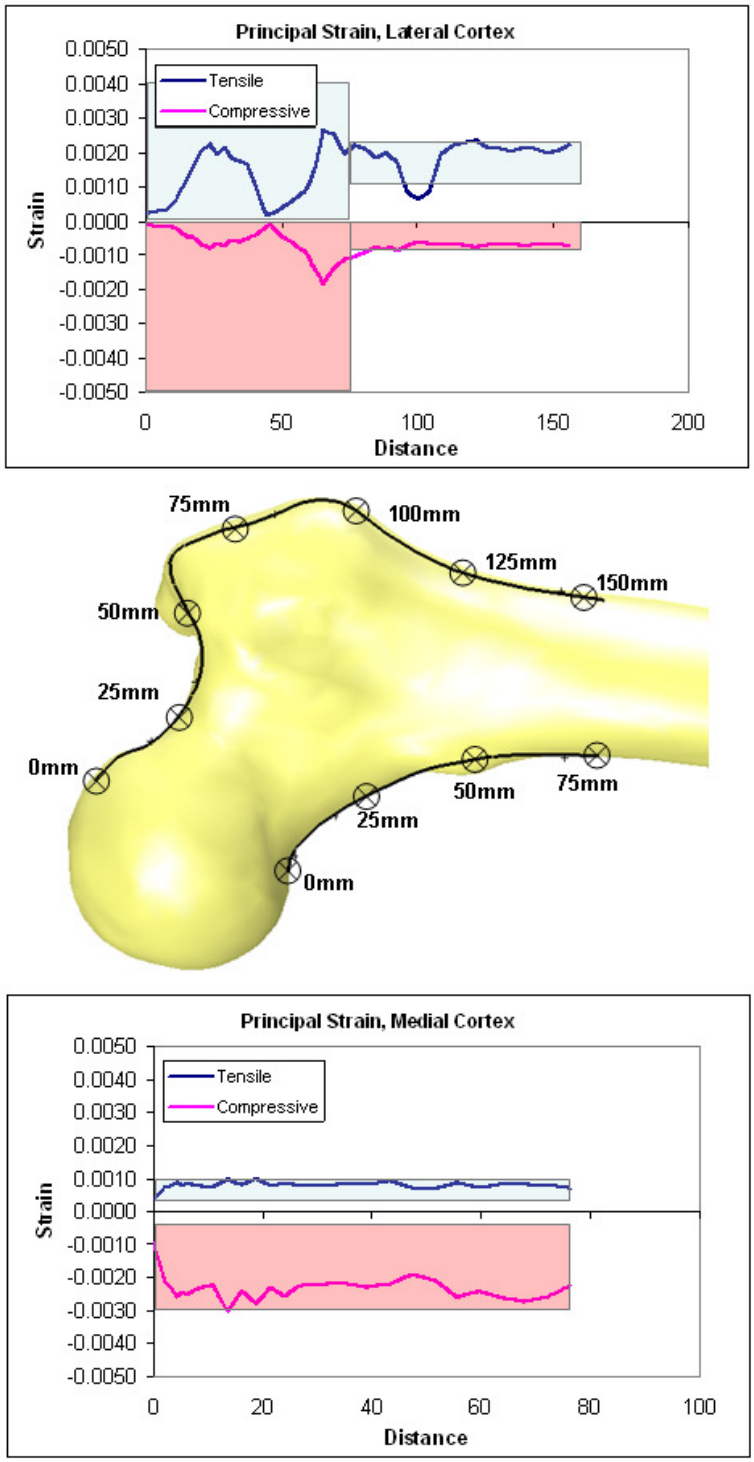

Figure 68: Path Plots of Principal Cortex Strains along the Medial and Lateral Aspects of the Proximal Femur. Boxes represent Strain Ranges reported in the Literature.

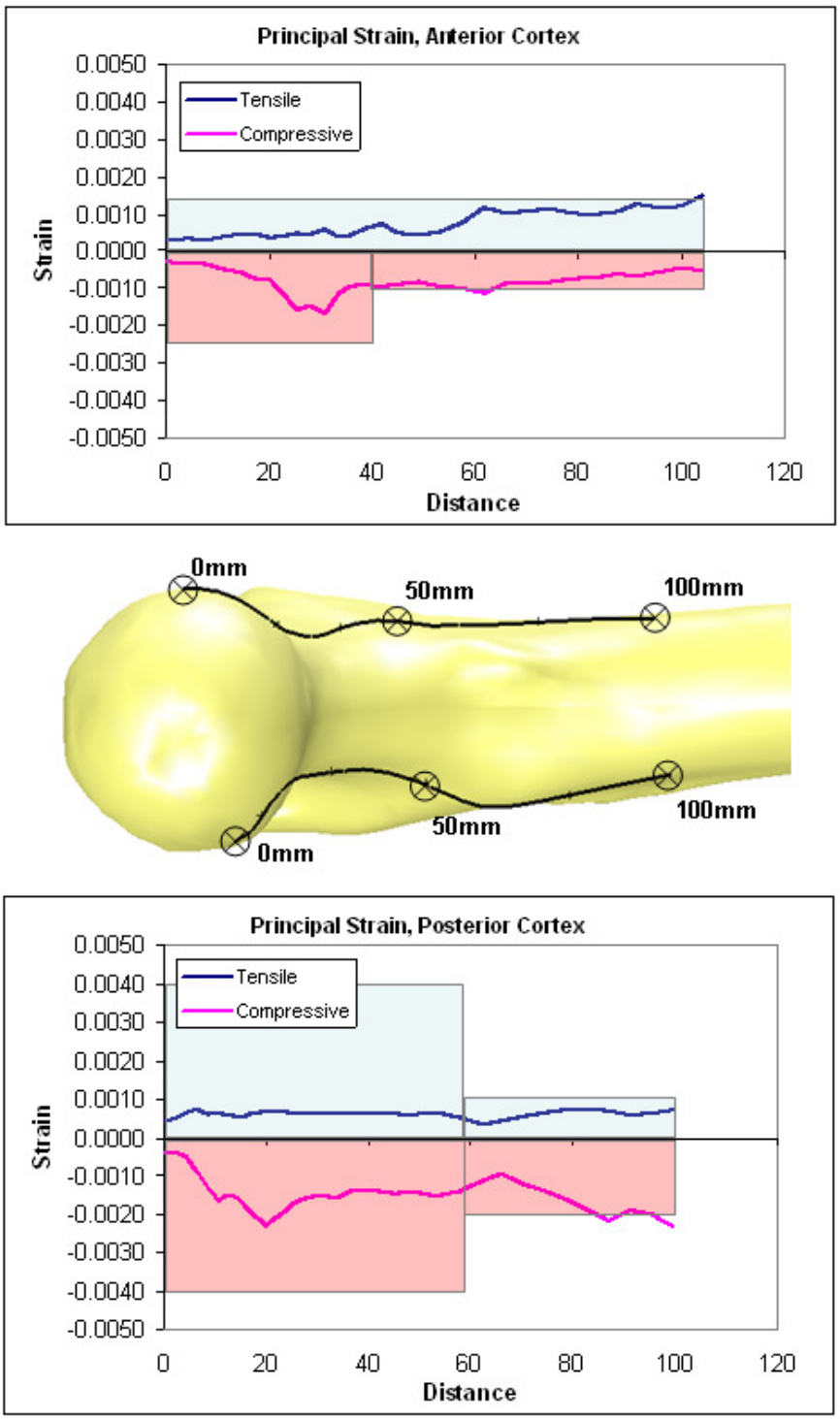

Figure 69: Path Plots of Principal Cortex Strains along the Anterior and Posterior Aspects of the Proximal Femur. Boxes represent Strain Ranges reported in the Literature.

Further confidence can be provided by comparing the model's predictions to *in-vivo* strain values. Such data is difficult to obtain, but there is strain gauge data from an *in-vivo* experiment reported by Aamodt et al [233]. This latter study showed, during gait, peak tensile and compressive strains of approximately 0.0012 and -0.0004 at a point 35mm distal of the greater trochanter on the lateral cortex, which are consistent with the results presented here.

4.4.3 Model Corroboration Conclusion

The risk of model corroboration with previous results from the literature is that previous errors become ingrained in subsequent studies. However, considering as broad a range of previous studies as possible, including six FE modelling studies and two cadaveric experiments, the results of this model were observed to corroborate well with past research. Further confidence can be provided by corroboration with clinical results, which is considered in detail in the discussion at the end of each of the three main study chapters.

5 STUDY 1: POST-OPERATIVE STATIC MODELS

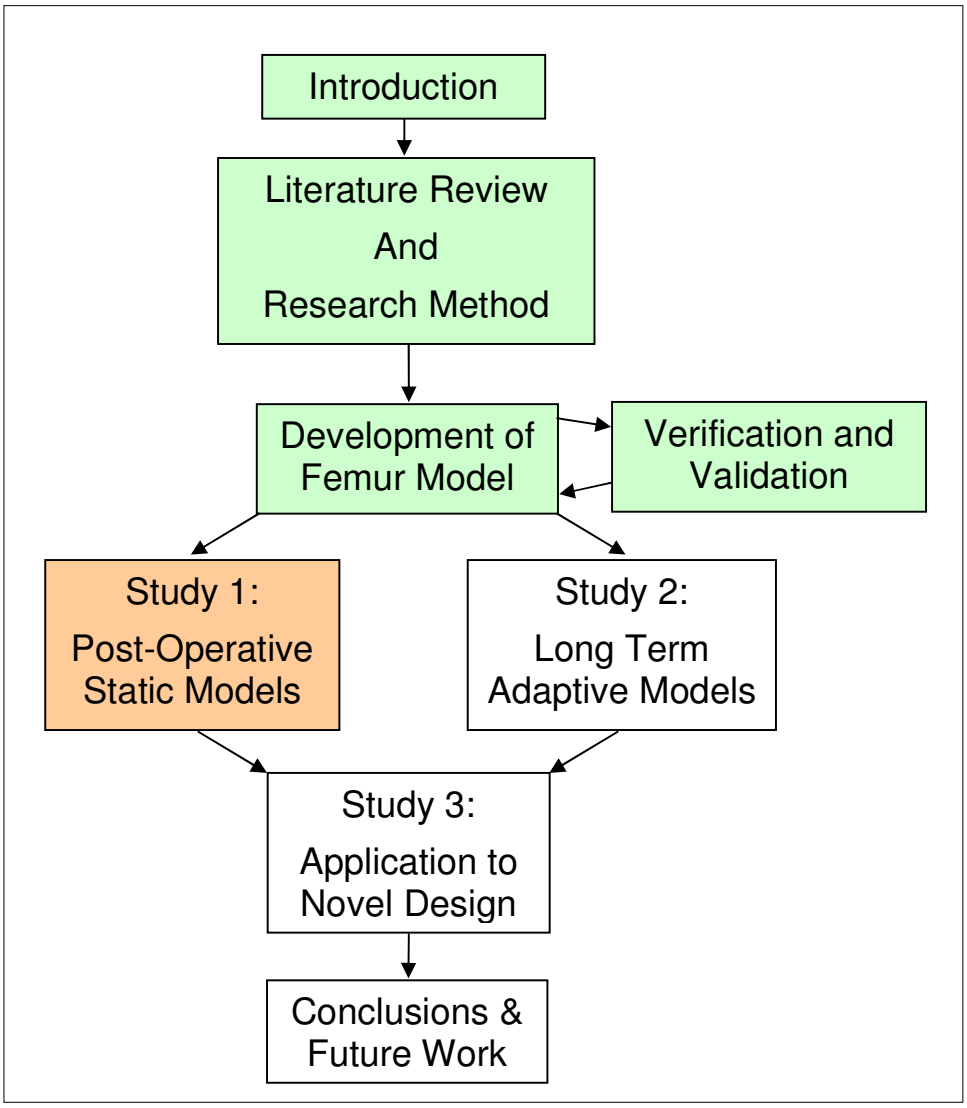

The results in this chapter were presented at the 54th Annual Meeting of the Orthopaedic Research Society, San Francisco, USA, March 2008 (preliminary form), and at the 22nd Annual Congress of the International Society for Technology in Arthroplasty, Hawaii, USA, October 2009 (completed form).

The work presented in this chapter has also been published in a journal article:

Dickinson, A S, Taylor, A C, Browne, M: *Performance of the Resurfaced Hip. Part 1: the Influence of the Prosthesis Size and Positioning on the Remodelling and Fracture of the Femoral Neck*. Proceedings of the Institution of Mechanical Engineers, Pt. H: Journal of Engineering in Medicine, 2010, 224: p427-439.

5.1 Introduction

In this chapter, a quasi-static version of the FE model was used to investigate the biomechanics of the resurfaced hip. This constituted a first pre-clinical analysis tool which would allow analysis of the two main femoral prosthesis failure modes: femoral neck fracture and femoral prosthesis loosening.

The model was used to investigate the influence of surgical variability on these two failure modes in an existing prosthesis design, including implant sizing and positioning, to allow the model's predictions to be corroborated with clinical evidence. Furthermore, the improved understanding of these failure modes allowed the influence of current prosthesis design features on the failure modes to be investigated, to inform the development of an improved resurfacing head prosthesis design.

5.2 Methods

The femoral FE model (with a natural femoral head diameter of 48mm) was implanted first with a 52mm diameter resurfacing head of the Finsbury Orthopaedics ADEPT design, according to the operative technique [234], as shown in Figure 70. The prosthesis was implanted in three orientations: first with the stem aligned with the neutral femoral neck axis, and then with 10° of relative varus and valgus rotation. The prosthesis was positioned so that the implant head centre was located in the same position as the natural head centre. The 52mm implant was the smallest head which allowed implantation in this location without notching the femoral neck or leaving exposed reamed cancellous bone, across the desired range of ±10° varus-valgus angular variation.

Figure 70 also shows two biomechanical measurements: the horizontal femoral offset, and the angle between the femoral shaft and the mechanical axis of the oriented bone. As the centre of rotation of the femoral head was maintained from the pre- to postoperative states, these measurements would be the same in all cases. However, this is not typically achieved clinically [10, 52]. Implant positioning is carried out using instrumentation which references the diameter of the femoral head-neck junction, allowing the surgeon to position the implant such that its opening is located at the highest point possible along the femoral neck where the maximum neck radius equals that of the mouth of the implant. As the surgeon aims to minimise the femoral head size in order to conserve acetabular bone, this often results in a shift of the prosthetic head centre location down the femoral neck [15], which

shortens the leg and reduces the horizontal femoral offset distance. Prosthesis positioning with prosthesis under-sizing was investigated, by resurfacing the femoral head with a 50mm prosthesis as shown in Figure 71. This figure also shows the reduction in the horizontal femoral offset which would result for the three varus-valgus angles modelled, and the changes in femoral shaft – mechanical axis angle, which were applied by tilting the femur such that the mechanical axis remained vertical.

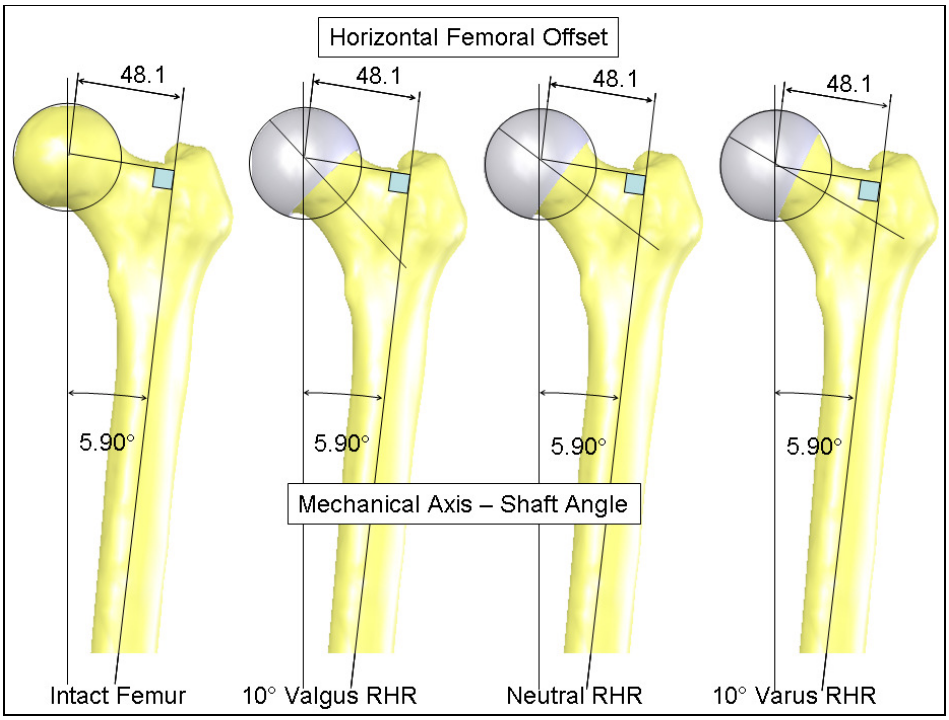

Figure 70: FE Model Prosthesis Positioning, with Biomechanical Measurements for the Proximal Femur (left to right) Intact, and Implanted with a 52mm Prosthesis in Valgus, Neutral and Varus Orientation.

The values of intact and implanted offsets are shown graphically in Figure 72 with their shift from the natural location. The offset was reduced least– by 3mm– when the prosthesis was placed with varus orientation. Conversely, the implanted joint centre vertical position was closest to that in the intact bone when implanted with valgus orientation.

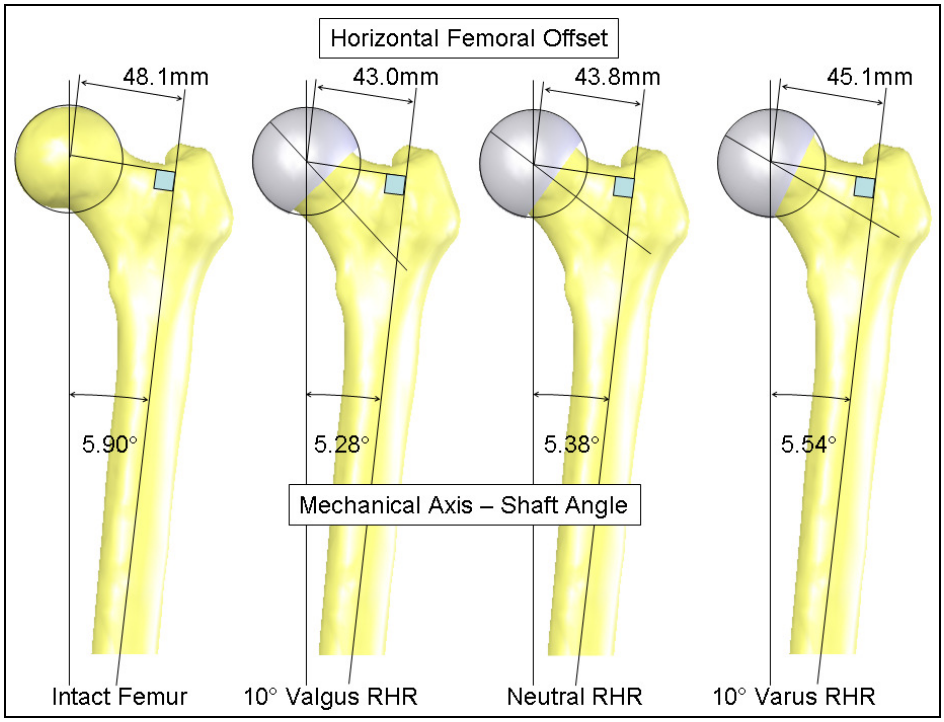

Figure 71: FE Model Prosthesis Positioning, with Biomechanical Measurements for the Proximal Femur (left to right) Intact, and Implanted with a 50mm Prosthesis in Valgus, Neutral and Varus Orientation.

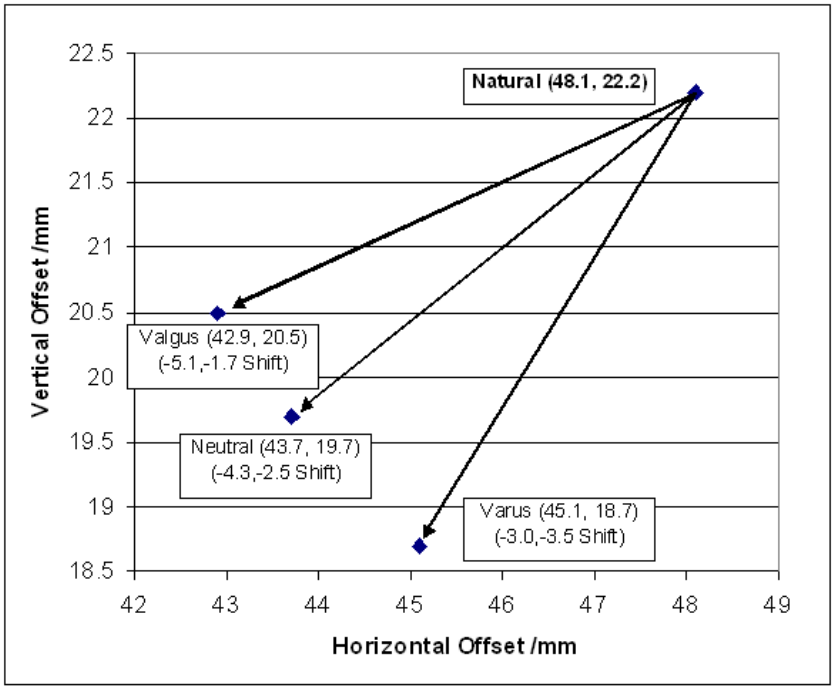

Figure 72: Horizontal and Vertical Hip Centre Offsets for the Natural Femur and Three Models Implanted with 50mm Prostheses.

5.3 Results

Under gait loading, stumbling and falling scenarios, the results were as follows:

5.3.1 Effect of Varus – Valgus Orientation on Fracture Strength

The femoral neck strain pattern was analysed for the intact bone, and bone yield was predicted to initiate at 6.0kN in stumbling, and 3.0kN in sideways falling. To illustrate the location of bone damage initiation, Figure 73 shows the distribution of yielding bone elements in the femoral head and neck under these loads. The figure also includes the bone damage distributions for the femur resurfaced with the 52mm prosthesis, showing how resurfacing alters the damage initiation pattern. Figure 73 does not contain results for the 50mm prosthesis because at 6.0kN in stumbling and 3.0kN in falling, no bone elements exceeded the yield strain. This indicates that for the 50mm prosthesis, the damage initiation load was greater than that of the intact bone.

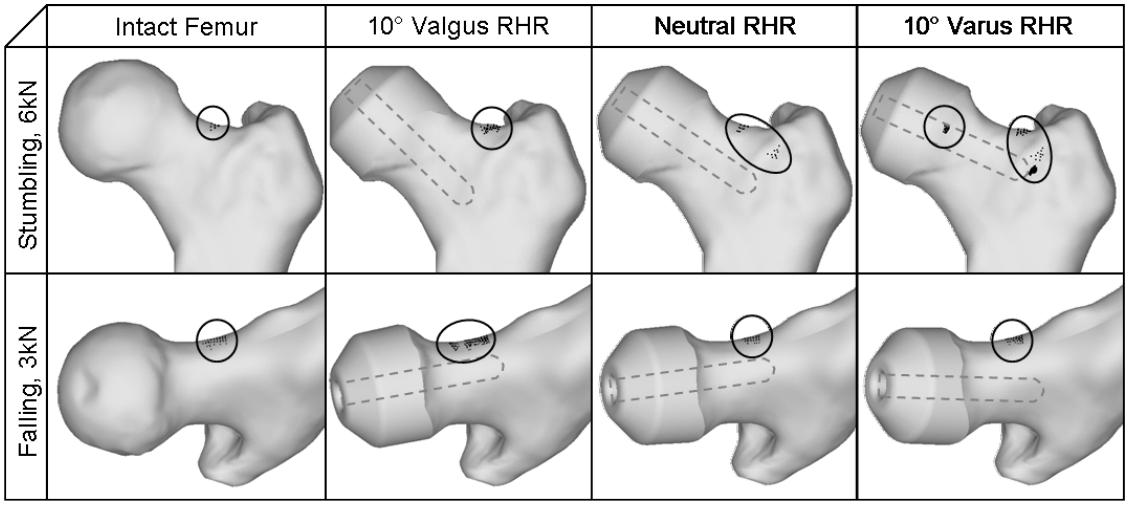

Figure 73: Distribution of Yielding Bone Elements under 6kN Stumbling and 3kN Falling Loads for the Proximal Femur Intact and Resurfaced with the 52mm Prosthesis in Valgus, Neutral and Varus Orientations. Dashed Line indicates Stem Bore.

Next, the femoral neck bone damage initiation load was predicted for the bone resurfaced with the 50mm and 52mm prostheses in varus, neutral and valgus orientations, and the results are given in Figure 74 for stumbling loading and in Figure 75 for falling loading.

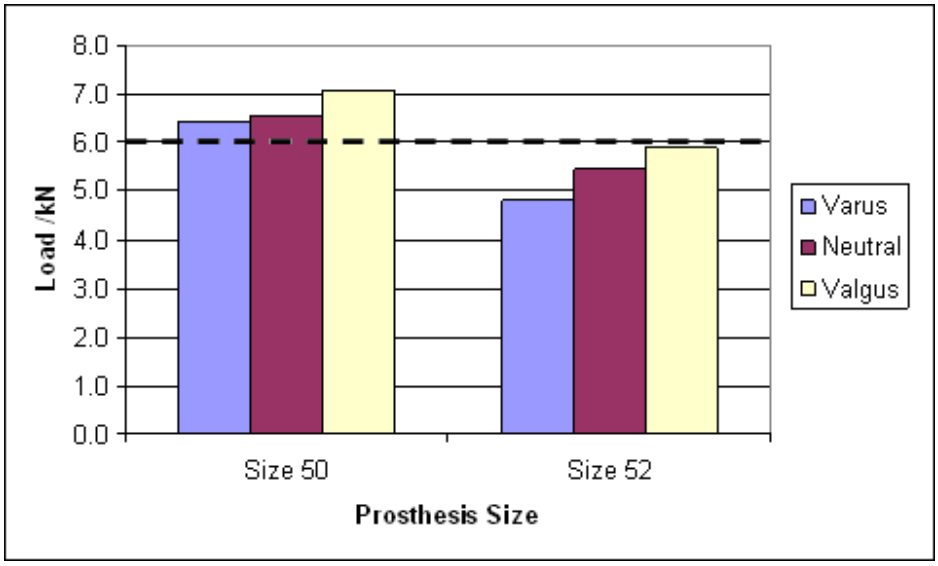

Figure 74: Predicted Femoral Neck Bone Damage Initiation Load under Stumbling Conditions, for the Femur Resurfaced with 50mm and 52mm Prostheses. The Dashed Line indicates the Damage Initiation Load for the Intact Bone.

Under stumbling loading, the model predicted that resurfacing the femoral head with the smaller, 50mm prosthesis would increase the femoral neck bone damage initiation load compared to the intact bone, by approximately 8%, 9% and 18% for varus, neutral and valgus orientations respectively. When the larger 52mm prosthesis was used, and the natural femoral head centre location was recreated post-operatively, the femoral neck bone damage initiation load was reduced by approximately 20% with a varus implant and approximately 9% with a neutral implant. With a valgus oriented implant, the predicted damage initiation load was within 2% of the strength of the intact bone. This implies an approximately linear correlation between femoral neck strength and valgus prosthesis orientation angle. These results indicate that two effects contribute to a reduction in the femoral neck fracture strength:

- **First, for large vs. small prostheses:** if the prosthesis is positioned some distance down the femoral neck, so that the horizontal femoral offset is reduced, the result is a lower femoral neck bending moment, which decreases load transfer in bending and shear at the root of the femoral neck, [10, 54]. Load is transferred instead as compression in the medial cortex, for which the yield strain is higher. This gives an increase in the load at which bone yield initiates, and therefore a likely increase in femoral neck fracture load. This positioning was achieved with the smaller, 50mm prosthesis, to avoid notching the femoral neck.

- **Second, for varus vs. valgus orientation:** implantation results in the introduction of strain concentrations around the prosthesis, which in some cases of prosthesis positioning can interact with the natural strain concentrations and cause bone yield at reduced loads. This is illustrated by Figure 73. In the valgus case, where the prosthesis does not approach the natural bone strain concentration, the neck strength is unaffected by resurfacing. However, the bone is weakened by a valgus implant, where the strain concentrating prosthesis stem bore is close to the natural strain concentration, allowing the strain concentrations to interact.
- **Combining the effects:** in this study, the worst case of femoral neck strength was predicted for the varus oriented 52mm prosthesis because this case had the combination of the longest horizontal femoral offset and the interference of the prosthetic stem bore strain concentration with the natural strain concentration. The result was a reduction in the femoral neck's bone yield initiation load by 20%.

For sideways falling, all fractures were predicted to originate from the anterior-medial femoral neck, as seen in Figure 73. A similar improvement in the bone damage initiation load with smaller prosthesis size and therefore reduced femoral offset can be identified in the results for sideways falling, as seen in Figure 75, where the strength was higher for the hips resurfaced with the 50mm implant, by up to 12% for the neutral orientation. However, the proximity of the prosthesis stem bore to the medial femoral neck when the prosthesis was in valgus orientation resulted in a lower implied fracture strength than in the other orientations, despite its lower offset; however, all predicted strength values were above that for the intact bone. The bone damage initiation load was lower for the larger prosthesis, but within 3% of the intact bone case for all orientations.

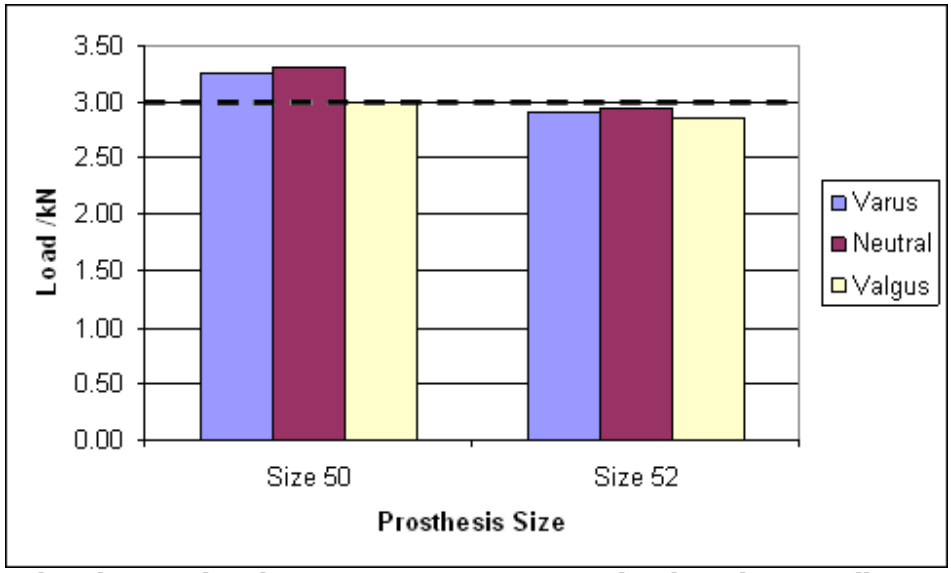

Figure 75: Predicted Femoral Neck Bone Damage Initiation Load under Sideways Falling Conditions, for the Femur Resurfaced with 50mm and 52mm Prostheses. The Dashed Line indicates the Bone Damage Initiation Load for the Intact Bone.

5.3.2 Effect of Varus – Valgus Orientation on Remodelling

The bone remodelling stimulus (percentage change in Strain Energy Density, SED) was calculated for the six implanted cases and is shown for a cross section coincident with the femoral neck axis in Figure 76. This indicates the locations in which bone resorption and densification would be expected, corresponding to a stimulus below -75% and above +75% respectively for an elderly patient, shown by the bottom and top contours on the charts. In all cases, extensive stress shielding was predicted within the superior femoral head, with densification around the stem bore, particularly around the narrowest point of the femoral neck, and at the tip of the stem bore. Apart from a small region in the inferior side of the stem bore, stress shielding was restricted to the interior of the femoral head for the elderly patient.

If a threshold remodelling stimulus of 50% is assumed, for a younger patient with a more active metabolism, stress shielding and bone densification are indicated by the bottom and top two contours. In that case, stress shielding was predicted to extend into the superior femoral neck when the smaller, 50mm prosthesis was used, for all orientations.

Figure 77 quantifies the relative extents of bone remodelling for the six models. These charts predict a trend for increased remodelling as the valgus angle of the prosthesis increases. The volumes of hypertrophic bone were predicted to be similar in all orientations for each size, but the results suggested that stress shielding would increase with valgus positioning, particularly for the smaller (50mm) prosthesis and the younger patient. The volumes of bone at the extreme magnitudes of remodelling stimulus (±75% threshold) were between 7.5% and 8.1% for the 50mm prosthesis, of which 6.5-7.0% represented stress shielding. There was a slight increase in stress shielding with increasing valgus orientation, and a hip resurfaced with the 52mm prosthesis was predicted to follow a similar trend with 6.9-8.1% of the proximal bone stress shielded. However, the volume of densifying bone was predicted to be higher for the larger prosthesis, in particular in the inferior femoral head and at the tip of the stem bore.

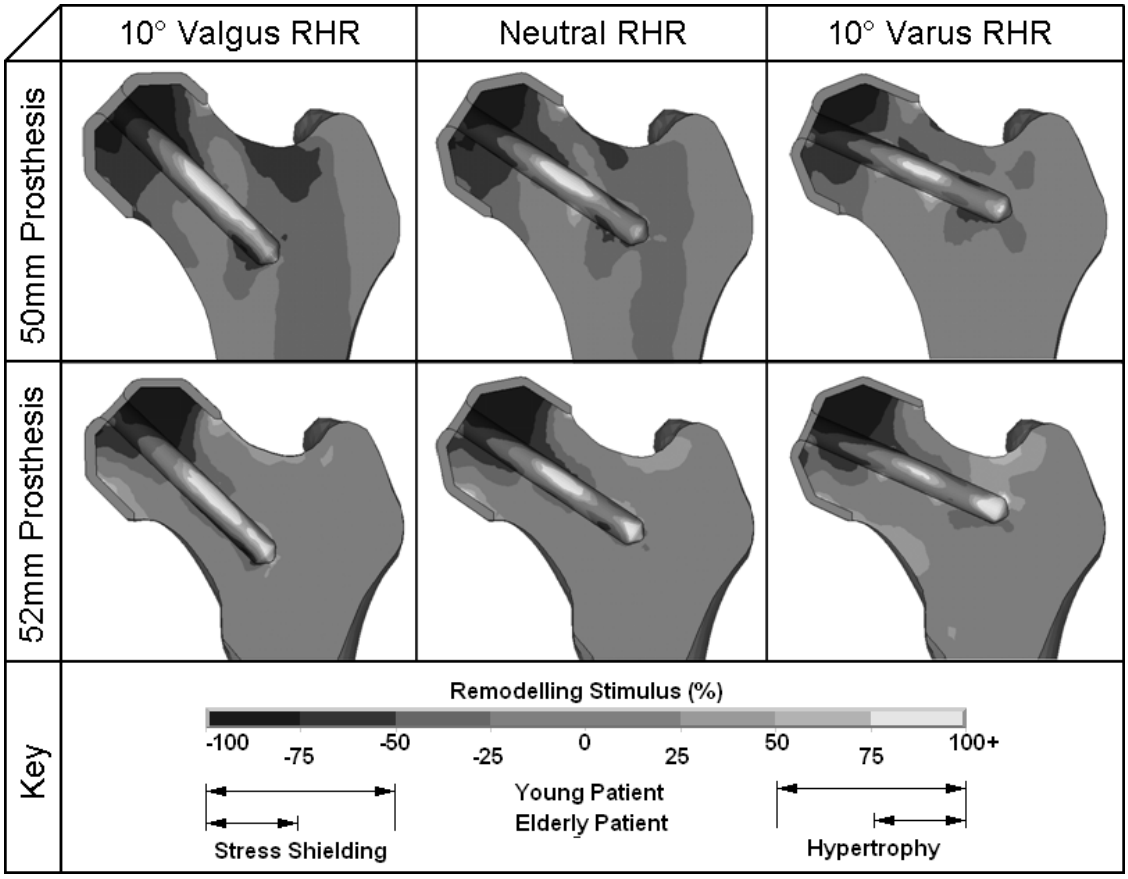

Figure 76: Remodelling Stimulus (Percentage Change in Strain Energy Density) for Resurfacing with Valgus, Neutral and Varus Oriented 50mm and 52mm Prostheses as Labelled. Approximated Mask Applied to Obscure Bone Cement Elements

Analysis of the volume of bone with a remodelling stimulus greater than the ±50% threshold representing the younger patient indicated that stress shielding in particular would be more severe if a

small prosthesis were used, in valgus orientation. From Figure 72 it may be hypothesized that this increase in stress shielding results from the reduction in the cantilever length of the femoral neck and therefore its bending moment, as a result of the shortened femoral offset. Analysis of the remodelling stimulus charts in Figure 76 shows that the extents of stress shielding inside the femoral head were similar for all prosthesis orientations, so this increased net remodelling stimulus arose instead from increased stress shielding in the superior femoral neck, which would be consistent with a reduced femoral neck bending moment. This theory is further supported by the fact that the volume of stress shielded bone was predicted to be considerably lower and almost unaffected by prosthesis varus-valgus orientation for the younger patient if the 52mm prosthesis were used, where the natural femoral offset was recreated postoperatively. In this scenario, irrespective of prosthesis orientation, stress shielding was predicted to be limited to the interior of the femoral head.

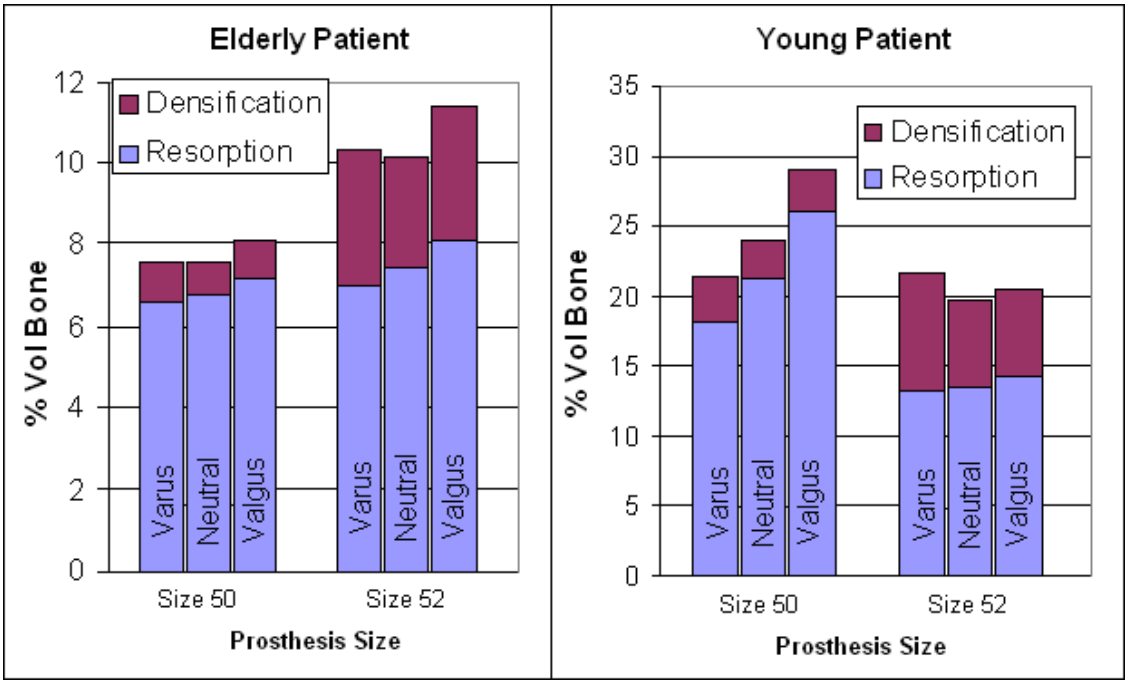

Figure 77: Percentage Volumes of Remodelling Femoral Head and Neck Bone, Resurfaced with 50mm and 52mm Prostheses, in Elderly (left) and Young Patients (right).

5.4 Discussion

5.4.1 Discussion of Study Results

Femoral Neck Fracture

The first part of this study looked at the effects of prosthesis positioning and sizing upon the femoral neck fracture load (implied by the bone damage initiation load) under stumbling and sideways falling scenarios. The predicted correlation between femoral neck fracture strength in stumbling and valgus prosthesis orientation was in agreement with clinical experience which has identified excessive varus orientation as a risk factor [10, 47]. The results were also in agreement with *in-vitro* mechanical test results [53] which identified the same approximately linear correlation between neck strength and varus-valgus angle and recreated natural fracture strength with a prosthesis at around 10° of valgus orientation. The predicted fracture origin in the natural bone- the superior femoral neck- was representative of one of the morphologies identified by Cristofolini et al's cadaveric tests [126] using the same loading conditions. The fracture origin only moved from this location when the prosthesis was oriented and sized to weaken the femoral neck. In this case, damage initiated in the bore for the prosthesis stem around the narrowest point of the femoral neck, and could feasibly propagate across to the prosthesis rim. This would be in agreement with the implanted fracture morphologies identified in Morlock et al's retrieval analysis [49]. Otherwise, Morlock's results indicate that fracture initiates at the superior head-neck junction in some patients. That fracture origin location was not identified in this model because this region of bone was modelled as cement penetrated, and therefore neglected from the bone fracture calculation. This is a limitation of the study. Future tests should include more clinically representative cement mantles which are thicker at the pole and thinner at the head periphery, or consider the fracture risk of cement penetrated bone.

At the time of writing, no equivalent computational or experimental studies of the femoral neck strength in sideways falling *on implanted joints* were found to allow corroboration, although the predicted fracture load and location for the intact bone were in agreement with the results in the literature [133, 235]. The model indicated that similar effects to the stumbling case were in action, including increased strength where implantation reduced the neck bending moment with a shorter femoral offset, and reduced neck strength when the strain concentrating stem bore was closest to the damage initiation site at the medial femoral neck. Considering the sensitivity of the FEA modelling approach, these results indicated that in a sideways fall onto the greater trochanter, within the bounds

of currently recommended prosthesis positioning there would be no significant increase in the femoral neck fracture risk following resurfacing.

Considering prosthesis design, these results indicated that the stem bore strain concentration is influential upon the femoral neck strength. The strength of the intact femoral neck may be recreated with current prosthesis designs, but only if the strain concentrations in the superior femoral neck and around the stem bore do not interfere, which is prevented with valgus orientation. A logical goal for improved prosthesis design is reduced dependence on surgical orientation, or improved tolerance to surgical variability. The results imply that maintaining an intact femoral neck by shortening or removing the prosthesis stem may achieve this, by removing the stem bore strain concentration.

Stress Shielding and Prosthesis Loosening

The second part of the study was concerned with the effects of the same surgical variability upon the remodelling occurring in the supporting femoral head and neck bone. Patterns of bone remodelling based on the immediate post-operative remodelling stimulus were predicted to be in agreement with previous modelling studies and clinical observations. This included bone resorption in the superior femoral head, observed in loosened implants [7-18, 199], and densification to form sclerotic 'pedestal lines' around the prosthesis stem tip and along its superior edge [4, 45]. These were predicted to occur for both prosthesis sizes and all implant orientations. Previous modelling studies have linked these pedestal lines to stem tip load transfer [8, 14], although in the immediate post-operative state there is no contact between the stem tip and the bone. These results are consistent with more recent modelling research by Ong et al [18] which indicated that the presence of the bore alone is sufficient to cause bone densification around the stem.

Additional bone densification was predicted to occur around the stem bore more proximally, on the anterior and posterior faces of the stem around the narrowest point of the femoral neck (Figure 76). This would be obscured by the stem, so densification in this region would not be visible on radiographs. Figure 78 shows an x-ray and retrieval photograph of a revised 50mm BHR prosthesis. Although no pre-operative x-ray was available to assess radiographic changes around the stem, there is relatively high medial neck trabecular density and the retrieval photo shows that a neo-cortex formed around the stem at the proximal femoral neck level. The figure provides corroborative evidence to suggest that

bone hypertrophy can occur in this region, and shows how this may be largely obscured by the radiopaque prosthesis stem; there is only a small dense region visible, superior to the stem around the resection level. This sign is most clear immediately after retrieval and before cleaning; that is, whilst the trabecular bone porosity is indicated by blood on the cut surface. In personal communication from three orthopaedic surgeons, a neo-cortex around the stem and some resistance on removing the prosthesis after neck resection are common observations in revision surgery.

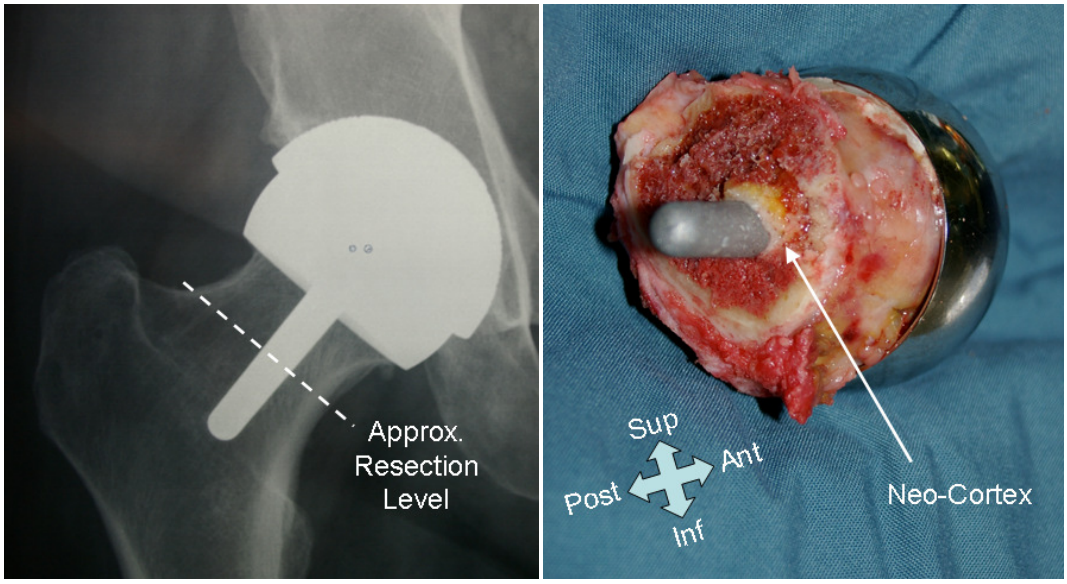

Figure 78: Pre-Revision Radiograph and Retrieved 50mm BHR Prosthesis showing formation of an Anterior and Posterior Neo-Cortex around the Proximal Stem, Largely Obscured Radiographically.

A more extreme case is shown in Figure 79 where extensive resorption has occurred around the cup and femoral head-neck junction, possibly due to an osteolytic response to metal debris from a high wearing, excessively steep acetabular cup (approx. 55°). This proximal resorption would lead to increased stem load bearing, which is indicated by bone densification around the stem tip. In this case, densification resulting from the proximal stem bore strain concentration is more widespread and can be seen superior to the stem. These photographs were kindly supplied by Dr David Young, of the Melbourne Orthopaedics Group.

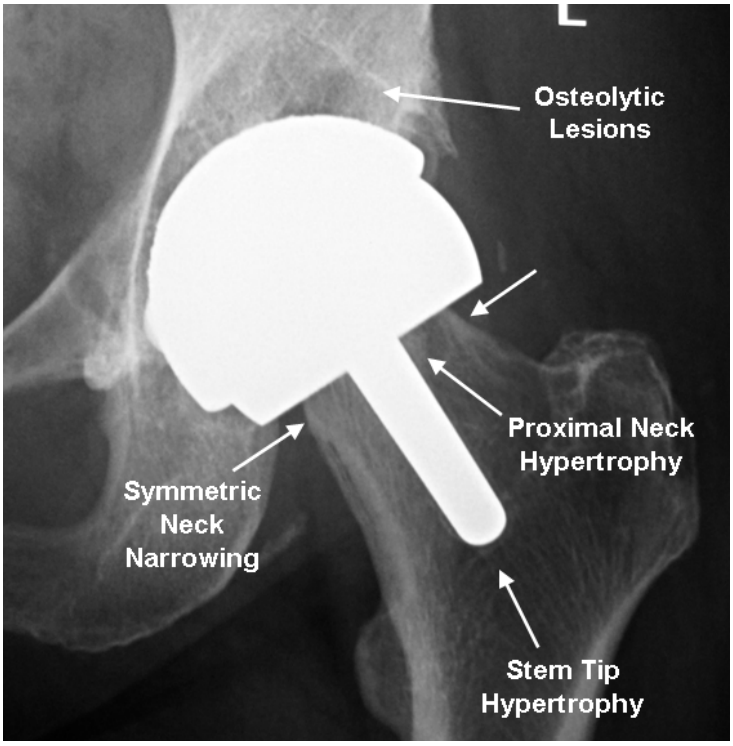

Figure 79: Radiograph of a 46mm BHR Prosthesis after 8 Years *in-vivo*, showing Acetabular and Femoral Osteolytic Lesions, and Densification around the Prosthesis Stem.

On first inspection, previous research has produced contrasting conclusions regarding the influence of varus-valgus prosthesis orientation on bone remodelling. Analysis of the figures from Ong et al's study [18] indicates that, in accordance with clinical outcomes, they reduced the femoral offset in resurfacing. Consistent with the 50mm prosthesis results in this study, they predicted a clear correlation between stress shielding and valgus prosthesis orientation. Conversely, Radcliffe and Taylor [16] concluded that valgus orientation was preferable, on the basis of a closer strain distribution to that in the natural bone. In their detailed discussion, they reported that the varus case increased the superior femoral neck strain (in agreement with this study's fracture analysis), whereas the valgus case was predicted to reduce the superior femoral neck strain (in agreement with this study's remodelling stimulus analysis), and trends were minor but statistically significant. Images of their model indicate that on implantation they recreated the natural femoral head centre and femoral offset irrespective of varus-valgus angle, which is consistent with the 52mm prosthesis results in this study for which a less strong trend was observed. The present study's attempt to decouple the effects of prosthesis varus-valgus angle and horizontal femoral offset clarifies the influence of the two separate effects.

Clinical data on hip resurfacing has enabled an understanding of the effects of prosthesis positioning and sizing on bone remodelling. Silva et al [52] reported in their study of 50 RHR patients that the pre- to postoperative horizontal offset was reduced by an average of 0.8mm but that osteoarthritic hips had a significantly reduced horizontal femoral offset compared to a healthy contralateral joint, by an average of 8.4mm. They identified that this horizontal offset decrease resulted largely from a shift of the natural neck-shaft angle into valgus, as an osteoarthritic deformity. However, all the operations were conducted by a highly experienced surgeon from a centre of excellence, so this may represent the best case of prosthesis positioning. Considering the clinical data on femoral neck narrowing, Hing et al [3] studied 163 hips, also resurfaced by experienced surgeons, and identified the female gender and a more valgus natural femoral neck-shaft angle as statistically significantly increased risk factors for neck narrowing. They also identified a slightly increased risk of neck narrowing where a smaller prosthesis head size was used. Similarly, Amstutz et al [67] reported on 400 patients and identified a statistically significantly increased risk of femoral neck radiographic changes and femoral component loosening with a smaller prosthesis size in males. The most recent, high volume clinical results for hip resurfacing come from the Australian Orthopaedic Association National Joint Replacement Registry [39], which show a clear trend for increased revision rates for smaller prostheses, and indicate that a good outcome can be achieved for female patients if they have a larger prosthesis.

Attempting to draw a link between prosthesis design and adverse bone remodelling, an influential factor was observed to be the high stiffness prosthesis shell, surrounding the entire femoral head and stress shielding a considerable proportion of it. However, unlike the prosthesis stem it would be more difficult to alter this aspect of the prosthesis design without affecting its primary function as a bearing. Again the prosthesis stem was observed to have an effect, with evidence of a distal shift in load transfer away from the femoral head and proximal neck, into the medial femoral neck. Thus, as in the analysis of femoral neck fracture, it may be beneficial to shorten the prosthesis metaphyseal stem. Compared to the trends in stress shielding with prosthesis positioning, the stem's effect appeared to be minor. However, this may be linked to the fact that this study considered the initial postoperative bone remodelling stimulus, before any load transfer is established along the tapering portion of the prosthesis stem with healing of the bore around it. The distal shift of load transfer by the stem could therefore become more pronounced as the stem bore heals and refills with tissue, as predicted by modelling studies which assumed perfect prosthesis-bone interface contact, and indicated by clinical

radiographic observations [4, 12, 14, 18, 196]. This will be considered in the dynamic bone adaptation study (Study 2, Chapter 6).

5.4.2 Discussion of Study Methods

This study has investigated the mechanical effects of the positioning and sizing of hip resurfacing prostheses upon the femoral neck fracture strength and the risk of implant loosening. It must be recognised that this consideration of mechanical effects alone is a great simplification of the complex *in-vivo* biomechanical situation. The following is a discussion of the limitations of the methods employed.

Stress shielding from altered biomechanics is only one potential cause of narrowing of the femoral neck. Other previously suggested causes include inflammatory response to wear particles, impingement, and bone necrosis, possibly caused by exothermic bone cement polymerisation or disruption of the blood supply to the femoral head, specifically the retinacular vessels [3, 51, 72, 236]. The reported incidence of femoral neck narrowing is high (up to 90%), but the extreme biomechanical conditions that this modelling study suggests are required for it to occur are not so common. Therefore, it is probable that a combination of the listed factors above is responsible. However, two quantified radiographic clinical studies [4, 72] report that neck narrowing occurs early and stabilises around two to three years postoperatively; therefore, adaptive effects including stress shielding must be a significant factor.

Considering the modelling more generally, the model is subject to several simplifications which must be noted. First, the model simulations were carried out on a model of a single femur. The model was generated from a CT scan of an ideal candidate, male patient, receiving a prosthesis from the most common size range [39]. To remove any effects of bone degeneration of the joint which would certainly be present, but subject to a very large range of variability, and to isolate the effects of prosthesis positioning, a disease-free candidate was selected from 15 available scans. This was considered to be reasonable because the effects of conditions such as sclerosis or destruction of the subchondral bone would be largely removed by the surgical cuts, and the isolated femur modelling method avoids the effects of narrowing of the joint space. Other effects such as formation of osteophytes and subchondral cysts, or avascular necrosis would be subject to greatest variability, but, if advanced, may be included in the list of contraindications for hip resurfacing. This ideal candidate, disease-free patient's CT scan was

used to allow reliable comparison of the variables of interest For the same reason, the investigated range of surgical variability was restricted to avoid surgical error scenarios such as incomplete prosthesis seating, notching of the femoral neck, and excessive cement penetration. The limitation of a single bone analysis is that results should be used to investigate the effects of surgical positioning and sizing variables in comparative quantitative terms rather than making absolute quantitative predictions. After research by Radcliffe [202] into necessary sample sizing in multi-femur analyses to obtain desired confidence levels in results, Bryan [211] conducted the first statistical analysis of geometric and materials properties of the proximal femur in a large scale multi-femur analysis of resurfaced hips. One aim of the research was to identify possible causes of inter-patient variability, in terms of geometric and material property differences between patients. The models predicted that inter-patient differences in femoral head and neck strains arise in particular from femoral neck geometric properties, including the femoral neck diameter, the head-neck diameter ratio, the femoral neck axis length, and the neck-shaft angle. The results were in clear agreement with clinically reported trends of the risks associated with small prosthesis sizes [39, 66], and demonstrate the importance of multi-femur analysis to capture the effects of inter-patient variability.

One simplification of the model boundary conditions was that the same joint contact force and abductor muscle force were applied to the model irrespective of changes to the biomechanical geometry due to joint centre repositioning with the 50mm prosthesis. It is argued though that this is a conservative simplification. The forces and moments about the hip joint are shown in Figure 80. Shortening the horizontal femoral offset (HFO) would reduce the range of abduction and the abductor muscle moment arm (AMA) length, and therefore increase the muscle force required to counteract the moment about the joint arising from the body weight in stance. This would increase the resultant joint contact force – the opposite of the goal of positioning in total hip replacement surgery [237, 238]. Conversely, joint 'medialisation', or shortening the bodyweight moment arm (BMA) is a surgical goal because it results in a lower JCF by reducing the moment generated across the joint by the bodyweight. These effects were quantified in a biomechanical modelling study by Johnston et al [239], who predicted the reduction in joint contact force and abductor muscle force resulting from up to 20mm joint centre medialisation and lateral trochanteric transfer (increasing femoral offset). Identical force magnitudes were applied to the models in this study, in order to isolate the *structural* effects of the prosthesis positioning. Similarly, any abductor muscle weakening from surgical incisions, or loss of soft tissue tension, was neglected. Based on the work of Johnston et al [239], this was judged to be an acceptable simplification. They predicted that joint centre medialisation had a greater effect upon the

joint force magnitudes than increasing the horizontal femoral offset. This may be extrapolated into a reduction of the HFO distance and the AMA length. Furthermore, Silva et al's study [52] reported that hip resurfacing resulted in a mean joint centre medialisation of 6.5mm, whereas the greatest reduction in AMA length in this study was 4.2mm. With linear interpolation of Johnston et al's data [239], this medialisation would give a 12% lower JCF, compared to, at most, only a 3% increase in JCF as a result of the horizontal femoral offset increase. As such, the observed effects of the reduced femoral neck strains associated with a shorter joint horizontal femoral offset are likely to become more marked if the associated joint contact and abductor muscle force reductions were taken into account. This study's models therefore represent a conservative case.

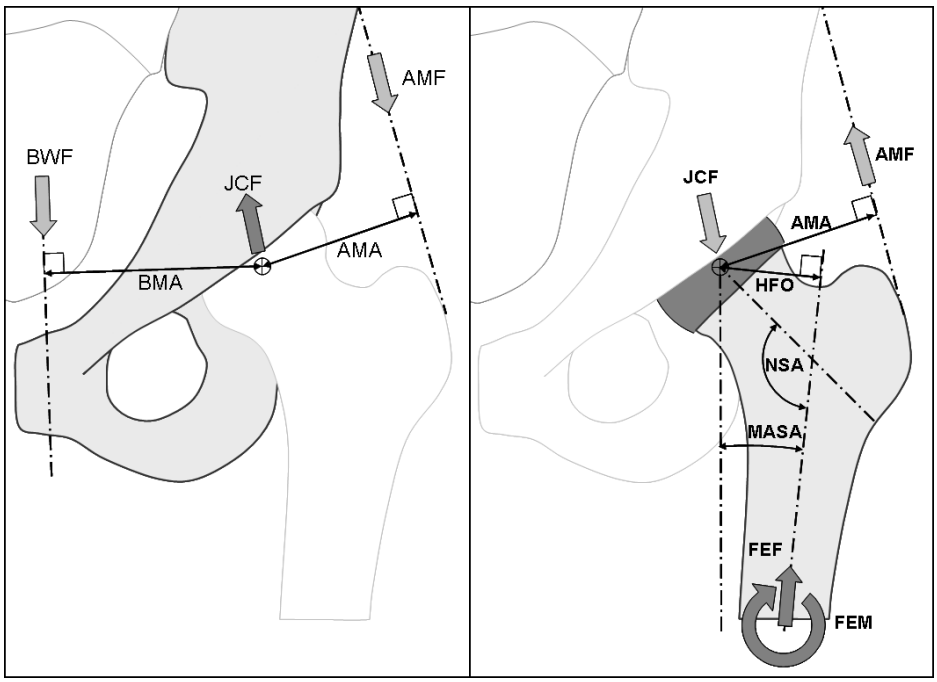

Figure 80: Biomechanical Measurements and Forces on Hip.
Left: Pelvic Frame of Reference, Right: Femoral Frame of Reference.
AMA=Abductor Moment Arm, AMF=Abductor Muscle Force, BMA=Bodyweight Moment Arm, BWF=Bodyweight Force, JCF=Joint Contact Force, FEF=Femur Equilibrium Force, FEM=Femur Equilibrium Moment, HFO=Horizontal Femoral Offset, MASA=Mech. Axis-Shaft Angle, NSA=Neck-Shaft Angle.

A further simplification of the force application method was the use of a single, gait load case for the bone remodelling study, rather than a set of variable amplitude loading (VAL) cases. This simplification has two implications. First, different load activities would be expected, particularly in a young hip resurfacing patient post-operatively. However, Morlock et al [240] reported the activities of 31 total hip replacement patients of mean age 62.5 years, and their data suggested that normal walking may account for as much as 96% of a standard day's dynamic loading. Any more strenuous loading conditions would be discouraged by the surgeon in the immediately postoperative period, which this

study aims to simulate. Second, the instantaneous peak load magnitude for this activity was selected for application to the model, as it generates the peak mechanical stimulus, but in reality a wider range of loading magnitudes in varying directions would be experienced by the joint. According to the originators of bone modelling and remodelling theory [176, 217, 241] it is a 'time-averaged value of typical repeated peak strains that enter or exceed the MES (Mean Effective Strain) range' that cause the greatest remodelling response. They theorise that occasional, large magnitude strains do not discernibly affect remodelling, provided they do not cause damage. This justifies neglecting occasional stumbling or higher magnitude (stair ascent or fast walking) loads. Furthermore, it is accepted that strains below the MES may also be neglected, no matter how frequently they occur, and this justifies the use of the peak load point in the gait cycle. This study's use of a single case may be a limitation, but considering that some simplification is needed to reduce computational expense, particularly in the adaptive models to be discussed later on, it is argued that this is reasonable.

Considering the traumatic loading scenarios modelled, again only single load cases were modelled but these were designed to replicate *in-vitro* simplifications of, again, widely variable *in-vivo* traumatic load events [126, 129, 131, 242]. Worst case loading conditions from these studies were used, so it was considered that these load cases were a fair representation of common traumatic events.

Finally, these remodelling results were based purely on the initial remodelling stimulus. Simulation of adaptive remodelling practically requires multiple solutions, and theoretically requires the assumption of several parameters to represent the interaction between internal and external remodelling, and damage. The initial stimulus may only provide a partial indication of the final remodelled state, but as it contains fewer assumed parameters its simple instantaneous predictions could be more reliable than detailed longer term predictions. Fundamentally, it is a reasonable assessment that of two designs or surgical positions, the one with lower initial remodelling stimulus will behave in a more physiological manner and be less prone to loosening. Dynamic bone adaptation simulation requires more detailed research, so the second study in this report is dedicated to that subject.

5.5 Conclusions

The following conclusions can be drawn from this study:

- The results from the femoral neck fracture model were in agreement with *in-vitro* and clinical studies, placing confidence in its use for further studies. The model suggested that positioning the prosthesis to reduce the femoral offset distance, and orienting it to prevent interaction of natural and prosthetic strain concentrations, can preserve or improve the femoral neck strength.
- The model's predictions of bone remodelling stimulus separated the effects of varus-valgus positioning and a reduced femoral offset. These two effects may have been confounded in previous modelling studies, and to the author's knowledge this study is the first to separate them. A reduced femoral offset was indicated to be more influential, contributing to femoral neck stress shielding.
- The prosthesis stem was predicted to contribute to both failure modes, and unlike the stiff shell which was also indicated to contribute to stress shielding, the stem is a feasible design aspect for modification to reduce femoral head and neck stress shielding and femoral neck fracture risk.

6 STUDY 2: LONG TERM ADAPTIVE MODELS

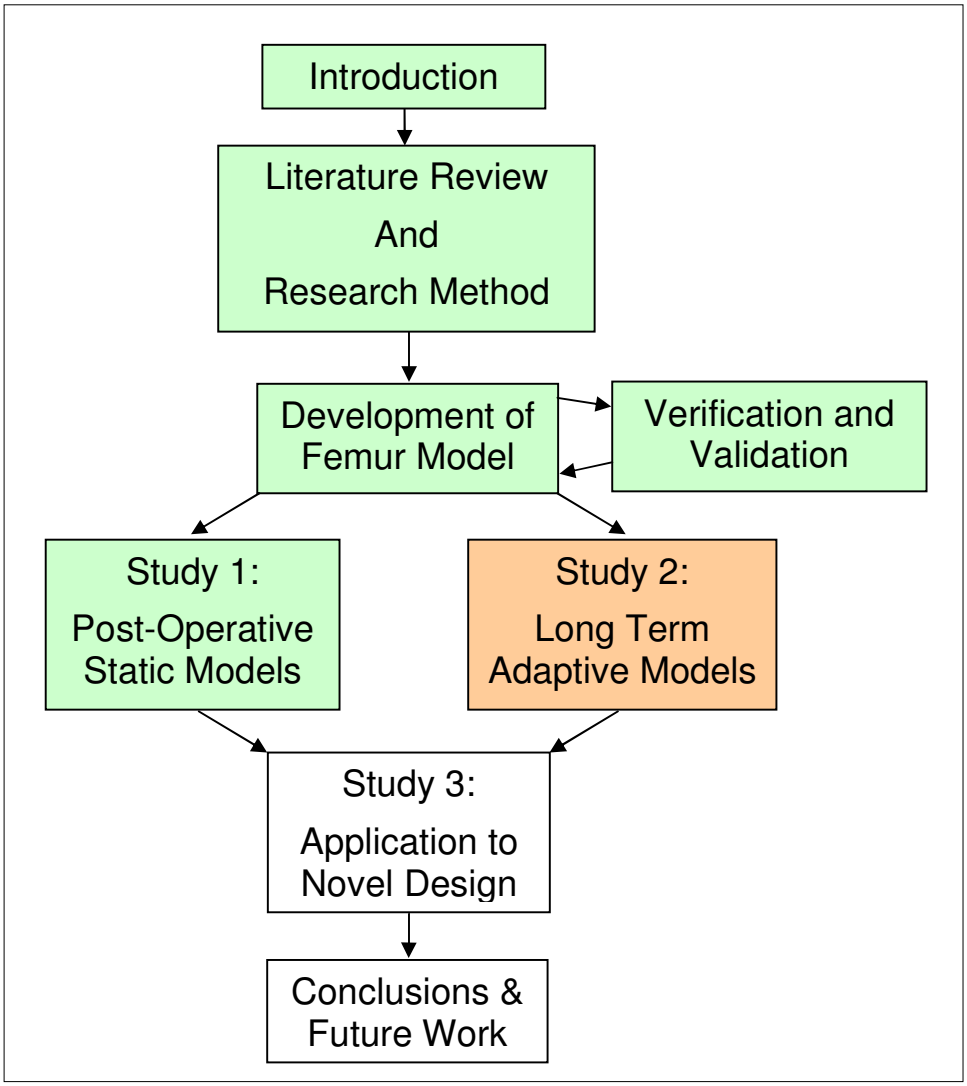

This chapter describes the process by which existing adaptive bone remodelling predictions were made for the resurfaced femoral head and neck. Adaptive remodelling methods from the literature were applied to the static model from the previous chapter, and an adaptive bone defect healing module was added.

These results were presented in preliminary form at the 18th European Conference on Orthopaedics, the meeting of the European Orthopaedic Research Society (EORS), Davos, Switzerland, June 2010.

The completed study was presented at the 6th World Congress on Biomechanics (WCB), Singapore, August 2010. It is also in review for publication as an Article in the journal Computer Methods in Biomechanics and Biomedical Engineering.

6.1 Introduction

Extensive radiographic changes are observed in the femoral neck following hip resurfacing [3, 4, 45, 67, 72]. Two of the most common changes indicate formation of a neo-cortex around the prosthesis stem, and densification of the medial femoral neck trabecular bone at the level of the stem. Remote from the stem, radiographically measurable narrowing of the femoral neck is sometimes observed, particularly at the superior head-neck junction. Finally, superior femoral head resorption has been identified in revised specimens [78]. These changes are observed more commonly in loosening prostheses [4]. Previous modelling studies have investigated the effects of a permanent gap around the stem, or perfect stem-bone contact [12, 18, 196], but clinical evidence suggests that each condition exists at some point in time:

- Immediately postoperatively, the tapering portion of the stem is unsupported as it is located in a parallel sided drilled bore.
- Radiographic changes suggest that later, bone re-fills this bore. This would be necessary for the dense bone regions identified as the neo-cortex to form around the stem.

In this study, a bone healing model was added to existing adaptive bone remodelling algorithms, to allow this gradual stem-bone contact to be simulated. The hypothesis was that simulation of gradual stem-bore gap refilling is necessary to allow FE models to simulate more closely the clinically observed bone adaptation behaviour around resurfacing head prostheses. As an ultimate goal, a bone adaptation algorithm which is capable of reproducing the bone remodelling response to traditional prosthesis designs would be a useful preclinical analysis tool for predicting the performance of new designs.

6.2 Methods

6.2.1 Finite Element Model

The proximal femur FE model was implanted with a 52mm diameter resurfacing head of the Finsbury Orthopaedics ADEPT design, with its bearing head centre located 4.5mm lateral to the natural femoral head centre, and in 10° of valgus orientation with respect to the natural femoral neck axis. This is an accepted, clinically representative case of prosthesis sizing and positioning [234]. As described in the Methods and Materials, a mapped mesh was created in the stem bore with a layered structure representing the healing defect. Adaptation of elements in this region was controlled by the combined

healing and remodelling algorithm, and elsewhere in the model the mature bone remodelling process alone was applied.

6.2.2 Study Approach: Bone Remodelling and Healing Process Parameters

The investigation was split in two stages:

Part 1: Benchmark Remodelling and Healing Investigations

The first part of the investigation aimed to determine simply whether the healing module was necessary to simulate bone adaptation. The approach was to test two extreme limits of stem-bone contact with remodelling alone, and then to add the stem-bore healing process to the bone adaptation algorithm using baseline remodelling and healing process parameters from the literature. These three cases were tested using the ADEPT prosthesis, as in all preceding models. For quantified comparison with clinical data, it was necessary to repeat the combined healing and remodelling test using the BHR prosthesis, as all the DEXA scan data reported in the literature for RHR [74, 75, 82] related to this implant. The two prosthesis geometries are compared schematically in Figure 81; although both nominally 9mm diameter, the BHR stem is longer and has a smaller taper angle into a larger tip radius. The four cases modelled were:

Table 10: Study Design: Part 1

Case	Model	Adaptation Algorithm	Stem-Bone Conditions
1	Extreme 1: ADEPT	Remodelling	No Contact
2	Extreme 2: ADEPT	Remodelling	Full Contact
3	Baseline Healing 1: ADEPT	Remodelling + Healing	Gradually Established Contact
4	Baseline Healing 2: BHR	Remodelling + Healing	Gradually Established Contact

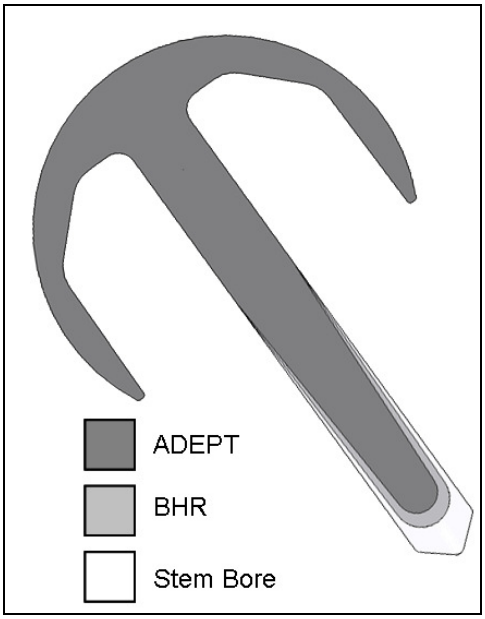

Figure 81: A Schematic Comparison of ADEPT and BHR Prosthesis Stem Geometries

Part 2: Remodelling and Healing Process Parameter Investigation

Trends from the first part of the investigation showed only a rough agreement with clinical observations. Review of the previously used remodelling and healing simulations in the literature suggested that only some of the process parameter values used were chosen on a biomechanically justified basis. The second part aimed to test the influence of these process parameters to identify a set of parameters which produced the best agreement with clinical observations.

As discussed in the Methods and Materials section (Chapter 3), the healing and adaptation algorithm employed the following parameters:

- 's', the threshold stimulus for bone remodelling (baseline s_{mature}=±75% [215] in mature bone, and $s_{healing}$=±33% [176, 219] in immature, modeling bone),
- 'τ_s', the rate constant for bone remodelling (baseline τ_s=130g^{2}mm^{-2}J^{-1}/month [169]), and
- 'D', the stem cell diffusion coefficient in the healing defect (2.37mm^2/day [196]).

Also, the parameter:

- 'M', the stem cell maturation rate in the healing defect,

can be defined for the algorithm. This refers to the healing tissue's Young's Modulus smoothing operation employed in previous studies [188, 189, 232], over a ten day smoothing period. This can be described as a fractional cell maturation rate of 10%/day, which is the percentage of remaining immature cells which mature per day. This approach makes gap filling follow an approximately exponential decay relationship.

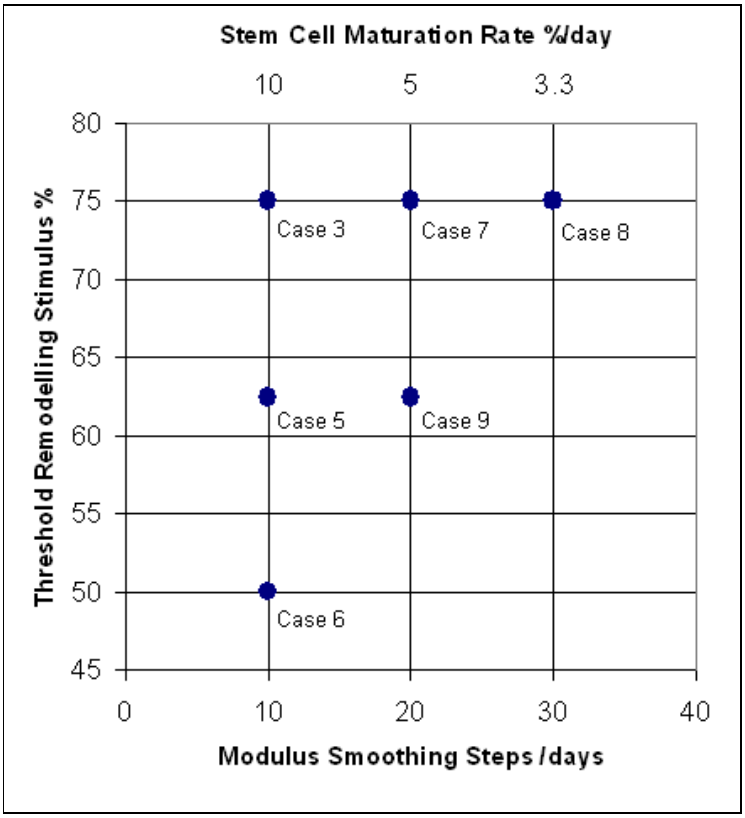

Figure 82: Study Design: Part 2, Remodelling and Healing Process Parameters

The threshold remodelling stimulus 's_{mature}' and the stem cell maturation rate 'M' were the two parameters investigated (justified below). The test matrix is shown in Figure 82, with the previously described Case 3 as the baseline healing case.

Compared to Case 3, Cases 5 and 6 tested the influence of the surrounding mature bone's threshold remodelling stimulus. In this case, the baseline value from the literature was first proposed by Weinans et al [215] who found that ±75% gave a 'moderate bone loss prediction' around a THR femoral stem, compared to ±35% which resulted in complete resorption of the bone surrounding the proximal third of the stem. This variable was investigated further because only two values were tested in that original

study, and since the remodelling predicted in this study with the baseline ±75% value was relatively low compared to the clinical DEXA data (see Results Section 6.3.1). Considering that a young RHR patient's metabolism is likely to be more active, lower values of ±62.5% and ±50% were tested in this study. The other parameters in the remodelling algorithm were not varied, as they were based upon clinically derived strain values ($s_{healing}$=0.33 [176, 219, 220]) or quantified analysis of quadratic errors between simulations and human experimental results (τ_s=130g^{2}mm^{-2}J^{-1}/month [169]).

Compared to baseline Case 3, Cases 7 and 8 tested the influence of the healing bone's stem cell maturation rate 'M'. Preliminary study of healing in an unloaded defect (Appendix 1) indicated that this parameter had a greater effect upon the rate of healing tissue stiffness than 'D', the stem cell diffusion coefficient. The baseline value from the literature (D=2.37mm^2/day [196]) was derived from a long bone fracture scenario where the distance over which cells diffuse is considerably higher than this model, where the maximum cell diffusion distance was only 5mm, explaining the low effect of this variable. However, no mathematical or biomechanical justification for the 10 day Young's Modulus smoothing period was found in the literature [195, 197], so the value of the implied stem cell maturation rate parameter 'M' *was* investigated. The baseline value of 10% was used, plus values of 5% and 3.3%, referring to averaged smoothing periods of 10, 20 and 30 days respectively.

Finally, Case 9 considered a combination of reduced threshold remodelling stimulus and stem cell maturation rate, with values of s_{mature}=±62.5% and M=5%/day.

The remaining process parameter values used in the algorithm were materials properties values (Table 6); these have firm theoretical and experimental justification so were not varied in this investigation.

6.2.3 Results Metrics

Qualitative analysis of the results was conducted using virtual X-Rays [216], generated at notable time points postoperatively as described in Appendix 2. This allowed the locations of particular regions of bone densification and resorption to be observed more completely than is possible using single planar sections through the bone, the regularly adopted approach in the literature.

Quantitative analysis used a virtual DEXA scan subroutine written in the FE post-processor, which calculated the areal Bone Mineral Density (BMD) associated with defined regions in the medial and lateral femoral neck (Figure 83). The *percentage change* in BMD was used to remove any patient size effects from BMD measurements [243], comparing the values at 3, 6, 12 and 24 postoperative months to the immediately postoperative values. To corroborate the model's predictions, these values were compared to clinical measurements of the changes in BMD following resurfacing at the same time points [74, 75, 82].

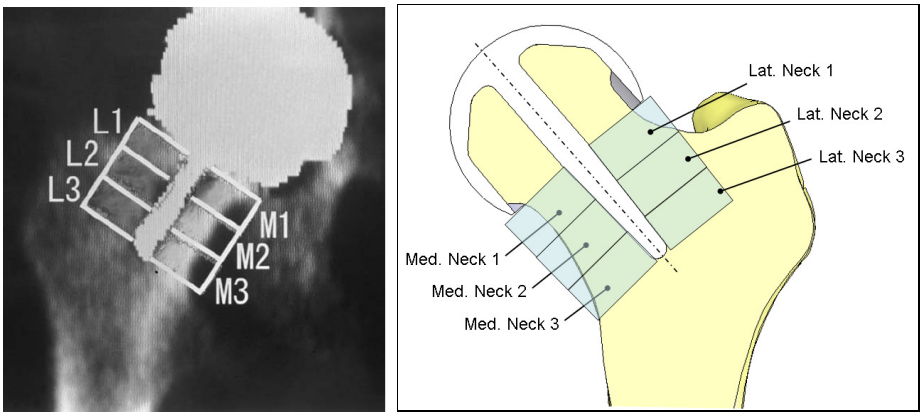

Figure 83: Femoral Neck Virtual DEXA Scan Zones from the Literature (left) and the Present Study's Model (right). Left image Reproduced and adapted with permission and copyright © of the British Editorial Society of Bone and Joint Surgery [74]

6.3 Results

6.3.1 Benchmark Remodelling and Healing Investigations

For the two extreme, pure remodelling situations (Cases 1 and 2), and the baseline healing situation (Case 3), bone density variations over the first two postoperative years were predicted and virtual X-Rays were generated. The postoperative, 3 and 24-Month follow-up virtual X-Rays are shown (Figure 84). Much like real X-Rays, some of the changes were subtle so they are best visualised in the detail views shown in Figure 85.

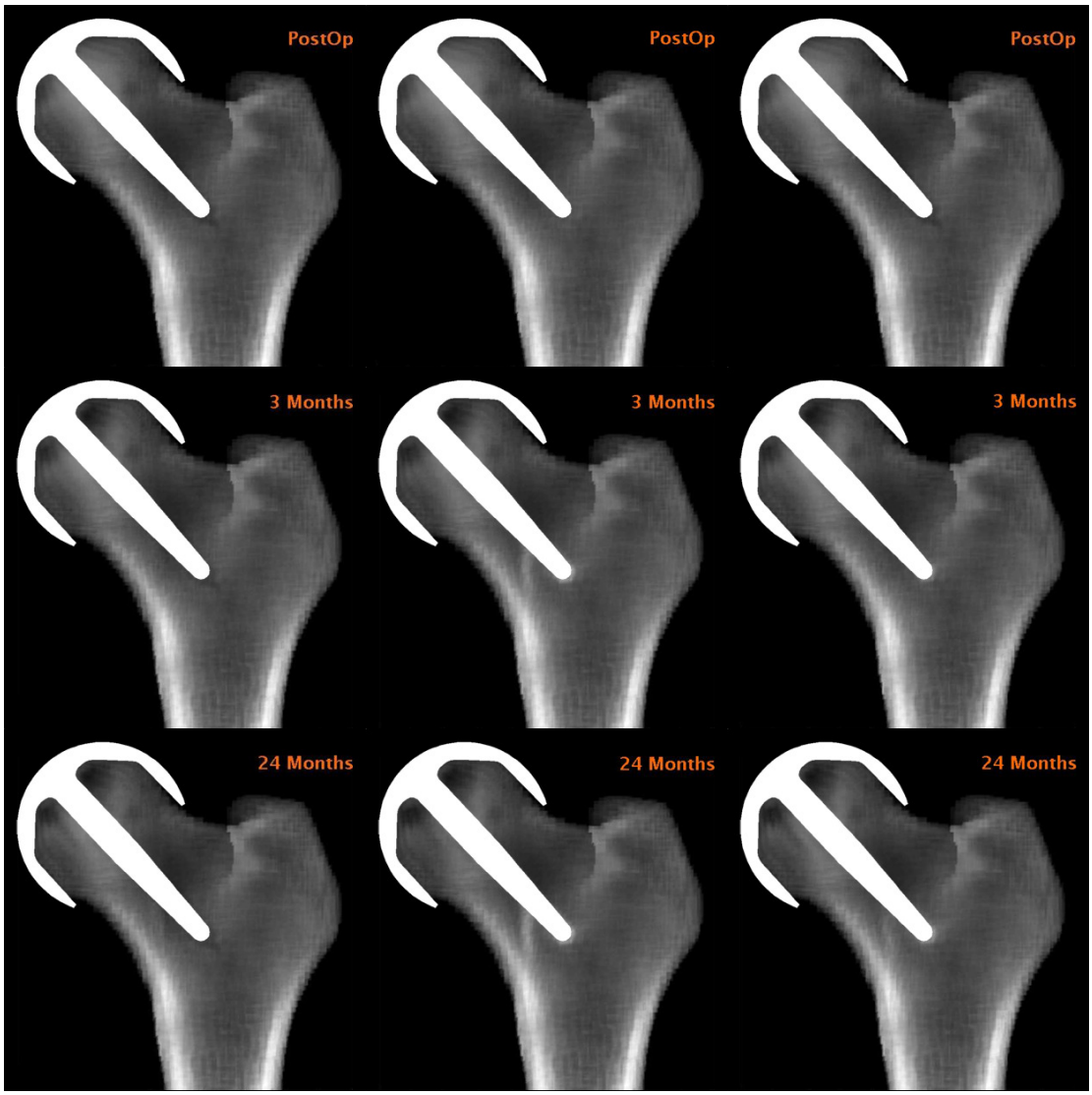

Figure 84: Virtual X-Rays at 0, 3 and 24 Months Follow-Up for Case 1 (Stem-Bone Gap, left), Case 2 (Stem-Bone Contact, centre) and Case 3 (Baseline Healing Gap, right).

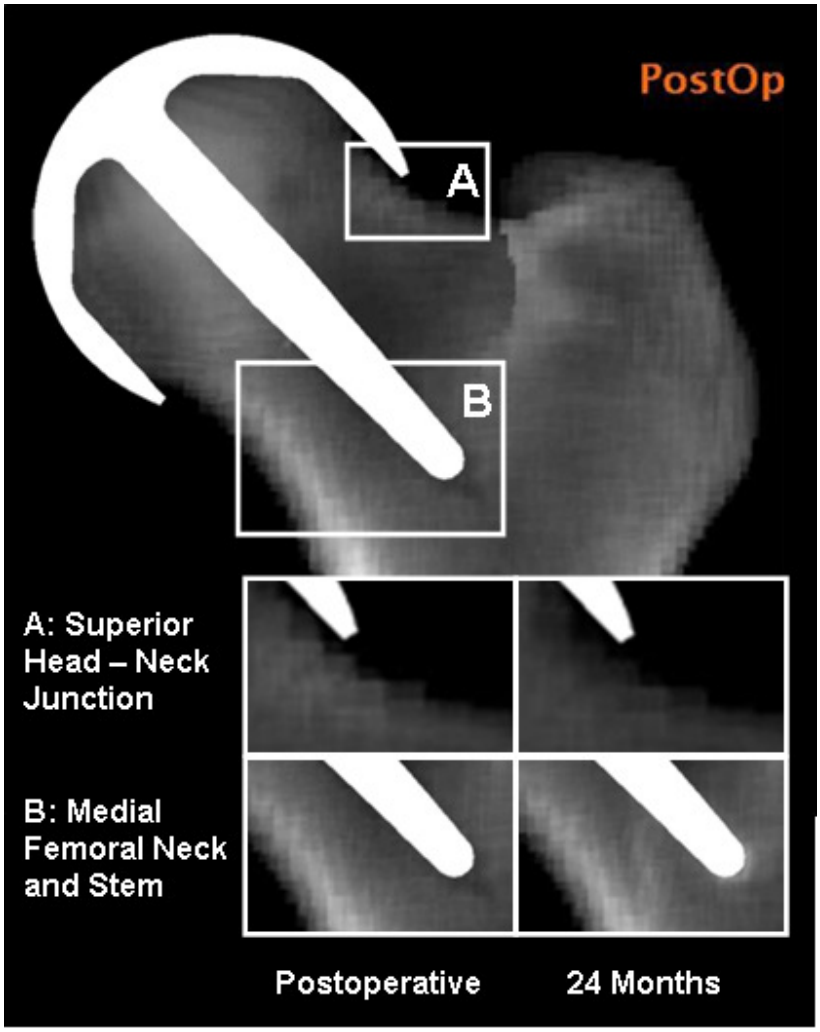

Figure 85: Details of Virtual X-Rays for a Healing Stem-Bone Gap

For quantified analysis, virtual DEXA scans were taken of the medial and lateral femoral neck regions in the FE models, and the resulting time history of percentage change in BMD was plotted. This data is included in the following charts (Figure 86):

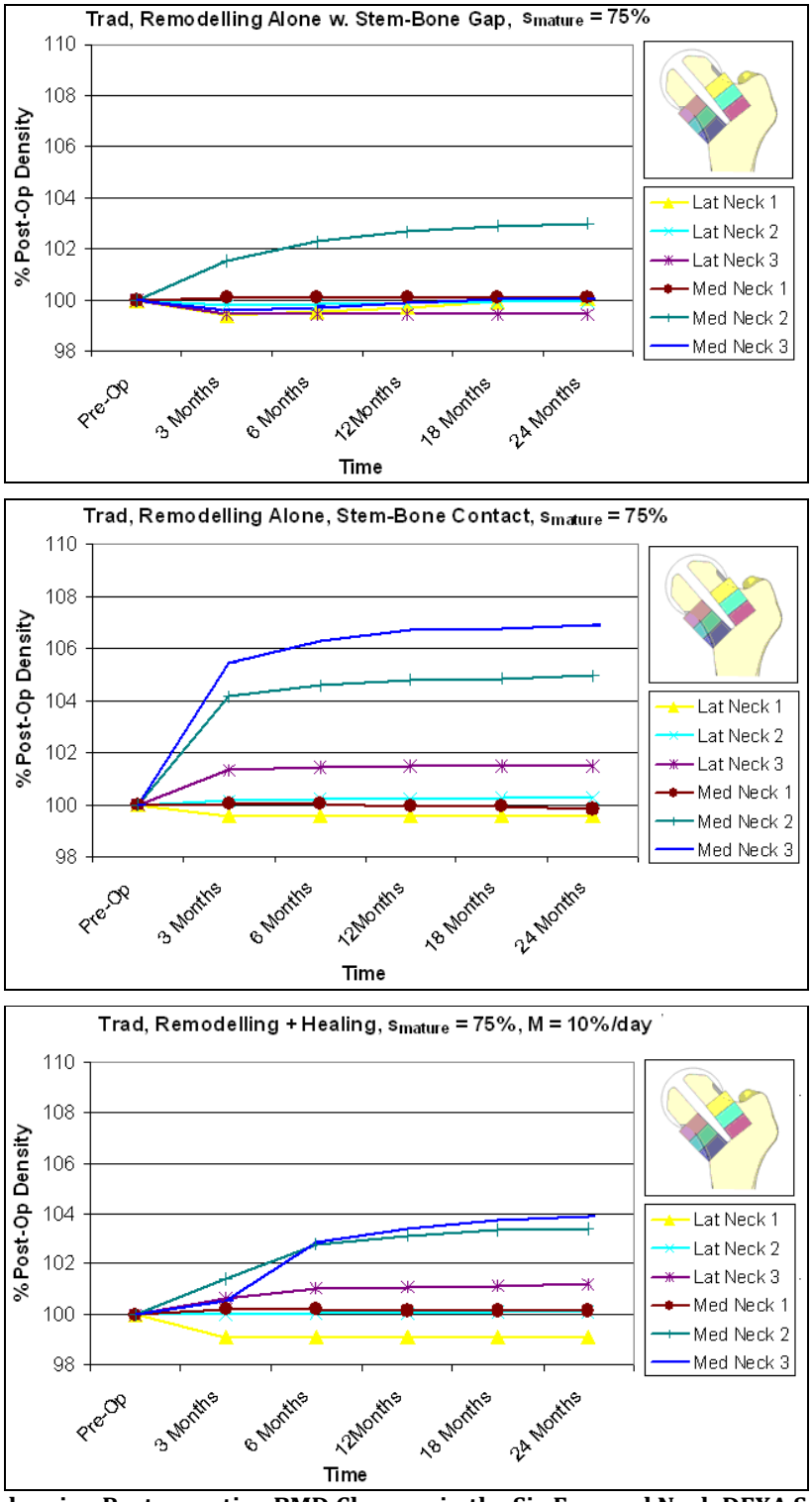

Figure 86: Charts showing Postoperative BMD Changes in the Six Femoral Neck DEXA Scan Zones for Case 1 (Stem-Bone Gap, Top), Case 2 (Stem-Bone Contact, Middle) and Case 3 (Baseline Healing Gap, Bottom).

These first results show bone adaptation predictions obtained using algorithms which simulate strain energy density (SED) stimulated bone remodelling alone, and combined bone remodelling and implant-bone interface defect healing. Both of the pure remodelling cases showed an incomplete set of the clinically observed radiographic changes, shown in virtual X-Rays (Figure 84). Both cases showed considerable resorption inside the femoral head, but much like real X-Rays, the changes in the femoral neck were subtle and are best understood with the charts of virtual DEXA scan data (Figure 86). Case 1, with no distal stem-bone contact, showed:

- a progressive increase in bone mineral density (BMD) in the medial femoral neck (zone M2),
- slight reductions in BMD around the tip of the stem (M3 and L3) due to the bore, and
- a reduction in BMD at the superior head-neck junction (L1), representative of femoral neck narrowing.

The BMD losses in regions M3 and L1 were both predicted to recover by 24 months, and the bore remained visible radiographically.

Case 2, with perfect stem-bone contact, showed:

- considerable increases in BMD in the medial neck, further down the stem (M2 and M3), in a focussed line between the stem and medial calcar, co-linear with the cortex,
- increased BMD at the stem tip similar to a 'pedestal' line indicating a stem neo-cortex (L3), and
- a sustained reduction in BMD at the superior head-neck junction (L1), indicating femoral neck narrowing.

The radiographic changes predicted in this case were a more complete representation of clinical observations. However, the densifications around the stem occurred immediately postoperatively and in a clearly focussed line, both of which are unrealistic.

Case 3, with progressively established stem-bone contact during healing, showed:

- more gradual increases in BMD in the medial neck (M2 and M3) and around the stem tip (L3), and
- sustained narrowing of the femoral neck at its superior edge (L1).

The results of this baseline healing case (Figure 85) lay between the two extreme cases of stem-bone contact. Superior femoral head resorption was similar for all three cases. The predicted radiographic changes were more consistent with clinical observations in that the changes occurred more progressively than in the full contact Case 2, and medial bone densification was slightly more evenly distributed. However, a focussed dense line still formed between the stem and the medial neck cortex which indicates that the changes still occurred fast in comparison to clinical reports, where medial densification is distributed more evenly [4, 72]. These observations indicate that with the baseline healing process parameters, stem-bore contact was established too quickly, in agreement with the findings of the unloaded healing case (Appendix 1).

The baseline healing model was then repeated using the BHR prosthesis geometry. The virtual X-Rays for the two prostheses are compared in Figure 87:

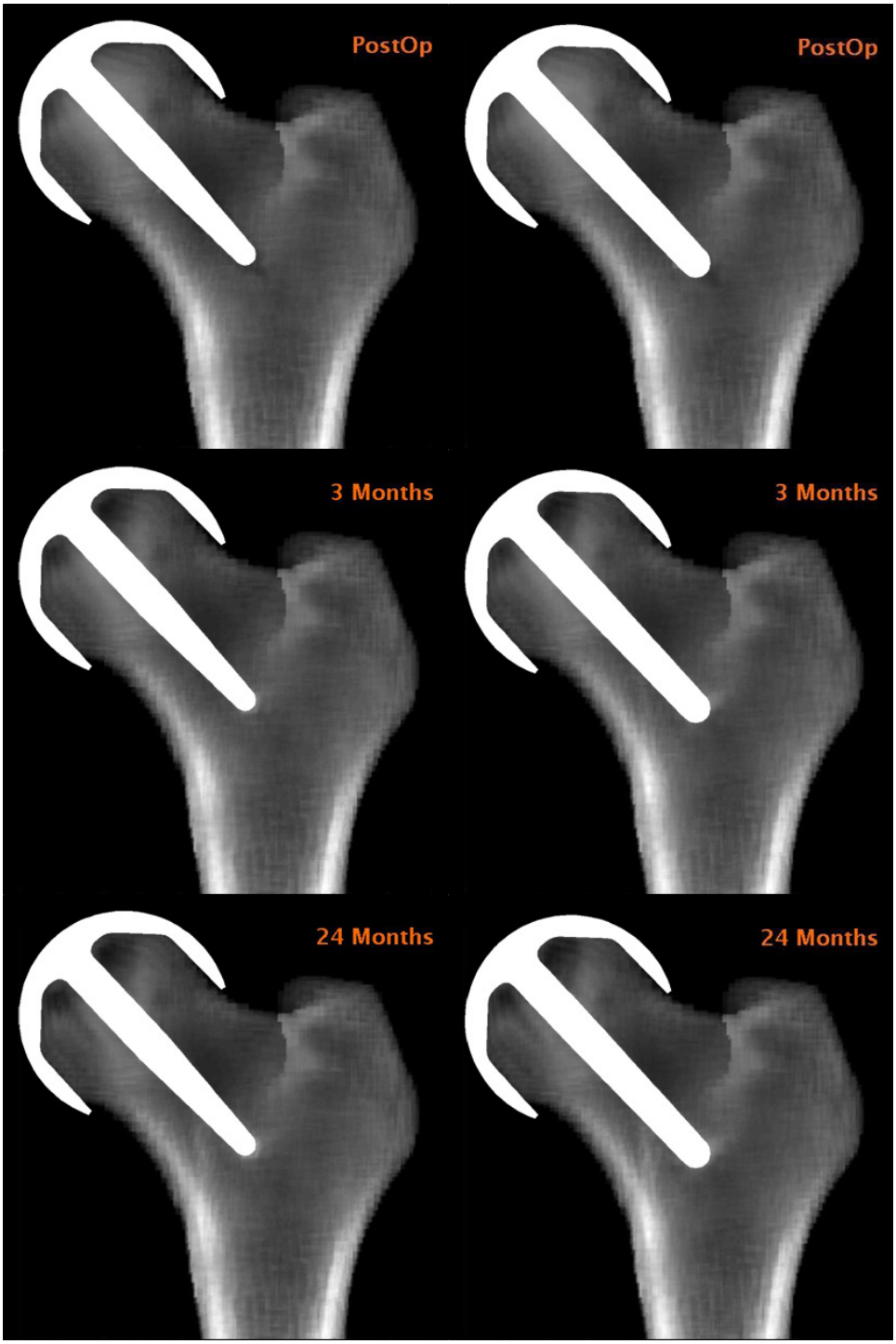

Figure 87: Virtual X-Rays at 0, 3 and 24 Months Follow-Up for the Two Baseline Healing Cases, Case 3 (ADEPT Prosthesis, left) and Case 4 (BHR Prosthesis, right).

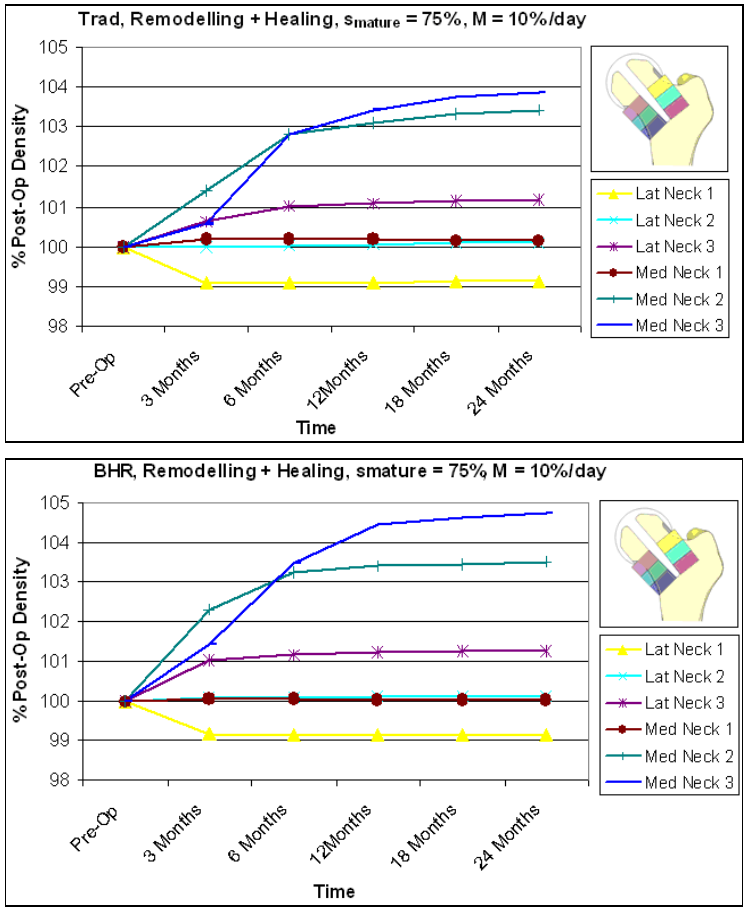

Figure 88: Charts showing BMD Changes Postoperatively in the Six Femoral Neck DEXA Scan Zones for the Baseline Healing Models, Case 3 (ADEPT Implant, Top) and Case 4 (BHR Implant, Bottom).

Comparison of the predictions for the ADEPT and BHR prostheses indicated that similar radiographic changes would be expected around both implants, despite the BHR's larger diameter stem. The BHR was predicted to cause slightly higher levels of bone densification in the medial femoral neck (M2 and M3), but in a less focussed distribution. The rate of densification around the stem and in the medial neck was higher for the BHR, indicated by changes in zones M2, M3 and L3, because the BHR stem tapers less and therefore its bore is a narrower gap to fill.

The BHR prosthesis was studied to allow the model's predictions to be compared to DEXA studies in the literature [74, 75, 82]. All three studies showed an initial postoperative reduction in BMD followed by a gradual recovery, with a more marked BMD reduction in the lateral neck and a greater BMD increase medially (Figure 89). However, data reported by two of these studies included additional data:

- Borg et al reported a slight increase in BMD in the contralateral hip following surgery [75] indicating increased postoperative activity, and
- Lian et al observed similar magnitude changes in the proximal femur remote from the prosthesis [82], indicating reduced activity or loading of the operated leg immediately postoperatively, and later increased activity level and favouring of the treated leg (Figure 90).

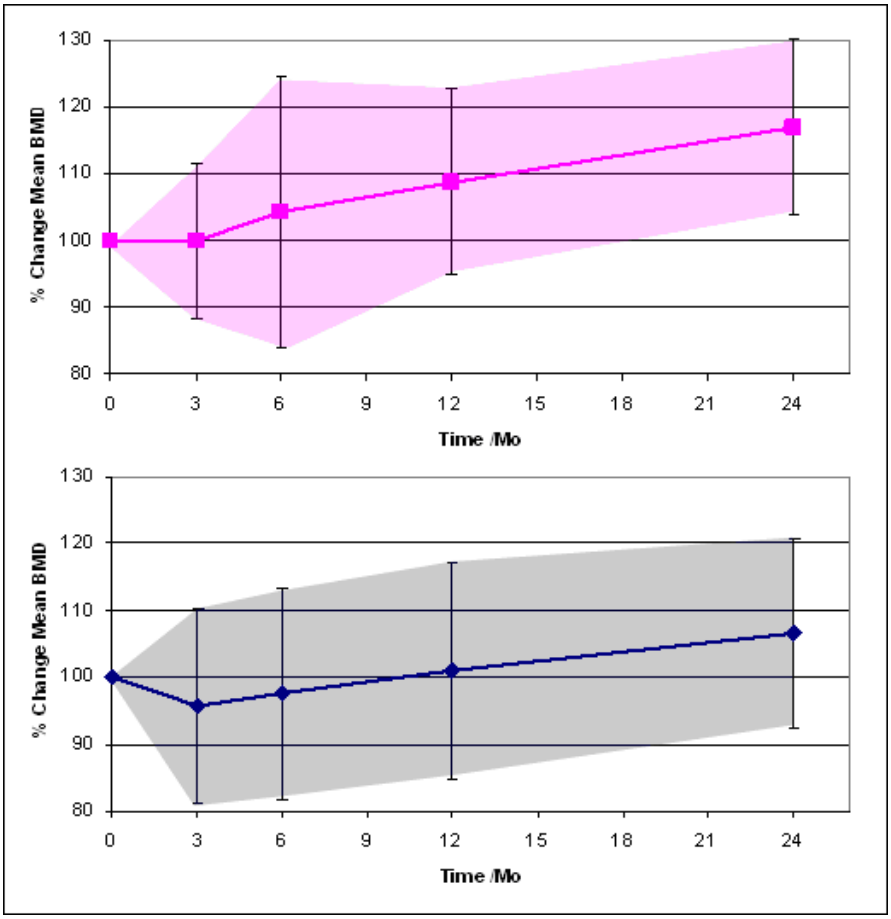

Figure 89: Mean % Change in BMD for the Medial (Top) and Lateral (Bottom) Femoral Neck following Hip Resurfacing. Data from Lian et al 2008 [82]. Error Bars indicate One S.D.

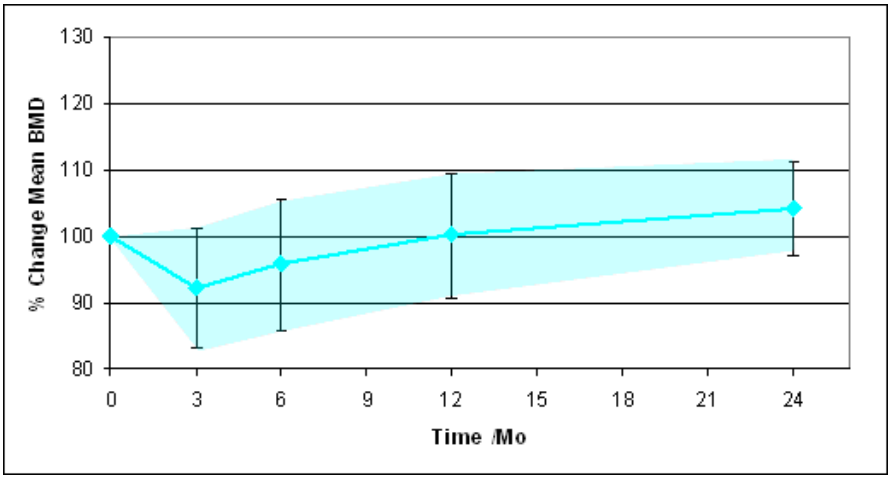

Figure 90: Background Mean % Change in BMD for the Proximal Femur Distant from the Femoral Neck following Hip Resurfacing. Data from Lian et al 2008 [82]. Error Bars indicate One S.D.

The FE model does not attempt to capture explicitly changes in activity and metabolism during and after recovery from surgery. However, these factors will have a considerable effect upon real bone adaptation. To account approximately for changes in patient activity levels, the data obtained from the FE model in this study were scaled with the background BMD percentage change data from Lian et al [82] and plotted on Figure 91. With this scaling it was possible to include implicitly the effects of increased postoperative activity levels, allowing direct comparison with the literature clinical data. To this end, Figure 91 contains envelopes of the literature study's mean ± one standard deviation medial and lateral femoral neck BMD changes.

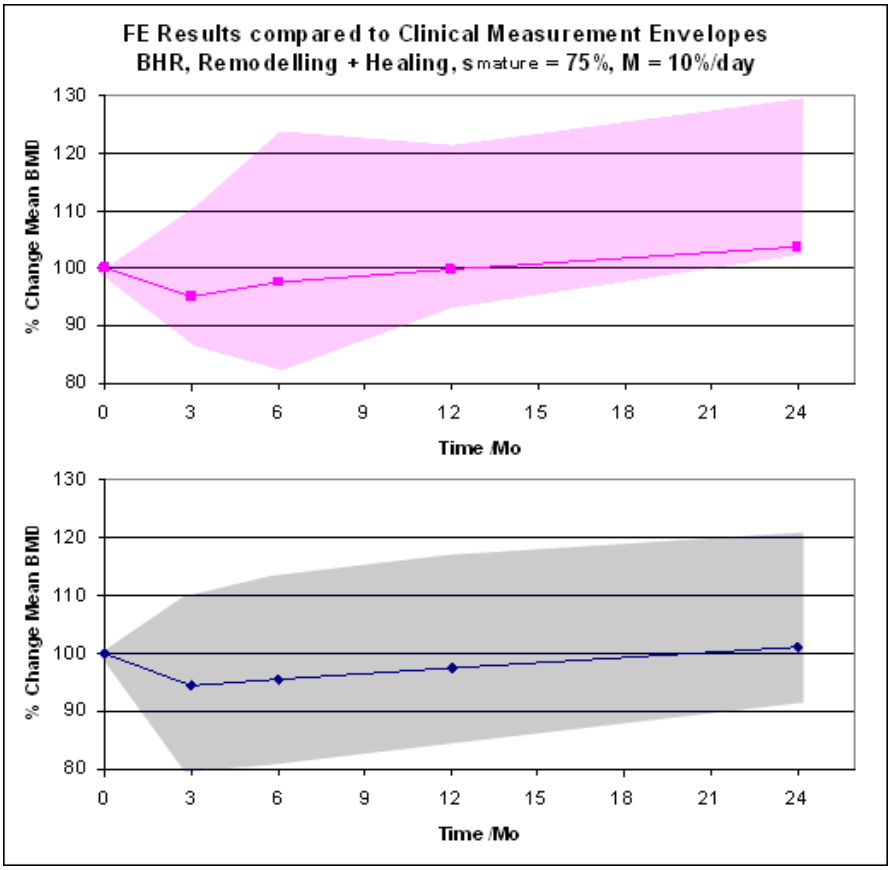

Figure 91: Charts showing BMD Changes Postoperatively in the Medial (Top) and Lateral (Bottom) Femoral Neck DEXA Scan Zones for the BHR Healing Model, Case 4, Scaled for Postoperative Activity Levels and Plotted within Mean ± One S.D. Envelopes of Clinical Data [82].

Comparing this study's FE models with clinical measurements showed an agreement in the trends of predicted BMD changes, particularly in the lateral femoral neck. The magnitude of BMD changes are towards the bottom of the clinical range in the medial neck. However, the FE model trends were small in comparison to the range of clinical measurement variability. This means that a quantitative interpretation is justifiable for the time scale, but is precluded for the BMD change magnitudes due to the high inherent variability of the clinical data. It was concluded that this data should be interpreted qualitatively, in conjunction with commonly reported X-Ray observations, for the selection of healing and remodelling process parameters for the algorithm.

On that basis, the remodelling process dominated in the first three months and appears to account well for the distributions and time for femoral head and neck bone resorption. However, after three months, once the healing process began to dominate in the femoral neck bone adaptations were

predicted to occur unrepresentatively fast and this may have contributed to the formation of an artificially focussed distribution of densifying bone between the prosthesis stem and the medial cortex. These observations help to structure the following investigation into the remodelling and healing process parameters, indicating that a lower stem cell maturation rate 'M' would be necessary to reduce the healing rate, and that a lower threshold mature bone remodelling stimulus 's_{mature}' would increase the magnitude of BMD changes.

6.3.2 Remodelling and Healing Process Parameter Investigation

In the second part of the study, the sensitivity of two remodelling and healing process parameters was investigated. For the baseline stem cell maturation rate (M=10%/day) and three values of the threshold bone remodelling stimulus 's_{mature}', bone density variations over the first two postoperative years were predicted and virtual X-Rays were generated. The postoperative, 3 and 24-Month follow-up virtual X-Rays are shown (Figure 92):

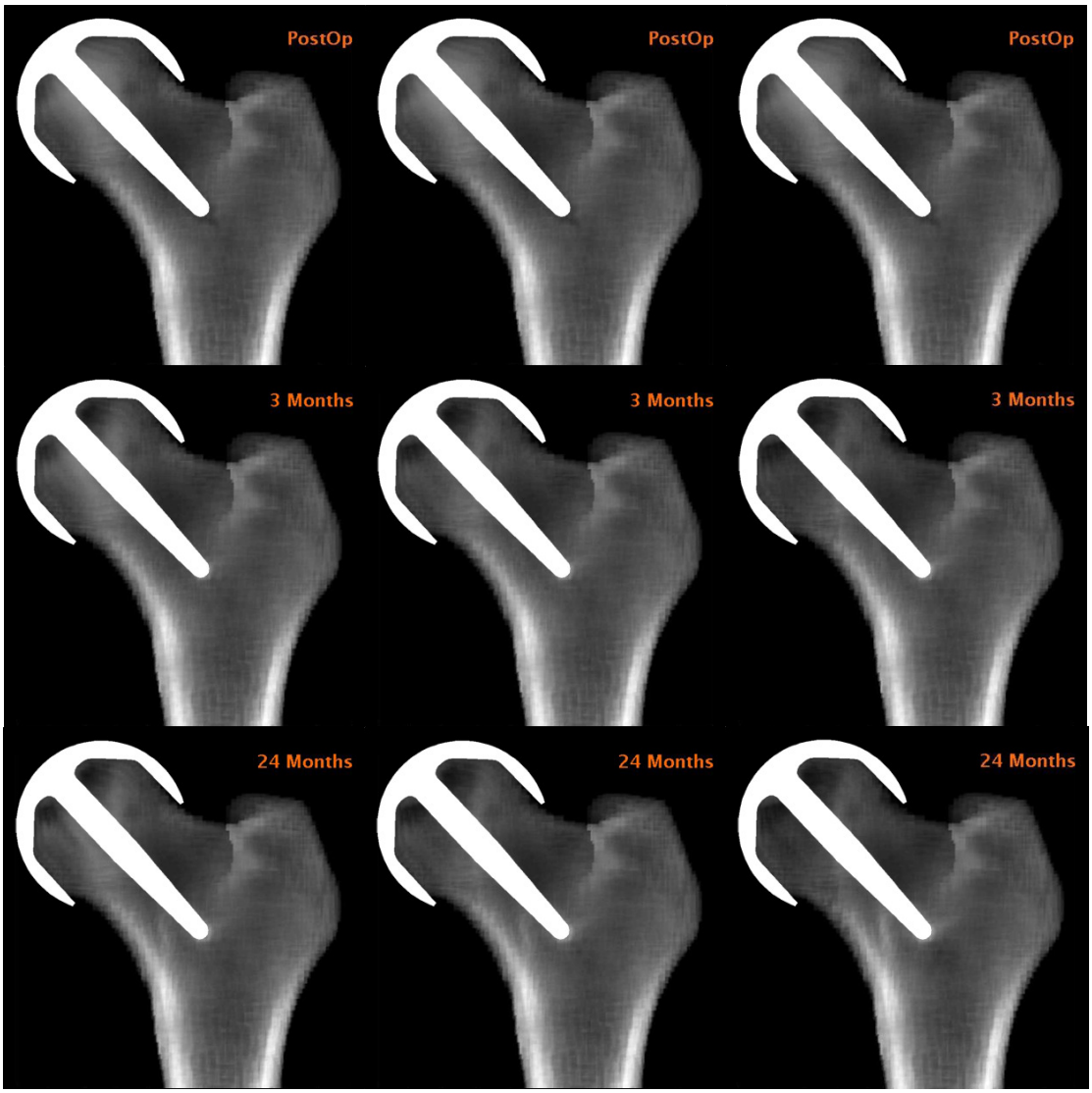

Figure 92: Virtual X-Rays at 0, 3 and 24 Months Follow-Up for Varying Threshold Remodelling Stimulus Values: Case 3 (±75%, left), Case 5 (±62.5%, centre) and Case 6 (±50%, right).

Virtual DEXA scans were taken of the medial and lateral femoral neck regions in the FE models from this sensitivity analysis, and the resulting time history of percentage change in BMD was plotted. This data is included in the following charts (Figure 93):

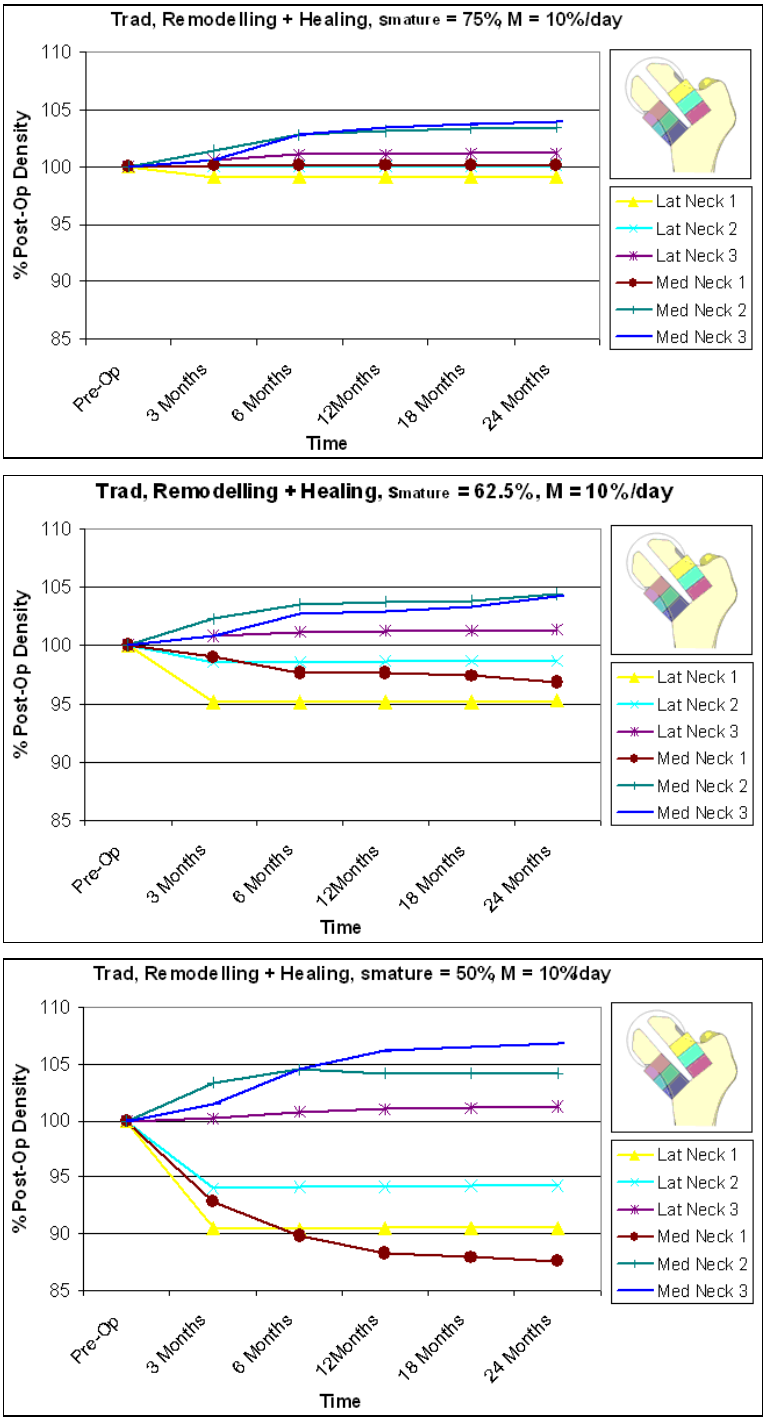

Figure 93: Charts showing BMD Changes Postoperatively in the Six Femoral Neck DEXA Scan Zones for Varying Threshold Remodelling Stimulus Values: Case 3 (75%, Top), Case 5 (62.5%, Middle) and Case 6 (50%, Bottom).

These results indicate that the magnitude of BMD changes in the femoral neck would be higher with a smaller threshold bone remodelling stimulus, as shown in the virtual X-Rays (Figure 92). With a ±50% threshold stimulus, observed BMD changes were increased resorption inside the femoral head and at the superior head-neck junction, indicating more extensive femoral neck narrowing. The extent of bone densification was also larger with a lower threshold remodelling stimulus, but this effect was less marked than the resorption. The radiographic changes predicted for the ±75% bone remodelling stimulus value commonly used in the literature, after Weinans et al [215], were representative of clinical radiographic observations. However, to the extent that quantitative analysis of these results in comparison to clinical data is valid (see Section 6.3.1), the results in the first half of this analysis with baseline parameters indicated that the magnitude of BMD changes was underestimated. Concurrently, the charts in Figure 93 suggest that a value of ±62.5% may produce more acceptable predictions for a younger hip resurfacing candidate patient, with more extensive adaptations resulting from a more active metabolism. The results indicated that reducing the threshold remodelling stimulus to ±50% would lead to unrepresentatively high levels of resorption.

Next, for the baseline bone remodelling stimulus change level (s_{mature}=±75%) and three values of the stem cell maturation rate 'M', bone density variations over the first two postoperative years were predicted and virtual X-Rays were generated. The postoperative, 3 and 24-Month follow-up virtual X-Rays are shown in Figure 94. Virtual DEXA scans were produced for medial and lateral femoral neck regions, and the resulting time history of percentage change in BMD was plotted (Figure 95).

This data shows that a lower stem cell maturation rate 'M' of 5%/day would lead to predictions of a similar magnitude of medial femoral neck BMD increase (zones M2 and M3) to the value used commonly in the literature (10%/day, or a 10 day averaged smoothing function [195, 197]). However, the densification rate was predicted to be slower, and the distribution of densifying medial trabeculae would be more even and therefore more clinically representative. In contrast, with a high stem cell maturation rate, an artificially focussed dense band of trabeculae was predicted to form between the prosthesis stem and the medial neck cortex. With a maturation rate of 3.3%/day, stem bore healing was not predicted to be complete at 24 months of follow-up, which clinical radiographic observations suggest is artificially slow [3, 72]. Extents of femoral head resorption and femoral neck narrowing were predicted to be similar in all three cases. These results, in agreement with the unloaded sensitivity

study (Appendix 1) suggest that in this application of a healing trabecular bone defect, a stem cell maturation rate of M=5%/day would produce the most clinically representative bone adaptation predictions.

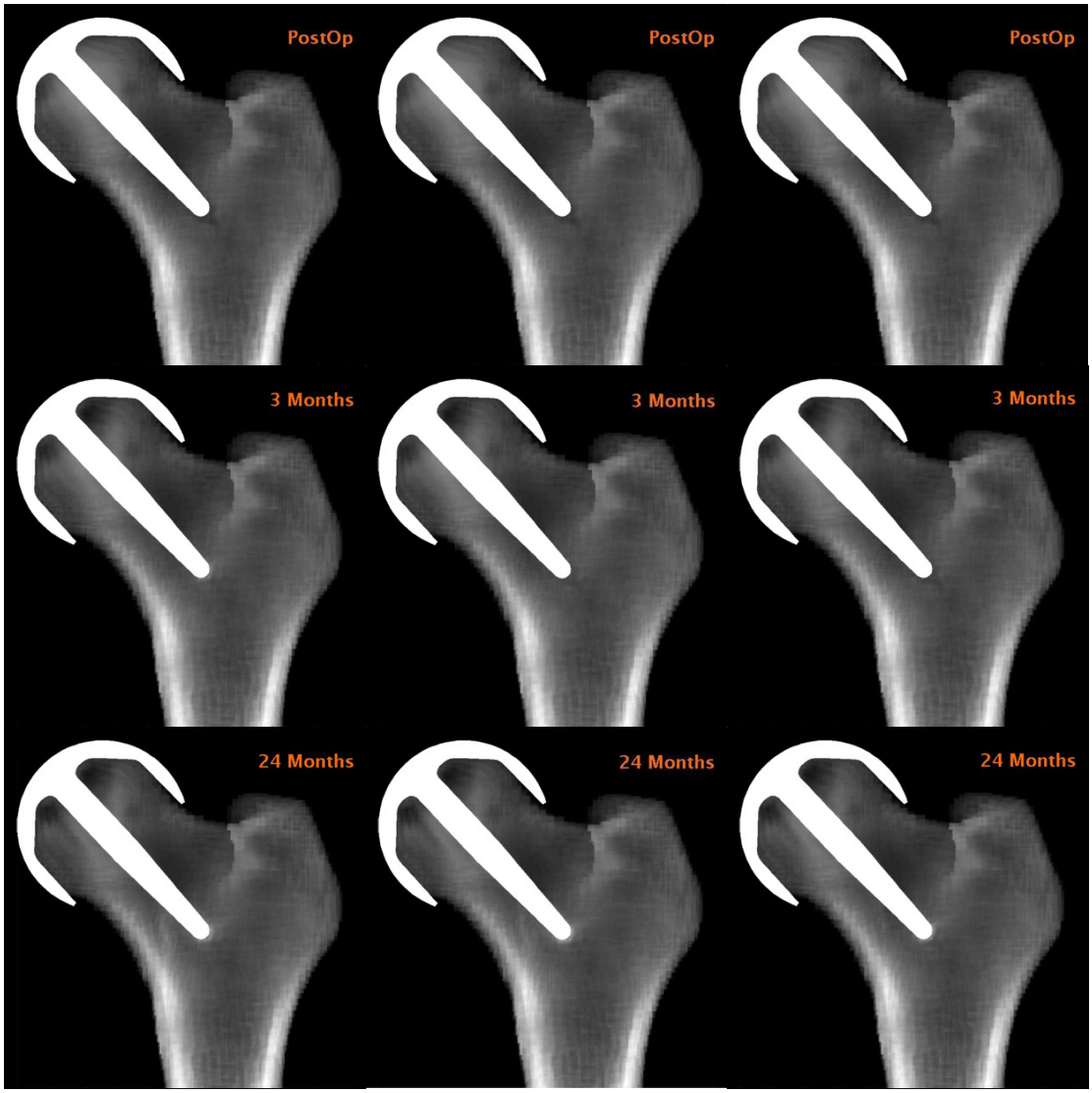

Figure 94: Virtual X-Rays at 0, 3 and 24 Months Follow-Up for Varying Stem Cell Maturation Rate Values: Case 3 (10%/day, left), Case 7 (5%/day, centre) and Case 8 (3.3%/day, right).

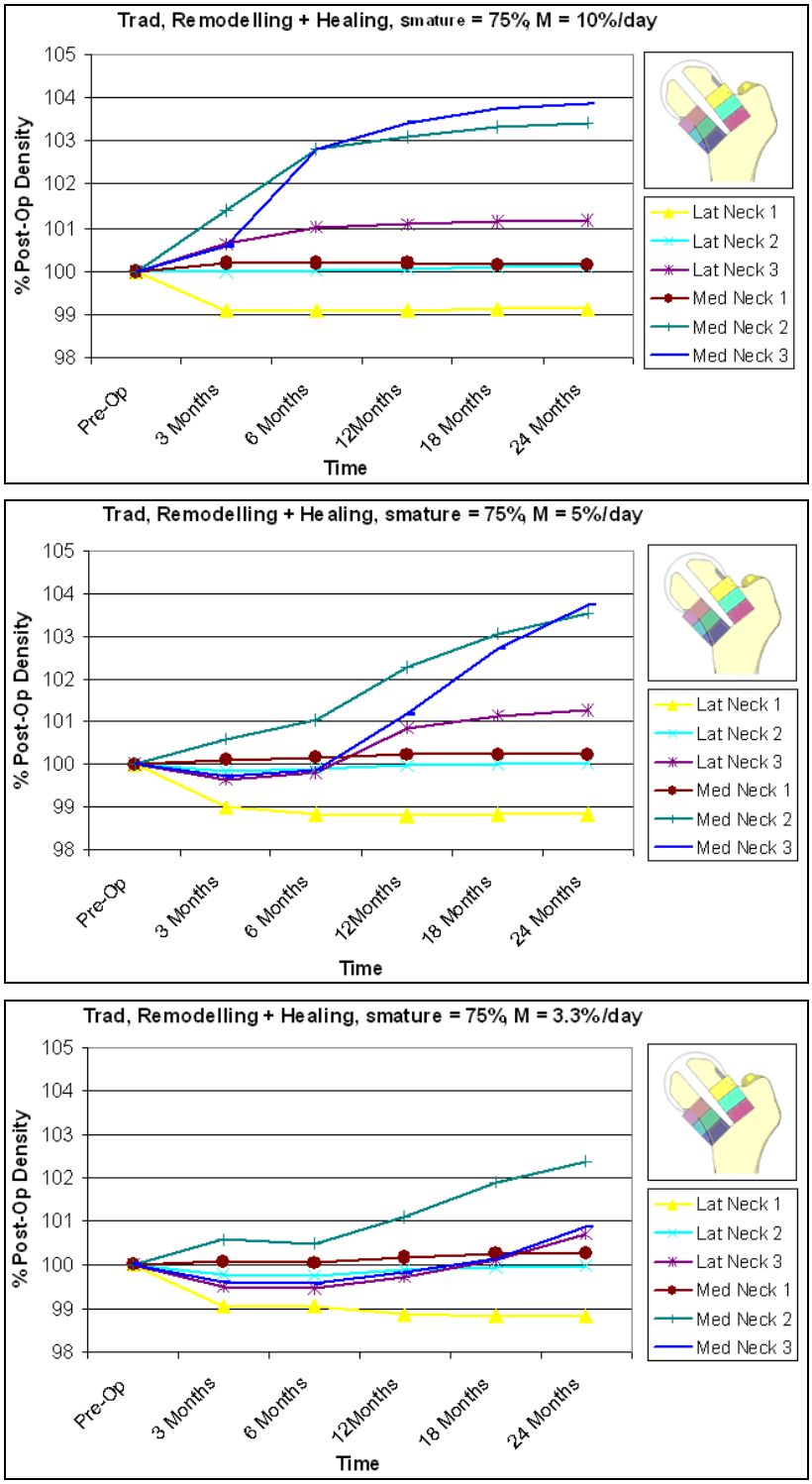

Figure 95: Charts showing BMD Changes Postoperatively in the Six Femoral Neck DEXA Scan Zones for Varying Stem Cell Maturation Rate Values: Case 3 (10%/day, Top), Case 7 (5%/day, Middle) and Case 8 (3.3%/day, Bottom).

Finally, the results produced by Case 9 are presented. This case considered a combination of reduced threshold remodelling stimulus (s_{mature}=±62.5%) and stem cell maturation rate (M=5%/day), and the postoperative virtual X-Rays are included in Figure 96. With these process parameter values, the full set of clinically observed radiographic changes were visible on the virtual X-Rays, and were produced without artificially focussed lines of bone densification.

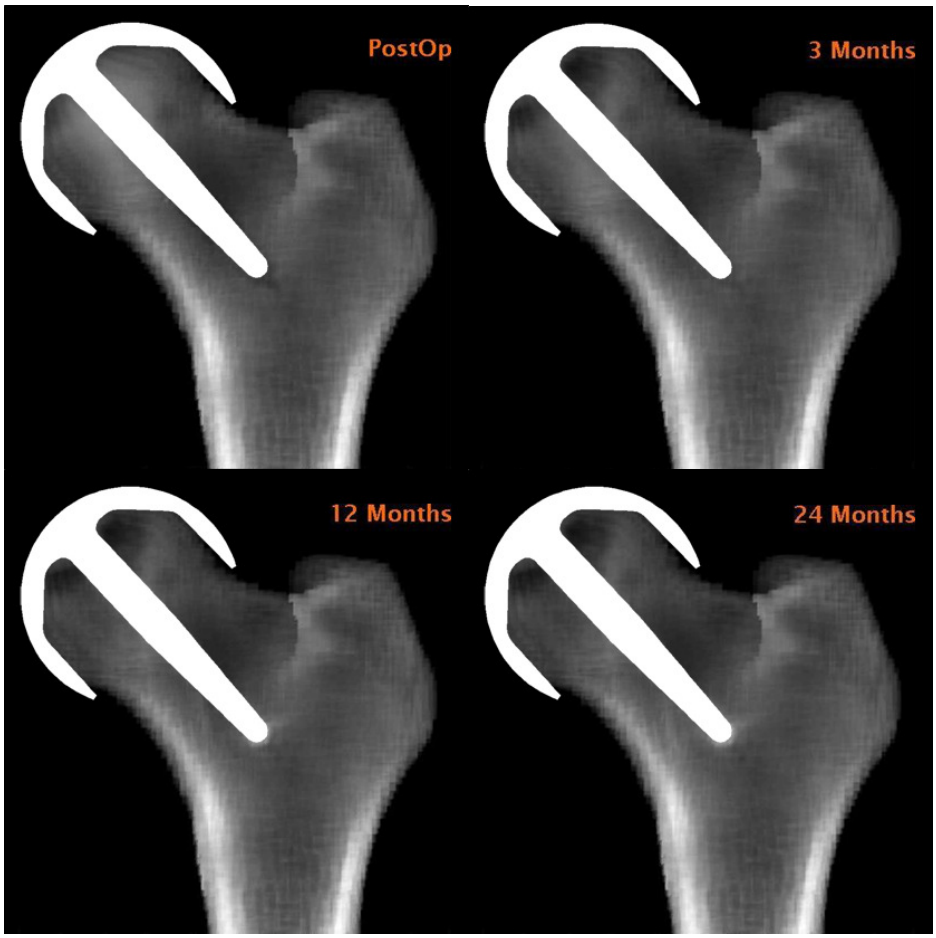

Figure 96: Virtual X-Rays at 0, 3, 12 and 24 Months Follow-Up for Case 9, the Combined Best Remodelling and Healing Process Parameter Values (s_{mature}=62.5%, M=5%/day).

Figure 97 shows the virtual DEXA scan results for this case, demonstrating medial trabecular densification (M2 and M3) predicted to stabilise between 12 and 18 months, and narrowing of the femoral neck both laterally and medially at the head-neck junction. Analysis of these Virtual X-Rays and DEXA scans indicates that a threshold remodelling stimulus of ±62.5% and a stem cell maturation rate of 5%/day gave the best fit to clinical observations of the values tested.

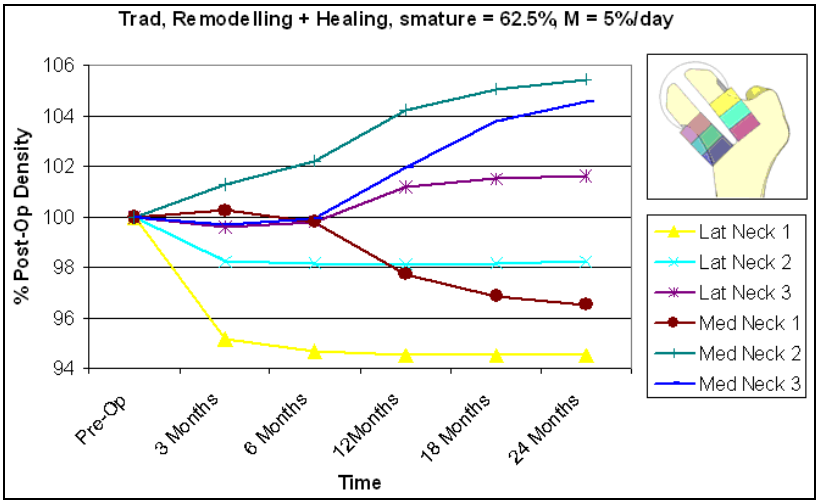

Figure 97: Chart showing BMD Changes Postoperatively in the Six Femoral Neck DEXA Scan Zones for Case 9, the Combined Best Remodelling and Healing Process Parameter Values (s_{mature}=62.5%, M=5%/day).

6.4 Discussion

The FE analysis predictions of adaptive bone remodelling around hip resurfacing implants were in agreement with radiographic clinical observations [3, 4, 45, 67, 72], demonstrating all of the typically observed changes. The model showed densification of medial femoral neck trabeculae, the formation of dense lines around the prosthesis stem tip, slight narrowing of the femoral neck and resorption inside the femoral head. Previous adaptive FE modelling studies [13, 203] have produced partial predictions of these changes, but none has simulated the full set, missing in particular femoral neck narrowing. This study attempted a quantified comparison of these changes to clinical DEXA data.

The study is subject to several limitations, as the FE model is a great simplification of the real biomechanical system. This simplification is necessary but must be justified. The major limitations are that the model is based on a single femur and was subjected to a single load case. These simplifications were necessary due to computational expense. A compromise between accuracy and solution time was made and since the goal of the study was the detailed reproduction of a biomechanical process, accuracy was favoured. For a multi-femur analysis attempting to capture a range of clinical variability, minimal solution time would be favoured and with the available computer hardware, solution accuracy would have been inadequate. Multi-femur analysis would also be precluded by the iterative approach to adaptive bone remodelling simulation, which required numerous solutions and considerable processing time for each model. Given this compromise, the femur was selected as an ideal candidate for hip resurfacing (discussed fully in Study 1, Chapter 5), and the single load case was chosen with

care. The peak joint contact force instant in the gait cycle was used, as this would produce the peak strain experienced by a large proportion of the bone. The justification for gait as the loading scenario was that, as explained by Frost [217, 244], modelling and remodelling are stimulated most by 'a time averaged value of repeated peak strains', whereas occasional high magnitude strain events have little influence, provided they do not cause damage. Furthermore, the single peak instant in the gait cycle was used instead of a number of time averaged instants in the cycle because low magnitude strains, below a 'minimum effective strain, MES' of perhaps 2000με do not evoke an osteocytic reaction. Finally, the effect of any simplifications in the applied load cases is minimised by the comparative stimulus, which considers only the change in the bone strain field as a result of implantation. This approach neglects changes in pre- to postoperative activity levels and loading, although these effects were applied implicitly in this study by superposition of background BMD changes from the literature.

Similarly, the choices of stimuli for bone modelling and remodelling are likely to be simplifications of the signals sensed by osteocytes *in-vivo*. Bone remodelling was stimulated by the strain energy density which employed an equivalent strain, analogous to the von Mises stress and containing contributions of principal strains and shear. Bone healing or modelling was stimulated by this equivalent strain and the hydrostatic pressure, representing deviatoric strains and interstitial fluid pressure. Although they arise from single studies [191, 245], these stimuli have been used repeatedly over many years of study reported in the literature, establishing their suitability through corroboration. Although they are unlikely to be precisely the *in-vivo* mechanical osteocyte stimuli, the behaviour that they predict is in good agreement with clinical observations so they can be considered acceptable analogies of the *in-vivo* stimuli. This study aimed to extend their use and combine the two biomechanical processes, so it was logical to base the methods upon established approaches. In particular, there is scope to improve the understanding of the healing of the cancellous bone defect around the prosthesis stem, using stem cell maturation rates which are linked to the stability provided by the prosthesis surface or surrounding trabecular surfaces, in a similar manner to Martin's free surface area principle [177]. In this study, an attempt was made to simulate more physiological rates of bone adaptation by capping the maximum bone deposition rate according to this free surface area and a value for the maximum osteoblast deposition rate [217], and other studies have applied limits to bone densification with bone damage stimulated resorption [185, 186]. However, the stimuli employed were able to produce predictions of the patterns of postoperative bone adaptation in overall agreement with clinical observations, which suggests that they are suitable for comparative investigations.

Finally, the ultimate conclusion should be interpreted with care. A set of process parameters (Case 9, s_{mature}=±62.5% and M=5%/day) were selected as they gave the best fit to clinically observed bone density changes. The threshold remodelling stimulus of ±62.5% was in agreement with a similar sensitivity analysis study from the literature [216]. Femoral neck narrowing is observed in the majority (up to 90%) of patients [3, 42, 45, 68, 70, 72]. Sclerotic lines around the stem are also common, and radiographically clear lines have been observed in 60-75% of cases [4, 45]. However, medial trabecular densification is less usual, observable in only 50% of these patients [4]. This study found remodelling and healing process parameters which forced these bone adaptations to occur in a particular patient. Instead of representing a standard patient's biomechanical response, they are perhaps best interpreted as worst cases for use in preclinical analysis, in the same manner that one uses a worst load case for a femoral neck fracture investigation. The model's best use in preclinical analysis is comparative: a proposed new design would be favoured if it is shown to generate a smaller bone adaptation response under these conditions than a traditional design.

6.5 Conclusions

The following conclusions can be drawn from this study:

- qualitatively, bone adaptations predicted by FE models were in closer agreement with clinically observed radiographic changes when combined bone interface healing and remodelling were used, than with remodelling alone.
- quantitatively, for variables of stem-bone contact conditions and the extent of the prosthesis stem taper, trends and magnitudes of BMD changes in the FE modelling study were predicted to be small in comparison to variability in clinical measurements. However,
- the cell diffusion and tissue differentiation based healing process used commonly in the literature led to unrepresentatively high healing rates and low levels of medial femoral neck bone densification in this application. An improved set of process parameter values for pre-clinical study was proposed.

7 STUDY 3: APPLICATION OF MODELLING METHODS TO NEW DESIGNS

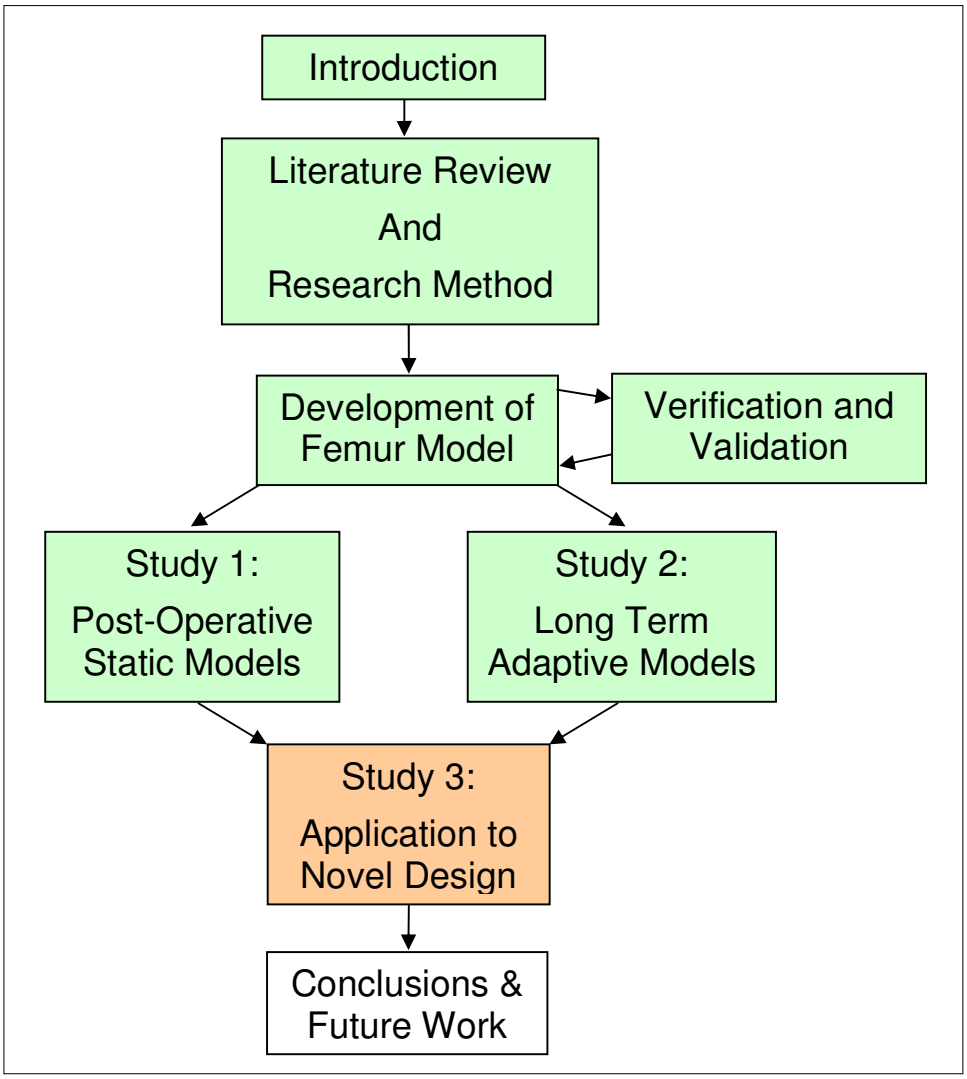

These results demonstrate the application of the previously developed modelling methods. This is a case study for their application to novel implant design concepts, evaluating a short stemmed resurfacing head.

The first part of these results was presented at the 54th Annual Meeting of the Orthopaedic Research Society (ORS) in San Francisco, USA, March 2008, and at the 22nd Annual Congress of the International Society for Technology in Arthroplasty, Hawaii, USA, October 2009.

This part of the study was also published in a journal article:

Dickinson, A S, Taylor, A C, Browne, M: *Performance of the Resurfaced Hip. Part 2: the Influence of Prosthesis Stem Design on the Remodelling and Fracture of the Femoral Neck*. Proceedings of the Institution of Mechanical Engineers, Pt. H: Journal of Engineering in Medicine, 2010, 224: p841-852.

The second part of the results was presented at the 6th World Congress on Biomechanics (WCB), Singapore, August 2010.

7.1 Introduction

While meticulous surgical technique and careful patient selection can serve to reduce the incidence of fracture under overloading, the conclusions drawn in Study 1 (Chapter 5) suggest that further improvements in neck fracture strength may be achievable through prosthesis design. In particular, the presence of a bore for the prosthesis stem was predicted to contribute to weakening of the femoral neck, especially in cases of poor prosthesis positioning.

Study 2 (Chapter 6) investigated the bone's adaptive response to resurfacing, considering in detail the extent of stem-bone contact. The results demonstrated a full set of clinically representative bone remodelling predictions, and indicated the role of the prosthesis stem in creating a distal load transfer shift, potentially contributing to proximal stress shielding and prosthesis loosening.

Changes in prosthesis design to reduce the risks of neck fracture and loosening must be achieved without adverse effects upon other performance factors such as the range of motion, and the amount of bone conserved in the arthroplasty procedure. There are constraints on prosthesis design to maintain the basic function of the joint, mainly relating to the geometry of the bearing surface and sizing relative to the host bone. Whilst the spherical bearing surface has been optimised for tribological performance and range of motion [246-248], research into the stem design has been within relatively confined limits and is not complete. As reported in the Literature Review, the stem diameter [12, 202] and extent of contact between the tapering stem and the host bone [12, 14] have been studied, but the stem length has only received limited attention [8, 194, 241].

The results of both studies presented so far in this thesis have suggested that a shorter prosthesis stem would have clinical benefits. In this final study, the hypothesis was tested that reducing the

prosthesis stem length would improve the biomechanics of the resurfaced femoral head and neck. It was proposed that an implant without a long stem could reduce the risk of femoral neck fracture because with a short stemmed or stemless implant, a long bore into the femoral neck would be unnecessary and the neck could be maintained intact. Furthermore the prosthesis loosening risk from adaptive remodelling could be diminished because the load transfer would not be shifted distally, so proximal stress shielding could be reduced. This chapter reports how the methods developed in the previous two studies were used as preclinical analysis tools for the assessment of a new design, testing short stemmed and stemless prosthesis concepts.

7.2 Methods

The FE modelling methods developed in the first two studies were used for the prosthesis design study. The design concepts were tested statically – in terms of bone remodelling stimulus and fracture risk – and adaptively – in terms of the predicted progressive bone healing and remodelling response. The FE model of the femur was resurfaced with two new implant designs for comparison to the traditional design, the ADEPT. The new designs are shown in Figure 98. In the static investigation, the prosthesis was implanted in three, 0 and ±10° varus-valgus orientations as in the first presented study. The 48mm diameter femoral head was resurfaced with 52mm prostheses, which allowed the intact joint centre location to be reproduced in the implanted joint. This isolated the prosthesis design from the effects of femoral offset, identified in Study 1.

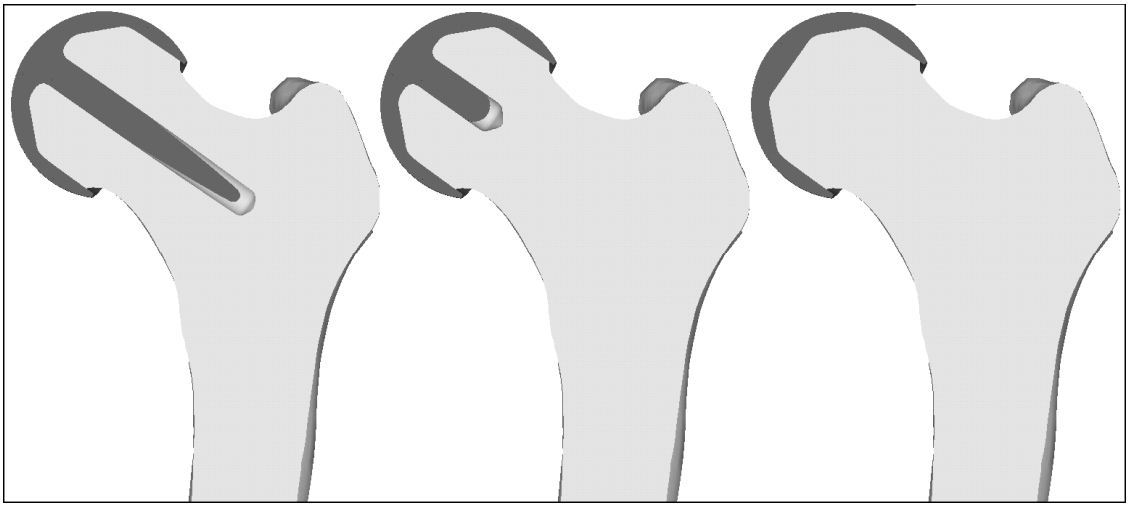

Figure 98: Current (ADEPT, left), Short Stemmed (centre) and Stemless (right) Implant Designs

These models were used to compare the performance of the three resurfacing designs under the three prosthesis orientations, and under gait, stumbling and falling loads. According to the static analysis results, the more successful proposed design was identified, and was then evaluated in more detail using Study 2's adaptive modelling techniques. For that study, the prosthesis was implanted in the clinically representative position described in Study 2: in 10° of valgus orientation and with 4.5mm of horizontal offset reduction. The remodelling and healing process parameter values identified in Study 2 to give the closest fit to clinical observations were used: in remodelling, s_{mature}=±62.5%, and in healing, D=2.37mm^2/day and M=5%/day.

7.3 Results

7.3.1 Static Remodelling Stimulus and Fracture Risk Predictions

Recalling Study 1, the femoral neck strain pattern was analysed for the intact bone, and bone yield was predicted to initiate in the superior femoral neck cortex at 6.0kN in stumbling, and in the anterior-medial femoral neck cortex at 3.0kN in sideways falling. To illustrate the effect of prosthesis stem design on the femoral neck fracture strength, the load at which bone damage initiation occurs was predicted for the bone resurfaced with the three prosthesis designs in varus, neutral and valgus orientations, and the results are given in Figure 99 for stumbling loading and in Figure 101 for falling loading. The distribution of yielding bone elements in the femoral head and neck was also predicted for the two scenarios, shown in Figure 100 for 6kN stumbling and Figure 102 for 3kN falling loading.

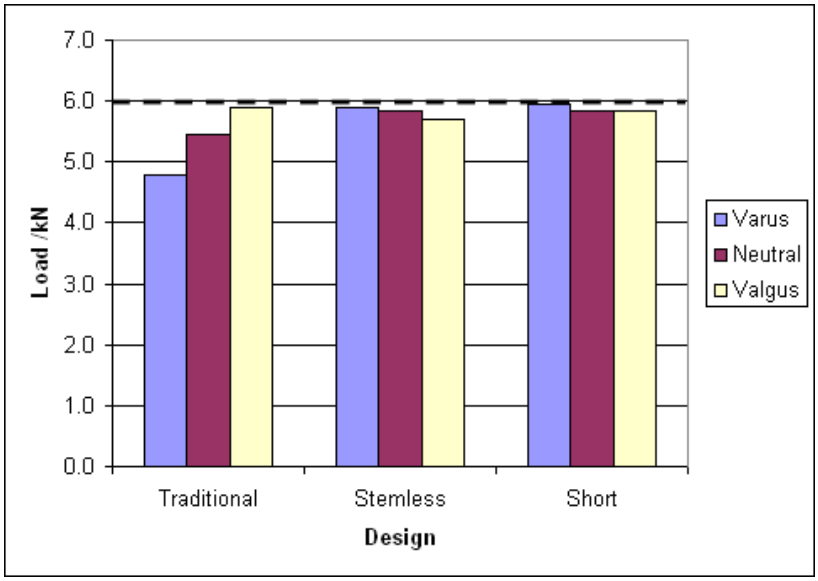

Figure 99: Predicted Femoral Neck Bone Damage Initiation Load under Stumble Loading Conditions, for the Femur Resurfaced with Traditional (Long Stemmed ADEPT), Stemless and Short Stemmed Prosthesis Designs. The Dashed Line indicates the Damage Initiation Load for the Intact Bone.

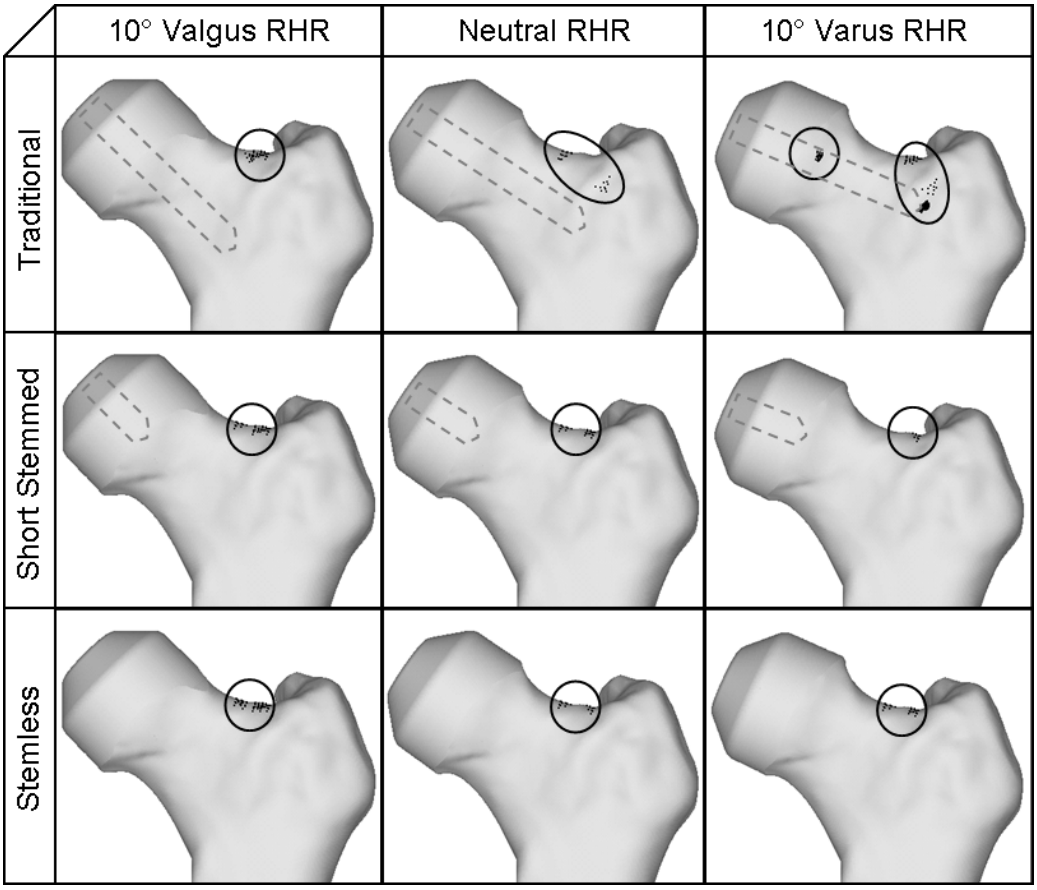

Figure 100: Distribution of Yielding Bone Elements under 6kN Stumbling Loads for the Proximal Femur Resurfaced with 52mm Prostheses of Three Stem Designs in Valgus, Neutral and Varus Orientations. Dashed Lines indicate Stem Bores.

A positive correlation between the damage initiation load in stumbling and a valgus implant orientation was predicted for the traditional design prosthesis (Figure 99, as reported in Chapter 5). The results indicated a 20% reduction in femoral neck damage initiation load with varus orientation, and 9% in neutral orientation. The natural femoral neck strength was predicted to be recreated with 10° of valgus orientation, within 2% of the intact case. Inspection of the damage location in Figure 100 indicates that this resulted from interference between the natural femoral neck root strain concentration and the prosthetic strain concentration at the tip of the stem bore. In valgus orientation, the two strain concentrations were distant from each other and did not interfere, so the natural femoral neck strength was preserved.

The short stemmed and stemless designs weakened the femoral neck less than the long stemmed, traditional design prosthesis. For the stemless design in all orientations, the load at which bone yield

initiated in the femoral neck was predicted to be within 5% of the intact bone, and the yield load with the short stemmed design was predicted to be within 2% of the intact case (Figure 99). The damaged bone distribution plots (Figure 100) suggest that this is related to the removal of the long stem and its bore, as both new designs led to the same bone damage initiation location as the intact bone: in the superior femoral neck.

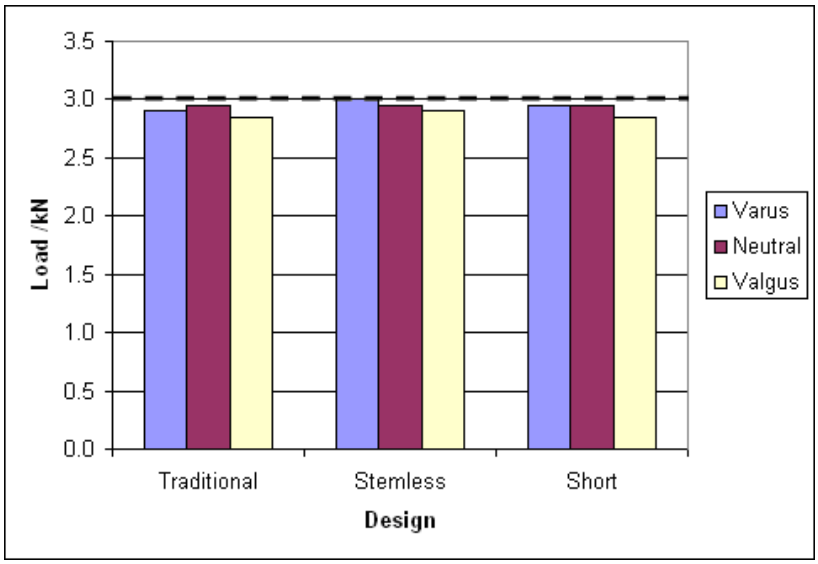

Figure 101: Predicted Femoral Neck Bone Damage Initiation Load under Sideways Falling Loads, for the Femur Resurfaced with Traditional (Long Stemmed ADEPT), Stemless and Short Stemmed Prosthesis Designs. The Dashed Line indicates the Damage Initiation Load for the Intact Bone.

Figure 101 shows the predicted damage initiation loads and Figure 102 the damage locations for the sideways falling scenario. All fractures were predicted to initiate at the anterior-medial surface of the femoral neck. All designs implanted in all orientations were predicted to give a femoral neck damage initiation load with 5% of the intact case, which implies that the proximity of the stem bore to the stress concentrated medial neck does not weaken the bone. Both new designs were therefore predicted to perform similarly to the traditional design under sideways falling loads.

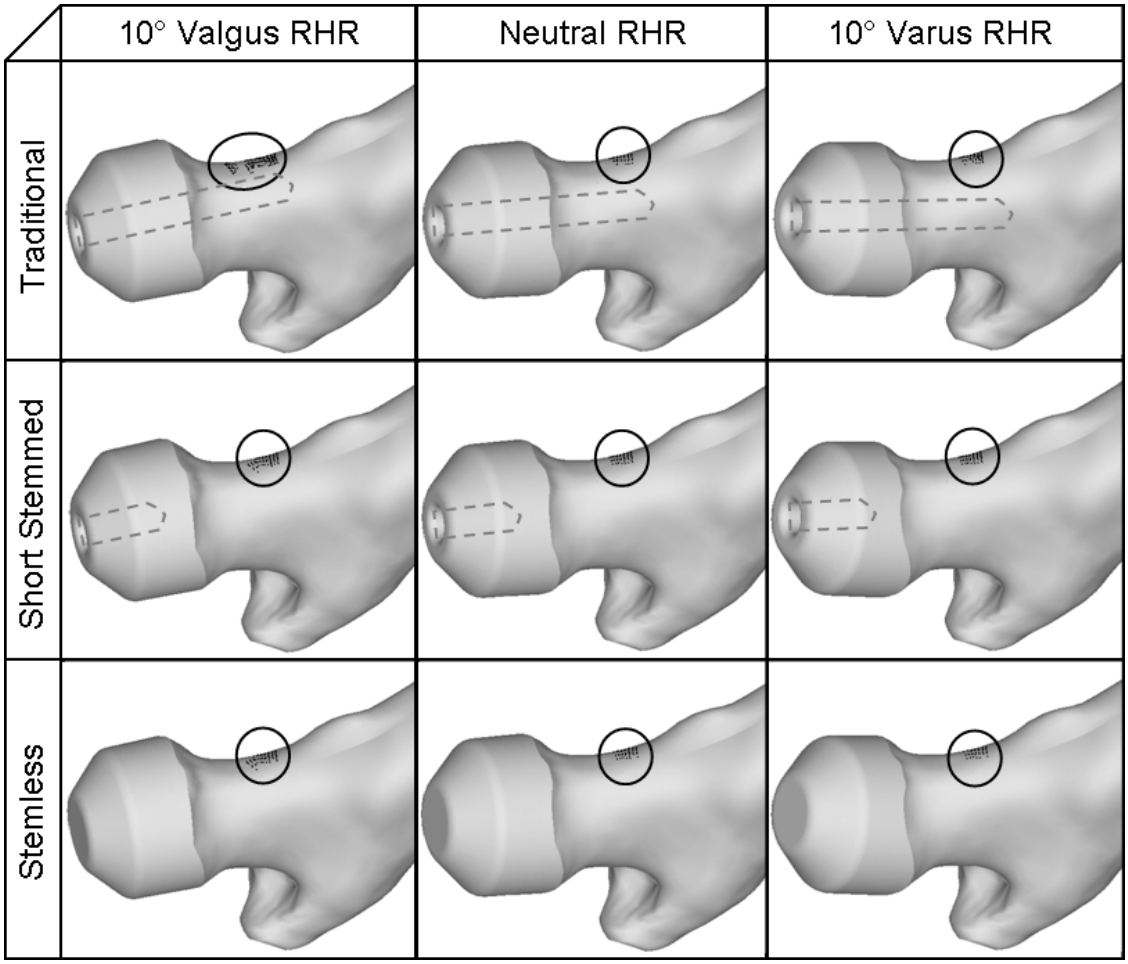

Figure 102: Distribution of Yielding Bone Elements under 3kN Falling Loads for the Proximal Femur Resurfaced with 52mm Prostheses of Three Stem Designs in Valgus, Neutral and Varus Orientations. Dashed Lines indicate Stem Bores.

The immediately postoperative bone remodelling stimulus was predicted for the nine implanted cases and is shown for a cross section along the femoral neck axis in Figure 103. This shows the locations at which bone resorption and densification would be expected. For an elderly patient, these correspond to a stimulus below -75% and above +75% respectively, shown by the bottom and top contours on the charts. For a younger patient an extreme stimulus of ±50% was considered[1]. In all cases, extensive stress shielding was predicted within the superior femoral head. For the traditional design prosthesis, densification was predicted around the stem bore, particularly around the narrowest point of the femoral neck and at the tip of the stem bore.

[1] Although the results of Study 2 indicated that ±50% would lead to excessive extents of bone remodelling, and ±62.5% was used for the young patient in the adaptive remodelling study, the ±50% value from Study 1 was kept for the static investigation for consistency.

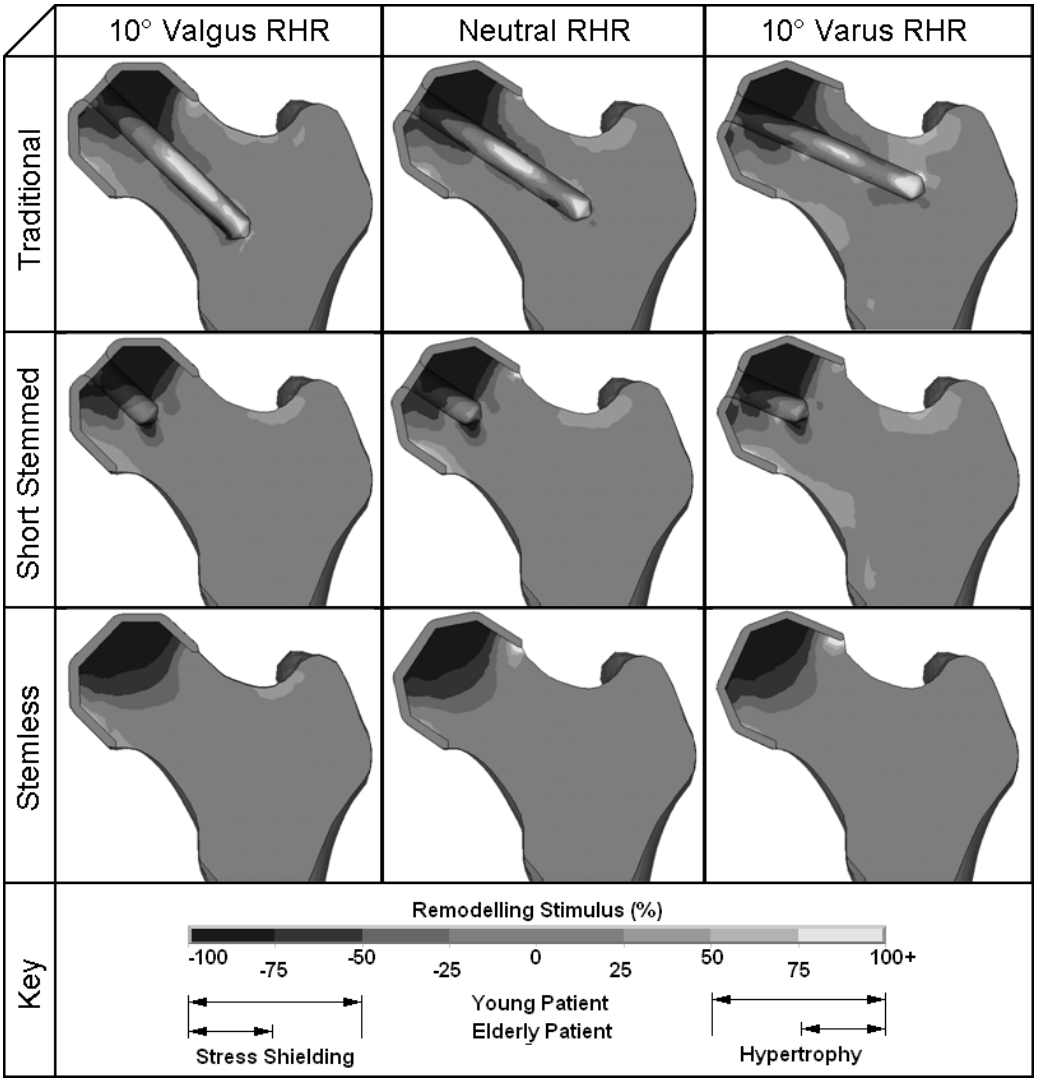

Figure 103: Strain Energy Density Remodelling Stimulus for Resurfacing with the Three Prosthesis Designs in Valgus (left), Neutral (middle) and Varus (right) Orientations. Approximated Mask Applied to Obscure Bone Cement Elements

Use of the stemless and short stemmed designs was not predicted to remove the stress shielding inside the femoral head. However, it can be seen in charts quantifying the extent of stress shielding and hypertrophy for the two stimulus levels (Figure 104) that stress shielding was reduced by 9-12% for the young patient and by 3-10% in the elderly patient with the short stemmed implant. The extent of hypertrophic bone was predicted to be reduced considerably with the removal of the long stem and its bore, particularly in neutral and valgus orientations, which led to an overall reduction in the volume of remodelling bone of up to 19% for the elderly patient and 21% for the young patient. This was when the prosthesis was in valgus positioning – the worst case for the traditional design.

The stemless prosthesis was predicted to stimulate an even lower volume of bone densification, as the stem is removed completely. However, retaining the entire internal volume of the femoral head led to the prediction of increased stress shielding, by 10-17% in the elderly patient and 4-13% in the young patient.

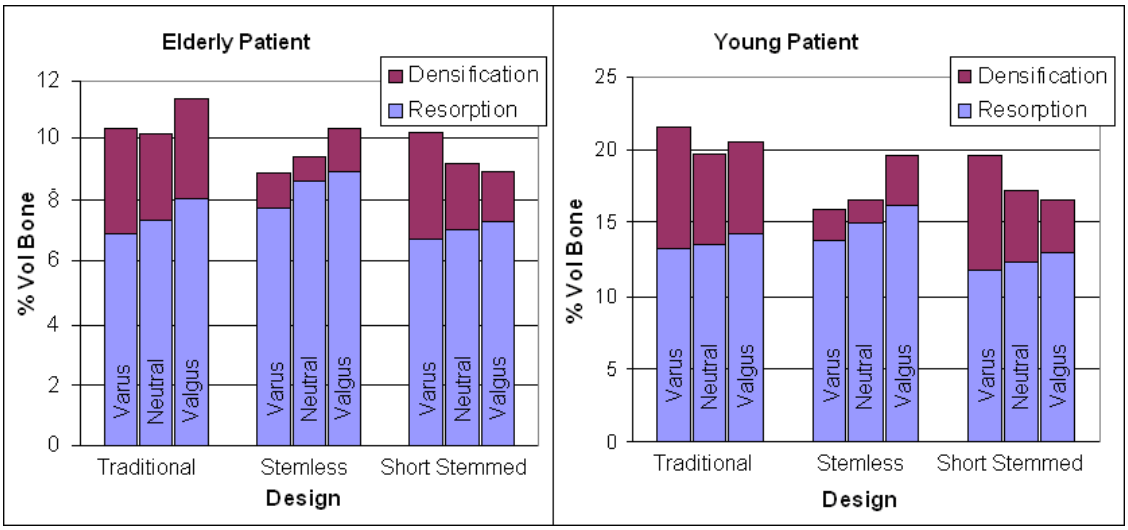

Figure 104: Strain Energy Density Remodelling Stimulus for Resurfacing with the Three Prosthesis Designs in Valgus (left), Neutral (middle) and Varus (right) Orientations

The results from the static models support the original hypothesis, that the shortening or removal of the long prosthesis stem and its bore may reduce the risks of femoral neck fracture and femoral prosthesis loosening. Recalling the limitations raised in the discussion of Study 1's results, it was argued that static remodelling stimulus models may only partially indicate the progressive bone adaptation behaviour following implantation. Therefore, the short stemmed design was taken forward for study in its ideal, valgus orientation using the adaptive healing and bone remodelling tool developed in Study 2. The purpose was to compare the final bone adaptations around the short stemmed design in comparison to the traditional prosthesis. In particular, the role of progressive load bearing at the tip of the short stemmed design was compared to that around the tapered long stem of the traditional design.

7.3.2 Adaptive Bone Remodelling Predictions

For the traditional (ADEPT) prosthesis design and the proposed short stemmed design, bone density variations were predicted and virtual X-Rays were generated. The postoperative, 3 and 24-Month follow-up virtual X-Rays are shown (Figure 105):

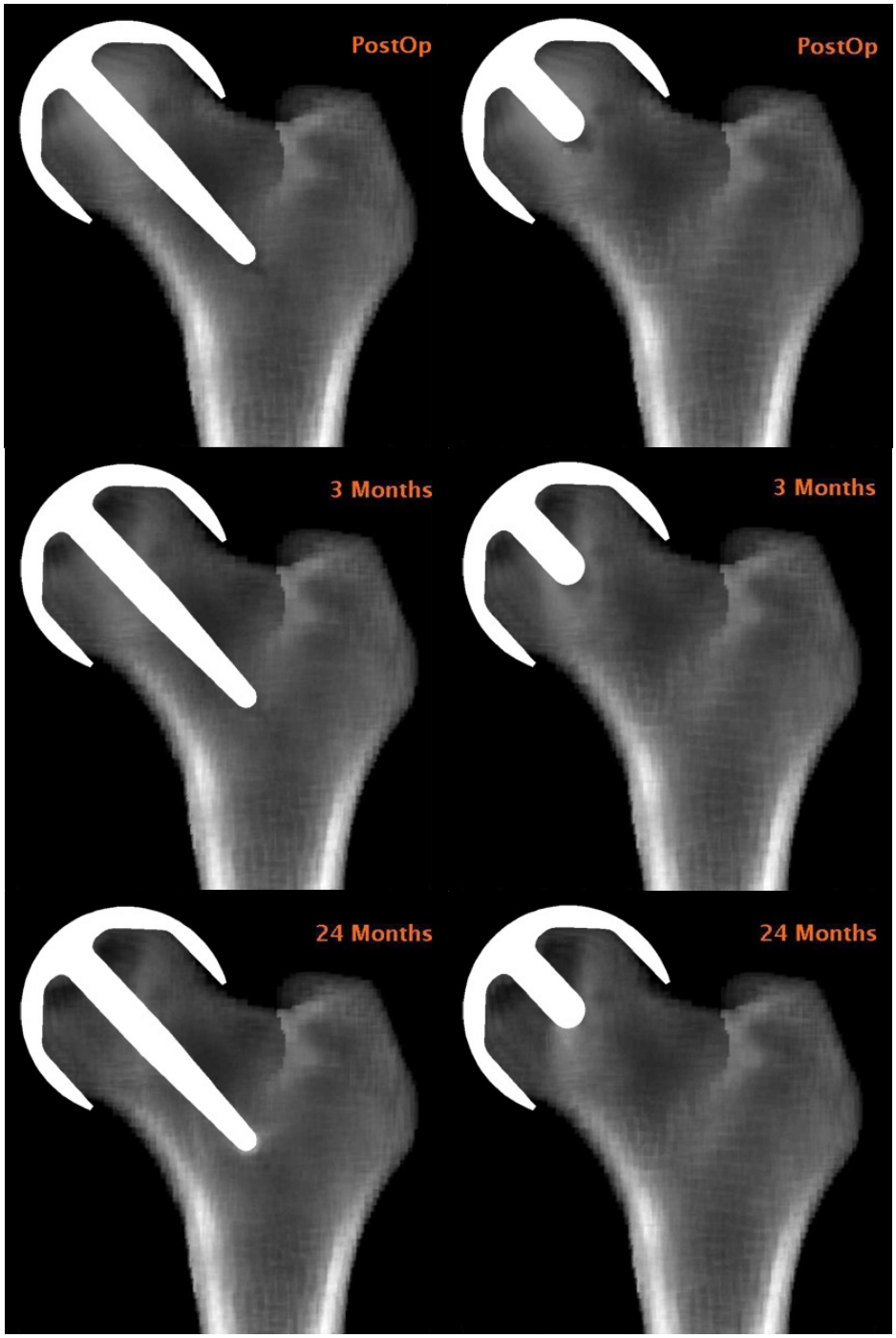

Figure 105: Virtual X-Rays at 0, 3 and 24 Months Follow-Up for the Traditional Design (ADEPT, Left), and the Proposed New Design (Short Stemmed, Right).

For quantified analysis, virtual DEXA scans were taken of the medial and lateral femoral neck regions in the FE models, and the resulting time history of percentage change in BMD was plotted. This data is included in the following charts (Figure 106):

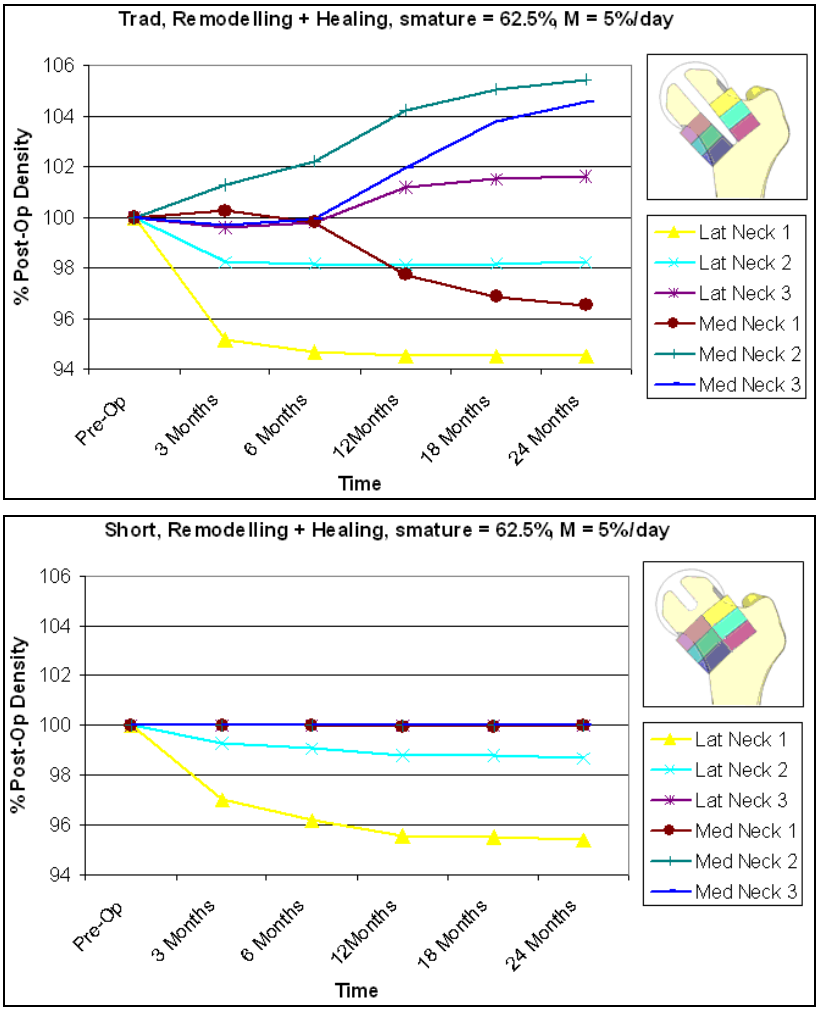

Figure 106: Charts showing Postoperative BMD Changes in the Six Femoral Neck DEXA Scan Zones for the Traditional Design (ADEPT, Top), and the Proposed New Design (Short Stemmed, Bottom).

These results allow the predicted long term performance of the new design to be compared to traditional prostheses. The progressive bone adaptations around the implant are shown in Figure 105, indicating that a similar extent of bone resorption would occur inside the femoral head for both designs. As observed in the postoperative bone remodelling stimulus results, both designs resurface the femoral head with a stiff metal shell and the stem design does not alter this. However, the radiographic changes in the femoral neck were predicted to be considerably reduced for the short stemmed design, and this is supported by the virtual DEXA data (Figure 106). The only region in which considerable bone density changes were predicted was at the superior head-neck junction (L1 and M1), with resorption indicative of femoral neck narrowing. Study 1's results indicated that prosthesis positioning is likely to have a considerable effect upon neck narrowing, where shortening the horizontal femoral

offset reduces the bending loads the femoral neck experiences naturally. However, these results imply that the extent of neck narrowing would be less marked for the short stemmed design.

These results indicated that a quantified measure of the influence of bone resorption inside the femoral head on prosthesis loosening was required. Therefore, the mean bone mineral density (BMD) was calculated over a layer of bone supporting the prosthesis stem and the cement fixation layer: the bone layer directly responsible for fixation of the implant. This density was measured over the two postoperative years and plotted (Figure 107):

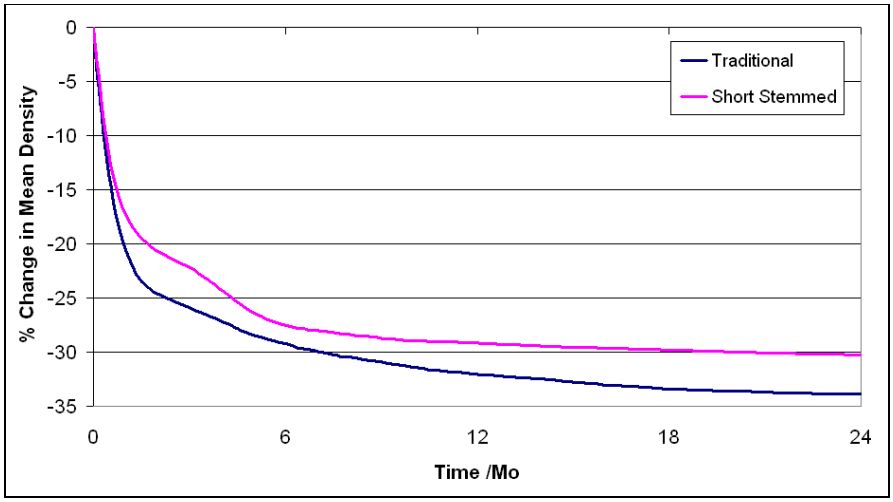

Figure 107: Chart showing Postoperative BMD Changes at the Cement/Stem Fixation Bone Layer for the Traditional Design (ADEPT), and the Proposed New Design (Short Stemmed).

This chart indicates that the progressive increase in stem load bearing for the traditional design does lead to additional proximal stress shielding over time, which may be avoided by the short stemmed design. Ultimately, the long stemmed design showed a reduction in implant-bone interface density of 34.0%, compared to 30.3% for the short stemmed design. The virtual X-Rays (Figure 105) indicate that over time the short stem would establish additional load bearing itself, at its tip. However, since this loading would be directed into the natural load path in the femoral head, this would cause less stress shielding in the proximal bone responsible for prosthesis fixation (Figure 107). These results show that the short stemmed design would be predicted to affect the load bearing and density of healthy bone less than traditional designs, as hypothesised.

7.4 Discussion

Studies 1 and 2 both concluded that the stem in traditional design femoral head resurfacing prostheses is likely to have a role in femoral neck fracture and prosthesis loosening. This third study took the methods developed in the first two studies and applied them to test a new prosthesis design, with a shortened or removed metaphyseal stem. The presented results indicate that the short stemmed prosthesis design would reduce the risks of femoral neck fracture and femoral prosthesis loosening compared to traditional, long stemmed implants.

The promising predicted biomechanical performance for short stemmed metal prostheses would indicate that a ceramic resurfacing head prosthesis would also be feasible. There would be concerns associated with tensile stresses generated at the root of a long ceramic stem [249], which could be solved by producing a short stemmed ceramic resurfacing head. This would go some way towards answering the concerns associated with the release of metal ions from MoM resurfacing heads, if used in a Ceramic-on-Metal or Ceramic-on-Ceramic combination.

There is clinical precedence for stemless resurfacing heads from the first attempts at surface arthroplasty, for example the Wagner prosthesis in metal-polyethylene [250] and MoM [34, 251] versions, and the Indiana Conservative prosthesis [244-246]. Failures of many these early prostheses were unacceptably common but could be explained by wear induced osteolysis: the Metal-on-Metal Wagner prosthesis had considerably higher survivorship than its metal-polyethylene predecessor, approaching the medium term survivorship of current technology.

The path of load transfer in the proximal femur is through the principal band of dense trabeculae in the femoral head and into the medial calcar, as shown in Figure 108. The hypothesis behind the short stemmed design was that if a stem is required for assistance with alignment in surgery, and it is known that the stem will bear load, positioning the tip of the stem in the load path will at least cause it to bear load in a more physiological manner. This would theoretically reduce the remodelling stimulus in comparison to current designs, and potentially reduce the volume of damaged bone under stumbling loading, because there would be no void bore in the narrow region of the femoral neck.

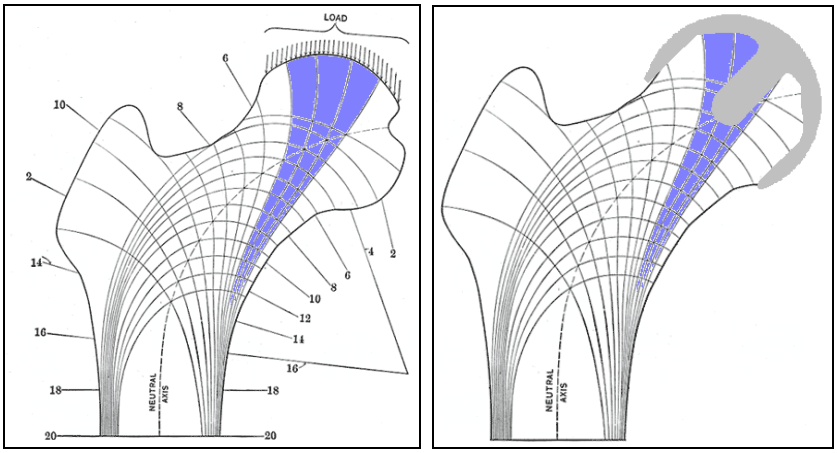

Figure 108: Load Transfer through the Proximal Femur, after Koch [252]

In FE modelling research, the stem diameter [12, 202] and extent of contact between the tapering stem and the host bone [12, 14] have been studied, but there has been limited investigation into the effects of representative length and shorter stems. de Waal Malefijt and Huiskes [8] compared the predicted biomechanics of the long stemmed TARA prosthesis to a design with a stem of similar length to current RHR prostheses (terminating in the femoral neck) and a stemless design. Their model was very simple (2D plane strain, side plated) and they analysed stress shielding qualitatively, in terms of the change in von Mises stress. More representative models were produced by Radcliffe [202], using multiple patient specific FE models and implant geometry based on the DePuy Orthopaedics ASR prosthesis. However, he considered only stems from 55-70mm in length, within the range of currently produced prostheses, and simulated the ASR's fully tapering stem out of contact with the parallel stem bore. Most recently, in 2010 Pal et al [205] reported the predicted effects of shortening the ASR implant's stem, simulating its adaptive bone remodelling behaviour. Again the stem-bone contact conditions were simplified to ideal contact. Rothstock et al [253] also shortened the femoral stem to the head centre and found reduced femoral head remodelling stimulus compared to long stemmed designs. However, their models used thinner stems than current prosthesis designs and investigated a very thin walled head which allowed the cortical shell to be preserved, so it is difficult to compare their findings directly with current clinical results. The present study investigated the clinical state of the art in detail as a control, including the predicted changing long term effects of stem-bone contact. The study then changed the stem design only, allowing its isolated effects to be established.

The limitations of the approach taken in this FE modelling study have been discussed in detail in the previous two chapters. That the model employs a single femur and a limited range of surgical

variability are perhaps greater limitations in an implant design study because the orthopaedic implant development process should investigate its performance across the full range of candidate patients. Clearly there is scope for further study. Multi-femur modelling would permit the implant's performance to be predicted across a range of patient variability. Probabilistic analysis and surrogate modelling could allow surgical variability and varying load cases to be investigated. However, both approaches would require process automation and statistical analysis of loads, bone geometry and materials properties that was beyond the scope of this investigation.

7.5 Conclusions

The following conclusions can be drawn from this study:

- shortening the stem of the resurfacing head may reduce the volume of damaged bone in a stumbling event because it is not necessary to bore into the narrowest region of the femoral neck for the stem.
- the short stem may also reduce the stress shielding effects in the femoral neck, particularly in valgus orientation- recommended to prevent femoral neck fracture- which is an indication of tolerance to surgical variability.
- the reduced risk of prosthesis loosening was indicated in a reduction of both the static postoperative bone remodelling stimulus, and the predicted long term bone adaptations around the implant.
- the biomechanical suitability of a short stemmed metal resurfacing head would indicate that a ceramic resurfacing head would also be feasible. This would begin to answer concerns associated with metal ions.
- these predictions consider only a limited range of patient and surgical variability, so extensive further research is necessary to assess the new design's predicted performance. However these first results for a representative candidate patient support the hypothesis and justify further investigation.

8 CONCLUSIONS AND FUTURE WORK

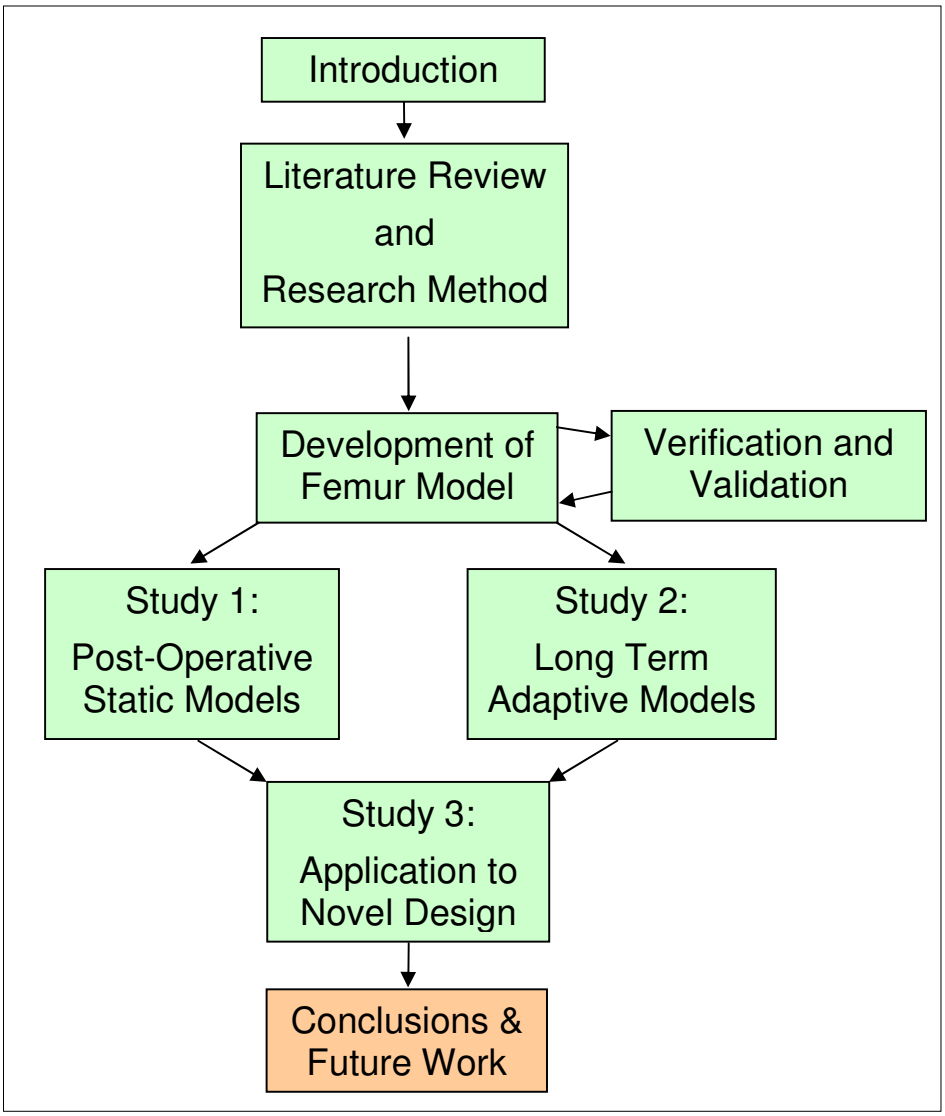

The methods and results of each of the three studies in this thesis were discussed in detail in their respective chapters; the following is a brief summary of the research motivation, approach, each study's methods and findings, a general discussion, a summary and suggestions for future research.

8.1 Summary of Motivation and Approach

The motivation behind this study was to develop computational tools to further the understanding of the biomechanics of resurfacing hip replacement prostheses. Hip resurfacing surgery is reported to produce successful outcomes as an osteoarthritis treatment for young, male patients in particular [1], but has lower success rates in older and female patients [2-5]. The two main femoral failure modes are reported to be femoral neck fracture and prosthesis loosening: both are multi-factorial phenomena with biomechanical involvement [6]. The range of clinical variation is great, so the efficiency and flexibility of computational analysis makes it a key tool for the predictive study of implant biomechanics. Before the range of clinical variability can be investigated, single deterministic models must be produced which are capable of capturing the clinically observed biomechanical effects, characterised by the prediction of trends in adaptations to implantation and failure modes. Considering hip resurfacing, several groups have produced computational biomechanical models using finite element analysis [11-18], and a detailed understanding of many aspects of the *in-vivo* behaviour of traditional design implants has been achieved.

When this study began, there was remaining scope for further research particularly in the simulation and understanding of femoral bone adaptation and implant loosening. Trends in the predicted stimulus for adaptive bone remodelling have been the subject of some contradiction, considering prosthesis positioning [15, 16, 18] and material [202, 205] in particular. Other variables likely to have biomechanical effects have received relatively little attention, including more design-related factors such as prosthesis stem length and profile [8, 195]. Finally, previously employed methods and available computer resources have precluded the detailed prediction of the bone adaptations around resurfacing implants, and resulted in limited agreement between modelling predictions and clinical observations. The effects of prosthesis stem-bone contact have been investigated in some detail using instantaneous remodelling stimulus models [12, 18, 196, 198], but predictions of the progressive changes in stem-bone contact, and their effects upon wider periprosthetic bone adaptation have not been considered by previously published adaptive remodelling studies [13, 203]. Achieving closer agreement between computational predictions of the biomechanics of traditional design implants and their clinical behaviour will improve the confidence in these tools for the pre-clinical analysis of new designs.

This research aimed to develop computational tools capable of closer agreement with clinical trends, to further the understanding of the biomechanics of the resurfaced hip. Two approaches were used: static modelling of the immediately postoperative condition, and dynamic modelling of progressive bone adaptation. These tools were developed and tested with commonly used traditional prosthesis designs, and as a proof of concept, the pre-clinical analysis of a new resurfacing prosthesis design was carried out.

8.2 Findings

Postoperative Static Models

The first study (Chapter 5) aimed to produce a static FE model of the resurfaced femur for basic biomechanical analysis, and to test a truer representation of clinically achieved prosthesis positioning. The static model represented the immediately postoperative state, from which the femoral neck fracture risk and the stimulus for adaptive bone remodelling could be predicted. The study indicated the importance of prosthesis sizing upon its final positioning, relating specifically to the horizontal femoral offset distance which controls the bending moment on the femoral neck. This detail may not have been captured in some previous idealised modelling studies which reproduce the natural joint centre location after implantation, something that is not necessarily a clinical goal. The results were corroborated by clinical observations, predicting an increased risk of femoral neck fracture with varus prosthesis positioning [10, 47], and an increased risk of femoral prosthesis loosening for smaller implants [39], especially in younger patients. This study isolated the effects of prosthesis sizing and varus-valgus positioning, allowing the effects to be observed independently. Finally, for the purposes of the development of a new prosthesis design, the results supported theories of:

- the involvement of the stem in proximal stress shielding, and
- the influence of a stem bore upon reduced femoral neck strength.

Long Term Adaptive Models

The second study (Chapter 6) aimed to produce a model of the bone adaptations around the resurfacing prosthesis, as previous adaptive models had not reproduced the full set of clinically observed radiographic bone density changes [3, 4, 45, 67, 72]. *In-vivo,* dense lines around the implant stem visible on x-rays show that contact must be established at the stem-bone interface from its initial, over-drilled state. In theory this would involve a gradual healing and bone modelling process. It was hypothesised that a bone adaptation model of the resurfaced femur should include a provision for this stem-bone defect to heal or re-fill progressively with tissue. Study of the literature allowed the identification of candidate algorithms for predicting bone remodelling [169] and orthopaedic defect healing though tissue differentiation [196], but highlighted the need to select values for several algorithm parameters. The investigation indicated first that the inclusion of the healing process in the bone adaptation model led to closer predictions of radiographic changes than using remodelling alone with either a stem-bone gap or perfect stem-bone contact. Second, a set of bone remodelling and healing process parameters was identified which gave a closer fit of predicted bone adaptations to qualitative virtual x-ray changes and quantitative virtual DEXA scan Bone Mineral Density (BMD) changes. This investigation highlighted again the involvement of the prosthesis stem in proximal stress shielding, plus its increasing effect with progressive stem load transfer. It also developed a new pre-clinical analysis tool for predicting postoperative bone adaptation, but demonstrated that the predicted BMD changes were small compared to the variability of clinical measurements.

Application of Modelling Methods to New Designs

The final study (Chapter 7) demonstrated the use of the preclinical analysis tools, employing the static and adaptive biomechanical models in the pre-clinical analysis of a new prosthesis design. When work began, resurfacing prosthesis stem length had been relatively rarely researched [8, 202] in comparison to stem diameter [12] and stem-bone contact conditions [12, 14, 15, 18, 196, 198]. However, the results of the first two studies indicated that shortening or removing the prosthesis stem could reduce the risk of femoral neck fracture and proximal stress shielding, and hence femoral prosthesis loosening. This hypothesis was tested using stemless and short stemmed designs. Static biomechanical modelling using Study 1's methods indicated that both designs would allow the intact femoral neck strength to be maintained following resurfacing. Results also indicated only slight changes in femoral neck strength across a range of prosthesis positioning, suggesting greater tolerance to surgical variability. Furthermore, the results implied that the extent of stimulated bone remodelling

would be lowest for the short stemmed resurfacing head, so this design was compared to a traditional prosthesis design using Study 2's progressive bone adaptation prediction model. This model reinforced the hypothesis, predicting that the density of the layer of bone supporting the prosthesis would be maintained closer to the preoperative density by the short stemmed design than the traditional prosthesis.

8.3 General Discussion of Limitations

A clear limitation of the modelling approaches employed in this thesis is the use of a single femur, and single load cases. At the time of writing, the focus of computational orthopaedic biomechanics research was moving from individual deterministic models towards consideration of surgical and inter-patient variability, using multi patient modelling and probabilistic techniques [202, 254]. This study was concerned with improvements in the ability of computational models to capture specific biomechanical effects, which could be applied in multi-femur studies or probabilistic analysis in the future. It is not appropriate to draw firm conclusions on the basis of the predictions of a single femur model, especially in pre-clinical analysis, but biomechanical analysis techniques must be developed at first in individual models. Where it was attempted to make initial predictions of clinical performance, this study took a comparative approach across a range of prosthesis positioning, or between proposed new and existing designs. Although inter-patient variability is huge, the limited patient scope for hip resurfacing would diminish the range of variability required for study, so the femur used in these models was selected carefully as representative of the target patient for resurfacing. In the same manner, where computational expense limited investigations to single load cases rather than full load spectra, the load case was selected carefully on the basis of worst clinical scenarios or the scenarios thought to have the greatest effect upon supposed biomechanical bone adaptation stimuli. For example:

- simulating stumbling and falling, loading directions found to give the minimum strength in mechanical tests [126, 129, 131] were used, and
- simulating remodelling, gait loading was selected according to evidence that it is repeated, peak gait cycle magnitude loads which evoke bone modelling and remodelling drifts most effectively [217].

A comparative study strategy was also used to minimise the effects of load case simplifications. Where there were known simplifications of boundary conditions and force application, these were kept consistent between models, and were shown to represent conservative cases, giving some confidence in the trends displayed by the models. This leaves a requirement for further research, testing

hypotheses such as those considered in this study using multiple load cases. This study was limited largely by computational expense, but multiple load case testing will become easier in the future as processing power increases. Ultimately, most confidence will be achieved from multi-femur [255], variable materials property [256], multiple activity load case studies including surgical positioning variability [257], in addition to the use of probabilistic techniques [254].

The precise nature of biomechanical failure criteria of bone and stimuli for bone remodelling and healing are also unknown, so the mechanical stimuli used to simulate these effects also represent a simplification of the *in-vivo* conditions. It is best to consider the strain energy density, deviatoric strain and dilatational hydrostatic pressure stimuli used in this study as analogous to the real biomechanical stimuli. That is, even if they are not perfect representations of physiologic stimuli, they do allow clinically observed behaviour of existing prosthesis designs to be reproduced by a model, and by extrapolation would allow the model to predict the behaviour of new designs. There is a risk in extrapolation that the models and stimuli have limited validity, so the pre-clinical analysis approach should follow an evolutionary path rather than revolutionary changes, and the initial predictions obtained from these models should be supported by testing. These models therefore represent only one step in the pre-clinical analysis process.

8.4 Future Work

The scope for future work is illustrated by the limitations of the present study. The work presented here involved the development of new computational models for analysis of the resurfaced femoral head, using a deterministic modelling approach. On this level, improvement may be warranted in the detail of the healing algorithm, to tailor the tissue differentiation approach to cancellous bone defect re-filling. This study employed a new physiologically-based maximum bone densification rate limit for modelling and remodelling. In a similar manner, further development could include variable, physiologically-based stem cell maturation rates, perhaps accounting for the stability provided by the implant and surrounding trabecular structure.

A particular focus for future research in orthopaedic biomechanics is probabilistic methods, so the major future computational work arising from this research should be to apply the tools developed here on a probabilistic basis. For reasons of computational expense, it will be necessary to identify reasonable modelling simplifications to permit multiple solutions. This point is reinforced when improved bone adaptation modelling methods are considered. Even on a deterministic basis [173, 174, 182-184], the latest methods which include material anisotropy and optimisation stimuli are expensive. Only recently have these approaches become feasible for single 3D intact bone models, through the use of multiscale modelling employing rapid neural network theories for microstructural adaptation [258]. It is accepted that the biomechanical adaptation stimuli used in this research are a simplification or an analogy to *in-vivo* physiology. The application of these more advanced algorithms could be of benefit, once computational resources and the methods themselves permit more complex implanted models to be solved cost effectively.

A further extension of the research relates to additional pre-clinical analysis of the new resurfacing head prosthesis design. Whilst this work has focussed on understanding the influence of biomechanics on the longevity of hip resurfacing prostheses, the original motivation also noted the requirement for improved prosthesis biocompatibility, considering the possibility of metal sensitivity reactions in female patients. Contemporary ceramic biomaterials demonstrate excellent biocompatibility and a clear objective of future hip resurfacing prosthesis development would involve these metal-free materials. Repeated analysis of this study's new, short stemmed prosthesis design would be necessary if ceramic materials are employed, again under several load cases and considering the range of

prosthesis positioning. The goals would be first to assess whether the stiffer ceramic material would stimulate additional stress shielding or femoral neck strain, and second to identify whether prosthesis stresses are sufficiently low to avoid fracture. Mechanical tests of prosthesis strength should be conducted to supplement the computational study, designed on the basis of the *in-vivo* FE analysis prosthesis stress distribution results. Prosthesis support fixtures would be designed to allow the main *in-vivo* stress concentrations to be recreated under *in-vitro* conditions with mechanical test machines. This research is particularly necessary because the existing suite of British Standard and International Standard tests are designed with THR prostheses in mind, and are not applicable to resurfacing prostheses for which the loading and supporting tissue structures are very different.

Considering mechanical testing, an extension of the digital image correlation validation tests conducted in this research would be the use of digital volume correlation (DVC) [228, 229]. The increase in size and resolution of CT-scanners and the capacity to conduct mechanical testing inside the scanner would permit experimental measurement of the percentage change in strain between intact and implanted bones. This would allow further model validation, of individual cases of the bone remodelling stimulus used in this research. Critically however, the DIC validation tests should be repeated using cadaver bone, to assess the validity of the assignation of materials properties to the model.

Finally, the place of this research in the state of the art is considered more broadly. The work focussed on femoral head resurfacing, but scope for improvement remains for the acetabular cup prosthesis for resurfacing. Evidence is accumulating that late RHR failures are associated with acetabular loosening [120], in addition to ongoing concerns associated with metal ion effects. If an ultimate goal is to produce a completely metal free conservative hip replacement prosthesis for female patients, an alternative material acetabular cup would be required, employing ceramic or advanced polymer materials. Simulations using methods such as those developed in this study could be applied to the pelvis with a natural and implanted acetabulum, guiding the design process of new acetabular cup prostheses and supporting the overall goals of improving prosthesis biocompatibility and longevity.

8.5 Conclusion

In line with the original goals of the research, the work presented in this thesis has developed two levels of biomechanical tool for analysis of the performance of traditional resurfacing hip replacement prosthesis technology and for the pre-clinical analysis of new implant designs. The tools were developed from existing techniques and their predictions compared to trends in clinical results. The models reproduced clinically observed behaviour more closely than previous investigations, in terms of predicted risks of femoral neck fracture and prosthesis loosening, compared to clinical fracture trends, radiographic observations and DEXA scan bone mineral density measurements.

The models were developed using a deterministic approach, but the findings have highlighted factors worthy of consideration in future probabilistic research, including prosthesis sizing and positioning, and prosthesis-bone interface conditions. Ultimately, a case study was presented which demonstrated how the tools can be used to identify areas for improvement in traditional designs to inform new prosthesis design. Combined with their application in pre-clinical analysis of the new designs, this represents a step in the development process of orthopaedic implants for improved clinical results.

9 References

1. Beaulé, P.E., Antoniades, J, *Patient Selection and Surgical Technique for Surface Arthroplasty of the Hip.* Orth. Clin North America, 2005. **36**: p. 177-185.
2. McMinn, D., Daniel, J, *History and modern concepts in surface replacement.* Proc IMechE H, 2006. **220**: p. 239-251.
3. Hing, C.B., Young, D A, Dalziel, R E, Bailey, M, Back, D L, Shimmin, A J, *Narrowing of the neck in resurfacing arthroplasty of the hip.* J Bone Joint Surg [Br], 2007. **89-B**: p. 1019-1024.
4. Pollard, T.C.B., Baker, R P, Eastaugh-Waring, S J, Bannister, G C, *Treatment of the Young Active Patient with Osteoarthritis of the Hip: A Five- to Seven-Year Comparison of Hybrid Total Hip Arthroplasty and Metal-on-Metal Resurfacing*. J Bone Joint Surg [Br], 2006. **88-B**: p. 592-600.
5. Pandit, H., Glyn-Jones, S, McLardy-Smith, P, Gundle, R, Whitwell, D, Gibbons, C L M, Ostlere, S, Athanasou, N, Gill, H S, Murray, D W, *Pseudotumours Associated with Metal-on-Metal Hip Resurfacings.* J Bone Joint Surg [Br], 2008. **90-B**: p. 847-851.
6. Amstutz, H.C., Campbell, P A, Le Duff, M J, *Fracture of the neck of the femur after surface arthroplasty of the hip.* J Bone Joint Surg [Am], 2004. **86**: p. 1874-1877.
7. Huiskes, R., Chao, E Y S, *A Survey of Finite Element Analysis in Orthopedic Biomechanics: the First Decade.* J Biomech, 1983. **16**: p. 385-409.
8. de Waal Malefijt, M.C., Huiskes, R, *A clinical, radiological and biomechanical study of the TARA hip prosthesis.* Arch Orthop Trauma Surg, 1993. **112**: p. 220-225.
9. Watanabe, Y., Shiba, N, Matsuo, S, Higuchi, F, Tagawa, Y, Inoue, A, *Biomechanical Study of the Resurfacing Hip Arthroplasty: Finite Element Analysis of the Femoral Component.* J Arthoplasty, 2000. **15**: p. 505-511.
10. Beaulé, P.E., Lee, J L, Le Duff, M J, Amstutz, H C, Ebramzadeh, E, *Orientation of the femoral component in surface arthroplasty of the hip. A biomechanical and clinical analysis.* J Bone Joint Surg [Am], 2004. **86**: p. 2015-2021.
11. Little, J.P., Taddei, F, Viceconti, M, Murray, D W, Gill, H S, *Changes in Femur Stress after Hip Resurfacing Arthroplasty: Response to Physiological Loads.* Clin Biomechanics, 2007. **22**: p. 440-448.
12. Taylor, M., *Finite element analysis of the resurfaced femoral head.* Proc IMechE H, 2006. **220**: p. 289-297.
13. Gupta, S., New, A M R, Taylor, M, *Bone remodelling inside a cemented resurfaced femoral head.* Clin Biomechanics, 2006. **21**: p. 594-602.
14. Ong, K.L., Kurtz, S M, Manley, M T, Rushton, N, Mohammed, N A, Field, R E, *Biomechanics of the birmingham hip arthroplasty.* J Bone Joint Surg [Br], 2006. **88-B**: p. 1110-1115.
15. Long, J., Bartel, DL, *Surgical Variables Affect Mechanics of a Hip Resurfacing System.* Clin Ortho Rel Res, 2006. **453**: p. 115-122.
16. Radcliffe, I.A.J., Taylor, M, *Investigation into the Effect of Varus-Valgus Orientation on Load Transfer in the Resurfaced Femoral Head: a Multi-Femur Finite Element Analysis.* Clin Biomechanics, 2007. **22**: p. 780-786.
17. Radcliffe, I.A.J., Taylor, M, *Investigation into the Affect of Cementing Techniques on Load Transfer in the Resurfaced Femoral Head: A Multi-Femur Finite Element Analysis.* Clin Biomechanics, 2007. **22**: p. 422-430.
18. Ong, K.L., Day, J S, Kurtz, S M, Field, R E, Manley, M T,, *Role of Surgical Positioning on Interface Stress and Initial Bone Remodelling Stimulus around Hip Resurfacing Arthroplasty.* J Arthroplasty, 2009. **24**: p. 1137-1142.
19. Gray, H., *Anatomy of the Human Body*. 20th, Online ed. 2000, Philadelphia: Lea & Febiger.
20. Hardinge, K., *Hip Replacement: The Facts*. 1983: Oxford University Press.
21. Mow, V.C., Hung, C T, *Biomechanics of Articular Cartilage*, in *Basic Biomechanics of the Musculoskeletal System*, N. Frankel, Editor. 2001, Lippincott, Williams & Wilkins. p. 59-100.
22. *The Swedish National Hip Arthroplasty Register Annual Report*. 2004, Joint Replacement Unit, Sahlgren Hospital, Sweden: Gothenburg.
23. *The 2004 Implant Yearbook on Orthopaedic Endoprostheses: Finnish Arthroplasty Register*. 2006, National Agency for Medicines: Helsinki.
24. *The Norwegian Arthroplasty Register*. 2005, Haukeland University Hospital: Haukeland.
25. *National Joint Registry for England and Wales 5th Annual Report*. 2008: Hemel Hempstead.
26. Lyons, A.R., *Clinical outcomes and treatment of hip fractures.* American J Med, 1997. **103(2A)**: p. 51S-64S.
27. Firestein, G.S., *Evolving concepts of rheumatoid arthritis.* Nature, 2003. **423**: p. 356-361.

28. Crawford Adams, J., Hamblen, D L, *Outline of Orthopaedics*. 12th ed. 1995, Edinburgh: Churchill Livingstone.
29. Amstutz, H.C., Le Duff, M J, *Background of Metal-on-Metal Resurfacing.* Proc IMechE H, 2006. **220**: p. 85-94.
30. Charnley, J., *Arthroplasty of the hip: a new operation.* Lancet, 1961. **1**: p. 1129-1132.
31. McKee, G.K., Watson-Farrar, J, *Replacement of Arthritic Hips by the McKee-Farrar Prosthesis.* J Bone Joint Surg [Br], 1966. **48-B**: p. 245-259.
32. Freeman, M., Swanson, Day, Thomas, *Conservative total replacement of the hip.* J Bone Joint Surg [Br], 1975. **57-B**: p. 114.
33. Amstutz, H.C., Clarke, I C, Cristie, J, Graff-Radford, A, *Total hip articular replacement by internal eccentric shells.* Clin Ortho Rel Res, 1977. **128**: p. 261-284.
34. Wagner, H., *Surface replacement arthroplasty of the hip.* Clin Ortho Rel Res, 1978. **134**: p. 102-130.
35. Gerard, Y., *Hip arthroplasty by matching cups.* Clin Ortho Rel Res, 1978. **134**: p. 25-35.
36. Furuya, K., Tsuchiya, M, Kawachi, S, *Socket-cup arthroplasty.* Clin Ortho Rel Res, 1978. **134**: p. 41-44.
37. Trentani, C., Vaccarino, *The Paltrinieri-Trentani hip joint resurface arthroplasty.* Clin Ortho Rel Res, 1978. **134**: p. 36-40.
38. Amstutz, H.C., Kilgus, Kabo, Dorey, *Porous surface replacement of the hip with chamfered-cylinder component.* Arch Ortho Trauma Surg, 1988. **107**: p. 73-85.
39. Australian Orthopaedic Association, *National Joint Replacement Registry Annual Report*. 2008, AOA: Adelaide.
40. Beaulé, P.E., Amstutz, H C, Le Duff, M, Dorey, F, *Surface Arthroplasty for Osteonecrosis of the Hip: Hemiresurfacing versus Metal-on-Metal Hybrid Resurfacing.* J Arthoplasty, 2004. **19**: p. S54-S58.
41. NICE, *Guidance on the use of metal on metal hip resurfacing arthroplasty. Technology Appraisal Guidance No 44*. 2002, NHS, London.
42. McMinn, D., Treacy, R, Lyn, K, Pynsent, P, *Metal-on-metal surface replacement of the hip.* Clin Ortho Rel Res, 1996. **329S**: p. S89-S98.
43. *Australian Orthopaedic Association National Joint Replacement Registry Annual Report*. 2004, AOA: Adelaide.
44. Bostrom, H., Bahnsen, B, Keusch, L, Chon, C, Mayur Tipnis, CFA, *Focus On Hip Resurfacing: A New Spring in the Orthopaedic Step.* Goldman Sachs Global Investment Research, October, 2005.
45. Steffen, R.T., Pandit, H P, Palan, J, Beard, D J, Gundle, R, McLardy-Smith, P, Murray, D W, Gill, H S, *The five-year results of the Birmingham Hip Resurfacing Arthroplasty.* J Bone Joint Surg [Br], 2008. **90-B**: p. 436-441.
46. Little, C.P., Ruiz, A L, Harding, I J, McLardy-Smith, P, Gundle, R, Murray, D W, Athansou, N A, *Osteonecrosis in retrieved femoral heads after failed resurfacing arthroplasty of the hip.* J Bone Joint Surg [Br], 2005. **87-B**: p. 320-323.
47. Shimmin, A.J., Back, D, *Femoral Neck Fractures Following Birmingham Hip Resurfacing: A National Review of 50 Cases.* J Bone Joint Surg [Br], 2005. **87-B**: p. 463-4.
48. Morlock , M.M., Bishop, N, Ruther, W, Delling, G, Hahn, M, *Biomechanical, Morphological and Histological Analysis of Early Failures in Hip Resurfacing Arthroplasty.* Proc IMechE H, 2006. **220**: p. 333-344.
49. Morlock, M.M., Bishop, N, Zustin, J, Hahn, M, Ruther, W, Amling, M, *Modes of Implant Failure after Hip Resurfacing: Morphological and Wear Analysis of 267 Retrieval Specimens.* J Bone Joint Surg [Am], 2008. **90**: p. 89-95.
50. Shimmin, A.J., Beaulé, P E, Campbell, P, *Metal-on-Metal Hip Resurfacing Arthroplasty: Current Concepts Review.* J Bone Joint Surg [Am], 2008. **90**: p. 637-654.
51. Beaulé, P.E., Campbell, P A, Hoke, R, Dorey, F, *Notching of the femoral neck during resurfacing arthroplasty of the hip. A vascular study.* J Bone Joint Surg [Br], 2006. **88-B**: p. 35-39.
52. Silva, M., Haeng Lee, K, Heisel, C, dela Rosa, M A, Schmalzried, T P, *The Biomechanical Results of Total Hip Resurfacing Arthroplasty.* J Bone Joint Surg [Am], 2004. **86**: p. 40-46.
53. Davis, E.T., Olsen, M, Zdero, R, Waddell, J P, Schemitsch, E H, *Femoral Neck Fracture Following Resurfacing.* J Bone Joint Surg [Br], 2008. **90-B**: p. 1522-1527.
54. Freeman, M.A.R., *Some Anatomical and Mechanical Considerations Relevant to the Surface Replacement of the Femoral Head.* Clin Ortho Rel Res, 1978. **134**: p. 19-24.
55. Little, J.P., Gray, H A, Murray, D W, Beard, D J, Gill, H S, *Thermal Effects of Cement Mantle Thickness for Hip Resurfacing.* J Arthroplasty, 2008. **23**: p. 454-458.
56. Gill, H.S. *Femoral neck fractures following resurfacing*. in *Engineers and Surgeons: Joined at the Hip*. 2007. London: IMechE.

57. Steffen, R.T., Foguet, P R, Krikler, S J, Gundle, R, Beard, D J, Murray, D W, *Femoral Neck Fractures after Hip Resurfacing.* J Arthoplasty, 2009. **24**: p. 614-619.
58. Menge, M. *Seven years of experience in MoM resurfacing: results and open questions*. in *11th BIOLOX Symposium: Bioceramics and Alternative Bearings in Joint Arthroplasty*. 2006. Rome: Steinkopff Darmstadt.
59. Treacy, R.B.C., McBryde, C W, Pynsent, P B, *Birmingham hip resurfacing arthroplasty.* J Bone Joint Surg [Br], 2005. **87-B**: p. 167-170.
60. Beaulé, P.E., Campbell, P, Lu, Z, Leunig-Ganz, K, Beck, M, Leunig, M, Ganz, R, *Vascularity of the arthritic femoral head and hip resurfacing.* J Bone Joint Surg [Am], 2006. **88**: p. 85-96.
61. Gautier, E., Ganz, K, Krugel, N, Gill, T, Ganz, R, *Anatomy of the medial femoral circumflex artery and its surgical implications.* J Bone Joint Surg [Br], 2000. **82-B**: p. 679-683.
62. Steffen, R.T., Smith, S R, Urban, J P G, McLardy-Smith, P, Beard, D J, Gill, H S, Murray, D W, *The Effect of Hip Resurfacing on Oxygen Concentration in the Femoral Head.* J Bone Joint Surg [Br], 2005. **87-B**: p. 1468-1474.
63. Amarasekera, H.W., Costa, M L, Foguet, P, Krikler, S J, Prakash, U, Griffin, D R, *The Blood Flow to the Femoral Head/Neck Junction during Resurfacing Arthroplasty.* J Bone Joint Surg [Br], 2008. **90**: p. 442-445.
64. Steffen, R.T., O'Rourke, K S, Beard, D J, Murray, D W, Hill, H S, *Hip Resurfacing: Antero-Lateral Approach is Less Damaging to Femoral Head Blood Supply than Posterior*, in *Engineers and Surgeons: Joined at the Hip*. 2007, IMechE: London.
65. Jameson, S.S., Langton, D J, Natu, S, Nargol, T V F, *The Influence of Age and Sex on Early Clinical Results after Hip Resurfacing.* J Arthroplasty, 2008. **23**: p. 50-55.
66. Shimmin, A.J., Walter, W L, Esposito, C, *The Influence of the size of the Component on the Outcome of Resurfacing Arthroplasty of the Hip.* J Bone Joint Surg [Br], 2010. **92-B**: p. 469-476.
67. Amstutz, H.C., Beaulé, P E, Dorey, F J, Le Duff, M J, Campbell, P A, Gruen, T A, *Metal-on-metal hybrid surface arthroplasty: two to six-year follow-up study.* J Bone Joint Surg [Am], 2004. **86**: p. 28-39.
68. Beaulé, P.E., Le Duff, M, Campbell, P, Dorey, F J, Hyun Park, S, Amstutz, H C, *Metal-on-metal surface arthroplasty with a cemented femoral component: a 7-10 year follow-up study.* J Arthoplasty, 2004. **19**(8): p. 17-22.
69. Heilpern, G.N.A., Shah, N N, Fordyce, M J F, *Birmingham Hip Resurfacing Arthroplasty: a Series of 110 Consecutive Hips with a Minimum Five-Year Clinical and Radiological Follow-Up.* J Bone Joint Surg [Br], 2008. **90-B**: p. 1137-1142.
70. Katrana, P., Crawford, J R, Vowler, S, Lilikakis, A, Villar, R N, *Femoral neck resorption after hip resurfacing arthroplasty- a comparison of cemented and uncemented prostheses.* J Bone Joint Surg [Br], 2006. **88-B Suppl 2**: p. 234.
71. De Haan, R., Campbell, P A, Su, E P, De Smet, K A, *Revision of Metal-on-Metal Resurfacing Arthroplasty of the Hip: The Influence of Malpositioning of the Components.* J Bone Joint Surg [Br], 2008. **90-B**: p. 1158-1163.
72. Spencer, S., Carter, R, Murray, H, Meek, R M D, *Femoral Neck Narrowing After Metal-on-Metal Hip Resurfacing.* J Arthroplasty, 2008. **23**: p. 1105-1109.
73. Ball, S.T., LeDuff, M J, Amstutz, H C, *Early Results of Conversion of a Failed Femoral Component in Hip Resurfacing Arthroplasty.* J Bone Joint Surg [Am], 2007. **89**: p. 735-741.
74. Kishida, Y., Sugano, N, Nishii, T, Miki, H, Yamaguchi, K, Yoshikawa, H, *Preservation of the bone mineral density of the femur after surface replacement of the hip.* J Bone Joint Surg [Br], 2004. **86-B**: p. 185-189.
75. Borg, H., Hakulinen, M A, Kiviranta, I, Jurvelin, J S, Anttila, E, Parviainen, T, Hakkinen, A. *Restoration of Bone Mineral Density after Hip Resurfacing*. in *Swedish Orthopaedic Society*. 2009. Halstad, Sweden.
76. Lian, Y., Pei, F, Yoo, M, Cheng, J, Fatou, C, *Changes of Bone Mineral Density in Proximal Femur following Total Hip Resurfacing Arthroplasty in Osteonecrosis of Femoral Head.* J Orth Res, 2009. **26**: p. 453-459.
77. Harty, J.A., Devitt, B, Harty, L C, Molloy, M, McGuinness, A, *Dual Energy X-Ray Absorptiometry Analysis of Peri-Prosthetic Stress Shielding in the Birmingham Resurfacing Hip Replacement.* Arch Ortho Trauma Surg, 2005. **125**: p. 693-695.
78. McMinn, D. *The History of Hip Resurfacing*. [cited March 2010; Available from: http://www.mcminncentre.co.uk/hipconcepts.htm.
79. Ong, K.L., Manley, M T, Kurtz, S L, *Have Contemporary Hip Resurfacing Designs Reached Maturity? A Review.* J Bone Joint Surg, 2008. **90**: p. 81-88.
80. Bengs, B.C., Sangiorgio, S N, Ebramzadeh, E, *Less Range of Motion with Resurfacing Arthroplasty than with Total Hip Arthroplasty: In Vitro Examination of 8 Designs.* Acta Othopaedica, 2008. **79**: p. 755-762.

81. Kluess, D., Zietz, C, Lindner, T, Mittelmeier, W, Schmitz, K-P, Bader, R, *Limited Range of Motion of Hip Resurfacing Arthroplasty due to Unfavourable Ratio of Prosthetic Head Size and Femoral Neck Diameter.* Acta Orthopaedica, 2008. **79**: p. 748-754.
82. Lian, Y., Pei, F, Yoo, M, Cheng, J, Fatou, C, *Changes of Bone Mineral Density in Proximal Femur following Total Hip Resurfacing Arthroplasty in Osteonecrosis of Femoral Head.* J Orth Res, 2008. **26**: p. 453-459.
83. Thompson, M.S., *The design of a novel hip resurfacing prosthesis*, in *Interdisciplinary Research Centre in Biomedical Materials*. 2001, Queen Mary and Westfield College, University of London: London.
84. Charnley, J., Kamangar, A, Longfield, M D, *The Optimum Size of Prosthetic Heads in Relation to the Wear of Plastic Sockets in Total Replacement of the Hip.* Med Biol Engng, 1969. **7**: p. 31-39.
85. Schmalzreid, T.P., Kwong, L M, Jasty, M, Sedlacek, R C, Haire, T C, O'Connor, D O, Bragdon, C R, Kabo, J M, Malcolm, A J, Path, M R C, Harris, W H, *The Mechanism of Loosening of Cemented Acetabular Components in Total Hip Arthroplasty. Analysis of Specimens Retrieved at Autopsy.* Clin Ortho Rel Res, 1992. **274**: p. 60-78.
86. Ingham, E., Fisher, J, *Biological Reactions to Wear Debris in Total Joint Replacement.* Proc IMechE Part H: J Eng Med, 2000. **214**: p. 21-37.
87. Goldsmith, A.A.J., Dowson, D, Isaac, G H, Lancaster, J G, *A Comparative Joint Simulator Study of the Wear of Metal-on-Metal and Alternative Material Combinations in Hip Replacements.* Proc IMechE Part H: J Eng Med, 2000. **214**: p. 39-47.
88. Doorn, P.F., Campbell, P A, Worrall, J, Benya, P D, McKellop, H A, Amstutz, H C, *Metal Wear Particle Characterisation from Metal on Metal Total Hip Replacements: Transmission Electron Microscopy Study of Periprosthetic Tissues and Isolated Particles.* J Biomed Mater Res, 1998. **42**: p. 103-111.
89. Firkins, P.J., Tipper, J L, Saadatzadeh, M R, Ingham, E, Stone, M H, Farrar, R, Fisher, J, *Quantitative Analysis of Wear and Wear Debris from Metal-on-Metal Hip Prostheses Tested in a Physiological Hip Joint Simulator.* Biomed Mater Engng, 2001. **11**: p. 143-157.
90. Doorn, P.F., Mirra, J M, Campbell, P A, Amstutz, H C, *Tissue Reaction to Metal on Metal Total Hip Prostheses.* Clin Orth, 1996. **329S**: p. 187-205.
91. Campbell, P.A., Wang, M, Amstutz, H C, Goodman, S B, *Positive Cytokine Production in Failed Metal-on-Metal Total Hip Replacements.* Acta Orthop Scand, 2002. **73**: p. 506-512.
92. Catelas, I., Campbell, P A, Dorey, F, Frausto, A, Mills, B G, Amstutz, H C, *Semi-quantitative Analysis of Cytokines in MM THR Tissues and their Relationship to Metal Particles.* Biomaterials, 2003. **24**: p. 4785-4797.
93. Korovessis, P., Petsinis, G, Repanti, M, Repantis, T, *Metallosis after Contemporary Metal-on-Metal Total Hip Arthroplasty. Five to Nine Year Follow-Up.* J Bone Joint Surg [Am], 2006. **88**(1183-1191).
94. Shanbhag, A.S., Jacobs, J J, Black, J, Galante, J O, Glant, T T, *Macrophage/particle Interactions: Effect of Size, Composition and Surface Area.* J Biomed Mater Res, 1994. **28**: p. 81-90.
95. Langton, D.J., Jameson, S S, Joyce, T J, Webb, J, Nargol, A V F, *The Effect of Component Size and Orientation on the Concentrations of Metal Ions after Resurfacing Arthroplasty of the Hip.* J Bone Joint Surg [Br], 2008. **90-B**: p. 1143-1151.
96. Szuszczewicz, E.S., Schmalzreid, T P, Petersen, T D, *Progressive Bilateral Pelvic Osteolysis in a Patient with McKee-Farrar Metal-Metal Total Hip Prostheses.* J Arthoplasty, 1997. **12**: p. 819-824.
97. Black, J., *Systemic Effects of Biomaterials.* Biomaterials, 1984. **5**: p. 11-18.
98. van Kampen, M., Scholes, S, Unsworth, A. *The Lubrication Regime in a Metal-on-Metal Total Hip Replacement*. in *IMechE International Conference: Engineers and Surgeons- Joined at the Hip*. 2002. London.
99. Brodner, W., Bitzan, P, Meisinger, V, Kaider, A, Gottsauner-Wolf, F, Kotz, R, *Serum Cobalt Levels After Metal-on-Metal Total Hip Arthroplasty.* J Bone Joint Surg [Am], 2003. **85**: p. 2168-2173.
100. Grubl, A., Weissinger, M, Brodner, W, Gleiss, A, Giurea, A, Gruber, M, Poll, G, Meisinger, V, Gottsauner-Wolf, F, Kotz, R, *Serum Aluminium and Cobalt Levels After Ceramic-on-Ceramic and Metal-on-Metal Total Hip Replacement.* J Bone Joint Surg [Br], 2006. **88-B**: p. 1003-1005.
101. Hart, A.J., Hester, T, Sinclair, K, Powell, J J, Goodship, A E, Pele, L, Fersht, N L, Skinner, J, *The Association Between Metal Ions From Hip Resurfacing and Reduced T-Cell Counts.* J Bone Joint Surg [Br], 2006. **88-B**: p. 449-454.
102. Ladon, D., Doherty, A, Newson, R, Turner, J, Bhamra, M, Case, C P, *Changes in Metal Levels and Chromosome Aberrations in the Peripheral Blood of Patients after Metal-on-Metal Hip Arthroplasty.* J Arthoplasty, 2004. **19**: p. S78-S83.
103. MacDonald, S.J., McCalden, R W, Chess, D G, Bourne, R B, Rorabeck, C H, Cleland, D, Leung, F, *Metal-on-Metal versus Polyethylene in Hip Arthroplasty: a Randomised Clinical Trial.* Clin Ortho Rel Res, 2003. **406**: p. 282-296.

104. Savarino, L., Greco, M, Cenni, E, Cavasinni, L, Rotini, R, Baldini, N, Giunti, A, *Differences in Ion Release After Ceramic-on-Ceramic and Metal-on-Metal Total Hip Replacement.* J Bone Joint Surg [Br], 2006. **88-B**: p. 472-476.
105. Skipor, A.K., Campbell, P A, Patterson, L M, Amstutz, H C, Schmalzreid, T P, Jacobs, J J, *Serum and Urine Levels in Patients with Metal-on-Metal Surface Arthroplasty.* J Mater Sci, 2002. **13**: p. 1227-1234.
106. Clarke, M.T., Lee, P T H, Arora, A, Villar, R N, *Levels of Metal Ions after Small- and Large- Diameter Metal-on-Metal Hip Arthroplasty.* J Bone Joint Surg [Br], 2003. **85**: p. 913-917.
107. Case, C.P., Langkamer, V G, James, C, Palmer, M R, Kemp, A J, Heap, P F, Solomon, L, *Widespread Dissemination of Metal Debris from Implants.* J Bone Joint Surg [Br], 1994. **76-B**: p. 701-712.
108. Urban, R.M., Tomlinson, M J, Hall, D J, Jacobs, J J, *Accumulation in Liver and Spleen of Metal Particles Generated at Nonbearing Surfaces in Hip Arthroplasty.* J Arthoplasty, 2004. **19 (Suppl. 3)**: p. 94-101.
109. Hallab, N.J., Anderson, S, Caicedo, M, Brasher, A, Mikecz, K, Jacobs, J J, *Effects of Soluble Metals on Human Peri-Implant Cells.* J Biomed Mater Res, 2005. **74A**: p. 124-140.
110. Willert, H.-G., Buchhorn, G H, Fayyazi, A, Flury, R, Windler, M, Koster, G, Lohmann, C H, *Metal-on-metal bearings and hypersensitivity in patients with artificial hip joints. A clinical and histomorphological study.* J Bone Joint Surg [Am], 2005. **87A**: p. 28-36.
111. Hallab, N., Merrit, K, Jacobs, J J, *Metal Sensitivity in Patients with Orthopaedic Implants.* J Bone Joint Surg [Am], 2001. **83A**: p. 428-436.
112. Cobb, A.G., Schmalzreid, T P, *The Clinical Significance of Metal Ion Release from Cobalt-Chromium Metal-on-Metal Total Hip Joint Arthroplasty.* Proc IMechE H, 2006. **220**: p. 385-398.
113. Silva, M., Heisel, C, Schmalzreid, T P, *Metal-on-Metal Total Hip Replacement.* Clin Orth Rel Res, 2005. **430**: p. 53-61.
114. Visuri, T.I., Pukkala, E, Pulkkinen, P, Paavolainen, P, *Cancer Incidence and Causes of Death Among Total Hip Replacement Patients: a Review Based on Nordic Cohorts with a Special Emphasis on Metal-on-Metal Bearings.* Proc IMechE H, 2006. **220**: p. 399-407.
115. Tharani, R., Dorey, F J, Schmalzried, T P, *The Risk of Cancer Following Total Hip or Knee Arthroplasty.* J Bone Joint Surg [Am], 2001. **83**: p. 774-780.
116. Brodner, W., Grohs, J G, Bancher-Todesca, D, Dorotka, R, Meisinger, V, Gottsauner-Wolff, F, Kotz, R, *Does the Placenta Inhibit the Passage of Chromium and Cobalt after Metal-on-Metal Total Hip Arthroplasty?* J Arthoplasty, 2004. **19 Suppl 3**: p. 102-106.
117. Zaiee, H., Daniel, J, Datta, A K, Blunt, S, McMinn, D J W, *Transplacental Transfer of Cobalt and Chromium in Patients with Metal-on-Metal Hip Arthroplasty.* J Bone Joint Surg [Br], 2007. **89-B**: p. 301-305.
118. Schmalzreid, T.P., Szuszczewicz, E S, Akizuki, K H, Petersen, T D, Amstutz, H C, *Factors Correlating with Long Term Survival of McKee-Farrar Total Hip Prosthesis.* Clin Ortho Rel Res, 1996. **329**: p. S48-S59.
119. Andrew, T.A., Berridge, D, Thomas, A, Duke, R N, *Long-Term Review of Ring Total Hip Arthroplasty.* Clin Ortho Rel Res, 1985. **201**: p. 111-122.
120. Tuke, M.A., Scott, G, Roques, A, Hu, X Q, Taylor, A C, *Design Considerations and Life Prediction of Metal-on-Metal Bearings: The Effect of Clearance.* J Bone Joint Surg [Am], 2008. **90**: p. 134-141.
121. Nordin, M., Frankel, V H, *Biomechanics of the Hip*, in *Basic Biomechanics of the Musculoskeletal System*, M. Nordin, Frankel, V H, Editor. 2001, Lippincott, Williams and Wilkins. p. 202-221.
122. Johnston, R.C., Smidt, G L, *Hip Motion Measurements for Selected Activities of Daily Living.* Clin Ortho Rel Res, 1970. **72**: p. 205.
123. Paul, J.P., *Force Actions Transmitted by Joints in the Human Body.* Proc Royal Soc London B: Biol Sci, 1976. **192**: p. 163-172.
124. Bergmann, G., Graichen, F, Rohlmann, A, *Hip joint loading during walking and running, measured in two patients.* J Biomech, 1993. **26**: p. 969-990.
125. Bergmann, G., Deuretzbacher, G, Heller, M, Graichen, F, Rohlmann, A, Strauss, J, Duda, G N, *Hip contact forces and gait patterns from routine activities.* J Biomech, 2001. **34**: p. 859-871.
126. Cristofolini, L., Juszczyk, M, Martelli, S, Taddei, F, Viceconti, M, *In Vitro Replication of Spontaneous Fractures of the Proximal Human Femur.* J Biomech, 2007. **40**: p. 2837-2845.
127. Majumder, S., Roychowdhury, A, Pal, S, *Simulation of Hip Fracture in Sideways Fall using a 3D Finite Element Model of Pelvis-Femur-Soft Tissue Complex with Simplified Representation of Whole Body.* Med Eng and Physics, 2007. **29**: p. 1167-1178.
128. Duchemin, L., Mitton, D, Jolivet, E, Bousson, V, Laredo, J D, Skalli, W, *An anatomical subject-specific FE-model for hip fracture load prediction.* Comp Meth Biomech Biomed Eng, 2008. **11**: p. 105-111.

129. Keyak, J.H., Rossi, S A, Jones, K A, Skinner, H B, *Prediction of femoral fracture load using automated finite element modelling.* J Biomech, 1998. **31**: p. 125-133.
130. Schileo, E., Taddei, F, Cristolfini, L, Viceconti, M, *Subject-specific finite element models implementing a maximum principal strain criterion are able to estimate failure risk and fracture location on human femurs tested in-vitro.* J Biomech, 2008. **41**: p. 356-367.
131. Lotz, J.C., Hayes, W C, *The Use of Quantitative Computer Tomography to Estimate Risk of Fracture of the Hip from Falls.* J Bone Joint Surg [Am], 1990. **72**: p. 689-700.
132. Keyak, J.H., Rossi, S A, *Prediction of femoral fracture load using finite element models: an examination of stress- and strain-based failure theories.* J Biomech, 2000. **33**: p. 209-214.
133. de Bakker, P.M., Manske, S L, Ebacher, V, Oxland, T R, Cripton, P A, Guy, P, *During Sideways Falls Proximal Femur Fracture Initiate in the Superolateral Cortex: Evidence from High-Speed Video of Simulated Fractures.* J Biomech, 2009. **42**: p. 1917-1925.
134. Keyak, J.H., Rossi, S A, Jones, K A, Les, C M, Skinner, H B, *Prediction of Fracture Location in the Proximal Femur using Finite Element Models.* Med Eng and Physics, 2001. **23**: p. 657-644.
135. Majumder, S., Roychowdhury, A, Pal, S, *Effects of Trochanteric Soft Tissue Thickness and Hip Impact Velocity on Hip Fracture in Sideways Fall through 3D Finite Element Simulations.* J Biomech, 2008. **41**: p. 2834-2842.
136. *Guidance Document for the Preparation of Premarket Notifications for Ceramic Ball Hip Systems*. 1995, Centre for Devices and Radiological Health: US Food and Drug Administration.
137. Dalla Pria, P., Pressacco, M, Benazzo, F, Fusi, S. *Evolution of Diameters Features and Results*. in *Ceramics in Orthopaedics: 12th BIOLOX Symposium: Bioceramics and Alternative Bearings in Joint Arthroplasty*. 2007. Seoul, Korea: Steinkopf Verlag.
138. Spence, A.P., *Basic Human Anatomy*. 1990: Benjamin-Cummings.
139. Jee, W.S.S., *Integrate Bone Tissue Physiology*, in *Bone Mechanics Handbook*, S.C. Cowin, Editor. 2001, CRC Press: Boca Raton.
140. Carter, D.R., Spengler, D M, *Mechanical Properties and Composition of Cortical Bone.* Clin Orth Rel Res, 1978. **135**: p. 192-217.
141. Reilly, D.T., Burstein, A H, *The Mechanical Properties of Cortical Bone.* J Bone Joint Surg [Am], 1974. **56**: p. 1001-1022.
142. Morgan, E.F., Keaveny, T M, *Dependence of yield strain of human trabecular bone on anatomic site.* J Biomech, 2001. **34**: p. 569-577.
143. Morgan, E.F., Bayraktar, H H, Keaveny, T M, *Trabecular Bone Modulus-Density Relationships Depend on Anatomic Site.* J Biomech, 2003. **36**: p. 897-904.
144. Schileo, E., Taddei, F, Malandrino, A, Cristolfini, L, Viceconti, M, *Subject-specific finite element models can accurately predict strain in long bones.* J Biomech, 2007. **40**: p. 2982-2989.
145. Wolff, J., *Das Gesetz der Transformation Der Knochen*, ed. Hirschwald. 1892, Berlin.
146. Bobyn, J.D., Mortimer, E S, Glassman, A H, Engh, C A, Miller, J E, Brooks, C E, *Producing and avoiding stress shielding: laboratory and clinical observations of noncemented total hip arthroplasty.* Clin Ortho Rel Res, 1992. **274**: p. 79-96.
147. Bruder, S.P., Kurth, A A, Shea, M, Hayes, W C, Jaiswal, N, Kadiyala, S, *Bone Regeneration by Implantation of Purified, Culture-Expanded Human Mesenchymal Stem Cells.* J Orth Res, 1998. **16**: p. 155-162.
148. Ponticiello, M.S., Schinagl, R M, Kadiyala, S, Barry, F P, *Gelatin-based Resorbable Sponge as a Carrier Matrix for Human Mesenchymal Stem Cells in Cartilage Regeneration Therapy.* J Biomed Mater Res, 2000. **52**: p. 246-255.
149. Barry, F.P., *Biology and Clinical Applications of Mesenchymal Stem Cells.* Birth Defects Research (Part C), 2003. **69**: p. 250-256.
150. Quarto, R., Mastrogiacomo, M, Cancedda, R, *Repair of Large Bone Defects with the Use of Autologous Bone Marrow Stromal Cells.* N Engl J Med, 2001. **344**: p. 385-386.
151. Matsuda, N., Morita, N, Matsuda, K, Wanatabe, M, *Proliferation and Differentiation of Human Osteoblastic Cells Associated with Differential Activation of MAP Kinases in Response to Epidermal Growth Factor, Hypoxia, and Mechanical Stress in-Vitro.* Biochem. and Biophys. Research Communications, 1998. **249**: p. 350-354.
152. Angele, P., Yoo, J U, Smith, C, Mansour, J, Jepsen, K J, Nerlich, M, Johnstone, B, *Cyclic Hydrostatic Pressure Enhances the Chondrogenic Phenotype of Human Mesenchymal Progenitor Cells Differentiated in vitro.* J Orth Res, 2003. **21**: p. 451-457.
153. Altman, G., Horan, R, Martin, I, Farhadi, J, Stark, P, Volloch, V, Vunjak-Novakovic, G, Richmond, J, Kaplan, D L, *Cell Differentiation by Mechanical Stress.* J FASEB, 2002. **16**: p. 270-272.

154. Brighton, C.T., *Principles of Fracture Healing*, in *Instructional Course Lectures*, J.A. Murray, Editor. 1984, Mosby Co.: St Louis, CV. p. 60-82.
155. Carter, D.R., Blenman, P R, Beaupré, G S, *Correlations Between Mechanical Stress History and Tissue Differentiation in Initial Fracture Healing.* J Orth Res, 1988. **6**: p. 736-748.
156. Speirs, A.D., Slomczykowski, M A, Orr, T E, Siebenrock, K, Nolte, L-P, *Three-Dimensional Measurement of Cemented Femoral Stem Stability: an in vitro Cadaver Study.* Clin Biomechanics, 2000. **15**: p. 248-255.
157. Perren, S.M., *Physical and Biological Aspects of Fracture Healing with Special Reference to Internal Fixation.* Clin Orth Rel Res, 1979. **138**: p. 175-195.
158. Pauwels, F., *A New Theory Concerning the Influence of Mechanical Stimuli on the Differentiation of the Supporting Tissues*, in *Biomechanics of the Locomotor Apparatus*, P. Manquet, Furlong, R, Editor. 1980, Springer: Berlin. p. 375-407.
159. Weinans, H., Prendergast, P J, *Tissue Adaptation as a Dynamical Process Far from Equilibrium.* Bone, 1996. **19**: p. 143-149.
160. Pilliar, R.M., Lee, J M, Maniatopoulos, C D D S, *Observations on the Effect of Movement on Bone Ingrowth into Porous-Surfaced Implants.* Clin Orth, 1986. **208**: p. 108-113.
161. Søballe, K., *Hydroxyapatite ceramic coating for bone-implant fixation. Mechanical and histological studies in dogs.* Acta Orthop Scand, 1993. **65 S255**: p. 1-58.
162. Burke, D.W., Bragdon, C R, O'Connor, D O, Jasty, M, Haire, T, Harris, W H, *Dynamic Measurement of Interface Mechanics in vivo and the Effect of Micromotion on Bone Ingrowth into a Porous Surface Device under Controlled Loads in vivo.* Trans ORS, 1991. **16**: p. 103.
163. Ruimerman, R., Hilbers, P, van Rietbergen, B, Huiskes, R, *A Theoretical Framework for Strain-Related Trabecular Bone Maintenance and Adaptation.* J Biomech, 2005. **38**: p. 931-941.
164. Lotz, J.C., Cheal, E J, Hayes, W C, *Fracture Prediction for the Proximal Femur using Finite Element Models: Part I- Linear Analysis.* J Biomech Eng, 1991. **113**: p. 353-360.
165. Lotz, J.C., Cheal, E J, Hayes, W C, *Fracture Prediction for the Proximal Femur using Finite Element Models: Part II- Nonlinear Analysis.* J Biomech Eng, 1991. **113**: p. 361-365.
166. Bayraktar, H.H., Morgan, E F, Niebur, G L, Morris, G E, Wong, E K, Keaveny, T M, *Comparison of the Elastic and Yield Properties of Human Femoral Trabecular and Cortical Bone Tissue.* J Biomech, 2004. **37**: p. 27-35.
167. Huiskes, R., Weinans, H, Grootenboer, H J, Dalstra, M, Fudala, B, Slooff, T J, *Adaptive bone remodelling theory applied to prosthetic design analysis.* J Biomech, 1987. **20**: p. 1135-1150.
168. Huiskes, R., Weinans, M S, van Rietbergen, M S, *The relationship between stress shielding and bone resorption around total hip stems and the effects of flexible materials.* Clin Ortho Rel Res, 1992. **274**: p. 124-134.
169. Weinans, H., Huiskes, R, van Rietbergen, B, Sumner, D R, Turner, T M, Galante, J O, *Adaptive Bone Remodelling around a Bonded Noncemented Total Hip Arthroplasty: a Comparison between Animal Experiments and Computer Simulation.* J Orth Res, 1993. **11**: p. 500-513.
170. Prendergast, P.J., Taylor, D, *Prediction of bone adaptation using damage accumulation.* J Biomech, 1994. **27**: p. 1067-1076.
171. Garcia, J.M., Martinez, M A, Doblaré, M, *An isotropic internal-external bone adaptation model based on a combination of CAO and continuum damage mechanics technologies.* Comp Meth Biomech Biomed Eng, 2001. **4**: p. 355-377.
172. Doblaré, M., Garcia, J M, *Application of an anisotropic bone-remodelling model based on a damage-repair theory to the analysis of the proximal femur before and after total hip replacement.* J Biomech, 2001. **34**: p. 1157-1170.
173. Jang, I.G., Kim, I Y, *Computational Study of Wolff's Law with Trabecular Architecture in the Human Proximal Femur using Topology Optimization.* J Biomech, 2008. **41**: p. 2353-2361.
174. Kowalczyk, P., *Simulation of Orthotropic Microstructure Remodelling of Cancellous Bone.* J Biomech, 2010. **43**: p. 563-569.
175. Carter, D.R., Orr, T E, Fyhrie, D P,, *Relationships between loading history and femoral cancellous bone architecture.* J Biomech, 1989. **22**: p. 231-244.
176. Frost, H.M., *Vital biomechanics: proposed general concepts for skeletal adaptations to mechanical usage.* Calcif Tissue Int, 1988. **42**: p. 145-156.
177. Martin, R.B., *Porosity and Specific Surface of Bone.* CRC Crit Rev Biomed Eng, 1984. **10**: p. 179-222.
178. Carter, D.R., Hayes, W C, Schurman, D J, *Fatigue life of compact bone- II: effects of microstructure and density.* J Biomech, 1976. **9**: p. 211-218.

179. Mattheck, C., Burkhardt, S, *A New Method of Structural Shape Optimisation based on Biological Growth.* Int J Fatigue, 1990. **12**: p. 185-190.
180. Martinez-Reina, J., Garcia-Aznar, J M, Dominguez, J, Doblare, M, *A Bone Remodelling Model Including the Directional Activity of BMUs.* Biomech Model Mechanobiol, 2009. **8**: p. 111-127.
181. Restrepo, J.M., Choksi, R, Hyman, J M, Jiang, Y, *Improving the Damage Accumulation in a Biomechanical Bone Remodelling Model.* CMBBE, 2009. **12**: p. 341-352.
182. Jang, I.G., Kim, I Y, Kwak, B B, *Analogy of Strain Energy Density Based Bone-Remodeling Algorithm and Structural Topology Optimization.* J Biomech Eng, 2009. **131**: p. 011012-1.
183. Harrigan, T.P., Hamilton, J J, *Bone Remodeling and Structural Optimization.* J Biomech, 1994. **27**: p. 323-328.
184. Jang, I.G., Kim, I Y, *Computational Simulation of Simultaneous Cortical and Trabecular Bone Change in Human Proximal Femur during Bone Remodeling.* J Biomech, 2010. **43**: p. 294-301.
185. McNamara, L.M., Prendergast, P J, *Bone remodeling algorithms incoroporating both strain and microdamage stimuli.* J Biomech, 2007. **40**: p. 1381-1391.
186. Scannell, P.T., Prendergast, P J, *Cortical and Interfacial Bone Changes around a Non-Cemented Hip Implant: Simulations using a Combined Strain/Damage Algorithm.* Med Eng and Physics, 2009. **31**: p. 477-488.
187. Carter, D.R., Wong, M, *The Role of Mechanical Loading Histories in the Development of Diarthrodial Joints.* J Orth Res, 1988. **6**: p. 804-816.
188. Prendergast, P.J., Huiskes, R, *Finite Element Analysis of Fibrous Tissue Morphogenesis - A Study of the Osteogenic Index with a Biphasic Approach.* Mechanics of Composite Materials, 1996. **32**: p. 144-150.
189. Giori, N.J., Ryd, L, Carter, D R, *Mechanical Influences on Tissue Differentiation at Bone-Cement Interfaces.* J Arthoplasty, 1995. **10**: p. 514-522.
190. Gardner, T.N., Mishra, S, Marks, L, *The Role of Osteogenic Index, Octahedral Shear Stress and Dilatational Stress in the Ossification of a Fracture Callus.* Med Eng and Physics, 2004. **26**: p. 493-501.
191. Claes, L.E., Heigele, C A, *Magnitudes of Local Stress and Strain Along Bony Surfaces Predict the Course and Type of Fracture Healing.* J Biomech, 1999. **32**: p. 255-266.
192. Heigele, C.A., Claes, L E. *Finite Element Analysis of the Local Strains and Hydrostatic Pressure in Drill Hole Defects*. in *11th Conference of the European Society of Biomechanics*. 1998. Tououse, France.
193. Prendergast, P.J., Huiskes, R, Soballe, K, *Biophysical Stimuli on Cells during Tissue Differentiation at Implant Interfaces.* J Biomech, 1997. **30**: p. 539-548.
194. Huiskes, R., van Driel, W D, Prendergast, P J, Soballe, K, *A Biomechanical Regulatory Model for Periprosthetic Fibrous-Tissue Differentiation.* J Mater Sci, 1997. **8**: p. 785-788.
195. Lacroix, D., Prendergast, P J. *A Homogenization Procedure to Prevent Numerical Instabilities in Poroelastic Tissue Differentiation Models*. in *Proceedings of the 8th Symposium on Computational Methods in Orthopaedic Biomechanics*. 2000. Florida, USA.
196. Lacroix, D., Prendergast, P J, Li, G, Marsh, D, *Biomechanical Model to Simulate Tissue Differentiation and Bone Regeneration: Application to Fracture Healing.* Medical & Biological Engineering & Computing, 2002. **40**: p. 14-21.
197. Lacroix, D., Prendergast, P J, *A Mechano-Regulation Model for Tissue Differentiation during Fracture Healing: Analysis of Gap Size and Loading.* J Biomech, 2002. **35**: p. 1163-1171.
198. Kelly, D.J., Prendergast, P J, *Mechano-Regulation of Stem Cell Differentiation and Tissue Regeneration in Osteochondral Defects.* J Biomech, 2005. **38**: p. 1413-1422.
199. Scannell, P.T., *Mechanoregulation Algorithms Predicting Peri-Prosthetic Bone Adaptations. PhD Thesis*. 2006, Trinity College: Dublin.
200. Pérez, M.A., Prendergast, P J, *Random-Walk Models of Cell Dispersal Included in Mechanobiological Simulations of Tissue Differentiation.* J Biomech, 2007. **40**: p. 2244-2253.
201. Isaksson, H., Wilson, W, van Donkelaar, C C, Huiskes, R, Ito, K, *Comparison of Biophysical Stimuli for Mechano-Regulation of Tissue Differentiation during Fracture Healing.* J Biomech, 2006. **39**: p. 1507-1516.
202. Radcliffe, I.A.J., *Multiple femur finite element analysis of the resurfaced femoral head. PhD Thesis*, in *Bioengineering Science Research Group*. 2007, University of Southampton: Southampton.
203. Pal, B., Gupta, S, New, A M, *A Numerical Study of Failure Mechanisms in the Cemented Resurfaced Femur: Effects of Interface Characteristics and Bone Remodelling.* Proc IMechE Part H: J Eng Med, 2009. **223**: p. 471-484.
204. Davis, E.T., Olsen, M, Zdero, R, Waddell, J P, Scemitsch, E H, *A Biomechanical and Finite Element Analysis of Femoral Neck Notching During Hip Resurfacing.* J Biomech Eng, 2009. **131**.
205. Pal, B., Gupta, S, New, A M R, *Design Considerations for Ceramic Resurfaced Femoral Head: Effect of Interface Characteristics on Failure Mechanisms.* CMBBE, 2010. **13**: p. 143-155.

206. Long, J., Santner, TJ, Bartel, DL, *Hip Resurfacing Increases Bone Strains Associated with Short-Term Femoral Neck Fracture.* J Orth Res, 2009: p. 1-7.
207. Stone, R.J., Stone, J A, *Atlas of Skeletal Muscles, 4th ed.* 2003, McGraw-Hill, New York.
208. Speirs, A.D., Heller, M O, Duda, G N, Taylor, W R, *Physiologically based boundary conditions in finite element modelling.* J Biomech, 2007. **40**: p. 2318-2323.
209. Polgar, K., Gill, H S, Viceconti, M, Murray, D W, O'Connor, J J, *Strain Distribution within the Human Femur due to Physiological and Simplified Loading: Finite Element Analysis using the Standardized Femur Model.* Proc IMechE Part H: J Eng Med, 2003. **217**: p. 173-189.
210. Stolk, J., Verdonschot, N, Huiskes, R, *Hip-Joint and Abductor-Muscle Forces Adequately Represent In-Vivo Loading of a Cemented Total Hip Prosthesis.* J Biomech, 2001. **34**: p. 917-926.
211. Bryan, R., *Large Scale, Multi Femur Computational Stress Analysis Using a Statistical Shape and Intensity Model*, in *Bioengineering Science Research Group*. 2010, University of Southampton.
212. Zannoni, C., Mantovani, R, Viceconti, M, *Material properties assignment to finite element models of bone structures: a new method.* Med Eng and Physics, 1998. **20**: p. 735-740.
213. Keyak, J.H., *Improved Prediction of Proximal Femoral Fracture Load using Nonlinear Finite Element Models.* Med Eng and Physics, 2001. **23**: p. 165-173.
214. Hertz, H., *On the contact of elastic solids.* J Reine und Angewandte Mathematik, 1882. **92**: p. 156-171.
215. Weinans, H., Huiskes, R, Verdonschot, N, van Rietbergen, B, *The Effect of Adaptive Bone Remodelling Threshold Levels on Resorption around Noncemented Hip Stems*, in *Advances in Bioengineering*, R. Vanderby, Editor. 1991, ASME: New York. p. 303-306.
216. Turner, A.W.L., Gillies, R M, Sekel, R, Morris, P, Bruce, W, Walsh, W R, *Computational Bone Remodelling Simulations and Comparisons with DEXA Results.* J Orth Res, 2005. **23**: p. 705-712.
217. Frost, H.M., *Skeletal Structural Adaptations to Mechanical Usage (SATMU): 1. Redefining Wolff's Law: The Bone Modeling Problem.* The Anatomical Record, 1990. **226**: p. 403-413.
218. Liu, X., Niebur, G L, *Bone Ingrowth into a Porous Coated Implant Predicted by a Mechano-Regulatory Tissue Differentiation Algorithm.* Biomech Model Mechanobiol, 2008. **7**: p. 335-344.
219. Carter, D.R., *Mechanical Loading Histories and Cortical Bone Remodelling.* Calcif Tissue Int, 1984. **36**: p. S19-S24.
220. Rubin, C.T., Lanyon, L E, *Regulation of Bone Mass by Mechanical Strain Magnitude.* Calcif Tissue Int, 1985. **37**: p. 411-417.
221. Viceconti, M., Olsen, S, Nolte, L-P, Burton, K, *Editorial: Extracting Clinically Relevant Data from Finite Element Simulations.* Clin Biomechanics, 2005. **20**: p. 451-454.
222. Gupta, S., van der Helm, F C T, Sterk, J C, van Keulen, F, Kaptein, B L, *Development and Experimental Validation of a Three-Dimensional Finite Element Model of the Human Scapula.* Proc IMechE Part H: J Eng Med, 2004. **218**: p. 127-142.
223. Taddei, F., Cristofolini, L, Martelli, S, Gill, H S, Viceconti, M, *Subject-Specific Finite Element Models of Long Bones: An in vitro Evaluation of the Overall Accuracy.* J Biomech, 2006. **39**: p. 2457-2467.
224. Coker, E.G., Filon, L N G, Jessop, H T, *A Treatise on Photo-Elasticity*. 1st ed. 1931, London: Cambridge University Press.
225. Kahn-Jetter, Z., Chu, T, *Three-Dimensional Displacement Measurements using Digital Image Correlation and Photogrammetric Analysis.* Experimental Mechanics, 1990. **30**: p. 10-16.
226. Peters, W.H., Ranson, W F, *Digital Imaging Techniques in Experimental Stress Analysis.* Optical Engineering, 1982. **21**: p. 427-431.
227. Sztefek, P., Vanleene, M, Olsson, R, Collinson, R, Pitsillides, A A, Shefelbine, S, *Using Digital Image Correlation to Determine Bone Surface Strains During Loading and After Adaptation of the Mouse Tibia.* J Biomech, 2010. **43**: p. 599-605.
228. Bay, B.K., Smith, T S, Fyrie, D P, Saad, M, *Digital Volume Correlation: Three-Dimensional Strain Mapping using X-ray Tomography.* Experimental Mechanics, 1999. **39**: p. 217-226.
229. Liu, L., Morgan, E F, *Accuracy and Precision of Digital Volume Correlation in Quantifying Displacements and Strains in Trabecular Bone.* J Biomech, 2007. **40**: p. 3516-3520.
230. *Sawbones Website, www.sawbones.com*. January 2010].
231. *Kulzer-Heraeus Website, www.kulzer-technik.de.*
232. Taylor, M.E., Tanner, K E, Freeman, M A R, Yettram, A L, *Stress and Strain Distribution within the Intact Femur: Compression or Bending?* Med Eng and Physics, 1998. **18**: p. 122-131.
233. Aamodt, A., Lund-Larsen, J, Eine, J, Andersen, E, Benum, P, Schnell Husby, O, *In Vivo Measurements Show Tensile Axial Strain in the Proximal Lateral Aspect of the Human Femur.* J Orth Res, 1997. **15**: p. 927-931.

234. *ADEPT Resurfacing Operative Technique*, Finsbury Orthopaedics Ltd: Leatherhead, UK.
235. Keyak, J.H., *Relationships between Femoral Fracture Loads for Two Load Configurations.* J Biomech, 2000. **33**: p. 499-502.
236. Berend, M.E., Bertrand, T, *Metal-Metal Hip Resurfacing: Solution to a Nonexistent Problem.* Orthopedics, 2007. **30**: p. 724-727.
237. Charnley, J., *Low Friction Arthroplasty of the Hip: Theory and Practice*. 1979, New York: Springer.
238. McGrory, B.J., Morrey, B F, Cahalan, T D, An, K-N, Cabanela, M E, *Effect of Femoral Offset on Range of Motion and Abductor Muscle Strength after Total Hip Arthroplasty.* J Bone Joint Surg [Br], 1995. **77-B**: p. 865-869.
239. Johnston, R., Brand, RA, Crowninshield, RD, *Reconstruction of the Hip: A Mathematical Approach to Determine Optimum Geometric Relationships.* J Bone Joint Surg [Am], 1979. **61**: p. 639-652.
240. Morlock, M.M., Schneider, E, Bluhm, A, Vollmer, M, Bergmann, G, Muller, V, Honl, M, *Duration and Frequency of Every Day Activities in Total Hip Patients.* J Biomech, 2001. **34**: p. 873-881.
241. Cowin, S.C., *Bone Mechanics*. 1988, Boca Raton, FL: C.R.C. Press.
242. Bessho, M., Ohnishi, I, Matsumoto, T, Ohashi, S, Tobita, K, Mastuyama, J, Nakamura, K, *Prediction of Strength and Fracture Location of the Proximal Femur by a CT-based Nonlinear Finite Element Method- Effect of Load Direction on Hip Fracture Load and Fracture Site.* Trans. Orthopaedic Research Society, 2008. **33**: p. 955.
243. Carter, D.R., Bouxsein, M L, Marcus, R, *New Approaches for Interpreting Projected Bone Densitometry Data.* J Bone Mineral Research, 1992. **7**: p. 137-145.
244. Frost, H.M., *Skeletal Structural Adaptations to Mechanical Usage (SATMU): 2. Redefining Wolff's Law: The Remodeling Problem.* The Anatomical Record, 1990. **226**: p. 414-422.
245. Carter, D.R., Fyhrie, D P, Whelan, R T, *Trabecular Bone Density and Loading History: Reguation of Connective Tissue Biology by Mechanical Energy.* J Biomech, 1987. **20**: p. 785-794.
246. Dowson, D., Hardaker, C, Flett, M, Isaac, G H, *A hip joint simulator study of the performance of metal-on-metal joints. Part 1: materials.* J Arthoplasty, 2004. **19**(8: Suppl 3): p. 124-130.
247. Dowson, D., Hardaker, C, Flett, M, Isaac, G H, *A hip joint simulator study of the performance of metal-on-metal joints. Part 2: design.* J Arthoplasty, 2004. **19**(8 Suppl 3).
248. Isaac, G.H., Siebel, Schmalzreid, Cobb, O'Sullivan, Oakeshott, Flett, Vail, *Development rationale for an articular surface replacement: a science-based evolution.* Proc IMechE H, 2006. **220**: p. 253-268.
249. Pal, B., *Biomechanical Analysis of Failure Mechanisms and Design Considerations for Femoral Resurfacing Implants: Numerical and Experimental Investigations*. 2009, Indian Institute of Technology, Kharagpur: PhD Thesis, Department of Mechanical Engineering.
250. Howie, D.W., Campbell, D, McGee, M, Cornish, B L, *Wagner resurfacing hip arthroplasty. The results of one hundred consecutive arthroplasties after eight to ten years.* J Bone Joint Surg [Br], 1990. **72**: p. 708-714.
251. Wagner, M., Wagner,, *Preliminary results of uncemented metal on metal stemmed and resurfacing hip replacement arthroplasty.* Clin Ortho Rel Res, 1996. **329S**: p. S78-S88.
252. Koch, J.C., *The Laws of Bone Architecture.* Am Jour Anat, 1917.
253. Rothstock, S., Gebert, A, Morlock, M M, *Influence of Resurfacing Cap Design on the Bone Remodelling Stimulus and Stress Distribution in the Proximal Femur.* J Biomech, 2008. **41(S1)**: p. S371.
254. Laz, P.J., Browne, M, *A Review of Probabilistic Analysis in Orthopaedic Biomechanics.* Proc IMechE Part H: J Eng Med, 2010. **224**: p. 927-943.
255. Bryan, R., Nair, P B, Taylor, M, *Use of a Statistical Model of the Whole Femur in a Large Scale, Multi-Model Study of Femoral Neck Fracture Risk.* J Biomech, 2009. **42**: p. 2171-2176.
256. Laz, P.J., Stowe, J Q, Baldwin, M A, Petrella, A J, Rullkoetter, P J, *Incorporating Uncertainty in Mechanical Properties for Finite Element-Based Evaluation of Bone Mechanics.* J Biomech, 2007. **40**: p. 2831-2836.
257. Dopico-Gonzalez, C., New, A M R, Browne, M, *Probabilistic Finite Element Analysis of the Uncemented Hip Replacement - Effect of Femur Characteristics and Implant Design Geometry.* J Biomech, 2010. **43**: p. 512-520.
258. Hambli, R., Katerchi, H, Benhamou, C-L, *Multiscale Methodology for Bone Remodelling Simulation using Coupled Finite Element and Neural Network Computation.* Biomech Model Mechanobiol, 2010. **10**: p. 133-145.
259. Sandborn, P.M., Cook, S D, Spires, W P, Kester, M A, *Tissue Response to Porous-Coated Implants Lacking Initial Bone Apposition.* J Arthroplasty, 1988. **3**: p. 337-346.
260. Brooks, R.A., DiChiro, G, *Principles of Computer-Assisted Tomography in Radiographic and Radioisotropic Imaging*. Phys Med Biol, 1976. **21**: p. 689-732.
261. Hobbie, R.K., *Intermediate Physics for Medicine and Biology*. 1988, New York: John Wiley & Sons.

APPENDIX 1: BONE HEALING PROCESS PARAMETERS

In the tissue differentiation algorithm used to model bone healing, two process parameters were used which influenced the healing rate: the stem cell diffusion coefficient 'D' [mm^2/day] and the stem cell maturation rate 'M' [%cells/day]. Baseline values of these parameters from the literature were D=2.37mm^2/day and M=10%/day [195, 197]. A parametric variation study was conducted to identify the suitability of the baseline values when applying the tissue differentiation algorithm to the healing of a small cancellous bone defect. An unloaded model was used, to isolate the effects of healing or bone modelling from mature bone remodelling. For this scenario, clinical data from Sandborn et al [259] was used to support the selection of parameter values. Their data showed that 56–79% gap filling was achieved in cancellous bone after 3 months (84 days), for gap widths of 0.25mm–1.0mm, although filling of wider gaps was slower. Within their limits of measurement variability, gap filling was approximately linear up to this point. However, their investigation used a canine model which would have a faster metabolism than humans, so for this study, a lower bound was used for parameter fitting. Parameters were fitted so that the stem bore would reach 50% of its steady state Young's Modulus value after 3 months, and exceed 95% of gap filling after 12 months, indicating completed healing. The healing algorithm was applied to the stem bore and the extent of gap filling quantified as the percentage of the steady state bone density.

First, the stem cell diffusion coefficient was investigated, with values of D=2.37, 1.19 and 4.74mm^2/day (the baseline value, halved and doubled). The percentage gap filling and the normalised percentage of mean stem cell concentration were plotted over time, in Figure 109 and Figure 110.

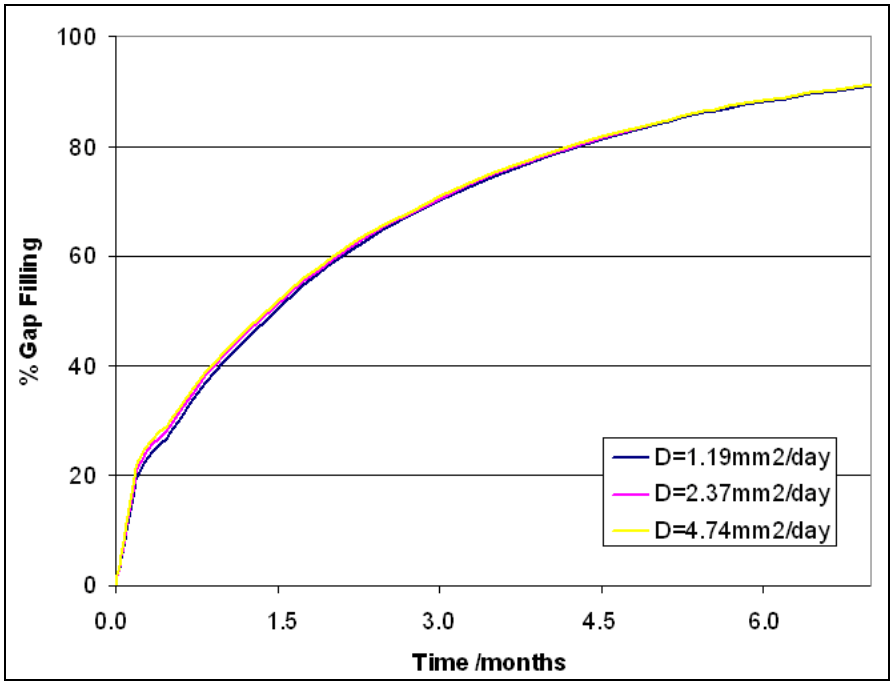

Figure 109: Percentage Gap Filling for Varying Stem Cell Diffusion Rates

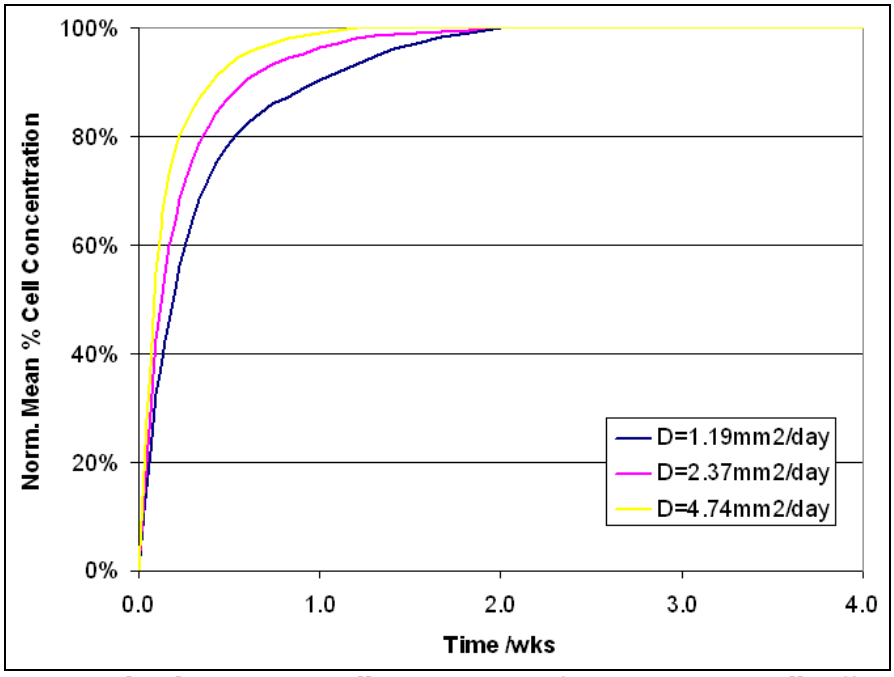

Figure 110: Normalised Percentage Cell Concentration for Varying Stem Cell Diffusion Rates

The stem cell diffusion rate 'D' had only a very slight effect upon the rate of gap filling, during the first postoperative month (Figure 109). It can be concluded that the stem cell diffusion is completed quickly in this scenario, because the cell diffusion distance is small (maximum 5mm) compared to the

cut surface area. Therefore, the final cell concentration pattern was achieved within the first two weeks (Figure 110), so the stem cell maturation process has the greater influence upon the rate of gap filling. In contrast, in the fracture fixation application for which the tissue differentiation healing process was designed, the stem cells originating at the marrow must diffuse over tens of millimetres to populate the whole fracture callus [196]. In that case, the stem cell origin location and diffusion coefficient were observed to have a greater effect upon the healing rate.

The effect of the stem cell maturation rate 'M' upon the gap filling rate was investigated next, with values of M=20, 10, 6.7, 5 and 3.3%/day. These were achieved using averaged smoothing periods of 5, 10, 15, 20 and 30 days respectively.

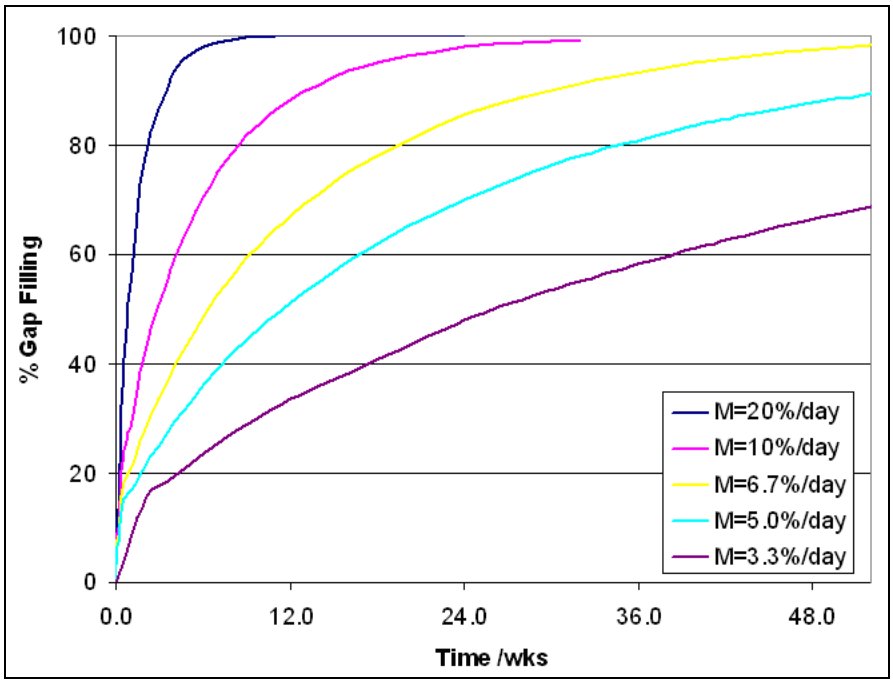

Figure 111: Percentage Gap Filling for Varying Stem Cell Maturation Rates

The stem cell maturation rate 'M' had a considerable effect upon the rate of gap filling, with higher maturation rates giving faster gap filling (Figure 111). The gap filling rate fitted the requirements best with a maturation rate of 5%/day, from an averaged smoothing period of 20 days; the gap filling was 51% at 3 months and 89% at 12 months.

In conclusion, an established tissue differentiation–based healing process from the literature was used to simulate the re-filling of a cancellous bone void. The literature value for the stem cell diffusion coefficient of D=2.37mm^2/day was kept for this study. However, a smaller stem cell maturation rate than that used in the literature, of M=5%/day, was proposed as suitable for this application. With limited clinical data for parameter fitting, this parameter was investigated further in the main study.

APPENDIX 2: VIRTUAL X-RAY ALGORITHM

To analyse the finite element model's bone density distribution and its adaptation, it is insufficient to inspect individual cross sections of the bone; changes will occur throughout its thickness. To obtain density change information throughout the bone, a virtual X-Ray algorithm was written in MATLAB (The MathWorks Inc, MA, USA) which took three-dimensional locations and equivalent density values for each node in the model from the FE software. For each node, taking its density value 'ρ' its equivalent Hounsfield Unit value (HU) was calculated using the fitted relationship from the original CT scan (Figure 39):

$$HU = 855\rho - 80 \qquad \textbf{Equation 37}$$

From this, the linear attenuation coefficient of the bone element was calculated using the rearranged equation from Brooks and DiChiro [260]:

$$\mu_{tissue} = \frac{HU\left(\mu_{water} - \mu_{air}\right)}{1000} + \mu_{water} \qquad \textbf{Equation 38}$$

where 'μ' is the linear attenuation coefficient of the tissue, and air and water references. Values were taken for 20keV incident X-Ray energy of μ_{water} = 0.796cm^{-1} and μ_{air} = 8.76x10^{-4}cm^{-1} [261].

In the MATLAB model, a grid of pixels was laid over the bone, and the elements overlapped by each pixel were found. Then the fractional incident intensity of received X-Rays transmitted through the bone was calculated by discretising the equation [261]:

$$\frac{I}{I_0} = e^{-\mu x} \qquad \textbf{Equation 39}$$

where 'I' is the transmitted ray intensity, 'I_0' is the incident intensity and 'x' is the depth of material through which the rays have passed. The discretised form for N elements, each with an attenuation coefficient 'μ_i' and half-tetrahedron height 'x_i' was:

$$\frac{I}{I_0} = e^{-\sum_{i=1}^{N} \mu_i x_i} \qquad \textbf{Equation 40}$$

This was displayed for the pixels as a greyscale contour plot, such as that included in Figure 112 for the intact proximal femur:

Figure 112: Example Virtual X-Ray of the Intact Femur

APPENDIX 3: PUBLISHED ARTICLES

To date, 6 conference papers have been published and presented from this work:

- Dickinson, A, Browne, M, Jeffers, J and Taylor, A (2008): *FE Analysis of the Effect of Hip Resurfacing Stem Design on Femoral Head and Neck Strains*, at the 54th Annual Meeting of the Orthopaedic Research Society.
- Dickinson, A S, Browne, M, Taylor, A C (2009): *Performance of the Resurfaced Hip: the Influence of Prosthesis Size and Positioning on Remodelling and Fracture of the Femoral Neck,* at the 22nd Annual Congress of the International Society for Technology in Arthroplasty (ISTA).
- Dickinson, A S, Browne, M, Jeffers, J R T, Taylor, A C (2009): *Performance of the Resurfaced Hip: the Influence of Prosthesis Stem Design on Remodelling and Fracture of the Femoral Neck,* at the 22nd Annual Congress of the International Society for Technology in Arthroplasty (ISTA).
- Dickinson, A S, Taylor, A C, Browne M (2010): *Simulating Healing and Adaptation of the Implant-Bone Interface in Resurfacing Hip Replacement*, at the 18th Annual Meeting of the European Orthopaedic Research Society,
- Dickinson, A S, Taylor, A C, Browne M (2010): *A Mechanobiological Model of Implant-Bone Interface Healing and Adaptation in Resurfacing Hip Replacement*, at the 6th World Congress of Biomechanics.
- Dickinson, A S, Taylor, A C, Ozturk, H, Browne, M (2010): *Experimental Validation of a Finite Element Model of the Proximal Femur using Digital Image Correlation*, at the 6th World Congress of Biomechanics.

Furthermore, three journal papers have been accepted for publication after peer review:

- Dickinson, A S, Taylor, A C, Browne, M (2010) *Performance of the Resurfaced Hip Part 1: the Influence of Prosthesis Size and Positioning on the Remodelling and Fracture of the Femoral Neck.* Proc. IMechE Part H: Journal of Engineering in Medicine, Vol. 224: 427-439.
- Dickinson, A S, Taylor, A C, Jeffers, J R T, Browne, M (2010) *Performance of the Resurfaced Hip Part 2: the Influence of Prosthesis Stem Design on Remodelling and Fracture of the Femoral Neck.* Proc. IMechE Part H: Journal of Engineering in Medicine, Vol. 224: 841-852.
- Dickinson, A S, Taylor, A C, Ozturk, H, Browne, M (2011) *Experimental Validation of a Finite Element Analysis Model of the Proximal Femur using Digital Image Correlation and a Composite Bone Model.* Journal of Biomechanical Engineering (Trans. ASME), Vol 133.

A fourth journal paper has been submitted for publication:

- Dickinson, A S, Taylor, A C, Browne, M, *Implant-Bone Interface Healing and Adaptation in Resurfacing Hip Replacement*. Revised version submitted to Computer Methods in Biomechanics and Biomedical Engineering after first peer review.